Continuing Dynamical Systems in Homogeneous Cosmologies Through The Big Bang Singularity

Joshua Hoffmann

Department of Physics

Lancaster University

A thesis submitted for the degree of

Doctor of Philosophy

September 2024

Abstract

General Relativity is the most successful theory of gravity developed so far. Among its many successes lie just as many open questions. This thesis is concerned primarily with the description of cosmological dynamical systems within General Relativity. The Hawking-Penrose theorems have shown General Relativity contains, quite generically, singular solutions for which it is not possible to uniquely and deterministically evolve dynamical systems describing the cosmology through these singular points. Possibly the most well known example of a such a singular point in the spacetime manifold is the Big Bang. Most conventional approaches to resolving this singularity impose some kind of quantization of the gravitational field, as one expects quantum gravity effects to be relevant under such conditions. In this work, we argue that if one takes the relationalist point of view, initially developed by Barbour and Bertotti, in which the measurable dynamical variables are dimensionless ratios, it is possible to find a description of cosmological dynamical systems defined on a contact manifold rather than the typical symplectic manifold of geometric classical mechanics. The framework of contact-reduction is applied to FLRW, Bianchi I and Bianchi IX cosmologies. We show that in the relational, shape space description there exist unique solutions to the equations of motion describing the cosmological dynamical system that pass smoothly through the Big Bang singularity. We also present work on addressing fundamental issues with several classes of cosmological inflation models, with a particular emphasis on the Quartic Hilltop model. These models are typically investigated under assumptions that make them physically unviable. We show that relaxing these assumptions and accounting for how they exit inflation significantly alters their predictions of the spectral index and tensor-to-scalar ratio.

Acknowledgements

First and foremost I dedicate this work to my mum, Jude. I simply cannot find the words to thank you, so I hope this does the job! I would like to thank my supervisor David Sloan for endless helpful discussions and above all his years of friendship and guidance. I must also thank Gavin Ayliffe and Mathew Kellet, without them I would certainly not have thought I was capable of an achievement of this kind. Likewise I owe a huge thank you to David Makepeace for continuing to inspire me to study physics long after I've left sixth form college! I must also thank my closest friends Roman, Archie, Luke Smith and Luke Georgiou. Each of you have affected my life profoundly in your own unique ways and I will always be grateful for your friendship.

Declaration

I declare that the work presented in this thesis is, to the best of my knowledge and belief, original and my own work. The material has not been submitted, either in whole or in part, for a degree at this, or any other university. Chapter 2 contains a review of background knowledge required to understand the work, following references clearly cited where relevant. Chapters 3 & 4 is based on original research carried out by myself and David Sloan and contained Published in Physical Review D [1, 2]. Chapter 5 is based on original research carried out by myself and David Sloan and is based on a paper published in Physical Review D [3] which I first authored. The work builds heavily on foundational results which are summarised and explicitly cited where relevant.

This thesis does not exceed the maximum permitted word length of 80,000 words including appendices and footnotes, but excluding the bibliography. A rough estimate of the word count is: 49440

Joshua Hoffmann

Publications

- Squared Quartic Hilltop Inflation: Josh Hoffmann & David Sloan `https://doi.org/10.1103/PhysRevD.104.123542`
- Regularization of Single Field Inflation Models: Josh Hoffmann & David Sloan `https://doi.org/10.1103/PhysRevD.107.023502`
- Continuation of Bianchi Spacetimes Through the Big Bang: Josh Hoffmann & David Sloan `https://doi.org/10.1103/PhysRevD.110.063539`

Contents

List of Figures

Chapter 1

Introduction

This thesis studies the behaviour of cosmological dynamical systems. The majority of the work is particularly concerned with alleviating the breakdown of these classical systems at the Big Bang singularity, particularly within the context of homogeneous Bianchi IX cosmologies. The work also touches on aspects on inflationary cosmology and attempts to show that previously ignored features of Quartic Hilltop potentials can have a significant effect on cosmological observable and the models consistency with data collected from the Planck survey. Section 2.1 provides a review of familiar symplectic Lagrangian and Hamiltonian mechanics and an introduction to contact manifolds and contact mechanics. A basic review of General Relativity is given, particularly from the perspective of a Lagrangian field theory. Features of homogeneous and isotropic cosmological solutions to the Einstein field equations are explored and an introduction to the basic motivations and ideas of inflation are given.

Sections 3 4 & 5 are based on original research by the author and David Sloan. In section 3 we discuss conceptual issues with a favourable inflationary potential candidate, the Quartic Hilltop model. It is argued that vacuum stabilising terms,which have previously been ignored in the literature, must be accounted for in to the Quartic Hilltop model in order for it to be physically viable. Furthermore we show that when accounted for, these stabilising terms can significantly affect the

predictions of the model and its consistency with observational data. In section 4 we extend this analysis to similar candidate models which suffer from the same issues as Quartic Hilltop.

In section 5 we develop a framework in which the dynamical systems describing Bianchi IX, Bianchi I and FLRW cosmologies may smoothly and uniquely evolved through the Big Bang singularity. Section 5 begins with a brief review of dynamical similarities and presents some foundational results from the literature. A review of the ADM formalism of General Relativity and the Bianchi classification of homogeneous spacetimes is then given, closely following references cited wherein. We then describe the process of symmetry reducing the ADM Hamiltonian by its scaling symmetry associated with the volume/scale factor to form a dynamical system defined on a contact manifold in section 5.6. In section 5.7 we show that in shape space, the equations of motion describing the cosmological dynamical systems have unique, smooth solutions passing through the Big Bang in the cases of FLRW, Bianchi I and Quiescent Bianchi IX spacetimes. In section 5.8 we provide numerical solutions to the equations of motion in a variety of examples and show explicitly continuation of the dynamical system through the initial singularity. Throughout this thesis we work in units for which $16\pi G = 1$ where G is the Newtonian gravitational constant and $c = 1$ unless stated otherwise.

Chapter 2

Background

2.1 Geometric Lagrangian and Hamiltonian Mechanics

2.1.1 Lagrangian and Hamiltonian Mechanics

In this section we will start by briefly recapping the standard Lagrangian and Hamiltonian mechanics that readers should be familiar with, before formalising these ideas in the context of differential geometry. The geometric formulation of Lagrangian and Hamiltonian mechanics has the benefit of being a coordinate-independent description of the evolution of dynamical systems, thus making it naturally suited for tackling problems in General Relativity.

The Lagrangian formulation of dynamical systems comes from considering a fundamental question. If the state of a physical system at some time t is described by a point in some configuration space Q, characterised by a set of generalised coordinates $q_i(t)$ labelled by and index $i = 1, ..., n$, knowing the initial and final states $q_0(t_0)$ and $q_1(t_1)$, what path does the system take through Q over the time interval $[t_0, t_1]$ between the two endpoints. Given two endpoints q_0 and q_1 there are of course many paths that can be drawn between them. The physical path γ through the configuration space is the one actually traced out by a classical system.

Thus the study of dynamical systems in classical mechanics has at it's core, the problem of finding this physical path. The guiding principle that determines the physical path of a system is the ***Principle of Stationary Action***. This states that the critical paths of the action functional are the physical paths of the system.The action of a dynamical system S is a functional of the Lagrangian function. The Lagrangian function takes as it's input the generalised coordinates $q_i(t)$ and velocities $\dot{q}_i(t)$. It may also be an explicit function of time, however in this section we will assume it is not unless stated otherwise.. The Lagrangian $L(q_i, \dot{q}_i)$ is defined in the first instance as the kinetic energy of the system minus it's potential energy.

$$L(q_i, \dot{q}_i) = K(q_i, \dot{q}_i) - V(q_i) \tag{2.1}$$

The action functional is defined as the integral of the Lagrangian over the time $t \in [t_0, t_1]$.

$$S[L(q_i, \dot{q}_i)] = \int_{t_0}^{t_1} L(q_i, \dot{q}_i)\, dt \tag{2.2}$$

Given fixed boundary conditions $q_i(t_0)$ & $q_i(t_1)$, we wish to find the stationary paths of the action, which will be the physical path of a classical system whose Lagrangian is $L(q_i, \dot{q}_i)$. In order to determine these paths we consider an infinitesimal variation of the generalised coordinates to the first order $q_i(t) \to q_i(t) + \delta q_i(t)$. If $q_i(t)$ are the generalised coordinates taken by the physical path of the system on the configuration space over time t, then the infinitesimal variation of the action must be zero with respect to an arbitrary infinitesimal variation $\delta q_i(t)$. The first order variation in the action is

$$\begin{aligned} \delta S &= \int_{t_0}^{t_1} \delta L(q_i, \dot{q}_i)\, dt \\ &= \int_{t_0}^{t_1} \frac{\partial L}{\partial q_i} \delta q_i(t) + \frac{\partial L}{\partial \dot{q}_i} \delta \dot{q}_i(t)\, dt \end{aligned} \tag{2.3}$$

Consider the second term in eq 2.3, which may be integrated by parts.

$$\begin{aligned} I &= \int_{t_0}^{t_1} \frac{\partial L}{\partial \dot{q}_i} \delta \dot{q}_i(t)\, dt \\ &= \left[\frac{\partial L}{\partial \dot{q}_i} \delta q_i(t) \right]_{t_0}^{t_1} - \int_{t_0}^{t_1} \frac{d}{dt} \left(\frac{\partial L}{\partial \dot{q}_i} \right) \delta q_i(t)\, dt \end{aligned} \tag{2.4}$$

The boundary points of the path $q_i(t_0), q_i(t_1)$ are taken to be fixed, and therefore the infinitesimal variations are zero at the boundaries $\delta q_i(t_0) = \delta q_i(t_1) = 0$ and thus the first term in the brackets of eq 2.4 is zero, and the first order infinitesimal action variation becomes

$$\delta S = - \int_{t_0}^{t_1} \left[\frac{d}{dt} \left(\frac{\partial L}{\partial \dot{q}_i} \right) - \frac{\partial L}{\partial q_i} \right] \delta q_i(t)\, dt \tag{2.5}$$

This variation must be zero with respect to arbitrary infinitesimal variations of the generalised coordinates, which is the case if and only if

$$\frac{d}{dt} \left(\frac{\partial L}{\partial \dot{q}_i} \right) - \frac{\partial L}{\partial q_i} = 0 \tag{2.6}$$

These are the Euler-Lagrange equations of motion, they are a set of n second-order ordinary differential equations, one for each of the generalised coordinates $q_i(t)$. The Lagrangian approach to classical mechanics is generally superior to the Newtonian approach, as we need only determine a single scalar function, the Lagrangian, which describes the dynamics of system and decide on $2n$ appropriate boundary conditions as initial data for the solutions of our differential equations. The Lagrangian approach is completely equivalent to Newtonian mechanics, and if one considers the Lagrangian of a point particle of mass m in n dimensions acting under a potential $V(q_i)$, for which the Lagrangian is

$$L(q_i, \dot{q}_i) = \frac{1}{2} m \sum_i \dot{q}_i^2 - V(q_i) \tag{2.7}$$

we obtain the standard Newtonian equation of motion.

$$m\ddot{q}_i = -\frac{\partial V}{\partial q_i} = F_i(q_i) \tag{2.8}$$

where $F_i(q_i)$ is the component in the i-direction of the force acting on the point particle. For simple classical systems the Newtonian equations of motion may be more convenient but for complicated systems, writing down Newtons second law for each particle will quickly become intractable, where as the Lagrangian offers a more sophisticated approach to analysing dynamical systems.

In particular, the Lagrangian framework makes it very apparent when the dynamical systems possesses a conserved quantity. If the Lagrangian is obtained, and is independent of a particular generalised coordinate, say $q_k(t)$, the coordinate is called a cyclic coordinate and the Euler-Lagrange equation for q_k will read

$$\frac{d}{dt}\left(\frac{\partial L}{\partial \dot{q}_k}\right) = 0 \tag{2.9}$$

The quantity $p^i = \partial L/\partial \dot{q}_i$ is known as the generalised momentum, as it is this term that in the familiar contexts such as point particles, gives exactly the particle momentum. Thus a cyclic coordinate has constant (generalised) momentum.

$$\frac{dp^k}{dt} = 0 \tag{2.10}$$

So far we have considered only Lagrangians with no explicit time dependence. It is a trivial exercise to show that relaxing this assumption does not change the Euler-Lagrange equations. Consider the total time derivative of a Lagrangian with explicit time dependence $\mathcal{L}(q_i, \dot{q}_i, t)$.

$$\frac{d\mathcal{L}}{dt} = \frac{\partial \mathcal{L}}{\partial q_i}\dot{q}_i + \frac{\partial \mathcal{L}}{\partial \dot{q}_i}\ddot{q}_i + \frac{\partial \mathcal{L}}{\partial t} \tag{2.11}$$

Assuming that the Euler-Lagrange equations are satisfied, one has

$$\frac{\partial \mathcal{L}}{\partial q_i} = \frac{d}{dt}\left(\frac{\partial \mathcal{L}}{\partial \dot{q}_i}\right) \tag{2.12}$$

and so equation 2.11 can be written as

$$\begin{aligned} \frac{d\mathcal{L}}{dt} &= \frac{d}{dt}\left(\frac{\partial \mathcal{L}}{\partial \dot{q}_i}\dot{q}_i\right) + \frac{\partial \mathcal{L}}{\partial \dot{q}_i}\ddot{q}_i + \frac{\partial \mathcal{L}}{\partial t} \\ &= \frac{d}{dt}\left(\dot{q}_i\frac{\partial \mathcal{L}}{\partial \dot{q}_i}\right) + \frac{\partial \mathcal{L}}{\partial t} \end{aligned} \tag{2.13}$$

The total derivative terms in equation 2.13 can be grouped together, giving the partial derivative of the Lagrangian with respect to time as

$$-\frac{\partial \mathcal{L}}{\partial t} = \frac{d}{dt}\left(\dot{q}_i\frac{\partial \mathcal{L}}{\partial \dot{q}_i} - \mathcal{L}\right) \tag{2.14}$$

We defined the Jacobi energy function $J(q_i, \dot{q}_i, t)$ by

$$\frac{dJ}{dt} = -\frac{\partial \mathcal{L}}{\partial t} \tag{2.15}$$

and therefore, up to an integration constant we have

$$J(q_i, \dot{q}_i, t) = \dot{q}_i\frac{\partial \mathcal{L}}{\partial \dot{q}_i} - \mathcal{L} \tag{2.16}$$

By it's definition through equation 2.15, the Jacobi energy function is conserved when the Lagrangian has no explicit time dependence. It is not immediately obvious that this function represents an energy associated with the dynamical system. To elucidate this, consider the simple case of a point particle of mass m moving under a potential $V(q)$ that only has explicit dependence on the generalised coordinates q_i. Furthermore, let the Cartesian coordinates have no explicit time dependence $\partial_t x_i = 0$. The Lagrangian of the point particle can be written in terms of kinetic

part K and the potential $V(q_i)$

$$\mathcal{L} = K - V(q_i) \tag{2.17}$$

where

$$K = \frac{1}{2} m \sum_r v_r^2 \tag{2.18}$$

The velocity of the r-th Cartesian coordinate can be written in terms of generalised coordinates

$$v_r = \frac{dx_r}{dt} = \frac{\partial x_r}{\partial q_j} \dot{q}_j \tag{2.19}$$

The kinetic term of the Lagrangian then becomes

$$K = \frac{1}{2} m \frac{\partial x_r}{\partial q_j} \frac{\partial x_r}{\partial q_k} \dot{q}_i \dot{q}_k \tag{2.20}$$

where summation over the Cartesian coordinates indexed by r is now implied. To calculate the Jacobi energy function we require the derivative

$$\frac{\partial L}{\partial \dot{q}_i} = \frac{1}{2} m \frac{\partial x_r}{\partial q_j} \frac{\partial x_r}{\partial q_k} \left(\delta^i_j \dot{q}_k + \delta^i_k \dot{q}_j \right) \quad = m \frac{\partial x_r}{\partial q_i} \frac{\partial x_r}{\partial q_k} \dot{q}_k \tag{2.21}$$

The Jacobi energy function is then

$$J(q_i, \dot{q}) = m \frac{\partial x_r}{\partial q_i} \frac{\partial x_r}{\partial q_k} \dot{q}_i \dot{q}_k - \mathcal{L} = K + V(q_i) \tag{2.22}$$

And thus we see that in this case the Jacobi energy function is always equal to the total energy of the system. The Jacobi energy function is really a more generalised case of the Hamiltonian, a function of fundamental importance in the study of dynamical systems.

So far we have explored the Lagrangian approach to classical dynamics, in which we construct a Lagrangian from a set of generalised coordinates q_i and velocities $\dot{q}_i$. The Lagrangian is a function of the space of coordinates and velocities (or possibly and extended space to include an interval of the real line if the Lagrangian is time

dependant). We have seen that for every velocity, there is an associated generalised momentum

$$p^i = \frac{\partial \mathcal{L}}{\partial \dot{q}_i} \tag{2.23}$$

If the Jacobian

$$J_{ij} = \frac{\partial p^i}{\partial \dot{q}_j} \tag{2.24}$$

is non singular, then by the implicit function theorem [6] $p^i = p^i(q_j, \dot{q}_j)$ has an inverse and there exists a one-to-one map between the velocities $\dot{q}_i$ and momenta p^i. The Hamiltonian is simply the Jacobi energy function written in terms of the momenta, rather than velocities when this particular regularity condition of the Hessian is satisfied

$$H(q_i, p^i, t) = p^i \dot{q}_i - \mathcal{L}(q_i, \dot{q}_i, t) \tag{2.25}$$

The Hamiltonian is a function defined on phase space (q_i, p_i) (or an extended phase space if it is time dependant), the space of generalised coordinates and momenta. From here on we will assume the Hamiltonian and Lagrangian to be time-independent unless specified. Each point in phase space is a state of the dynamical system, specifying its position and momentum, and as we shall now see, physical systems move through phase space in a manner determined by the Hamiltonian.

Just as we derived equations of motion generated by the Lagrangian through the stationary action principle, the same can be done for the Hamiltonian. Consider the action

$$S = \int \mathcal{L}\, dt \tag{2.26}$$

From equation 2.25 we have $\mathcal{L} = p^i \dot{q}_i - H$ and thus

$$S = \int p^i \dot{q}_i - H\, dt \tag{2.27}$$

Consider now a path through phase space $\gamma(t) = (q_i(t), p^i(t))$. By the stationary action principle, physical paths through phase space will be critical paths of the

action, and so for infinitesimal variations that vanish on the boundaries

$$\begin{aligned} q_i(t) &\to q_i(t) + \delta q_i(t) \\ p^i(t) &\to p^i(t) + \delta p^i(t) \end{aligned} \tag{2.28}$$

we must have $\delta S = 0$. Taking the infinitesimal variation of the action in equation 2.27 we have

$$\delta S = \int \delta p^i \dot{q}_i + p^i \delta \dot{q}_i - \delta H \, dt \tag{2.29}$$

The variation of the Hamiltonian can be written as

$$\delta H = \frac{\partial H}{\partial q_i} \delta q_i + \frac{\partial H}{\partial p^i} \delta p^i \tag{2.30}$$

The second term in equation 2.29 can be integrated by parts, with the boundary terms vanishing

$$\int p^i \delta \dot{q}_i \, dt = - \int \dot{p}^i \delta q_i \, dt \tag{2.31}$$

and so we have

$$\delta S = \int - \left(\dot{p}^i + \frac{\partial H}{\partial q_i} \right) \delta q_i + \left(\dot{q}_i - \frac{\partial H}{\partial p^i} \right) \delta p^i \, dt \tag{2.32}$$

To have $\delta S = 0$ for arbitrary infinitesimal variations δq_i & δp^i we must have

$$\dot{q}_i = \frac{\partial H}{\partial p^i}, \quad \dot{p}^i = - \frac{\partial H}{\partial q_i} \tag{2.33}$$

These are Hamiltons equations of motion. The change of variables going between the Lagrangian and the Hamiltonian description is a Legendre transform, and provided that it does indeed exist then we may move between the two equivalent descriptions of the same physical system.

The Hamiltonian is an object of fundamental importance in the study in dynamical systems. In a conservative system, it represents the total energy of the system, which we saw when we introduced the Jacobi energy function. The fact that

the Hamiltonian is a conserved energy in this case hints at the fact that it is relation to time translation symmetry. Noethers theorem [7–10] tells us that continuous symmetries are associated with conserved quantities. To see how the Hamiltonian is the generator of time evolution, consider an arbitrary smooth function of phase space $F(q_i, p^i)$ and its total time derivative along a physical path

$$\frac{dF}{dt} = \frac{\partial F}{\partial q_i}\dot{q}_i + \frac{\partial F}{\partial p^i}\dot{p^i} \tag{2.34}$$

Physical paths satisfy Hamiltons equations 2.33 and so we have

$$\frac{dF}{dt} = \frac{\partial F}{\partial q_i}\frac{\partial H}{\partial p^i} - \frac{\partial F}{\partial p^i}\frac{\partial H}{\partial q_i} \tag{2.35}$$

The Hamiltonian induces a Poisson bracket structure on the phase space

$$\{F, H\} := \frac{\partial F}{\partial q_i}\frac{\partial H}{\partial p^i} - \frac{\partial F}{\partial p^i}\frac{\partial H}{\partial q_i} \tag{2.36}$$

which gives the time derivative of phase space functions along solutions to the equations of motion

$$\frac{dF}{dt} = \{F, H\} \tag{2.37}$$

Consequently, we see that the Hamiltonian is conserved along solutions to the equations of motion, since its Poisson bracket with itself is always zero.

2.1.1.1 Point and Canonical Transformations

By this point we have developed two different frameworks in which can analyse a classical dynamical system, which are the Lagrangian and Hamiltonian descriptions. In former, we construct a Lagrangian from a set of generalised coordinates and velocities $(q_i, \dot{q}_i)$, physical paths through the velocity space satisfy the Euler-Lagrange equations generated by the Lagrangian. There should not be anything special about our particular choice of coordinates, so it's natural at this point to ask whether the Euler-Lagrange equations are invariant under an arbitrary change

of coordinates. Such a change of coordinates is called a point transformation, and the Euler-Lagrange equations are indeed invariant under point transformations as we shall show. Consider defining a new set of generalised coordinates $Q(q_i, t)$ which we assume are invertible functions and q_i are solutions to the Euler-Lagrange equations. We want to determine if the Euler-Lagrange equations hold in these arbitrary coordinates. To that end, consider calculating the partial derivatives

$$\begin{aligned} \frac{\partial \mathcal{L}}{\partial Q_i} &= \frac{\partial \mathcal{L}}{\partial q_j}\frac{\partial q_j}{\partial Q_i} + \frac{\partial \mathcal{L}}{\partial \dot{q}_j}\frac{\partial \dot{q}_j}{\partial Q_i} \\ \frac{\partial \mathcal{L}}{\partial \dot{Q}_i} &= \frac{\partial \mathcal{L}}{\partial q_j}\frac{\partial q_j}{\partial \dot{Q}_i} + \frac{\partial \mathcal{L}}{\partial \dot{q}_j}\frac{\partial \dot{q}_j}{\partial \dot{Q}_i} \end{aligned} \tag{2.38}$$

The Point transformation does not depend on the velocities and so we have $\frac{\partial q_j}{\dot{Q}_i} = 0$ and so the second line in equation 2.38 simplifies to

$$\frac{\partial \mathcal{L}}{\partial \dot{Q}_i} = \frac{\partial \mathcal{L}}{\partial \dot{q}_j}\frac{\partial \dot{q}_j}{\partial \dot{Q}_i} \tag{2.39}$$

We also have

$$\frac{dq_j}{dt} = \frac{\partial q_j}{\partial Q_k}\dot{Q}_k + \frac{\partial q_j}{\partial t} \tag{2.40}$$

and so we may calculate the partial derivative term

$$\begin{aligned} \frac{\partial \dot{q}_j}{\partial \dot{Q}_i} &= \frac{\partial}{\partial \dot{Q}_i}\left(\frac{\partial q_j}{\partial Q_k}\dot{Q}_k + \frac{\partial q_j}{\partial t}\right) \\ &= \delta^i_k \frac{\partial q_j}{\partial \dot{Q}_k} \\ &= \frac{\partial q_j}{\partial Q_i} \end{aligned} \tag{2.41}$$

Substituting this into equation 2.39 gives

$$\frac{\partial \mathcal{L}}{\partial \dot{Q}_i} = \frac{\partial \mathcal{L}}{\partial \dot{q}_j}\frac{\partial q_j}{\partial Q_i} \tag{2.42}$$

These pieces can now be brought together to show invariance of the Euler-Lagrange

equations.

$$\begin{aligned}\frac{d}{dt}\left(\frac{\partial \mathcal{L}}{\partial \dot{Q}_i}\right) - \frac{\partial \mathcal{L}}{\partial Q_i} &= \frac{d}{dt}\left(\frac{\partial \mathcal{L}}{\partial \dot{q}_j}\frac{\partial q_j}{\partial Q_i}\right) - \frac{\partial \mathcal{L}}{\partial q_j}\frac{\partial q_j}{\partial Q_i} - \frac{\partial \mathcal{L}}{\partial \dot{q}_j}\frac{\partial \dot{q}_j}{\partial Q_i} \\ &= \frac{\partial q_j}{\partial Q_i}\left[\frac{d}{dt}\left(\frac{\partial \mathcal{L}}{\partial \dot{q}_j}\right) - \frac{\partial \mathcal{L}}{\partial q_j}\right] + \frac{\partial \mathcal{L}}{\partial \dot{q}_j}\left[\frac{d}{dt}\left(\frac{\partial q_j}{\partial Q_i}\right) - \frac{\partial \dot{q}_j}{\partial Q_i}\right]\end{aligned} \tag{2.43}$$

The fist term in equation 2.43 is zero since the q_i are solutions to the Euler Lagrange equations. To show that the second term is zero, consider the time derivative

$$\frac{d}{dt}\left(\frac{\partial q_j}{\partial Q_i}\right) = \frac{\partial}{\partial Q_k}\left(\frac{\partial q_j}{\partial Q_i}\right)\dot{Q}_k + \frac{\partial}{\partial t}\left(\frac{\partial q_j}{\partial Q_i}\right) \tag{2.44}$$

Assuming that the point transformation is at least C^2 smooth, the ordering of partial derivatives does not matter, so we may write

$$\begin{aligned}\frac{d}{dt}\left(\frac{\partial q_j}{\partial Q_i}\right) &= \frac{\partial}{\partial Q_i}\left(\frac{\partial q_j}{\partial Q_k}\dot{Q}_k + \frac{\partial q_j}{\partial t}\right) \\ &= \frac{\partial}{\partial Q_i}\frac{dq_j}{dt}\end{aligned} \tag{2.45}$$

We then have the required result

$$\frac{d}{dt}\left(\frac{\partial \mathcal{L}}{\partial \dot{Q}_i}\right) - \frac{\partial \mathcal{L}}{\partial Q_i} = 0 \tag{2.46}$$

showing that the Euler-Lagrange equations do not depend on our choice of generalised coordinates and are therefore covariant. In the Hamiltonian framework however, a change of coordinates on phase space is not always guaranteed to preserve the form of Hamilton equations. Only a particular subset of coordinate transformations leave Hamiltons equations invariant, which are known as canonical transformations. Consider a Hamiltonian, possibly time dependant in a set of generalised coordinates $H(q_i, p^i, t)$ and a transformations to a new set of coordinates $Q_i(q, p, t)$ and $P^i(q, p, t)$. This is a canonical transformation if there exists a new Hamiltonian $K(Q, P, t)$ such that the form of Hamiltons equations is preserved in the new coordinates

$$\dot{Q}_i = \frac{\partial K}{\partial P^i}, \quad \dot{P}^i = -\frac{\partial K}{\partial Q_i} \tag{2.47}$$

Hamiltons equations, which we derived from a variational principle, hold in both sets of variables and thus we must have

$$\begin{aligned} \delta S &= \delta \int p^i \dot{q}_i - H(q_i, p^i, t)\, dt \\ &= \delta \int P^i \dot{Q}_i - K(Q_i, P^i, t)\, dt \\ &= 0 \end{aligned} \tag{2.48}$$

Recall that when we have fixed boundary conditions, the variation is insensitive to total derivative terms, and so for equation 2.48 to hold we must have

$$\lambda \left(p^i dq_i - H dt \right) = P^i dQ_i - K dt + dF \tag{2.49}$$

where F is an unknown function, called the generating function and lambda is some non-zero scale factor which we shall simply set to unity and ignore. There are four independent generating functions that one can use to find canonical transformations. Consider the case when $F = F_1(q_i, Q_i, t)$, then

$$dF = \frac{\partial F_1}{\partial q_i} dq_i + \frac{\partial F_1}{\partial Q_i} dQ_i + \frac{\partial F_1}{\partial t} dt \tag{2.50}$$

Comparing equation 2.50 to equation 2.49 yields

$$p^i = \frac{\partial F_1}{\partial q_i}, \quad P^i = -\frac{\partial F_1}{\partial Q_i}, \quad K = H + \frac{\partial F_1}{\partial t} \tag{2.51}$$

At a first glance it can be confusing to see how a generating function generates a canonical transformation. It is best elucidated through an example. Consider the Hamiltonian of a 1-dimensional harmonic oscillator in Cartesian coordinates

$$H = \frac{p^2}{2m} + \frac{1}{2} m\omega^2 q^2 \tag{2.52}$$

The Hamiltonian for this system involves a mixture of position and momentum variables, we would like to find a canonical transformation that simplifies the Hamiltonian. To that end consider changing to a new set of variables (Q, P) such that

$$p = f(P)\cos Q, \quad q = Af(P)\sin Q \tag{2.53}$$

where A is some scalar and $f(P)$ an unknown function of the new momentum variable P. If we choose $A = 1/m\omega$ then the Hamiltonian takes a simple form

$$H = \frac{f(P)^2}{2m} \tag{2.54}$$

Now let $F_1(q, Q)$ be the first generating function as defined in equation 2.51, then we have

$$f(P)\cos Q = \frac{\partial F_1}{\partial q} \tag{2.55}$$

and

$$f(P) = \frac{m\omega q}{\sin Q} \tag{2.56}$$

which is obtained from plugging in the chosen value of A into equation 2.53 and rearranging for $f(P)$. We therefore have

$$\frac{\partial F_1}{\partial q} = m\omega q \cot Q \implies F_1(q, Q) = \frac{1}{2} m\omega q^2 \cot Q + G(Q) \tag{2.57}$$

where $G(Q)$ is some arbitrary function which we may set to zero. The new momentum variable is then given by the generator function as

$$P = -\frac{\partial F_1}{\partial Q} = \frac{m\omega q^2}{2\sin^2 Q} \implies q^2 = \frac{2P}{m\omega}\sin^2 Q \tag{2.58}$$

Thus we identify the function

$$f(P) = \sqrt{2m\omega P} \tag{2.59}$$

We are left with a new Hamiltonian that is far simpler than the one we started with

$$K = \omega P \tag{2.60}$$

with preserved Hamiltons equations and Poisson bracket structure

$$\begin{aligned} \dot{Q} &= \frac{\partial K}{\partial P} = \omega \\ \dot{P} &= -\frac{\partial K}{\partial Q} = 0 \end{aligned} \tag{2.61}$$

with solutions $Q(t) = Q_0 + \omega t$ and $P = K/\omega$ where the Hamiltonian K is conserved.

The other 3 generating functions are found by investigating equation 2.49 when F is a function of different pairs of independent variables. In all cases one finds

$$\begin{aligned} &F = F_1(q_i, Q_i, t), \quad p^i = \frac{\partial F_1}{\partial q_i}, \quad P^i = -\frac{\partial F_1}{\partial Q_i} \\ &F = F_2(q_i, P^i, t), \quad p^i = \frac{\partial F_2}{\partial q_i}, \quad Q_i = \frac{\partial F_2}{\partial P^i} \\ &F = F_3(p^i, Q_i, t), \quad P^i = -\frac{\partial F_3}{\partial Q_i}, \quad q_i = -\frac{\partial F_3}{\partial p_i} \\ &F = F_4(p^i, P^i, t), \quad q_i = -\frac{\partial F_4}{\partial p^i}, \quad Q_i = \frac{\partial F_4}{\partial P^i} \end{aligned} \tag{2.62}$$

and the new Hamiltonian is given by

$$K = H + \frac{\partial F}{\partial t} \tag{2.63}$$

such that

$$\dot{Q}_i = \frac{\partial K}{\partial P^i}, \quad \dot{K} = -\frac{\partial K}{\partial \dot{Q}_i} \tag{2.64}$$

2.1.1.2 Symplectic Geometric Mechanics

So far we have looked at two related frameworks for describing classical dynamical systems, by constructing either a Lagrangian from a set of generalised coordinates q_i and velocities $\dot{q}_i$ or a Hamiltonian from the coordinates and a set of momenta p^i. In the Lagrangian case, we saw that the equations of motion were invariant under a point transformation of the generalised coordinates. To some extent, a result along these lines should be expected, since physics shouldn't depend on our choice of coordinates, which is simply a way of labelling physical points in space. To this end we seek a coordinate-free description of classical dynamical systems, for which we will appeal to the language of differential geometry.

In the study of dynamical systems, we often start with a set of n coordinates q_i which can be thought of as labelling points $q = (q_i)_{i=1,..,n}$ in "***Configuration Space***". We assume that the configuration space is a smooth n-dimensional manifold M [7, 11, 12]. The generalised velocities $\dot{q}_i$ belong to the tangent space T_qM of $q \in M$ which are fibers of the tangent bundle TM. The Lagrangian is a smooth map from each point $q \in M$ and the vectors $q_i \in T_qM$ to the reals, so we have $\mathcal{L} : TM \to \mathbb{R}$. Likewise, the Hamiltonian is a map from the cotangent bundle to the reals $H : T^*M \to \mathbb{R}$. The tangent and cotangent bundles are themselves $2n$-dimensional manifolds.

The geometric description of conservative classical dynamical systems makes use of ***Symplectic Geometry*** [7, 12–14], which we will give an overview of here. A symplectic manifold is a pair (M, ω), consisting of an even dimensional manifold M and a closed, non-degenerate 2-form ω called the symplectic form. The non-degererate symplectic form allows us to define a volume form $\omega^n \neq 0$ on M. Darboux's theorem [12] states that given a point $p \in M$, one can always find local coordinates in a neighbourhood of p such that $\omega = dq_i \wedge dp^i$. The fact that one can always find coordinates such that the symplectic form ω has this canonical structure is essentially the statement that symplectic manifolds have the same local structure, since the Darboux coordinates can be constructed in any arbitrary neighbourhood.

Symplectic manifolds are thus set apart by their global properties, rather than local structure.

Given a Hamiltonian on the contangent bundle manifold $H(q_i, p^i) : T^*M \to \mathbb{R}$, the symplectic form allows us to define a vector field X_H which is the unique solution of

$$i_{X_H}\omega = dH \tag{2.65}$$

where "i" denotes the interior product operator. The vector field X_H is called the "***Hamiltonian Vector Field***", and equation 2.65 is actually a geometric, coordinate-independent statement of Hamiltons equations of motion. Expanding X_H in the basis of local Darboux coordinates we have

$$X_H = X_q^i \frac{\partial}{\partial q_i} + X_p^i \frac{\partial}{\partial p^i} \tag{2.66}$$

and so we have the interior product

$$\begin{aligned} i_{X_H}\omega &= i_{X_H}\left(dq_i \wedge dp^i\right) \\ &= i_{X_H}\left(dq_i \otimes dp^i - dp^i \otimes dq_i\right) \\ &= dq_i(X_H)dp^i - dp^i(X_H)dq_i \\ &= X_q^i dp^i - X_p^i dq_i \end{aligned} \tag{2.67}$$

Comparing this result with

$$dH = \frac{\partial H}{\partial q_i}\frac{\partial}{\partial q_i} + \frac{\partial H}{\partial p^i}\frac{\partial}{\partial p^i} \tag{2.68}$$

we have

$$X_H = \frac{\partial H}{\partial p^i}\frac{\partial}{\partial q_i} - \frac{\partial H}{\partial q_i}\frac{\partial}{\partial p^i} \tag{2.69}$$

Thus the integral curves of the Hamiltonian vector field satisfy Hamiltons equations of motion 2.33 and the Hamiltonian vector field generates a 1-parameter group of diffeomorphisms on the phase space manifold

$$\phi_t(q_i(0), p^i(0)) = (q_i(t), p^i(t)) \tag{2.70}$$

called the Hamiltonian flow. Liouvilles theorem [12] states that volume form provides an invariant, volume preserving measure under the Hamiltonian flow

$$\mathcal{L}_{X_H}\omega^n = 0 \tag{2.71}$$

where $\mathcal{L}_{X_H}$ is the Lie derivative along X_H. As a consequence of the symplectic form being closed, it too is preserved along the flow. By Cartans formula we have

$$\begin{aligned} \mathcal{L}_{X_H}\omega &= i_{X_H}d\omega + d(i_{X_H}\omega) \\ &= i_{X_H}(0) + d(dH) \\ &= 0 \end{aligned} \tag{2.72}$$

One can in fact associate any smooth function $F \in C^\infty(M)$ with a vector field X_F satisfying

$$i_{X_F}\omega = dF \tag{2.73}$$

The symplectic form thus induces a natural Poisson bracket structure on the manifold and generates time evolution along the flow

$$\omega(X_F, X_H) = \frac{\partial F}{\partial q_i}\frac{\partial H}{\partial p^i} - \frac{\partial F}{\partial p^i}\frac{\partial H}{\partial q_i} := \{F, H\} = \frac{dF}{dt} \tag{2.74}$$

Time evolution of smooth functions on the symplectic manifold can also be seen as simply the action of the Hamiltonian vector field on the function

$$\frac{dF}{dt} = X_H(F) \tag{2.75}$$

since the flow of X_H generates time evolution of the bundle coordinates (q_i, p^i).

As a consequence, one can clearly see that the Hamiltonian is conserved along its flow, as we have

$$\frac{dH}{dt} = \{H, H\} = 0 \tag{2.76}$$

The requirement that the Hamiltonian be conserved means that physical paths through the cotangent bundle T^*M are restricted to a subset of the phase space. Given initial data $(q_i(0), p_i(0))$, the solution to Hamiltons equations of motion is one that evolves on a surface of constant H. This also helps to shed some light on the interpretation of the Hamiltonian vector field, which up until now plays the role of a rather abstract tool that we have constructed in order to find equations of motion, or in other words the Hamiltonian flow. For each point on the manifold $p \in M$ and $X_H|_p \in T_pM$, the Hamiltonian is a constant of the motion along translations in the X_H direction. An example where this can be seen clearly is the infinite 2-cylinder $S \times \mathbb{R}$, choosing a chart where points on the cylinder are parameterised by the azimuthal angle ϕ and height from the origin z, with the symplectic form $\omega = d\phi \wedge dz$. Consider a Hamiltonian that is a function of the height only, $H = H(z)$. The Hamiltonian vector field is then

$$X_H = \frac{\partial H}{\partial z}\frac{\partial}{\partial \phi} - \frac{\partial H}{\partial \phi}\frac{\partial}{\partial z} = \frac{\partial H}{\partial z}\frac{\partial}{\partial \phi} \tag{2.77}$$

Thus translations in the ∂_ϕ direction, which are rotations around the cylinders central axis, preserve the Hamiltonian, as one would expect since it is only a function of the height of a point on the cylinder.

In more physical examples, the interpretation of the direction the Hamiltonian vector field is not always so clear. Consider as an example a particle moving on the 2-sphere S^2 with symplectic form $\omega = d\theta \wedge dp_\theta + d\phi \wedge dp_\phi$, and the Hamiltonian function

$$H = \frac{1}{2}p_\theta + \frac{1}{2}\frac{p_\phi^2}{\sin^2\theta} \tag{2.78}$$

Firstly, we note that the Hamiltonian is independent of ϕ and so from Hamiltons

equations of motion 2.33, p_ϕ is a constant along the Hamiltonian flow. The Hamiltonain vector field is

$$X_H = p_\theta \frac{\partial}{\partial \theta} + \frac{p_\phi \cos\theta}{\sin^3\theta} \frac{\partial}{\partial p_\theta} + \frac{p_\phi}{\sin^\theta} \frac{\partial}{\partial \phi} \tag{2.79}$$

In this case, the Hamiltonian vector field involves terms pointing in the $\partial_\theta, \partial_{p_\theta}$ and ∂_ϕ directions, so it is not quite a simple as the cylinder case where the Hamiltonian vector field was just a rotation of the azimuthal angle ϕ. In the case of the particle on S^2, would could have anticipated that X_H would contain no contribution from ∂_{p_ϕ}, since it is a conserved quantity along Hamiltonian flows, and thus moving in the p_ϕ direction would be to go off-shell. In the particular case where $p_\phi = 0$, the Hamiltonian is only dependant on p_θ, which becomes a conserved quantity since $\partial H/\partial\theta = 0$ and the Hamiltonian vector field reduces to

$$X_H = p_\theta \frac{\partial}{\partial \theta} \tag{2.80}$$

Now it is clear that for this specific value of the p_ϕ momentum, the direction of X_H is easy to interpret, θ is the only dynamical variable left, and translations in the ∂_θ direction conserve the angular momentum p_θ and Hamiltonian.

In the case of an explicitly time dependant Hamiltonian, one can quite simply define an extended phase space $\tilde{M} = M \times \mathbb{R}$. Physical paths on the extended manifold are integral curves of

$$\tilde{X}_H = X_H + \frac{\partial}{\partial t} \tag{2.81}$$

and the time evolution of smooth functions on the extended phase space is given by

$$\frac{dF}{dt} = X_H(F) = \{F, G\} + \frac{\partial F}{\partial t} \tag{2.82}$$

So far we have looked at the Hamiltonian description of dynamical systems in the framework of differential geometry, so we also ought to be able to write the

Lagrangian description in coordinate-independent manner. Recall the Legendre transform

$$\mathbf{L} : TM \to T^*M \tag{2.83}$$

which converts our description of the dynamical system from one in terms of coordinates q_i and velocities q_i living on the tangent bundle TM to coordinates and momenta p^i living on the cotangent bundle T^*M where

$$\mathbf{L}(q_i, \dot{q}_i) = \left(q_i, \frac{\partial \mathcal{L}}{\partial \dot{q}_i} \right) \tag{2.84}$$

Provided that the Hessian $W_{ij} = \partial^2 \mathcal{L} / \partial \dot{q}_i \partial \dot{q}_j$ is regular, the symplectic form $\omega \in \Omega^2(T^*M)$ can be puled back to the tangent bundle TM by the Legendre transform.

$$\begin{aligned} \Omega &= \mathbf{L}^* \omega \\ &= \mathbf{L}^* (dq_i \wedge p^i) \\ &= dq_i \wedge d(\mathbf{L}^* dp^i) \\ &= dq_i \wedge d \left(\frac{\partial \mathcal{L}}{\partial \dot{q}_i} \right) \end{aligned} \tag{2.85}$$

In the third line of equation 2.85 we have used the fact that the Legendre transform (specifically its pullback in this case) acts on the momenta and not the coordinates, which are essentially passive variables as far as $\mathbf{L}$ is concerned. This is because the Legendre transform is exactly the fiber derivative at a fixed point [15]. Given a smooth $\mathcal{L} : TM \to \mathbb{R}$, the fiber derivative $\mathbb{L}_{\mathcal{L}}$ is a bijective diffeomorphism that maps a fiber in the tangent bundle TM over a point in the base manifold $p \in M$ to a fiber in the cotangent bundle T^*M over the same base point $p \in M$.

For the exterior derivative of $\partial \mathcal{L} / \partial \dot{q}_i$ we have

$$d \left(\frac{\partial \mathcal{L}}{\partial \dot{q}_i} \right) = \frac{\partial^2 \mathcal{L}}{\partial q_j \partial \dot{q}_i} dq_j + W_{ij} d\dot{q}_j \tag{2.86}$$

where

$$W_{ij} = \frac{\partial^2 \mathcal{L}}{\partial \dot{q}_i \partial \dot{q}_j} \tag{2.87}$$

is the Hessian matrix, which is symmetric by the smoothness of $\mathcal{L}$. The pullback of the symplectic form can then be written as

$$\Omega = \frac{\partial^2 \mathcal{L}}{\partial q_j \partial \dot{q}_i} dq_i \wedge dq_j + W_{ij} dq_i \wedge d\dot{q}_j \tag{2.88}$$

We then define the "***Lagrangian Vector Field***" $X_{\mathcal{L}}$ as the unique vector field satisfying

$$i_{X_{\mathcal{L}}} \Omega = dJ \tag{2.89}$$

where J is the Jacobi energy function as defined in equation 2.16. This is in direct analogy of the defining equation for the Hamiltonian vector field. Expanding the Lagrangian vector field in the local coordinates

$$X_{\mathcal{L}} = X_i^q \frac{\partial}{\partial q_i} + X_i^{\dot{q}} \frac{\partial}{\partial \dot{q}_i} \tag{2.90}$$

the interior product on the left hand side of equation 2.140 is

$$\begin{aligned} i_{X_{\mathcal{L}}} \Omega &= \left(\frac{\partial^2 \mathcal{L}}{\partial q_j \partial \dot{q}_i} \left(dq_i \otimes dq_j - dq_j \otimes dq_i \right) + W_{ij} \left(dq_i \otimes d\dot{q}_j - d\dot{q}_j \otimes dq_i \right) \right) (X_{\mathcal{L}}) \\ &= \left(\frac{\partial^2 \mathcal{L}}{\partial q_i \partial \dot{q}_j} X_i^q - \frac{\partial^2 \mathcal{L}}{\partial q_j \partial \dot{q}_i} X_j^q - W_{ij} X_j^{\dot{q}} \right) dq_i + W_{ij} X_j^q d\dot{q}_i \end{aligned} \tag{2.91}$$

The exterior derivative of the Jacobi energy function is

$$\begin{aligned} dJ &= d \left(\dot{q}_j \frac{\partial \mathcal{L}}{\partial \dot{q}_j} - \mathcal{L} \right) \\ &= \left(\dot{q}_j \frac{\partial^2 \mathcal{L}}{\partial q_i \partial \dot{q}_j} - \frac{\partial \mathcal{L}}{\partial q_i} \right) dq_i + \dot{q}_j W_{ij} d\dot{q}_i \end{aligned} \tag{2.92}$$

Equating these two we have

$$X_j^q = \dot{q}_j, \quad W_{ij} X_j^{\dot{q}} = \frac{\partial L}{\partial q_i} - \dot{q}_j \frac{\partial^2 \mathcal{L}}{\partial q_j \partial \dot{q}_i} \tag{2.93}$$

It is clear from equation 2.93 that in order for a unique solution to exist, the Hessian must be non-singular, so that its inverse W_{ij}^{-1} exists. Assuming that this is the case, the Lagrangian vector field is

$$X_{\mathcal{L}} = \dot{q}_j \frac{\partial}{\partial q_j} + W_{ij}^{-1} \left(\frac{\partial L}{\partial q_i} - \dot{q}_j \frac{\partial^2 \mathcal{L}}{\partial q_j \partial \dot{q}_i} \right) \frac{\partial}{\partial \dot{q}_j} \tag{2.94}$$

Integral curves of the Lagrangian vector field satisfy a system of ODE's which are equivalent to the Euler-Lagrange equations as follows. For such an integral curve $(q_i, \dot{q}_i)$ we have

$$\begin{aligned} \frac{d}{dt} q_i &= \dot{q}_i \\ \frac{d}{dt} \dot{q}_i &= W_{ij}^{-1} \left(\frac{\partial L}{\partial q_i} - \dot{q}_j \frac{\partial^2 \mathcal{L}}{\partial q_j \partial \dot{q}_i} \right) \end{aligned} \tag{2.95}$$

The first equation is trivial but the second equation can be manipulated into a form that makes the equivalence to the Euler-Lagrange equations clearer. Multiplying both sides by the Hessian we have

$$\begin{aligned} \dot{q}_j \frac{\partial^2 \mathcal{L}}{\partial q_j \partial \dot{q}_i} + \frac{\partial^2 \mathcal{L}}{\partial \dot{q}_i \partial \dot{q}_j} \ddot{q}_j &= \frac{\partial \mathcal{L}}{\partial q_i} \\ \frac{\partial}{\partial q_j} \left(\frac{\partial \mathcal{L}}{\partial \dot{q}_i} \right) \dot{q}_j + \frac{\partial}{\partial \dot{q}_j} \left(\frac{\partial \mathcal{L}}{\partial \dot{q}_i} \right) \ddot{q}_j &= \frac{\mathcal{L}}{\partial q_i} \end{aligned} \tag{2.96}$$

Recognising that the left hand side of the last line is simply the total time derivative of $\partial \mathcal{L} / \partial \dot{q}_i$, we see that this is simply the Euler-Lagrange equation

$$\frac{d}{dt} \left(\frac{\partial \mathcal{L}}{\partial \dot{q}_i} \right) - \frac{\partial \mathcal{L}}{\partial q_i} = 0 \tag{2.97}$$

2.1.1.3 Contact Geometric Mechanics

In this work we will make heavy use of the machinery of contact manifolds [12, 13, 16, 17]. Contact manifolds are a natural generalisation of a symplectic manifold, to the case where the manifold M is of odd dimension. Specifically, a contact manifold (M, η) is a pair consisting of an odd dimensional manifold M and a non-degenerate 1-form η satisfying $\eta \wedge (d\eta)^n \neq 0$. This definition is in direct analogy with the definition of a contact manifold. Much like how ω^n defines a volume form on (M, ω), $\eta \wedge (d\eta)^n$ defines an odd-dimensional volume form on the contact manifold. In some of the literature, a contact manifold is instead defined in terms of the odd-dimensional manifold M and a contact structure ξ. The contact structure is a maximally non-integrable hyperplane field, which is a sub bundle of the tangent bundle TM such that $\xi \in \ker(\eta)$. The maximal non-integrability condition is precisely that the contact volume form is non-degenerate $\eta \wedge (d\eta)^n \neq 0$. . There exists an equivalent Darboux theorem for contact manifolds [18], stating that we may always find local coordinates in which the contact form may be expressed as

$$\eta = -dS + p^i dq_i \tag{2.98}$$

where we now have an additional global coordinate S on the odd dimensional manifold, as well as q_i and p^i which we will continue to interpret as the generalised coordinates and momenta. Just like symplectic forms, contact forms locally all look the same, and are distinguished by their global structures.

In the symplectic case, every Hamiltonian function $H : M \to \mathbb{R}$ was associated with a unique Hamiltonian vector field generating the Hamiltonian flow on the phase space manifold. Likewise in the contact case, one can define a contact Hamiltonian vector field X_H whose integral curves are the physical paths on the manifold. The contact Hamiltonian vector field is the unique vector field satisfying

$$i_{X_H}\eta = H \tag{2.99}$$

and generates 1-parameter group of diffeomorphisms on the contact manifold, expressed through the Lie derivative

$$\mathcal{L}_{X_H}\eta = f_H\eta \tag{2.100}$$

for some unknown function $f_H \in C^\infty(M)$. Every contact manifold is endowed with a unique Reeb vector field $\mathcal{R} \in \ker(d\eta)$ such that

$$i_{\mathcal{R}}\eta = 1 \tag{2.101}$$

From the definition of the Reeb vector field, and the Darboux theorem on contact manifolds, it's components in the basis of Darboux coordinates can be calculated explicitly as follows. We write the Reeb vector field as

$$\mathcal{R} = R_i^q \frac{\partial}{\partial q_i} + R_i^p \frac{\partial}{\partial p^i} + R^s \frac{\partial}{\partial S} \tag{2.102}$$

The exterior derivative of the contact form is

$$d\eta = dp^i \wedge dq_i = dp^i \otimes dq_i - dq_i \otimes dp^i \tag{2.103}$$

Since $\mathcal{R} \in \ker(d\eta)$, we have $i_{\mathcal{R}} d\eta = 0$ and thus

$$\begin{aligned} dp^i(\mathcal{R})dq_i - dq_i(\mathcal{R})dp^i = 0 \\ R_i^p dq_i - R_i^q dp^i = 0 \end{aligned} \tag{2.104}$$

Which is satisfied if $R_i^q = R_i^p = 0$. From Equation 2.101 we have

$$\begin{aligned} -dS(\mathcal{R}) + p^i dq_i(\mathcal{R}) = 1 \\ -R^s + p^i R_i^q = 1 \end{aligned} \tag{2.105}$$

Since $R_i^q = 0$ we have $R^s = -1$ and the Reeb vector field is

$$\mathcal{R} = -\frac{\partial}{\partial S} \tag{2.106}$$

We know wish to determine the unknown function f_H in equation 2.100. Cartans formula allows us to write the Lie derivative term as

$$\mathcal{L}_{X_H} = i_{X_H} d\eta + d\left(i_{X_H}\eta\right) \tag{2.107}$$

Recalling that the contact Hamiltonian vector field satisfies equation 2.99, we have

$$dH = f_H \eta - i_{X_H} d\eta \tag{2.108}$$

Since $i_{\mathcal{R}}\eta = 1$ and $i_{\mathcal{R}} d\eta = 0$, acting the Reeb vector field on both sides of equation 2.108 yields

$$\begin{aligned} dH(\mathcal{R}) &= f_H \eta(R) - i_{X_H} d\eta(R) \\ dH(\mathcal{R}) &= f_H \implies f_H = -\frac{\partial H}{\partial S} \end{aligned} \tag{2.109}$$

Now that the Reeb vector field and f_H have been identified, we are left with two equations defining the contact Hamiltonian vector field

$$i_{X_H}\eta = H, \quad dH = -\frac{\partial H}{\partial S}\eta - i_{X_H} d\eta \tag{2.110}$$

Expanding the contact Hamiltonian vector field X_H in the basis of Darboux coordinates

$$X_H = X_i^q \frac{\partial}{\partial q_i} + X_i^p \frac{\partial}{\partial p^i} + X^s \frac{\partial}{\partial S} \tag{2.111}$$

the defining conditions 2.110 reduce to

$$-X^s + p^i X_i^q = H, \quad \frac{\partial H}{\partial q_i} dq_i + \frac{\partial H}{\partial p^i} dp^i + \frac{\partial H}{\partial S} dS = \left(-X_i^p - p^i \frac{\partial H}{\partial S}\right) dq_i + X_i^q dp^i \tag{2.112}$$

Equation 2.112 fixes the components X_H in the Darboux basis, giving

$$X_i^q = \frac{\partial H}{\partial p^i}, \quad X_i^p = -\frac{\partial H}{\partial q_i} - p^i \frac{\partial H}{\partial S}, \quad X^s = p^i \frac{\partial H}{\partial p^i} - H \tag{2.113}$$

The integral curves of the contact Hamiltonian vector field satisfy the equations of motion

$$\dot{q}_i = \frac{\partial H}{\partial p^i}, \quad \dot{p}^i = \quad X_i^p = -\frac{\partial H}{\partial q_i} - p^i \frac{\partial H}{\partial S}, \quad \dot{S} = p^i \frac{\partial H}{\partial p^i} - H \tag{2.114}$$

One can immediately see that when the contact Hamiltonian is independent of the global coordinate S, the equations of motion for (q_i, p^i) reduce to that of a symplectic Hamiltonian system. Time evolution of smooth functions on the contact manifold $F \in C^\infty(M)$ is again generated by the flow of the (contact) Hamiltonain vector field

$$\begin{aligned} \frac{dF}{dt} &= \frac{\partial F}{\partial q_i}\dot{q}_i + \frac{\partial F}{\partial \dot{p}^i}\dot{p}^j + \frac{\partial F}{\partial S}\dot{S} \\ &= X_H(F) \end{aligned} \tag{2.115}$$

Unlike in the symplectic case, the contact Hamiltonian is not generally conserved along its flow.

$$\frac{dH}{dt} = X_H(H) = -H\frac{\partial H}{\partial S} \tag{2.116}$$

From equation 2.116, we can see that the Hamiltonian will only be conserved if it is independent of the global bundle coordinate S or everywhere zero. Consequently, contact Hamiltonian mechanics are a popular choice when modelling non-conservative systems, particularly in classical and quantum thermodynamics [19–23]. Since the contact Hamiltonian is no longer generically conserved, one might expect that Liouvilles theorem does not hold on a contact manifold, and this is indeed the case. We have shown already that the Lie drag of the contact form along the Hamiltonian vector field is

$$\mathcal{L}_{X_H}\eta = -\frac{\partial H}{\partial S}\eta \tag{2.117}$$

It follows from this result that the Lie drag of the volume form $d\text{Vol} = \eta \wedge (d\eta)^n$ is [24]

$$\mathcal{L}_{X_H} d\text{Vol} = -(n+1)\frac{\partial H}{\partial S} d\text{Vol} \tag{2.118}$$

In [24] it shown that there does in fact exist and invariant measure on contact manifolds

$$d\mu = |H|^{-(n+1)} d\text{Vol} \tag{2.119}$$

for which there is a direct analogy of the Liouville theorem

$$\mathcal{L}_{X_H} d\mu = 0 \tag{2.120}$$

As an example of a simple classical system on a contact manifold, consider the damped harmonic oscillator. Let $T^*M \times \mathbb{R}$ be a contact manifold with coordinates (q, p, S) and contact form $\eta = -dS + pdq$. Let the contact Hamiltonian function be

$$H = \frac{p^2}{2m} + \frac{1}{2} m\omega^2 q^2 + \gamma S \tag{2.121}$$

The contact Hamiltonian equations of motion 2.114 for this system read

$$\dot{q} = \frac{p}{m}, \quad \dot{p} = -m\omega^2 q - p\gamma, \quad \dot{S} = \frac{p^2}{2m} - \frac{1}{2} m\omega^2 q^2 - \gamma S \tag{2.122}$$

From which we have

$$\begin{aligned} \ddot{q} &= \frac{\dot{p}}{m} \\ &= -\omega^2 q - \frac{p}{m}\gamma \\ &= -\omega^2 q - \gamma \dot{q} \end{aligned} \tag{2.123}$$

Which is simply the familiar equation of motion of a damped oscillator

$$\ddot{q} + \gamma \dot{q} + \omega^2 q = 0 \tag{2.124}$$

On close inspection, one might see that the equation for the global coordinate

S looks similar to a kinetic term minus a sort of potential term, which we may be tempted to identify as a Lagrange of sorts. In fact we shall see that this is exactly the contact equivalent of the Lagrangian function, known as the "***Herglotz Lagrangian***". Consider an odd dimensional manifold $TM \times \mathbb{R}$ formed from the cross product of the tangent bundle TM of a configuration space manifold M and the reals. Let $(q_i, \dot{q}_i, S)$ be the local coordinates on the manifold, where $(q_i, \dot{q}_i)$ are the coordinates of the cotangent bundle. The tangent bundle comes equipped with a natural canonical endomorphism [11,16] $E : TM \to TM$, which may be expressed in the local coordinates as

$$E = dq_i \otimes \frac{\partial}{\partial \dot{q}_i} \tag{2.125}$$

Let $L : TM \times \mathbb{R}$ be a Lagrangian function on the manifold. The pullback of the canonical endomorphism allows us to construct a contact form on the manifold.

$$\begin{aligned} \eta &= -dS + E^*(dL) \\ &= -dS + \frac{\partial L}{\partial \dot{q}_i} dq_i \end{aligned} \tag{2.126}$$

If the Lagrangian as a regular Hessian matrix, the volume form constructed from η is non-degenerate $\eta \wedge (d\eta)^n \neq 0$ and thus we have a contact manifold (M, η). As we have already discussed, associated with the contact manifold is a unique Reeb vector field satisfying

$$i_{\mathcal{R}} d\eta = 0, \quad i_{\mathcal{R}} \eta = 1 \tag{2.127}$$

Expanding the Reeb vector field in the basis of Darboux coordinates

$$\mathcal{R} = R_i^q \frac{\partial}{\partial q_i} + R^{\dot{q}} \frac{\partial}{\partial \dot{q}_i} \frac{\partial}{\partial \dot{q}_i} + R^s \frac{\partial}{\partial S} \tag{2.128}$$

The first condition $i_{\mathcal{R}} d\eta = 0$ reads

$$\begin{aligned} i_{\mathcal{R}} d\eta &= i_{\mathcal{R}} \left[d\left(\frac{\partial L}{\partial \dot{q}_i}\right) \wedge dq_i \right] \\ &= i_{\mathcal{R}} \left[\left(\frac{\partial}{\partial q_j}\left(\frac{\partial L}{\partial \dot{q}_i}\right) dq_j + \frac{\partial}{\partial \dot{q}_j}\left(\frac{\partial L}{\partial \dot{q}_i}\right) d\dot{q}_j + \frac{\partial}{\partial S}\left(\frac{\partial L}{\partial \dot{q}_i}\right) dS \right) \wedge dq_i \right] \\ &= i_{\mathcal{R}} \left[\frac{\partial^2 L}{\partial q_j \partial \dot{q}_j} dq_j \wedge dq_i + W_{ij} d\dot{q}_j \wedge dq_i + \frac{\partial^2 L}{\partial S \partial \dot{q}_i} ds \wedge dq_i \right] \\ &= \left[R^q_j \left(\frac{\partial^2 L}{\partial q_j \partial \dot{q}_i} - \frac{\partial^2 L}{\partial q_i \partial \dot{q}_j} \right) + R^{\dot{q}}_j W_{ij} + R^s \frac{\partial^2 L}{\partial S \partial \dot{q}_i} \right] dq_i - R^q_j W_{ij} d\dot{q}_i - R^q_i \frac{\partial^2 L}{\partial S \partial \dot{q}_i} dS \\ &= 0 \end{aligned} \tag{2.129}$$

For this condition to hold for a generic Lagrangian $L(q_i, \dot{q}_i, S)$ we must have

$$R^q_i = 0, \quad R^{\dot{q}}_i = -W^{ij} \frac{\partial^2 L}{\partial S \partial \dot{q}_j} R^s \tag{2.130}$$

where W^{ij} is the inverse Hessian, which we have assumed to be regular. This eliminates the R^q_i component, which is zero, the second condition $i_{\mathcal{R}} \eta = 1$ is required to full constrain the $R^{\dot{q}}$ and R^s components.

$$\begin{aligned} i_{\mathcal{R}} \eta &= -dS(\mathcal{R}) + \frac{\partial L}{\partial \dot{q}_i} dq_i(\mathcal{R}) \\ &= -R^s \\ &= 1 \end{aligned} \tag{2.131}$$

We therefore have $R^s = -1$ and hence the Reeb vector field in the local Darboux coordinates is

$$\mathcal{R} = -\frac{\partial}{\partial S} + W^{ij} \frac{\partial^2 L}{\partial \dot{q}_j \partial S} \frac{\partial}{\partial \dot{q}_i} \tag{2.132}$$

We now define the Herglotz Lagrangian vector field X_L to be the unique solution of

$$I(X_L) = dJ + (J - \mathcal{R}(J))\, \eta \tag{2.133}$$

where J is the Jacobi energy function as defined in equation 2.16 and $I : T(TM \times$

$\mathbb{R}) \to T^*(TM \times \mathbb{R})$ is a bundle isomorphism associated with the contact form

$$I(v) = (i_v\eta)\eta - i_v(d\eta) \tag{2.134}$$

Expanding the Herglotz Lagrangian vector field in the basis of Darboux coordinates we have

$$X_L = X_i^q \frac{\partial}{\partial q_i} + X_i^{\dot{q}} \frac{\partial}{\partial \dot{q}_i} + X^s \frac{\partial}{\partial S} \tag{2.135}$$

The bundle isomorphism in terms of the components of X_L can then be calculated as

$$\begin{aligned} I(X_L) = &\left[\frac{\partial L}{\partial \dot{q}_i}\left(-X^s + X_j^q \frac{\partial L}{\partial \dot{q}_j}\right) + X_j^q \frac{\partial^2 L}{\partial q_i \partial \dot{q}_j} - X_j^q \frac{\partial^2 L}{\partial q_j \partial \dot{q}_i} - X_j^{\dot{q}} W_{ij} - X^s \frac{\partial^2 L}{\partial S \partial \dot{q}_i}\right] dq_i \\ &+ X_j^q W_{ij} d\dot{q}_i + \left[X^s - X_i^q \frac{\partial L}{\partial \dot{q}_i} + X_i^q \frac{\partial^2 L}{\partial S \partial \dot{q}_i}\right] dS \end{aligned} \tag{2.136}$$

We next need to calculate the left hand side of equation 2.133. Recall that the Jacobi energy function is

$$J(q_i, \dot{q}_i, S) = \dot{q}_i \frac{\partial L}{\partial \dot{q}_i} - L \tag{2.137}$$

and so we have the exterior derivative

$$\begin{aligned} dJ &= \frac{\partial L}{\partial \dot{q}_i} d\dot{q}_i + \dot{q}_j d\left(\frac{\partial L}{\partial \dot{q}_j}\right) - dL \\ &= \left[\dot{q}_j \frac{\partial^2 L}{\partial q_i \partial \dot{q}_j} - \frac{\partial L}{\partial q_i}\right] dq_i + \dot{q}_j W_{ij} d\dot{q}_i + \left[\dot{q}_i \frac{\partial^2 L}{\partial S \partial \dot{q}_i} - \frac{\partial L}{\partial S}\right] dS \end{aligned} \tag{2.138}$$

Given the Reeb vector field in equation 2.132, we have

$$\begin{aligned} \mathcal{R}(J) &= -\frac{\partial J}{\partial S} + W^{ij} \frac{\partial^2 L}{\partial S \partial \dot{q}_j} \frac{\partial J}{\partial \dot{q}_i} \\ &= -\left[\dot{q}_i \frac{\partial^2 L}{\partial S \partial \dot{q}_i} - \frac{\partial L}{\partial S}\right] + W^{ij} \frac{\partial^2 L}{\partial S \partial \dot{q}_j} \left(\delta_k^i \frac{\partial L}{\partial \dot{q}_k} + \dot{q}_k W_{ik} - \frac{\partial L}{\partial \dot{q}_i}\right) \\ &= \frac{\partial L}{\partial S} \end{aligned} \tag{2.139}$$

Combining the results of equations 2.137, 2.138 and 2.139, the right hand side of equation 2.133 is

$$dJ + (J - R(J))\,\eta = \left[\dot{q}_j \frac{\partial^2 L}{\partial q_i \partial \dot{q}_j} - \frac{\partial L}{\partial q_i} + \dot{q}_j \frac{\partial L}{\partial \dot{q}_i}\frac{\partial L}{\dot{q}_j} - L\frac{\partial L}{\partial \dot{q}_i} - \frac{\partial L}{\partial \dot{q}_i}\frac{\partial L}{\partial S}\right] dq_i + \dot{q}_j W_{ij} d\dot{q}_i + \left[\dot{q}_i \frac{\partial^2 L}{\partial S \partial \dot{q}_i} - \dot{q}_i \frac{\partial L}{\partial \dot{q}_i} + L\right] dS \tag{2.140}$$

Equation 2.140 can now be equated with the calculation of the bundle isomorphism in terms of the components of X_L in equation 2.136. By inspecting the coefficients of dq_i, $d\dot{q}_i$ and dS the components of X_L can be determined. Firstly from the $d\dot{q}_i$ terms on both sides, we see that we must have

$$X_i^q = \dot{q}_i \tag{2.141}$$

Next, by inspecting the dS terms on both sides, we must have

$$\begin{aligned} X^s - \dot{q}_i \frac{\partial L}{\partial \dot{q}_i} + \dot{q}_i \frac{\partial^2 L}{\partial S \partial \dot{q}_i} &= \dot{q}_i \frac{\partial^2 L}{\partial S \partial \dot{q}_i} - \dot{q}_i \frac{\partial L}{\partial \dot{q}_i} + L \\ \implies X^s &= L \end{aligned} \tag{2.142}$$

Finally by inspecting the dq_i terms on both sides, we must have

$$X_j^{\dot{q}} W_{ij} = \frac{\partial L}{\partial q_i} + \frac{\partial L}{\partial \dot{q}_i}\frac{\partial L}{\partial S} - \dot{q}_j \frac{\partial^2 L}{\partial q_j \partial \dot{q}_i} - L\frac{\partial^2 L}{\partial S \partial \dot{q}_i} \tag{2.143}$$

It is clear from equation 2.143 why the Lagrangian must have a regular Hessian, we require the inverse of W_{ij} to exist in order for our system of equations to be solvable. Assuming that the Hessian is indeed regular, the flow generated by X_L satisfied

$$\dot{q}_i - \dot{q}_i, \quad \ddot{q}_j W_{ij} = \frac{\partial L}{\partial q_i} + \frac{\partial L}{\partial \dot{q}_i}\frac{\partial L}{\partial S} - \dot{q}_j \frac{\partial^2 L}{\partial q_j \partial \dot{q}_i} - L\frac{\partial^2 L}{\partial S \partial \dot{q}_i}, \quad \dot{S} = L \tag{2.144}$$

The first equation in 2.144 is the trivial relation $\dot{q}_i = \dot{q}_i$, the third relation is telling us that in contact Lagrangian systems, the Lagrangian is actually a function of the action itself

$$S = \int L(q_i, \dot{q}_i, S)dt \tag{2.145}$$

The contact Lagrangian is typically referred to in the literature as the Herglotz Lagrangian as we have mentioned. The second equation in 2.144 encodes the Herglotz-Lagrange equations of motion, which are a generalisation of the Euler-Lagrange equations to a contact manifold. They are derived from the second equation as follows. Consider the total time derivative

$$\begin{aligned} \frac{d}{dt}\left(\frac{\partial L}{\partial \dot{q}_i}\right) &= \frac{\partial^2 L}{\partial q_j \partial \dot{q}_i}\dot{q}_j + \frac{\partial^2 L}{\partial \dot{q}_j \partial \dot{q}_i}\ddot{q}_j + \frac{\partial^2 L}{\partial S \partial \dot{q}_i}\dot{S} \\ &= \frac{\partial^2 L}{\partial q_j \partial \dot{q}_i}\dot{q}_j + W_{ij}\ddot{q}_j + \frac{\partial^2 L}{\partial q_j \partial \dot{q}_i}L \\ \implies W_{ij}\ddot{q}_j &= \frac{d}{dt}\left(\frac{\partial L}{\partial \dot{q}_i}\right) - \frac{\partial^2 L}{\partial q_j \partial \dot{q}_i}\dot{q}_j - \frac{\partial^2 L}{\partial q_j \partial \dot{q}_i}L \end{aligned} \tag{2.146}$$

Equating this to the second equation in 2.144 we have

$$\frac{d}{dt}\left(\frac{\partial L}{\partial \dot{q}_i}\right) - \frac{\partial L}{\partial q_i} = \frac{\partial L}{\partial \dot{q}_i}\frac{\partial L}{\partial S} \tag{2.147}$$

These are the "***Herglotz-Lagrange equations of motion***". One can see that in the case where the Lagrangian is independent of the global coordinate S, they reduce to the standard Euler-Lagrange equations for $(q_i, \dot{q}_i)$. The integral curves of the Herglotz Lagrangian vector field satisfy the Herglotz-Lagrange equations if and only if they are critical paths of the action 2.145. A detailed discussion of the variational approach to the Herglotz-Lagrange equations can be found in [25], as well as an alternative that approach using Lagrange multipliers to enforce $\dot{S} = L$ in [26].

It now remains to show that the Herglotz-Lagrange equations are equivalent to the contact Hamiltonian equations under a Legendre transform. Given a contact

form $\eta = -dS + p^i dq_i$ on $T^*M \times \mathbb{R}$ and a Legendre transform $\mathbf{L} : TM \times \mathbb{R} \to T^*M \times \mathbb{R}$ such that

$$\mathbf{L}(q_i, \dot{q}_i, S) = (q_i, p^i, S), \quad p^i = \frac{\partial L}{\partial \dot{q}_i} \tag{2.148}$$

The pullback of the contact form by the Legendre transform is exactly

$$\mathbf{L}^*(\eta) = -dS + \frac{\partial L}{\partial \dot{q}_i} dq_i \tag{2.149}$$

which is the contact form on $TM \times \mathbb{R}$ which generates the Herglotz-Lagrange equations.

2.2 General Relativity

2.2.1 Lagrangian Field Theory of General Relativity

Einsteins theory of General Relativity [27–30], which is to date our most comprehensive and well tested theory of gravity, is built in the language of differential geometry. Einsteins key insights that allowed the development of this theory were his "***Equivalence Principle"*** and general covariance. These two concepts are often misconceived as the same, but there is an important distinction which allowed Einstein to construct a mathematical description of gravity as the curvature of spacetime. Firstly, general covariance is the statement that physical laws should be independent of any coordinate frame. Fundamentally, a set of coordinates is an entirely human construct and thus a physical, axiomatic law need no reference to them at all. Newtons laws of motion have covariance under the Galilean group, one may transform to any inertial frame of reference and the equations of motion will take the same form. This is not the case if one transforms to an accelerating frame of reference, thus Einstein knew that Newtons laws of motion could only be an approximation of a higher order theory in which one may make any coordinate transformation and retain general covariance.

The equivalence Principle, not to be confused with general covariance, was Einsteins insight that, in small enough regions of spacetime, one cannot distinguish through any experimental means between an accelerating frame of reference and the effect of a gravitational field in an inert frame. This means that at any given point of spacetime, we may always choose locally inertial coordinates provided we look at a sufficiently small region around the point. Over small regions, observers see spacetime has having a local Minkowski structure, but the global structure of spacetime may be very different. In particular, while the local Minkowski structure may be flat, the spacetime globally may be curved. The mathematical formalism that describes such structures is the differential geometry of manifolds.

In General Relativity, spacetime is assumed to be a 4-dimensional Lorentzian manifold $\mathcal{M}$ equipped with a non-degenerate metric g. We demand that the connection on the manifold Γ be metric compatible

$$\nabla_\sigma g_{\mu\nu} = 0 \tag{2.150}$$

and torsion free

$$T^\rho_{\mu\nu} := \Gamma^\rho_{\mu\nu} - \Gamma^\rho_{\nu\mu} - C^\rho_{\mu\nu} = 0 \tag{2.151}$$

where $C^\rho_{\mu\nu}$ are the commutation coefficients of the basis vectors $[\hat{e}_\mu, \hat{e}_\nu] = C^\rho_{\mu\nu}\hat{e}_\rho$ (which are vanishing for a coordinate basis $\hat{e}_\mu = \partial_\mu$). The unique connection satisfying conditions 2.150 & 2.151 is the Levi-Civita connection, with connection coefficients

$$\Gamma^\rho_{\mu\nu} = \frac{1}{2} g^{\rho\sigma} \left(\partial_\mu g_{\nu\sigma} + \partial_\nu g_{\mu\sigma} - \partial_\sigma g_{\mu\nu} \right) \tag{2.152}$$

With this specification the connection is not independent from the metric, in fact it is completely determined by it. Thus in order to determine the intrinsic curvature of the manifold topology, one needs only specify a metric $g_{\mu\nu}$. Test particles will then move on geodesics determined by this metric at each point.

General Relativity as such can be considered as a field theory of the metric, in which the goal is, given a spacetime with some particular matter components, how do we determine the metric and the motion of that matter?

Since the metric $g_{\mu\nu}$ is the dynamical variable of General Relativity, we seek equations of motion that tell us how the metric changes from point to point across the manifold in response to it's matter content, and how the matter moves in response to the geometry of the manifold determined by the metric. The Einstein Field equations are usually introduced in the context of Lagrangian mechanics, making use of the principle of stationary action discussed in section 2.1.1.2. In order to make use of such a principle, one first needs to determine an appropriate scalar Lagrangian, that is a function of the metric and it's derivatives. There is indeed a subtlety here that we should be aware of. In section 2.1.1 we studied Lagrangains that were functions of the degrees of freedom on the tangent bundle $(q_i, \dot{q}_i)$. In that context we are working with a particle theory, where there are a finite number of degrees of freedom. General Relativity is a field theory, where we are concerned with the dynamics of a field which is as function of the degrees of freedom on the tangent bundle and is defined at every point $p \in TM$. In total there is an uncountably infinite number of degrees of freedom, but a finite number per point. Thankfully the variational principle is still well-defined for field theories and there is a natural generalisation of the Euler-Lagrange equations for field theories. In this section we are only concerned with the field theory of the metric so we will derives its equation of motion by considering its variation explicitly.

The action that produces the Einstein Field Equations (EFEs) in a vacuum is the Einstein-Hilbert action

$$S = \int d^4x\sqrt{-g}\, R \tag{2.153}$$

When considering the possible actions we could construct, one must consider the fact that at in a neighbourhood of any point $p \in \mathcal{M}$, we may construct a locally inertial set of coordinates x^a in which the metric takes it's canonical form $g_{ab} = \eta_{ab}$

where η is the Minkowski metric. In particular, these coordinates are the Riemann normal coordinates at p [27,30]. The Riemann normal coordinates at p are provided through the exponential map

$$\exp_p : T_pM \to M \tag{2.154}$$

which associates a vector $k \in T_pM$ with the point $\gamma(1) \in M$ where $\gamma(\lambda)$ is the unique geodesic satisfying $\gamma(0) = p$ and $\gamma'(0) = k$. For a sufficiently small neighbourhood of p, the exponential map exists and is one-to-one [31]. The exponential map thus defines a set of coordinates

$$\exp_p(k) = x^\mu(\lambda = 1) \tag{2.155}$$

where $x^\mu(\lambda)$ is the unique solution to the geodesic equation with tangent vector k^μ at $\lambda = 0$. In the Riemann normal coordinates, the connection coefficients at p are zero, and thus metric compatibility implies the first derivatives of the metric are zero at p in the Riemann normal coordinates.

$$\nabla_\sigma g_{\mu\nu} = 0 \implies \partial_\sigma g_{\mu\nu}(p) = 0 \tag{2.156}$$

Thus for any Lagrangian to produce dynamics of the metric, it must be constructed from at terms at least second order in the metric and it's derivatives. The Riemann tensor $R_{\mu\nu\sigma\rho}$ plays an important role in this consideration, as it is the only linear, non-trivial tensor that can be constructed from the metric and it's derivatives up to second order [32]. Thus the Ricci scalar, is the only independent choice for a scalar constructed from, at most second order derivatives of the metric.

Let us now return to the Einstein-Hilbert action, and show that variation with respect to the metric produces the correct vacuum field equations of General

Relativity. We start with the proposed Einstein-Hilbert action

$$S = \int d^4x\sqrt{-g}R \tag{2.157}$$

and consider its variation with respect to the metric. In particular, it is convenient to vary with respect to the inverse metric components $g^{\mu\nu}$, so that when the functional derivative $\delta S[g]/\delta g^{\mu\nu}$ is set equal to zero the resulting equation of motion is in terms of the metric tensor components $g_{\mu\nu}$.

$$\begin{aligned}\delta S &= \int d^4x\,\delta\left(\sqrt{-g}R\right) \\ &= \int d^4x\,\delta(\sqrt{-g})R + \sqrt{-g}\delta R\end{aligned} \tag{2.158}$$

Considering first the variation of the metric determinant term

$$\delta S_1 = \int d^4x\,\delta(\sqrt{-g})R = -\int d^4x\,\frac{1}{2\sqrt{-g}}\delta g R \tag{2.159}$$

the variation of the metric determinant δg with respect to the components $\delta^{\mu\nu}$ can be obtained by first considering Jacobi's formula [33] which states the following.

Let $A(t)$ be a differentiable and invertible map from the reals to the space of $n \times n$ matrices $A(t) : \mathbb{R} \to \mathbb{R}^{n\times n}$ then the following holds

(2.160)

$$\frac{d}{dt}\text{Det } A(t) = (\text{Det } A(t))\,\text{Tr}\left(A^{-1}(t)\frac{d}{dt}A(t)\right) \tag{2.161}$$

We may then define a curve through $\mathbb{R}^{n\times n}$ by fixing a $n \times n$ matrix B and defining the map $A(t) = e^{tB}$. Thus by eq. 2.161 we have

$$\begin{aligned}\frac{d}{dt}\left[\text{Det } e^{tB}\right] &= \left[\text{Det } e^{tB}\right]\text{Tr}\left(e^{-tB}\frac{d}{dt}\left(e^{tB}\right)\right) \\ &= \left[\text{Det } e^{tB}\right]\text{Tr}\left(e^{-tB}e^{t^B}B\right) \\ &= \left[\text{Det } e^{tB}\right]\text{Tr}B\end{aligned} \tag{2.162}$$

Since B is a fixed matrix, eq. 2.162 can be viewed as differential equation on the reals of the function $f(t) = \text{Det } e^{tB}$

$$\frac{d}{dt} f(t) = (\text{Tr} B)\, f(t) \tag{2.163}$$

with the solution $f(t) := \text{Det } e^{tB} = e^{t\text{Tr}B}$. Letting the parameter $t = 1$ we have

$$\text{Det } e^{B} = e^{\text{Tr}B} \tag{2.164}$$

Equation 2.164 can be used to find the variation in the metric determinant, if we define the matrix $M = e^B$ we have

$$\ln\left[\text{Det } M\right] = \text{Tr} \ln M \tag{2.165}$$

Taking the matrix M to be the metric $g_{\mu\nu}$, we have the infinitesimal variation of both sides

$$\frac{1}{g}\delta g = g^{\mu\nu}\delta g_{\mu\nu} \implies \delta g = g g^{\mu\nu}\delta g_{\mu\nu} \tag{2.166}$$

In eq. 2.166 the variation is with respect to the metric components $\delta g_{\mu\nu}$. This can be swapped to a variation with respect to the inverse components simply by considering that $\delta(g^{\mu\nu} g_{\mu\nu}) = 0$ and thus $g^{\mu\nu}\delta g_{\mu\nu} = -g_{\mu\nu}\delta g^{\mu\nu}$. Therefore we have the final variation of the metric determinant with respect to the components of the inverse metric

$$\delta g = -g g_{\mu\nu}\delta g^{\mu\nu} \tag{2.167}$$

We may plug this back into the variation of the action 2.159 & 2.158 to obtain

$$\delta S = -\int d^4x \, \frac{1}{2}\sqrt{-g} g_{\mu\nu}\delta g^{\mu\nu} R + \int d^4x \, \sqrt{-g}\delta R \tag{2.168}$$

The Ricci curvature scalar R is the contraction of the metric tensor and Ricci curvature tensor $R = g^{\mu\nu} R_{\mu\nu}$, and thus the variation δR with respect to the inverse

metric components is simply $\delta R = R_{\mu\nu}\delta g^{\mu\nu} + g^{\mu\nu}\delta R_{\mu\nu}$. Thus eq 2.168 becomes

$$\delta S = \int d^4x \sqrt{-g} \left(R_{\mu\nu} - \frac{1}{2} R g_{\mu\nu} \right) \delta g^{\mu\nu} + \int d^4x \sqrt{-g} g^{\mu\nu} \delta R_{\mu\nu} \tag{2.169}$$

We now need only consider the final term in eq. 2.169

$$\delta S_2 = \int d^4x \sqrt{-g} g^{\mu\nu} \delta R_{\mu\nu} \tag{2.170}$$

The Ricci curvature tensor is the non-metric contraction of the Riemann curvature tensor with it's first and third indices $R_{\mu\nu} = R^{\rho}_{\mu\rho\nu}$, with the Riemann tensor given in terms of the Levi-Civita connection coefficients as

$$R^{\rho}_{\mu\sigma\nu} = \partial_\sigma \Gamma^{\rho}_{\nu\mu} + \Gamma^{\rho}_{\sigma\lambda}\Gamma^{\lambda}_{\nu\mu} - \partial_\nu \Gamma^{\rho}_{\sigma\mu} - \Gamma^{\rho}_{\nu\lambda}\Gamma^{\lambda}_{\sigma\mu} \tag{2.171}$$

Thus the first order infinitesimal variation of the Riemann tensor with respect to the Levi-Civita connection coefficients (which are functions of the metric g_{mu}) is

$$\delta R^{\rho}_{\mu\sigma\nu} = \partial_\sigma \delta\Gamma^{\rho}_{\nu\mu} + \Gamma^{\rho}_{\sigma\lambda}\delta\Gamma^{\lambda}_{\nu\mu} + \delta\Gamma^{\rho}_{\sigma\lambda}\Gamma^{\lambda}_{\nu\mu} - \partial_\nu \delta\Gamma^{\rho}_{\sigma\mu} - \Gamma^{\rho}_{\nu\lambda}\delta\Gamma^{\lambda}_{\sigma\mu} - \delta\Gamma^{\rho}_{\nu\lambda}\Gamma^{\lambda}_{\sigma\mu} \tag{2.172}$$

We will now write the variation of the Riemann tensor 2.173 in terms of covariant derivatives by considering that the infinitesimal variation of the Levi-Civita connection $\delta\Gamma(g_{\mu\nu})$ is in fact the difference between two different connections

$$\delta\Gamma(g_{\mu\nu}) = \Gamma(g_{\mu\nu} + \delta g_{\mu\nu}) - \Gamma(g_{\mu\nu}) \tag{2.173}$$

Therefore it is a tensor in its own right as it defines a multilinear map from the space of differential forms and vector field on the manifold $\mathcal{M}$ to the reals [11]. As such, we may take its covariant derivative with respect to $\Gamma(g_{\mu\nu})$

$$\nabla_\sigma \delta\Gamma^{\rho}_{\mu\nu} = \partial_\sigma \delta\Gamma^{\rho}_{\mu\nu} + \Gamma^{\rho}_{\sigma\lambda}\delta\Gamma^{\lambda}_{\mu\nu} - \Gamma^{\lambda}_{\sigma\mu}\delta\Gamma^{\rho}_{\lambda\nu} - \Gamma^{\lambda}_{\sigma\nu}\delta\Gamma^{\rho}_{\mu\lambda} \tag{2.174}$$

from which it is clear that we may write eq 2.173 as

$$\delta R^{\rho}_{\mu\sigma\nu} = \nabla_{\sigma}\delta\Gamma^{\rho}_{\nu\mu} - \nabla_{\nu}\delta\Gamma^{\rho}_{\sigma\mu} \tag{2.175}$$

Thus the infinitesimal variation of the Ricci tensor can also be written in terms of covariant derivatives as it is simply the non-metric contraction of the Riemann tensor over the indices ρ and σ

$$\delta R_{\mu\nu} = \nabla_{\rho}\delta\Gamma^{\rho}_{\nu\mu} - \nabla_{\nu}\delta\Gamma^{\rho}_{\rho\mu} \tag{2.176}$$

Finally, we may use this to show that the second term in the variation of the action eq 2.170 is simply a boundary term. Substituting in eq 2.176 we have

$$\begin{aligned}
\delta S_2 &= \int d^4x\sqrt{-g}\, g^{\mu\nu}\delta R_{\mu\nu} \\
&= \int d^4x\sqrt{-g}\, g^{\mu\nu}\left(\nabla_{\rho}\delta\Gamma^{\rho}_{\nu\mu} - \nabla_{\nu}\delta\Gamma^{\rho}_{\rho\mu}\right) \\
&= \int d^4x\sqrt{-g}\, \nabla_{\rho}\left(g^{\mu\nu}\delta\Gamma^{\rho}_{\nu\mu} - g^{\mu\rho}\delta\Gamma^{\sigma}_{\sigma\mu}\right)
\end{aligned} \tag{2.177}$$

where in the final equality we have used metric compatibility of the Levi-Civita connection as well as relabelled dummy indices. In many cases, specifically those where the manifold is compact and without boundary, i.e. closed, one can argue that this final term is zero since by Stokes theorem it is the term inside the bracket evaluated at infinity where we requite the variations in the metric to be zero. This will be the case for all manifolds considered in this work but it is worth mentioning an important subtlety. In the case that the manifold $\mathcal{M}$ has a boundary ∂M, this boundary term cannot be so easily ignored. If the manifold has a boundary, applying stokes theorem to eq 2.177 results in terms proportional to the derivatives of the first order variations of the metric on the boundary, which are not in general zero. Thus a correction term must be added to the Einstein-Hilbert action 2.157 in order to cancel these derivative terms, so that the condition $\delta g_{\mu\nu}|_{\partial\mathcal{M}} = 0$ is sufficient for the variational principle to be well defined.

This term is the Gibbons-Hawking-York (GHY) term [34–36]

$$S_{\text{GHY}} = 2\int_{\partial\mathcal{M}} K \tag{2.178}$$

where K is the trace of the extrinsic curvature on the boundary. Some contexts where the GHY term becomes particularly relevant are path integral approaches to quantum gravity, black hole entropy and transition amplitudes in Loop Quantum Gravity [37–39]

As we are considering only contexts where the spacetime manifold is compact, the variational term 2.177 can be set equal to zero and we arrive at the final infinitesimal variation of the action with respect to $\delta g^{\mu\nu}$.

$$\delta S = \int d^4x \sqrt{-g}\left(R_{\mu\nu} - \frac{1}{2}Rg_{\mu\nu}\right)\delta g^{\mu\nu} \tag{2.179}$$

The metric is assumed to be non-degenerate $g \neq 0$, so for the infinitesimal variation of the action to be zero for arbitrary infinitesimal variations of the (inverse) metric $\delta g^{\mu\nu}$, we arrive at the vacuum Einstein Field Equations

$$R_{\mu\nu} - \frac{1}{2}Rg_{\mu\nu} = 0 \tag{2.180}$$

$G_{\mu\nu} = R_{\mu\nu} - Rg_{\mu\nu}/2$ is referred to as the Einstein tensor,as such the vacuum EFE's read simply

$$G_{\mu\nu} = 0 \tag{2.181}$$

The Einstein tensor is a (0,2)-tensor on the 4-dimensional spacetime manifold $\mathcal{M}$, and thus has 16 components. The EFE's define a set of partial differential equations in the metric, one for each of it's components. However not all of these components are independent. by symmetry of the Einstein tensor $G_{\mu\nu} = G_{\nu\mu}$, there are actually 6 dependant equations.

One may use the Bianchi identity of the Riemann tensor

$$\nabla_\lambda R_{\mu\nu\rho\sigma} + \nabla_\rho R_{\mu\nu\sigma\lambda} + \nabla_\sigma R_{\mu\nu\lambda\rho} = 0 \tag{2.182}$$

to determine that the divergence of the Einstein tensor is everywhere zero as follows. Contracting the Bianchi identity with $g^{\mu\rho}$ and using metric compatibility gives

$$\nabla_\lambda R_{\nu\sigma} + \nabla^\mu R_{\mu\nu\sigma\lambda} + \nabla_\sigma R^\rho_{\nu\lambda\rho} = 0 \tag{2.183}$$

The Riemann tensor is antisymmetric in first two and last two indices $R_{\mu\nu\rho\sigma} = -R_{\nu\mu\rho\sigma} = -R_{\mu\nu\sigma\rho}$. Using antisymmetry in the last two indices eq. 2.183 becomes

$$\nabla_\lambda R_{\nu\sigma} + \nabla^\mu R_{\mu\nu\sigma\lambda} - \nabla_\sigma R_{\nu\lambda} = 0 \tag{2.184}$$

Contracting once more with $g^{\nu\sigma}$ and using antisymmetry if the Riemann tensor in its first two indices yields

$$\nabla^\mu \left(R_{\mu\nu} - \frac{1}{2} g_{\mu\nu} R \right) \tag{2.185}$$

after relabelling dummy indices. The term in the brackets of eq. 2.185 is the Einstein tensor $G_{\mu\nu}$, thus we have the covariant divergence equation

$$\nabla^\mu G_{\mu\nu} = 0 \tag{2.186}$$

This constitutes a constraint on the components of the metric, in particular 4 constraint equations. thus the true number of degrees of freedom per point is 4. Contracting the Einstein tensor with the metric reveals that the vacuum EFE's state that the Ricci curvature of the spacetime must indeed be flat

$$R_{\mu\nu} = 0 \tag{2.187}$$

This agrees with the intuition of General Relativity, as there is no matter content

present in the spacetime telling it how to curve. The non-vacuum EFE's can eb derived considering the simple addition of a matter term S_M to the action 2.157

$$\begin{aligned} S &= S_H + S_M \\ &= \int d^4x\sqrt{-g}\ (R + \mathcal{L}_m) \end{aligned} \tag{2.188}$$

where $\mathcal{L}_m$ is the matter Lagrangian density. The variation principle, which we write more precisely as

$$\frac{1}{\sqrt{-g}}\frac{\delta S}{\delta g^{\mu\nu}} = 0 \tag{2.189}$$

gives the field equations

$$R_{\mu\nu} - \frac{1}{2}Rg_{\mu\nu} = T_{\mu\nu} \tag{2.190}$$

where we have defined the stress-energy tensor $T_{\mu\nu}$ by

$$\delta S_M = -\int d^4x\sqrt{-g}T_{\mu\nu}\delta g^{\mu\nu} \iff T_{\mu\nu} = -\frac{1}{\sqrt{-g}}\frac{\delta S_M}{\delta g^{\mu\nu}} \tag{2.191}$$

In the second line of equation 2.188 with have implicitly assumed that the matter content on the spacetime manifold is minimally coupled to gravity. The matter Lagrangian couples to the metric only through its determinant term in the proper volume element $dV = d^4x\sqrt{-g}$, rather than through higher order interactions which would involve couplings to the curvature tensors.

As an example consider the case of a scalar field minimally coupled to gravity as described above. The total action which describes both the gravitational and matter sectors of the theory is

$$S = \int d^4x\sqrt{-g}\left[R + \left(\frac{1}{2}\nabla^\mu\phi\nabla_\mu\phi - V(\phi)\right)\right] \tag{2.192}$$

where the matter Lagrangian of the scalar field with potential $V(\phi)$ is

$$\mathcal{L}_m = \frac{1}{2}\nabla^\mu\phi\nabla_\mu\phi - V(\phi) \tag{2.193}$$

If one considers the case in which the global spacetime metric is Minkowski $ds^2 = -dt^2 + d\mathbf{x}^2$ and the covariant derivatives become partial derivatives $\nabla_\mu = \partial_\mu$, the variational definition of the stress-energy tensor 2.191 leads to the familiar familiar stress-energy of a relativistic scalar field [1] [40, 41].

$$T_{\mu\nu} = -\frac{1}{\sqrt{-g}}\frac{\delta S_M}{\delta g^{\mu\nu}} = \frac{1}{4}g_{\mu\nu}\partial^\sigma\phi\partial_\sigma\phi - \frac{1}{2}\partial_\mu\phi\partial_\nu\phi - \frac{1}{2}V(\phi)g_{\mu\nu} \tag{2.194}$$

As we have introduced a matter field ϕ into the theory, there will also be a variational principle associated with this field

$$\frac{1}{\sqrt{-g}}\frac{\delta S}{\delta\phi} = 0 \tag{2.195}$$

The gravitational sector of the theory S_H is not coupled directly to the field, and thus the variation with respect to the matter field involves only minimally coupled matter action

$$\delta S = \delta S_M = \int d^4x\sqrt{-g}\,\delta\mathcal{L}_m(\phi, \partial_\mu\phi) \tag{2.196}$$

which results in the well know Klein-Gordon equation for a relativistic scalar field

$$\Box\phi = -\frac{dV(\phi)}{d\phi} \tag{2.197}$$

where $\Box = \partial^\mu\partial_\mu$ is the d'Alembertian derivative operator in Minkowski space. In the general case, where we introduce a set of minimally coupled field ϕ_a on the spacetime manifold with metric $g_{\mu\nu}$ one has the action

$$S = \int d^4x\sqrt{-g}\,R + \int d^4\sqrt{-g}\,\mathcal{L}_m(\phi_a, \nabla_\mu\phi_a) \tag{2.198}$$

one has the Einstein Field Equations as defined in eq 2.190, with stress-energy tensor

[1] In this work we use units of $16\pi G = 1$, in literature which is more concerned with making the low-energy agreement with Newtonian gravity more apparent this factor is often left in and the stress-energy tensor is defined with an additional factor of 2 so that the EFE's read $G_{\mu\nu} = 8\pi G T_{\mu\nu}$

as defined in eq 2.191 and the generalised Euler-Lagrange field equation

$$\nabla_\mu \left(\frac{\partial \mathcal{L}_m}{\partial(\nabla_\mu \phi_a)} \right) - \frac{\partial \mathcal{L}_m}{\partial \phi_a} = 0 \tag{2.199}$$

We showed previously that the covariant divergence of the Einstein tensor is zero as per eq. 2.186. This is due to the symmetry relations of the Riemann tensor, which can be traced back to properties of the Levi-Civita connection [2]. The vanishing covariant divergence of the Einstein tensor holds regardless of whether we include an a matter term in the action or not, thus on-shell we must also have a vanishing divergence of the stress-energy tensor

$$\nabla^\mu T_{\mu\nu} = 0 \tag{2.200}$$

which should not come as a surprise, as it is the statement of local conservation of energy-momentum generalised to a curved spacetime manifold. Importantly, equation 2.200 states that energy-momentum is conserved only locally, not globally. Global energy conservation is associated with a Noether symmetry in time translation. The stress-energy tensor is defined on a geometry with a (potentially) time varying metric, thus such a Noether charge does not generally exist globally. The stress-energy tensor is associated with the matter content that exists in the spacetime, and does not represent a stress-energy associated with the gravitational field itself. In the context of special relativity, we need only account for the stress-energy of the matter content, as the background is non-dynamical as well as flat which leads to a well defined notion of globally conserved energy $\partial_\mu T^{\mu\nu} = 0$. But in the context of General Relativity, the background geometry is itself dynamical but there is no natural way to isolate the dynamical sector of the metric, and so one can't talk about a well-defined gravitational stress-energy. The stress-energy of the matter field $T^{\mu\nu}$ really represents an incomplete picture if one wishes to account for

[2] In fact, for any torsion-free connection one has the required symmetry properties of the Riemann tensor to enforce a vanishing covariant divergence of the Einstein tensor

both the matter fields and the gravitational field. The statement of only having local conservation of energy can be physically interpreted as the curvature of spacetime doing work on the matter content. In sufficiently small regions of spacetime, this amount of work is negligible and one has approximate conservation of energy, but over larger regions, the capacity of the curvature to do work on the matter content becomes significant. We shall see in section 2.2.3.2 that a physically observable consequence of this is that of cosmological redshift. We will return to the statement of local energy conservation in GR after a discussion of symmetries.

2.2.1.1 Symmetries and Killing Vectors

The spacetime of General Relativity really consists of a pair $(\mathcal{M}, g)$ of a manifold equipped with a Lorentzian metric g, since the manifold topology exists independent of the metric we equip it with. General Relativity insists on the general covariance of physical laws, in the sense that we are really concerned with an equivalence class of spacetimes $(\mathcal{M}, g) \sim (\mathcal{M}', g')$ that are isometric to each other. This means that there exists a diffeomorphism $\phi : \mathcal{M} \to \mathcal{M}'$ whose pull back maps g into g'

$$\phi^* g = g' \tag{2.201}$$

Consider a 1-parameter group of diffeomorphism $\phi_t : M \times \mathbb{R} \to M$, where the index $t \in \mathbb{R}$ labels a the continuous group parameter. One can think of the diffeomorphism as defining a curve through the manifold M as such. For a fixed $p \in \mathcal{M}$, $\phi_t(p)$ maps from the point p to another point in the manifold in a smoothly varying way with the group parameter t. The diffeomorphisms form a group with identity element $\phi_0(p) = p$. Hence $\phi_t(p) : \mathbb{R} \to \mathcal{M}$ defines a curve on the manifold. Choosing local coordinates x^μ at p, we may then define a tangent vector to the curve in the coordinate basis ∂_μ

$$v = \frac{dx^\mu}{dt}\partial_\mu \tag{2.202}$$

The converse argument is also true. Given a smooth vector field v on the manifold, one can construct a local coordinate system at p such that there exists a unique solution to the integral curve equation of v passing through p at $t = 0$, so the vector field generates a flow ϕ_t. Thus each diffeomorphism ϕ is associated with a vector field v which is the infinitesimal generator of the transformation.

The case of particular interest is that of isomorphism, where the pullback of any element in the group of diffeomorphisms is a symmetry of the metric

$$\phi_t^* g = g \tag{2.203}$$

In this particular case, the associated vector field is called a Killing vector field ξ. Since the metric is invariant under the flow ϕ_t, the Lie derivative along the Killing vector field is zero

$$L_\xi g_{\mu\nu} = \lim_{t\to 0}\left(\frac{\phi_t^* g_{\mu\nu} - g_{\mu\nu}}{t}\right) = 0 \tag{2.204}$$

Equation 2.204 is true by virtue of the Killing vector field being a generator of an isomorphism (equivalently by ϕ_t being a group of isomorphisms which defines a vector flow ξ) and by writing out the Lie derivative in component form one may show that a vector field ξ is a Killing vector field if and only if it satisfies Killings equation, which we derive as follows.

For an arbitrary (k, r)-tensor field T on a manifold, the Lie derivative of T along a vector field v is

$$\begin{aligned} L_v T^{a_1\ldots a_k}_{b_1\ldots b_r} &= v^c \nabla_c T^{a_1\ldots a_k}_{b_1\ldots b_r} \\ &\quad - T^{c\ldots a_k}_{b_1\ldots b_r}\nabla_c v^{a_1} - T^{a_1 c\ldots a_k}_{b_1\ldots b_r}\nabla_c v^{a_2} - \ldots - T^{a_1\ldots c}_{b_1\ldots b_r}\nabla_c v^{a_k} \\ &\quad + T^{a_1\ldots a_k}_{c\ldots b_r}\nabla_{b_1} v^c + T^{a_1\ldots a_k}_{b_1 c\ldots b_r}\nabla_{b_2} v^c + \ldots + T^{a_1\ldots a_k}_{b_1\ldots c}\nabla_{b_r} v^c \end{aligned} \tag{2.205}$$

The metric tensor is a type (0,2) tensor, and thus its Lie derivative along the vector field ξ associated with the group of isometries ϕ_t in component form is

$$L_\xi g_{\mu\nu} = \xi^\sigma \nabla_\sigma g_{\mu\nu} + g_{\sigma\nu}\nabla_\mu \xi^\sigma + g_{\mu\sigma}\nabla_\nu \xi^\sigma \tag{2.206}$$

The connection in equation 2.205 is generic, but we are considering the context of a spacetime manifold with a Levi-Civita connection which is metric compatible, so equation 2.206 simplifies to

$$L_\xi g_{\mu\nu} = \nabla_\mu \xi_\nu + \nabla_\nu \xi_\mu \tag{2.207}$$

Since the Killing vector field is the generator of a group of isometries, the Lie drag of the metric along it is zero as per eq. 2.204, and thus it's components in a local coordinate basis ∂_μ must satisfy

$$\nabla_\mu \xi_\nu + \nabla_\nu \xi_\mu = 0 \tag{2.208}$$

Equation 2.208 is known as Killings equation. A vector field is a Killing vector field if and only if it satisfies Killings equation, we have proved the statement in one direction above and the converse can be shown trivially. Killing vectors are an important practical and conceptual tool when looking for solutions of the EFEs. As we mentioned, Killing vectors are associated with symmetries of the metric. Symmetries in physics come hand in hand with conserved quantities, and represent a redundancy in the description of the physical system we are modelling. In general, a spacetime may have no symmetries, there is no apriori reason for them to exist. But in the case that a (or possibly many) Killing vector field does exist on the spacetime, thee satisfy a number of useful properties.

Firstly, given a Killing vector field ξ on a spacetime, one may always find a local coordinate system x^μ which is adapted to the Killing vector such that $\xi = \partial_{\mu^*}$ where $x^{\mu*}$ is a fixed coordinate in system. In such an adapted coordinate system, the metric can be shown to be independent of $x^{\mu*}$ as follows.

Using metric compatibility, Killings equation 2.208 can be written in the form

$$g_{\nu\sigma} \nabla_\mu \xi^\sigma + g_{\mu\sigma} \nabla_\nu \xi^\sigma = 0 \tag{2.209}$$

In the adapted coordinate system the Killing vector field components are $\xi^\sigma = \delta^\sigma_{\mu*}$, where the $\mu*$ index is fixed. Thus the covariant derivative terms are

$$\begin{aligned} \nabla_\mu \xi^\sigma &= \partial_\mu \xi^\sigma + \Gamma^\sigma_{\mu\nu}\xi^\nu \\ &= \partial_\mu \delta^\sigma_{\mu*} + \Gamma^\sigma_{\mu\nu}\delta^\nu_{\mu*} \\ &= \Gamma^\sigma_{\mu\mu*} \end{aligned} \tag{2.210}$$

Thus Killings equation 2.209 becomes

$$g_{\nu\sigma}\Gamma^\sigma_{\mu\mu*} + g_{\mu\sigma}\Gamma^\sigma_{\nu\mu*} = 0 \tag{2.211}$$

At which point we can use the explicit form of the Christoffel symbols given in eq. 2.152 to determine

$$\begin{aligned} g_{\nu\sigma}\Gamma^\sigma_{\mu\mu*} &= \frac{1}{2} g_{\nu\sigma} g^{\sigma\rho} \left(\partial_\mu g_{\mu*\rho} + \partial_{\mu*} g_{\mu\rho} - \partial_\rho g_{\mu\mu*}\right) \\ &= \frac{1}{2}\left(\partial_\mu g_{\mu*\nu} + \partial_{\mu*} g_{\mu\nu} - \partial_\nu g_{\mu\mu*}\right) \end{aligned} \tag{2.212}$$

Thus equation 2.211 finally reduces to

$$\partial_{\mu*} g_{\mu\nu} = 0 \tag{2.213}$$

which is true if and only if the metric components $g_{\mu\nu}$ are independent of $x^{\mu*}$. We have shown here that given a Killing vector field, there exists a local coordinate system in which the metric is independent of a particular fixed coordinate, the converse is also true. One can show trivially that if $\partial_{\mu*} g_{\mu\nu} = 0$ for some particular coordinate $x^{\mu*}$, then the vector $\xi = \partial_{\mu^*}$ satisfies Killings equation, which is a necessary and sufficient condition for being a Killing vector field on the spacetime manifold.

Killing vector fields, should they exist on the spacetime in question, allow us to define conserved quantities along geodesics. Consider a spacetime $(\mathcal{M}, g)$ with Killing vector field ξ and let $\gamma(\lambda)$ be a geodesic on the spacetime with tangent vector $v^\mu(\lambda)$.

Consider the quantity

$$\begin{aligned} v^\mu \nabla_\mu (\xi \cdot v) &= n^\mu \nabla_\mu (\xi^\nu v_\mu) \\ &= v^\mu v^\nu \nabla_\mu \xi_\nu + \xi_\nu v^\mu \nabla_\mu v^\nu \end{aligned} \tag{2.214}$$

Geodesics by definition are those curves whose tangent vectors are parallel transported $v^\mu \nabla_\mu v^\nu = 0$ thus the second term in eq. 2.214 is zero. The second term is also zero by the symmetry of Killings equation, thus we are left with the conservation equation, satisfied along the geodesic $\gamma(\lambda)$

$$v^\mu \nabla_\mu (\xi^\mu v_\mu) = 0 \tag{2.215}$$

In this sense we can understand the existence of a Killing vector field as generating a conserved quantity for observers moving along through the spacetime in geodesic motion. At this point it is appropriate to return to the stress-energy tensor $T_{\mu\nu}$. The stress-energy is conserved locally as it must satisfy $\nabla_\mu T^{\mu\nu} = 0$, but it is not in general possible to define a globally conserved energy. However, when there exists a timelike killing vector, one can define the current

$$J^\mu = T^{\mu\nu} \xi_\nu \tag{2.216}$$

Calling E the integral of this current over a spacelike hypersurface Σ one has .

$$E = \int_\Sigma \sqrt{|\gamma|} n_\mu J^\mu \tag{2.217}$$

where γ is the metric induced on the hypersurface by the spacetime metric g and n^μ is the unit normal to the spacelike hypersurface. At this point Stokes theorem

can be invoked (particularly as the hypersurface is not null and thus there exists a well defined natural volume element on Σ) to write the quantity E as an integral of a 4-divergence over the volume enclosed by the hypersurface $\mathcal{V}$

$$E = \int_{\mathcal{V}} d^4x\sqrt{-g}\nabla_\mu J^\mu \tag{2.218}$$

The 4-divergence of the current may be calculated explicitly from the properties of the stress-energy tensor and the Killing vector field

$$\nabla_\mu J\mu = T^{\mu\nu}\nabla_\nu + \xi_\nu\nabla_\mu T^{\mu\nu} = 0 \tag{2.219}$$

Equation 2.219 implies that the quantity we have defined as E, which can be interpreted as a total flux of the current J^μ passing through $\mathcal{V}$, will be zero regardless of the choice of spatial hypersurface Σ. Thus, given a timelike Killing vector field on the spacetime, it is possible to construct a globally conserved quantity from the stress-energy tensor.

The existence of a Kiliing vector field on a spacetime is not guaranteed but it is possible to determine the maximum possible number of linearly independent Killing vector fields on a spacetime by determining a well-defined system of ODEs the Killing vector field components a such.

Starting with the definition of the Riemann curvature tensor. for any given connection ∇ on a manifold the components for the Riemann tensor satisfy

$$\nabla_\mu\nabla_\nu v_\sigma - \nabla_\nu\nabla_\mu v_\sigma = R_{\mu\nu\sigma}{}^\rho v_\rho \tag{2.220}$$

for arbitrary v^ρ. Equation 2.220 may be applied to a Killing vector field and Killings equation can be used to swap the μ and σ indices on the second term at the expense of a minus sign.

$$\nabla_\mu\nabla_\nu\xi_\sigma + \nabla_\nu\nabla_\sigma\xi_\mu = R_{\mu\nu\sigma}{}^\rho\xi_\rho \tag{2.221}$$

By permuting the set of indices (μ, ν, σ) one can determine the relation

$$2\nabla_\nu \nabla_\sigma \xi_\mu = \left(R_{\mu\nu\sigma}{}^\rho + R_{\nu\sigma\mu}{}^\rho - R_{\sigma\mu\nu}{}^\rho \right) \xi_\rho \tag{2.222}$$

The components of the Riemann tensor satisfy anti-symmetry relation

$$3! R_{[\mu\nu\sigma]}{}^\rho = R_{\mu\nu\sigma}{}^\rho - R_{\nu\sigma\mu}{}^\rho + R_{\sigma\mu\nu}{}^\rho = 0 \tag{2.223}$$

Invoking these symmetry relations and relabelling indices, equation 2.222 becomes

$$\nabla_\mu \nabla_\nu \xi_\sigma = -R_{\nu\sigma\mu}{}^\rho \xi_\rho \tag{2.224}$$

Equation 2.224 constitutes a system of partial differential equations for the components of a Killing vector field. In the theory of PDEs, this system of equations at most one solution, provided that the functions $R_{\mu\nu\sigma}{}^\rho$ are suitably smooth. To find such solutions one needs two pieces of initial data at a point $p \in \mathcal{M}$, the value of the Killing vector field $\xi(p)$ and the value of the covariant derivative $(\nabla_\mu \xi_\nu)(p)$. Thus any Killing vector field will be uniquely determined by a point in the space of initial data at p, $(\xi_\mu, \nabla_\mu \xi_\nu)_p$. Thus the maximum possible number of linearly independent Killing vector fields possible on the spacetime manifold will be the dimension of this space. If the spacetime were of dimension n, then there would be n linearly independent components of a given killing vector, and since the covariant derivative $\nabla_\mu \xi_\nu$ is antisymmetric by Killings equation, it has $\frac{1}{2}n(n-1)$ independent components. Therefore the dimension of the space of initial data is $n + \frac{1}{2}n(n-1) = \frac{1}{2}n(n+1)$. Thus this is the maximum possible number of linearly independent Killing vector fields on a spacetime of dimension n. Maximally symmetric spacetimes are those spacetimes with the maximum number of Killing vector fields.

A final important property of Killing vector fields is that they form a Lie algebra on the manifold. A Lie algebra [33] is a vector space $\mathbf{v}$ equipped with a bilinear map

$[\cdot,\cdot] : \mathbf{v} \times \mathbf{v} \to \mathbf{v}$ satisfying the Jacobi identity

$$[x,[y,z]] + [y,[z,x]] + [z,[x,y]] = 0 \,\forall\, x, y, z, \in \mathbf{v} \tag{2.225}$$

Given a set of k linearly independent killing vectors ξ_k on a spacetime manifold, one can show trivially that the Lie drag of the metric along the commutator of two Killing vector fields is zero

$$L_{[\xi_k,\xi_r]} g_{\mu\nu} = 0 \tag{2.226}$$

Recalling that Killing vector fields generate isomorphims of the metric, for which the Lie drag is zero as per eq. 2.204, we see that the commutator $[\xi_k, \xi_r]$ is itself a Killing vector field. Therefore the set of all linearly independent Killing vector fields on a spacetime manifold of dimension n, should they exist, form the basis of a Lie algebra of dimension N bounded by

$$0 \leq N \leq \frac{1}{2} n(n+1) \tag{2.227}$$

We may then apply the standard theory of Lie algebras to the Killing vector fields, if we are able to find them. In particular, since the Lie bracket $[\cdot,\cdot]$ is closed, we may write the commutator of any two elements of the Killing vector Lie algebra in terms of structure constants C^c_{ab}.

$$[\xi_a, \xi_b] = C^c_{ab} \xi_c \tag{2.228}$$

2.2.2 Homogeneous and Isotropic Cosmological Spacetimes

In section 2.2.1 we developed the basic Lagrangian formalism of General Relativity, arriving at the Einstein Field Equations which describe the evolution of the spacetime geometry and the dynamics of matter fields that exist on the spacetime

$$\begin{aligned} R_{\mu\nu} - \frac{1}{2} R g_{\mu\nu} &= T_{\mu\nu} \\ \nabla_\mu T^{\mu\nu} &= 0 \end{aligned} \tag{2.229}$$

These equations represent a complicated set of coupled partial differential equations for components of the metric $g_{\mu\nu}$ and the matter fields introduced through the stress-energy tensor as defined in equation 2.191, which requires a specific choice of matter Lagrangian. In general the Einstein Field Equations cannot be solved, one needs to impose more information about the underlying spacetime and matter field (if they are present) in order to look for solutions. If we hope to be able to describe the dynamical evolution of our universe through the framework of General Relativity, we must appeal to observational evidence as a means to inform further assumptions about the spacetime geometry. At this point one can then look for solutions to the EFEs that describe the evolution of the universe under such assumptions and search for predictions that may be tested against observational data. One of the most significant observations in cosmology is the existence of the Cosmic Microwave Background (CMB), thermal radiation present everywhere in the universe that has been measured at a temperature of approximately $T = 2.7K$ [42]. The CMB contains only very small anisotropies, on the order of $\delta T \sim 10^{-}5$ [43], on large cosmological scales the correlator of fluctuations in the temperature field is approximately invariant under rotations. In fact a proportion of these small anisotropies can be explained by the fact that there is only one frame in which the entire universe looks isotropic. The frame of an observer on Earth is not exactly at rest relative to the CMB frame and therefore we observe small dipole anisotropies resulting from the Doppler shifting of it's blackbody spectrum [44–46].

Although an observer on Earth measures CMB anisotropies from a particular frame of reference, there is no reason to believe that this is a preferred frame of reference of the universe. This is the ***Copernicun principle***, that no observer inhabits a privileged reference frame. Thus is there is good reason to believe that the universe is approximately isotropic on cosmological scales as measured on Earth, then it should also be so at any point in the universe. A universe that is both spatially isotropic at every point must also be spatially homogeneous. Given that the temperature fluctuations of the CMB are so incredibly small,it is feasible that the matter content of the universe is smoothed out on cosmological scales and the spacetime is approximately homogeneous. These two assumptions of, that the universe should be approximately homogeneous and isotropic on sufficiently large scales form the ***Cosmological Principle***.

Assuming that the Universe is spatially homogeneous and isotropic allows us to greatly reduce the space of allowed solutions to the Einstein Field Equations, and in fact find explicit solutions. Before doing so, should first develop a formal notion of spatial homogeneity and isotropy of the spacetime manifold. Qualitatively, spatial homogeneity means that metric on spatial slices looks the same at any point. We recognise this as a symmetry of the (spatial metric) which we discussed in section 2.2.1.1. We define a spatially homogeneous spacetime $(\mathcal{M}, g)$ as one which may be foliated into spatial hypersurfaces $\mathcal{M} = \mathbb{R} \times \Sigma_t$, labelled by a single parameter $t \in \mathbb{R}$. Such that $\forall\, p, q \in \Sigma_t$ there exists an isometry ϕ_t for which $\phi_t(p) = q$. This statement of homogeneity tells us essentially that on any of the spatial hypersurfaces Σ_t, there exists an smooth, invertible map which takes us from any point $p \in \Sigma_t$ to any other point $q \in \Sigma_t$ and leaves the metric looking the same at the new point q. The statement of spatial isotropy concerns, qualitatively, the geometry of spacetime looking the same under rotations. Formally we define a spatially isotropic spacetime $(\mathcal{M}, g)$ as one for which, given any point $p \in \mathcal{M}$ and unit spacelike vectors in the tangent space $v, w \in T_p\mathcal{M}$, there exists an isometry ϕ such that $\phi(p) = p$ and $\phi_*(v) = w$ where ϕ_* is the pushforward of ϕ. In other words, there is a symmetry

transformation of the metric that maps p into itself but rotates one vector in the tangent space $T_p\mathcal{M}$ into another.

With these requirements of spatial homogeneity and isotropy, one can show that the spatial geometry must be one of constant curvature. Thus the problem simply reduces to finding those spatial geometries. There will exist an isomorphism between any two geometries of the same constant curvature (as long as the manifolds are of identical dimension and metric signature). Thus all of the spatial geometries are in fact already known. For positive curvature, the isomoprhism is to the geometry of the 3-sphere, whose metric is

$$ds^2 = d\psi^2 + \sin^2\psi d\theta^2 + \sin^2\psi \sin^2\theta d\phi^2 \tag{2.230}$$

and we refer to the manifold as ***closed FLRW*** which has the topology of $\mathbb{R} \times S^3$. For zero curvature, the spatial geometry is isomorphic to flat 3-Euclidean space with metric

$$ds^2 = dx^2 + dy^2 + dz^2 \tag{2.231}$$

with the simple topology of $\mathbb{R}^3$, which we call ***flat FLRW***. For negative curvature, the geometry is isomorphic to a 3-hyperboloid with metric

$$ds^2 = d\psi^2 + \sinh^2\psi d\theta^2 + \sinh^2\psi \sin^2\theta d\phi^2 \tag{2.232}$$

and the manifold is referred to as ***open FLRW***. The geometries are in fact the maximally symmetric geometries with constant curvature.

Assuming that we must satisfy the cosmological principle, one can write the full spacetime metric as

$$ds^2 = -dt^2 + a^2(t)d\Sigma^2 \tag{2.233}$$

where $a^2(t)$ is an arbitrary positive function of the timelike coordinate and $d\Sigma^2$ is the metric on the spatial slice. The conditions of homogeneity and isotropic require $d\Sigma^2$ to be either flat, closed or open, each of which corresponding to constant zero,

positive or negative curvature respectively. In each of these three cases, the spatial metric can be written in terms of polar coordinates (r, θ, ϕ) and a scalar curvature parameter $k = 0, 1, -1$ corresponding to each of the three cases.

$$d\Sigma^2 = \frac{1}{1 - kr^2} dr^2 + r^2 d\Omega^2 \tag{2.234}$$

where $d\Omega^2$ is the metric on S^2 and ψ and r are related through the coordinate transformation

$$d\psi = \frac{1}{\sqrt{1 - kr^2}} dr \tag{2.235}$$

The metric of eq. 2.234 is referred to as the Friedman-Lemaître-Robertson-Walker (FLRW) metric. It describes three spacetimes with distinct spatial topologies. The overall geometry is also dependant on an undetermined the scalar function $a(t)$, referred to as the scale factor. Understanding the significance of the scale factor is of fundamental importance in homogeneous cosmological models and we will discuss it at length shortly. The coordinates (r, θ, ϕ) are referred to as the comoving coordinates. Given this specific anszat for the metric, in terms of a curvature parameter k and an undetermined scale factor $a(t)$, we may write down explicitly the Einstein Field Equations in terms, which will turn out to be a set of ordinary differential equations for $a(t)$ and any matter fields we choose to introduce.

Given the form of the metric

$$ds^2 = -dt^2 + a^2(t) \left[\frac{1}{1 - kr^2} dr^2 + r^2 \left(d\theta^2 + \sin^2 \theta d\phi^2 \right) \right] \tag{2.236}$$

one may compute the non-zero components of the Ricci tensor

$$\begin{aligned} R_{tt} &= -3\frac{\ddot{a}}{a} \\ R_{rr} &= \frac{a\ddot{a} + 2\dot{a}^2 + 2k}{1 - kr^2} \\ R_{\theta\theta} &= r^2 \left(a\ddot{a} + 2\dot{a}^2 \ + 2k \right) \\ R_{\phi\phi} &= r^2 \left(a\ddot{a} + 2\dot{a}^2 + 2k \right) \sin^2 \theta \end{aligned} \tag{2.237}$$

and the Ricci scalar

$$R = 6\left[\frac{\ddot{a}}{a} + \left(\frac{\dot{a}}{a}\right)^2 + \frac{k}{a^2}\right] \tag{2.238}$$

At this point we also note that, following our discussion of Killing vector fields in section 2.2.1.1, we see that in this set of local coordinates the metric is independent of ϕ, therefore $\xi = \partial_\phi$ will be one of the Killing vector fields of this spacetime. This is vector field which we associate with generating a conserved angular momentum along the geodesic of an observer.

At this point we stop to discuss a further modification of the Einstein-Hilbert action that should be considered when discussing cosmological solutions. It is well understood that when measuring, say the energy of a system, only relative changes in the energy of the system are measurable. These are changes with respect to some ground state. This is manifest in both classical Newtonian mechanics and quantum mechanics. In Newtonian mechanics one may define the zero of the potential energy arbitrarily with no effect to the equations of motion. A foundational result of quantum mechanics is that when solving the Schrodinger equation for the states of a quantum harmonic oscillator, the energy eigenstates become discretely quantified with a constant non-zero vacuum state energy. It is not unreasonable to ask if there is a vaccum energy present in spacetime that may contribute to its dynamics. In fact it is this vaccuum energy term that Einstein added to the gravitational action after first publishing his theory of General Relativity. At the time of Einstein publishing his General Theory of Relativity, there was no evidence to suggest that the universe on cosmological scales was anything other than static in time. Einstein initially looked for such static solutions of the gravitational field equations but the field equations predicted a spatial geometry that could change with time through the scale factor $a(t)$. Einstein looked for static solutions to the field equations by adding a constant parameter Λ to the action as such [47]

$$S_{EH} \to \frac{1}{16\pi G}\int d^4x\sqrt{-g}\,(R - 2\Lambda) \tag{2.239}$$

where we have reinserted factors of $16\pi G$ in order to make better contact with the standard literature. With the addition of the constant term Λ, called the cosmological constant the Einstein Field Equations become

$$R_{\mu\nu} - \frac{1}{2}Rg_{\mu\nu} + \Lambda g_{\mu\nu} = 8\pi G T_{\mu\nu} \tag{2.240}$$

It is reasonable to ask if the cosmological constant Λ is equivalent to an energy density. If one considers the stress-energy of a perfect fluid with normalised 4-velocity u^μ, constant pressure p^{vac} and constant energy density ρ^{vac}

$$T^{\text{vac}}_{\mu\nu} = \rho^{\text{vac}} u_\mu u_\nu + p^{vac}(u_\mu u_\nu + g_{\mu\nu}) \tag{2.241}$$

Letting the pressure be the negative of the energy density $p^{\text{vac}} = -\rho^{\text{vac}}$, the EFEs with no cosmological constant would be

$$R_{\mu\nu} - \frac{1}{2}Rg_{\mu\nu} = 8\pi G\left(T_{\mu\nu} - \rho^{\text{vac}} g_{\mu\nu}\right) \tag{2.242}$$

which can be rearranged to give

$$R_{\mu\nu} - \frac{1}{2}Rg_{\mu\nu} + 8\pi G\rho^{\text{vac}} g_{\mu\nu} = 8\pi G T_{\mu\nu} \tag{2.243}$$

Clearly this is equivalent to a cosmological constant term. Thus one can define the vacuum energy associated with a cosmological constant as

$$\rho_\Lambda = \frac{\Lambda}{8\pi G} \tag{2.244}$$

As we have mentioned, Einstein originally introduced the cosmological solution to produce a static universe. If one considers the vacuum case of the Einstein Field Equations with cosmological constant 2.240, Looking at the R_{tt} component we have

$$R_{tt} - \frac{1}{2}Rg_{tt} + \Lambda g_{tt} = 0 \implies 3\left(\frac{\dot{a}}{a}\right)^2 + \frac{3k}{a^2} = \Lambda \tag{2.245}$$

Thus a static solution for which $\dot{a} = 0$ is possible if

$$\frac{k}{a^2} = \frac{1}{3}\Lambda = \frac{8}{3}\pi G\rho^{\text{vac}} \tag{2.246}$$

In the case of a zero cosmological constant, and thus zero vacuum energy density, the spatial topology is that of flat Euclidean space with the global spacetime being Minkowskian. If the cosmological constant is positive one has a closed universe with S^3 spatial topology. And finally with a negative cosmological constant the spacetime is open with the spatial topology of a 3-hyperboloid.

2.2.2.0.1 The Hubble Parameter Shortly after Einstein published his static universe Edwin Hubble presented highly convincing evidence that the universe was not static and that it was in fact expanding [48]. Through observing the red shift of distant comoving galaxies, Hubble determined that their radial velocities were proportional to their proper distance. If the spacetime is allowed to be non-static, the proper distance between a local observer and a comoving galaxy is $D(t) = a(t)R$ where R is the comoving distance, which is constant time assuming that the observer and the galaxy are indeed truely comoving. In the frame of the observer, the galaxy is thus een to be moving at a velocity

$$\begin{aligned} v = \dot{D} &= \dot{a}R + a\dot{R} = \dot{a}R \\ &= \frac{\dot{a}}{a}D \end{aligned} \tag{2.247}$$

The function $H(t) = \dot{a}/a$ appears frequently with some of the relevant quantities we have calculated, in particular the scalar curvature R. $H(t)$ is known as the Hubble parameter and arguably one of the most important quantities in cosmology. Simply by inspection one can see that the Hubble parameter represents a normalised measure of the universes expansion $H(t) \sim \dot{a}$. As we shall see shortly, the FLRW universe is insensitive to a rescaling of its size, and thus the magnitude of $a(t)$ is of no physical significance. As such it is conventional to define $a(t_0) = 1$,

where t_0 is present day of an observer on Earth. The time scales over which we make observations on Earth are negligibly small within the context of cosmological timescale, so it is appropriate to consider the Hubble parameter measured in recent years (since the start of modern cosmological observations) as a constant. Thus we define the Hubble constant as $H_0 = \dot{a}(0)$. General Relativity is therefore able to predict a linear relationship between the velocity of a comoving galaxy and its proper distance to the observer as equation 2.247 becomes

$$v = H_0 D \tag{2.248}$$

Equation 2.248 is known as Hubbles Law. In the 2022 publication of data collected from the Hubble Space Telescope, the value of the Hubble constant was determined to be $H_0 = 73.30 \pm 1.04 \mathrm{km\,s^{-1}\,Mpc^{-1}}$ [49,50]. There are however large discrepancies in the measured values of the Hubble constant from different experiments, this is known as the "Hubble Tension". For detailed discussions we refer the reader to [51–53]. To outline the problem briefly, local determinations of Hubbles constant such as by inferring it from the red shifts of (approximately) comoving galaxies or the brightness of "standard candles" [49, 54, 55], differ significantly from the inferred values from measurements of the CMB Temperature fluctuations [4]. The discrepancy is significant enough to warrant extensive discussion and research in the academic community, on the order of 8% [51].

2.2.2.1 The Friedmann Equations

We will now proceed to analyse the equations of motion for a homogeneous and isotropic universe filled with a perfect fluid. As we have discussed in section 2.2.2, such spacetime manifolds are equipped with the FLRW metric 2.236 from which one derives the non-zero components of the Ricci tensor 2.237 and the Ricci scalar 2.238, repeated here for convenience.

$$
\begin{aligned}
R_{tt} &= -3\frac{\ddot{a}}{a} \\
R_{rr} &= \frac{a\ddot{a} + 2\dot{a}^2 + 2k}{1 - kr^2} \\
R_{\theta\theta} &= r^2\left(a\ddot{a} + 2\dot{a}^2 \ + 2k\right) \\
R_{\phi\phi} &= r^2\left(a\ddot{a} + 2\dot{a}^2 + 2k\right)\sin^2\theta
\end{aligned}
\tag{2.249}
$$

$$
R = 6\left[\frac{\ddot{a}}{a} + \left(\frac{\dot{a}}{a}\right)^2 + \frac{k}{a^2}\right] \tag{2.250}
$$

Recall that the stress-energy tensor of a perfect fluid with energy density ρ, pressure p and normalised 4-velocity $u^\mu = (1, 0, 0)$ can be written as $T_{\mu\nu} = \rho u_\mu u_\nu + p(u_\mu u_\nu + g_{\mu\nu})$, as such the non-zero components are

$$
\begin{aligned}
T_{tt} &= \rho \\
T_{ii} &= p g_{ii} = p a^2(t)\gamma_{ii} \quad \text{(no summation over } i\text{)}
\end{aligned}
\tag{2.251}
$$

where the Latin index i runs over spatial coordinates and γ_{ij} is the scale-free part of the induced metric on spatial slices Σ_t. The total (matter) stress-energy tensor will be a linear combination of contributions from different classifications of matter. In this case one may write

$$
\begin{aligned}
\rho &= \sum_i \rho_i \\
p &= \sum_i p_i
\end{aligned}
\tag{2.252}
$$

We will treat the cosmological constant as entering into the Einstein Field Equations through the contribution of a perfect fluid with $\rho_\Lambda = -p_\Lambda$. Thus considering all non-zero components of the EFEs

$$
R_{\mu\nu} - \frac{1}{2}R g_{\mu\nu} = 8\pi G T_{\mu\nu} \tag{2.253}
$$

one has the following equations of motion from the non-trivial Einstein Field

Equations.

$$\begin{aligned} tt: &\quad \left(\frac{\dot{a}}{a}\right)^2 + \frac{k}{a^2} = \frac{8\pi G}{3}\rho \\ ii: &\quad 2\frac{\ddot{a}}{a} + \left(\frac{\dot{a}}{a}\right)^2 + \frac{k}{a^2} = -8\pi G p \end{aligned} \tag{2.254}$$

The tt equation may be used to eliminate the first derivative term H^2 term and the intrinsic curvature term proportional to k in the ii equation of 2.254, resulting in the Friedmann equations.

$$\begin{aligned} \left(\frac{\dot{a}}{a}\right)^2 + \frac{k}{a^2} &= \frac{8\pi G}{3}\rho \\ \frac{\ddot{a}}{a} &= -\frac{4\pi G}{3}\left(\rho + 3p\right) \end{aligned} \tag{2.255}$$

To summarise what we have established thus far. A homogeneous and isotropic spacetime filled with a perfect fluid (or many perfect fluids, each contributing linearly to the overall matter stress-energy) is described in terms its scale factor $a(t)$ and constant spatial curvature. Simply by inspecting the Friedmann equations, one can see that the overall size of the scale factor has no effect on the dynamics of the spacetime. Rescaling $a(t)$ by a positive scalar multiple $a \to \lambda a$ leaves the equations of motion invariant. One particular subtly arises related to the spatial curvature k. In the case $k \neq 0$ one may think that the equations of motion are not invariant under a rescaling of $a(t)$ due to the k/a^2 term in the first equation of 2.255. However not that only the sign of k is meaningful, it determines which of the three distinct spatial topologies the spacetime manifold possesses. It's magnitude is always taken to be $1, 0, -1$ and therefore the rescaled term $\lambda k/a^2$ is equivalent to k'/a^2 where $k' = 1, 0, -1$. Therefore the Friedmann Equations truly are insensitive to the overall scale of the universe.

We have already mentioned the Hubble parameter, as well as this the first Friedmann equation of 2.255 may be used to define some important cosmological parameters known as the density parameters. The first Friedmann equation may be written in the form

$$\frac{k}{H^2 a^2} = \frac{8\pi G}{3H^2}\rho - 1 \tag{2.256}$$

We define a quantity called the critical density ρ_c as

$$\rho_c = \frac{3H^2}{8\pi G} \tag{2.257}$$

and define the density parameters Ω_i as the ratios ρ_i/ρ_c. Equation 2.256 becomes

$$\frac{k}{H^2a^2} = \Omega - 1 \tag{2.258}$$

where $\Omega = \sum_i \Omega_i$ is the total density parameter. In this form the interpretation of the critical energy density is clearer. It is the total energy density of the universe that enforces flat spatial curvature i.e. if $\rho = \rho_c$ we must have $k = 0$. Finally, we treat the spatial curvature term as equivalent to a density parameter term, although it is important to mention that this is simply a convenience, and that this does not represent an energy density associated with the gravitational field. Defining the curvature density parameter as $\Omega_k = k/H^2a^2$, the first Friedmann equation becomes

$$\Omega_k = \Omega - 1 \tag{2.259}$$

The density parameters are not only important because they represent the matter content in spacetime and thus are a necessary piece of information in determine the evolution of the spacetime geometry, but because the from the value of Ω one can determine the spatial topology of the manifold. As we have shown, the cosmological principle restricts us to 3 distinct and fixed spatial topologies. If one has for the overall energy density $\rho > \rho_c$, the clearly from equation 2.259 and the definitions of the density parameters $k > 0$ and thus the spacetime is closed with spatial S^3 topology. By the same reasoning, if $\rho = \rho_c$ the spacetme is flat and if $\rho < \rho_c$ the the spacetime is open with 3-hyperboloid spatial topology.

As well as the Friedmann equations we also have the local conservation of the stress-energy tensor $\nabla_\mu T^{\mu\nu} = 0$, taking the $\nu = t$ component we have

$$\dot{\rho} + 3\frac{\dot{a}}{a}(\rho + p) = 0 \tag{2.260}$$

At this point it is useful to discuss some basic classifications used to describe the cosmological matter content. In particular, consider in the case in which there is a dominant contribution to the stress-energy tensor from one type of matter (i.e. photons, relativistic or non relativistic massive particles), and that all other contributions are negligible. Typically we assume a linear "equation of state", the relationship between the perfect fluids pressure and energy-density.

$$p = w\rho \tag{2.261}$$

where the state parameter w is usually assumed to be constant, as we shall do in this work. In this case the conservation equation 2.260 becomes

$$\dot{\rho} = -3H\rho(1 + w) \tag{2.262}$$

since we assume the only significant contribution to the overall stress-energy is from one source with $p = w\rho$. Recalling the definition of the Hubble parameter $H = \dot{a}/a$, equation 2.262 can be written in the more enlightening form

$$\frac{1}{\rho}\dot{\rho} = -3(1 + w)\frac{\dot{a}}{a} \tag{2.263}$$

This is a simple ODE to which there clearly exists an exact solution

$$\rho(t) = \rho_0 a(t)^{-3(1+w)} \tag{2.264}$$

where ρ_0 is a constant. In particular it is a well known result that a photon gas confided to, and in thermal equilibrium with, a box exerts a pressure equal

to 1 third of it's energy density [56]. If one considers the spacetime to be dominated by a perfect fluid with such state parameter $w = 1/3$, the energy density will scale with a^{-4} as per equation 2.264. One may expect that the energy density of such a "radiation dominated" would scale with a^{-3}, since the photons are essentially confined to a box of length $L \sim a(t)$ and would therefore form stationary waves of wavelength $\lambda_n = a/n\pi$. But the spacetime itself is expanding (or contracting depending on the sign of $\dot{a}$) and as we have mentioned in section 2.2.1, the gravitational field has the capacity to do work on the photons. The photon wavelengths are stretched out along with the scale factor and they become cosmologically redshifted. The cosmological redshift of photons shall be discussed in more detail in section 2.2.3.2.

Another basic classification of matter that is often considered is that of dust. In the late universe, on cosmological scales the matter content of the universe can be approximated as consisting of uniformly spread out structures such as galaxies, or clusters thereof. If one considers the perfect fluid filling the spacetime to be primarily dominated by slow moving, massive "dust" particles that exert approximately zero pressure, then clearly the state parameter $w = 0$. Thus from equation 2.264 we see that the energy density scales with a^{-3}. In contrast to the case of a radiation dominated energy density, this agrees with our naive intuition. If the total number of matter particles is held fixed during expansion of the spacetime, the number density will scale as a^{-3} and thus the total energy density also scale in the same manner.

At the start of this section we decided to treat the vacuum energy contribution as equivalent to a perfect fluid with $\rho_\Lambda = -\rho_\Lambda$. Clearly this corresponds to a state parameter $w = -1$, for which the vacuum energy density does not scale with $a(t)$ at all, in fact it is constant $\rho_\Lambda = \rho_0$ as we should expect from a vaccuum energy.

We have considered thus far three situations in which the matter content of the universe is approximated as having only a single non-negligible contribution from a perfect fluid with state parameter w. The cases of $w = 1/3, 0, -1$ are referred to as ***radiation dominated***, ***dust/matter dominated*** and ***vacuum dominated***

respectively. One could also consider the a case in which the energy density of the universe is dominated by the contribution from the spatial curvature term. Recall that we defined a density parameter related to the curvature term in analogy to the matter density parameters $\Omega_i = \rho_i/\rho_c$. In this fashion we may define an energy density term associated with the spatial curvature

$$\rho_k = \Omega_k \rho_c \tag{2.265}$$

The critical density ρ_c is defined in eq. 2.265 and thus the energy density term associated with the curvature is

$$\rho_k = \frac{3k}{8\pi G a^2} \tag{2.266}$$

We see that the curvature energy density scales with a^{-2}, so by comparison with eq. 2.264, this is acts like a perfect fluid with state parameter $w = -\frac{1}{3}$.

In each of the radiation, matter, vacuum and ***curvature dominated*** approximations it is possible to solve the Friedmann equations directly and determine the scale factor $a(t)$.

2.2.2.2 The Radiation Dominated Solution

As described in section 2.2.2.1, in a radiation dominated universe the energy density is given in terms of the scale factor as

$$\rho(t) = \rho_0 a(t)^{-4} \tag{2.267}$$

Which follows from the conservation of stress-energy and the equation of state $p = \rho/3$. The Friedmann equations have not yet been employed. Subsisting eq. 2.267 into the first Friedmann equation 2.255 one has

$$\left(\frac{\dot{a}}{a}\right)^2 + \frac{k}{a^2} = \frac{8\pi G}{3}\rho_0 a^{-4} \tag{2.268}$$

In the case of a flat spatial topology with $k = 0$, the Friedmann equation 2.268 reduces to

$$\begin{aligned} a^2\dot{a}^2 &= \frac{8\pi G}{3}\rho_0 \\ \implies a\dot{a} &= \pm 2\sqrt{\frac{2\pi G}{3}}\rho_0 \end{aligned} \tag{2.269}$$

We have the solution

$$a_{\pm}(t) = \left(\frac{32\pi G\rho_0}{3}\right)^{\frac{1}{4}}\sqrt{\pm t} \tag{2.270}$$

There are in fact two solutions here, $a_+(t)$ defined on $0 \leq t \leq \infty$ and $a_(t)$ defined on $-\infty \leq t \leq 0$. The $a_+(t)$ solution is expanding as the time coordinate evolves forward, and the $a_(t)$ solution is contracting. Both both solutions meet at $t = 0$ where $a(0) = 0$. With one eye looking towards the future, even from this simple solution in a toy model, one can see that the theory of GR will contain singular solutions. In equation 2.270 as $t \to 0$ the scale factor shrinks to zero. The determinant of the metric tensor is proportional to $a(t)^6$ and therefore at $t = 0$ the metric becomes degenerate. The degeneracy of the metric is not a sufficient condition for identifying a singular point, as it may well indicate a coordinate singularity in which the chosen chart is no longer suitable. It does however indicate that the points at which the metric becomes degenerate certainly warrens further investigation. Typically one would calculate the curvature invariant and look at their regularity at points for which $g \to 0$. The solution can be checked for consistency against the second Friedmann equation. Additionally, the Hubble parameter can also be calculated exactly as

$$H_{\pm}(t) = \frac{\dot{a}_{\pm}(t)}{a_{\pm}(t)} = \pm\frac{1}{2t} \tag{2.271}$$

In the closed and open cases with $k = 1$ and $k = -1$ respectively, the Friedmann Equations can also be solved exactly. In the radiation-dominated closed spacetime, the first Friedmann equation becomes

$$\left(\frac{\dot{a}}{a}\right)^2 + \frac{1}{a^2} = \frac{8\pi G}{3}\rho_0 a^{-4} \tag{2.272}$$

which has the solution

$$a(t) = \sqrt{\frac{8\pi G\rho_0}{3} - t^2} \tag{2.273}$$

where we have set the integration constant to zero. This is a solution defined on a bonded domain $|t| \leq \sqrt{8\pi G\rho_0/3}$ where the scale factor goes to zero at the boundaries and reaches a global maximum at $a(0) = \sqrt{8\pi G\rho_0/3}$. Again we see that this solution has two points in time for which the metric becomes degenerate and the equations of motion are indeterminate. Just as with the flat dust filled universe we can also calculate the Hubble parameter explicitly as

$$H(t) = \frac{3t}{3t^2 - 8\pi G\rho_0} \tag{2.274}$$

Lastly in the open case with $k = -1$, one has the Friedmann Equation

$$\left(\frac{\dot{a}}{a}\right)^2 - \frac{1}{a^2} = \frac{8\pi G\rho_0}{3} a^{-4} \tag{2.275}$$

Equation 2.275 has the branching solution (where the integration constant has been set to zero)

$$a(t) = \sqrt{t^2 - \frac{8\pi G\rho_0}{3}} \tag{2.276}$$

defined on $|t| \geq \sqrt{8\pi G\rho_0/3}$. Similarly to the radiation dominated closed solution, $a(t) = 0$ on the boundaries $t = \pm\sqrt{8\pi G\rho_0/3}$ at which point the Friedmann equations become indeterminate. The Hubble parameter for the radiation dominated open solution is

$$H(t) = \frac{3t}{3t^2 - 8\pi G\rho_0} \tag{2.277}$$

Functionally, this is the same as the Hubble parameter for the closed solution in eq. 2.274, however it is defined on a different time interval. The two solutions are defined on non-intersecting branches of the same overall global function $H(t) = 3t/(t^2 - 8\pi G\rho_0)$.

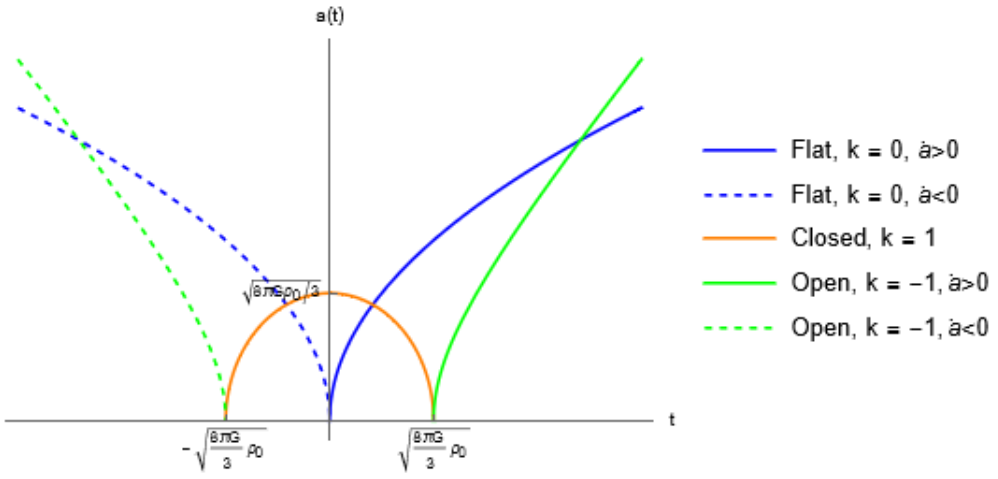

Figure 2.1: Plots of the scale factor solutions to the Friedmann Equations for a radiation dominated universe. In blue, the spatially flat $k = 0$ solution given by eq. 2.270. In orange, the closed $k = 1$ solution given by eq. 2.273. In green, the open $k = -1$ solution given by eq. 2.276. The contracting branches of the Flat and open solutions have been displayed in dashed to emphasise that they are separate solutions, defined on a different domain than the expanding solutions.

In figure 2.1 we plot the three solutions of the Friedmann Equations for a radiation dominated universe. In the case of flat spatial hypersurfaces, there exists an expanding and a contracting solution (blue, and blue/dashed respectively.), Likewise, in the open spacetime, there exist expanding and contracting solutions, in which the scale factor shrinks to zero at $t_0 = \pm\sqrt{8\pi G\rho_0/3}$. However the identification of $a(t_0) = 0$ is arbitrary as the time at which the scale factor becomes zero can simply be set to $t = 0$ with an appropriate choice of integration constant. As mentioned above we have simply set all integration constants to zero without loss of generality. It is important to note at this point that the solid and dashed curves in figure 2.1 represent separate solutions. In both solutions, the scale factor becomes zero at $t = 0$, at which point the equations of motion become undefined and GR does not tell us how to uniquely continue the dynamical variables beyond this point.

The closed universe has a much different dynamic than the flat and open cases. In the closed spacetime the scale factor is initially zero and the universe begins to expand at a decelerating rate before the scale factor reaches a maximum at

$a_{\max} = \sqrt{8\pi G\rho_0/3}$ in finite time. After reaching this maximum the spatial slices contract to zero size back to zero size. Thus the closed universe exists only for a finite amount of time, where as the flat and open universes can exist for arbitrarily long periods.

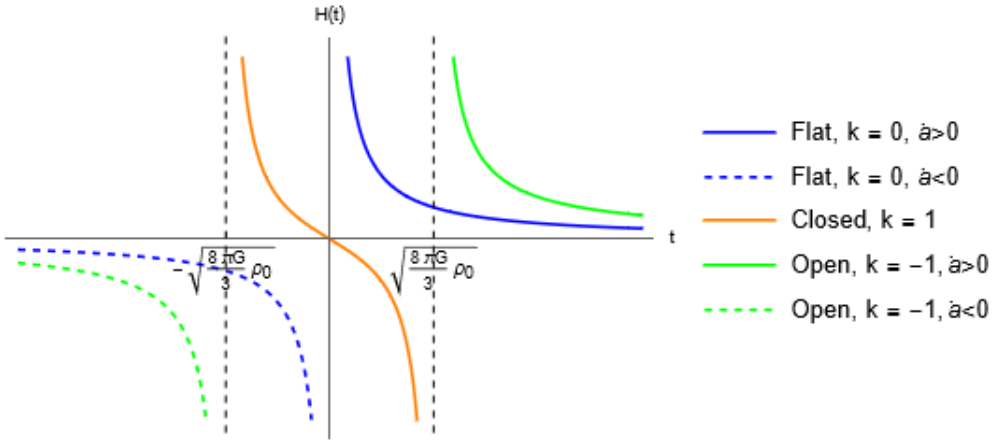

Figure 2.2: Plots of the Hubble parameters for a radiation dominated universe. In blue, the spatially flat $k = 0$ solution given by eq. 2.270. In orange, the closed $k = 1$ solution given by eq. 2.273. In grange, the open $k = -1$ solution given by eq. 2.276. For flat and open universes, the expanding solutions are given in bold and the contracting solutions in dashed.

In figure 2.2 we plot the Hubble parameters for a radiation dominated universe in the flat, closed and open spacetimes given by $k = 0, 1, -1$ respectively. The Hubble parameter can be interpreted as a normalised expansion rate of the universe. As such we see that in all three cases, as the scale factor approaches zero, the Hubble parameter grows unboundedly. In the particular case of the open universe the Hubble factor goes to zero at $t = 0$ which is when the scale factor reaches its maximum, as we should expect since $H = \dot{a}/a$ and therefore the Hubble factor is zero when the scale factor is instantaneously stationary.

2.2.2.3 Dust/Matter Dominated Solution

In section 2.2.2.1 we described an approximation in which the matter content of spacetime can be considered, on cosmological scales, to consist of non-relativistic, slow moving massive dust particles, with an equation of state $p = 0$, and hence

state parameter $w = 0$. In which case the matter energy density scales with $a(t)$ as $\rho = \rho_0 a(t)^{-3}$, given by eq. 2.264. The Friedmann Equations 2.255 can be solved exactly in this case. The first Friedmann Equation for a matter dominated universe becomes

$$\dot{a}^2 + k^2 = \frac{8\pi G}{3}\rho_0 a^{-1} \tag{2.278}$$

We consider first the case of flat spatial slices for which $k = 0$ and one has

$$a^{\frac{1}{2}}\dot{a} = \pm\sqrt{\frac{8\pi G}{3}\rho_0} \tag{2.279}$$

Equation 2.279 has an expanding solution defined on $t \geq 0$

$$a(t) = (6\pi G\rho_0)^{\frac{1}{3}}\, t^{\frac{2}{3}} \tag{2.280}$$

and a contracting solution defined on $t \leq 0$ given by

$$a(t) = (6\pi G\rho_0)^{\frac{1}{3}}\, (-t)^{\frac{2}{3}} \tag{2.281}$$

With the respective Hubble parameters given by the $t > 0$ and $t < 0$ branches of

$$H(t) = \frac{2}{3t} \tag{2.282}$$

In the closed spacetime with $k = 1$, the Friedmann Equation is

$$\left(\frac{\dot{a}}{a}\right)^2 + \frac{1}{a^2} = \frac{8\pi G\rho_0}{3}a^{-3} \tag{2.283}$$

In this case, the equation of motion for a is most easily solved by making a coordinate transformation to conformal time η. The conformal time is a change of the timelike coordinate given by

$$d\eta = \frac{1}{a}dt \tag{2.284}$$

or equivalently

$$\eta(t) = \int \frac{1}{a(t)} dt \tag{2.285}$$

In conformal time the FLRW metric 2.236 takes the form

$$ds^2 = a(\eta)^2 \left(-d\eta^2 + \frac{1}{1-kr} dr^2 + r^2 d\theta^2 + r^2 \sin^2\theta d\phi^2 \right) \tag{2.286}$$

Thus it derives its name "conformal time" from that fact that in the case of flat spatial slices the metric is related to the Minkowski metric of special relativity by a conformal transformation

$$g_{\mu\nu}(x) = a^2(x)\eta_{\mu\nu} \tag{2.287}$$

The conformal transformation is a change of coordinates that acts as an angle-preserving rescaling of the lengths measured by the metric. Conformal transformations are not ot be confused with Weyl transformations, they look alike but there is a subtle distinction to be aware of. A conformal transformation is fundamentally a change of coordinates which pulls a positive factor out of the metric. Whereas a Weyl transformation involves no coordinate transformation, and simply defines a new metric which is a positive scalar multiplied by the old metric.

In conformal time, the Friedmann equation for a matter dominated closed spacetime 2.283 becomes

$$a' = \pm\sqrt{\frac{1}{3} a \left(8\pi G\rho_0 - 3a\right)} \tag{2.288}$$

where $'$ denotes a derivative with respect to conformal time η. As with previous solutions, we expect to find two solutions defined on separate domains. This can be seen explicitly as follows. Equation 2.288 is separable, and letting $x = 3a/8\pi G\rho_0$ one finds

$$\int \frac{1}{\sqrt{x(1-x)}} dx = \pm(\eta - \eta_0) \tag{2.289}$$

The integral in eq. 2.289 is calculated using the substitution $\sqrt{1-x} = \sin\theta$ which

results in

$$\theta = \pm\frac{1}{2}\eta \tag{2.290}$$

where we have set the integration constant $\eta_0 = 0$ without loss of generality. We then have

$$\sqrt{1-x} = \pm\sin\frac{1}{2}\eta \tag{2.291}$$

From equation 2.291 it is clear that in the case $a' \geq 0$ the solution is restricted to $0 \leq \eta \leq 2\pi$ and in the case $a' \leq 0$ the solution is restricted to $-2\pi \leq \eta \leq 0$. In both cases solutions, the functional form of the scale factor, once we have traced back the transformation of variables, is the same

$$a(\eta) = \frac{4\pi G\rho_0}{3}\left(1-\cos\eta\right) \tag{2.292}$$

But just as has been mentioned in section 2.2.2.2, these are two separate solutions defined on domains with a single point of intersection $\eta = 0$, but the equations of motion cannot be defined at this point. The information contained in both solutions however is fully captured by considering only one branch, say $0 \leq \eta \leq 2\pi$, as one can move between solutions by a time translation $\eta \pm 2\pi$. Therefore we need only consider the solution over $0 \leq \eta \leq 2\pi$. Having changed to conformal time, we must account for this when computing the Hubble parameter

$$H(\eta) = \frac{1}{a(\eta)}\frac{da}{dt} = \frac{1}{a^2}\frac{da}{d\eta} \tag{2.293}$$

Thus the Hubble parameter for a matter-dominated closed spacetime is

$$H(\eta) = \frac{3}{4\pi G\rho_0}\frac{\sin\eta}{\left(1-\cos\eta\right)^2} \tag{2.294}$$

Similarly to the radiation dominated closed universe, the spacetime scale factor is initially at zero and then begins to grow causing the spatial slices of the manifold to expand before becoming stationary at $\eta = \pi$, at which point the scale factor is at a

local maximum of $a_{\max} = 8\pi G\rho_0/3$. For $\pi < \eta \leq 2\pi$ the scale factor begins to shrink and the universe collapses back to zero size at $\eta = 2\pi$. Again we have a scenario where the closed universe can only exist for a finite amount of time $\Delta\eta = 2\pi$.

Lastly we have the open solution, for which the equation of motion in terms of coordinate time t is

$$\left(\frac{\dot{a}}{a}\right)^2 - \frac{1}{a^2} = \frac{8\pi G\rho_0}{3}a^{-3} \tag{2.295}$$

Again, this is most easily solved in conformal time, for which the equation of motion is

$$a' = \pm\sqrt{\frac{1}{3}a\left(8\pi G\rho_0 + 3a\right)} \tag{2.296}$$

In this case there are again two solutions with the same functional form, but defined on the domains $-\infty < \eta \leq 0$ and $0 \leq \eta < \infty$

$$a(\eta) = \frac{4\pi G\rho_0}{3}\left(\cosh\eta - 1\right) \tag{2.297}$$

with Hubble parameter

$$H(\eta) = \frac{3}{4\pi G\rho_0}\frac{\sinh\eta}{\left(\cosh\eta - 1\right)^2} \tag{2.298}$$

For the sake of consistency with the closed and open solutions, we may also write the flat solution 2.280 in terms of conformal time, which can be easily calculated as

$$a(\eta) = \frac{2\pi G\rho_0}{3}\eta^2 \tag{2.299}$$

with Hubble parameter

$$H(\eta) = \frac{3}{\pi G\rho_0}\frac{1}{\eta^3} \tag{2.300}$$

We can see explicitly that if one calculates the coordinate time $t(\eta)$ given by eq. 2.285

$$t(\eta) = \int a(\eta)d\eta = \frac{2\pi G\rho_0}{9}\eta^3 \tag{2.301}$$

then the Hubble parameter in terms of conformal time 2.300 reduces to exactly the Hubble parameter calculated in coordinate time 2.282.

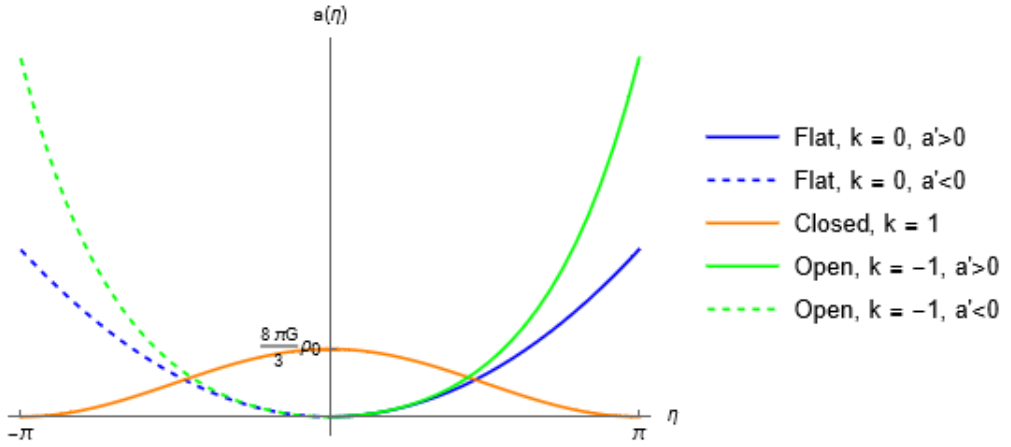

Figure 2.3: Plots of the scale factor solutions to the Friedmann Equations as functions of conformal time η, for a matter dominated universe. In blue, the spatially flat $k = 0$ solution given by eq. 2.299. In orange, the closed $k = 1$ solution given by eq. 2.292, where we have translated by $\eta + \pi$ without loss of generality, so that the function is centred on $\eta = 0$. In green, the open $k = -1$ solution given by eq. 2.297. The contracting branches of the flat and open solutions have been displayed in dashed to emphasise that they are separate solutions, defined on a different domain than the expanding solutions.

In figure 2.3 we plot the solutions to the matter dominated Friedmann Equations for the three distinct spatial topologies. In the case of flat spatial slices, we see that there are expanding (and contracting) solutions just as in the case of a radiation dominated universe, where the scale factor grows unboundedly as $\eta \to \infty$ and approaches zero as $\eta \to 0$. The open solution has the same qualitative behaviour but with the scale factor taking a different functional form. In the matter dominated closed solution, we also have the same qualitative behaviour as the radiation dominated closed universe, the scale factor initially starts at zero and the spatial slices expand at a decreasing rate until the scale factor reaches a maximum value $a_{\max} = 8\pi G\rho_0/3$, after which the universe undergoes recollapse back to zero size.

In figure 2.4 we plot the Hubble parameters for matter dominated solutions of the Friedmann equations in the three distinct spatial topology cases. As we would now come to expect, the Hubble parameters grow unboudedly where $a \to 0$, and in

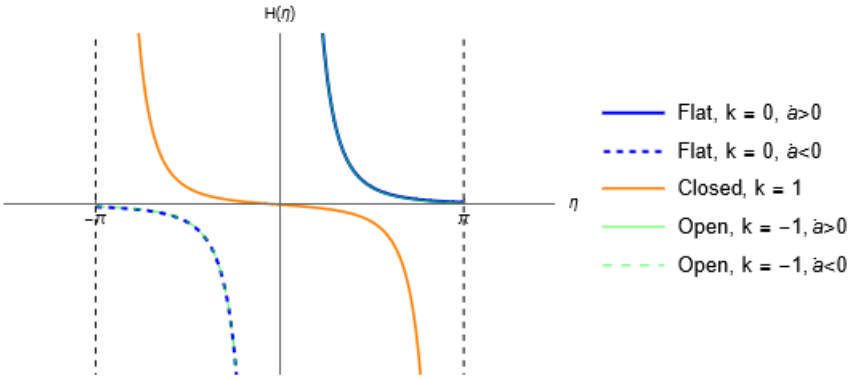

Figure 2.4: Plots of the Hubble parameters as functions of conformal time η, for a matter dominated universe. In blue, the spatially flat $k = 0$ solution given by eq. 2.299. In orange, the closed $k = 1$ solution given by eq. 2.292. As in figure 2.3 we have translated by $\eta + \pi$ without loss of generality, so that the Hubble parameter function is centred on $\eta = 0$. In green, the open $k = -1$ solution given by eq. 2.297. The open solution lies almost on top of the flat solution. The contracting branches of the flat and open solutions are displayed in dashed.

the case of a closed universe the Hubble factor is zero where $a(\eta)$ is stationary. We see also that the Hubble parameters for spatially flat and open solutions lie almost on top of each other, particularly for $|\eta| << \pi$. This should not come as too much of a surprise. If we consider the functional form of the open Hubble parameter

$$H(\eta; k = -1) = \frac{3}{4\pi G\rho_0} \frac{\sinh \eta}{(\cosh \eta - 1)^2} \tag{2.302}$$

and the flat Hubble parameter

$$H(\eta; k = 0) = \frac{3}{\pi G\rho_0} \frac{1}{\eta^3} \tag{2.303}$$

For sufficiently small η we have the truncated Taylor series

$$\sinh \eta \approx \eta, \quad \cosh \eta \approx 1 + \frac{1}{2}\eta^2 \tag{2.304}$$

and thus we calculate explicitly

$$H(\eta; k = -1) \approx \frac{3}{\pi G\rho_0} \frac{1}{\eta^3} := H(\eta; k = 0) \tag{2.305}$$

2.2.2.4 Vacuum Dominated Solution

In section 2.2.2.1 we treated the possible presence of a cosmological vacuum energy as equivalent to a contribution to the stress energy tensor from matter with a state parameter $w = -1$. As one would expect from a vacuum energy, the energy density is constant $\rho(t) = \rho_\Lambda$. This considerably simplifies the Friedmann Equations 2.255. In this case the first Friedmann equation becomes

$$\left(\frac{\dot{a}}{a}\right)^2 + \frac{k}{a^2} = \frac{8\pi G}{3}\rho_\Lambda \tag{2.306}$$

Just as in the radiation and matter dominated cases, eq. 2.306 can be solved for each of the three distinct spatial topologies.

$$\begin{aligned}
\underline{\textbf{Flat, k = 0:}} \quad & a(t) = e^{\pm Ht} \\
& H = \pm\sqrt{\frac{8\pi G\rho_\Lambda}{3}} \\
\underline{\textbf{Closed, k = 1:}} \quad & a(t) = \sqrt{\frac{3}{8\pi G\rho_\Lambda}}\cosh\left(\sqrt{\frac{8\pi G\rho_\Lambda}{3}}t\right) \\
& H(t) = \sqrt{\frac{8\pi G\rho_\Lambda}{3}}\tanh\left(\sqrt{\frac{8\pi G\rho_\Lambda}{3}}t\right) \\
\underline{\textbf{Open, k = -1:}} \quad & a(t) = \begin{cases} \sqrt{\frac{3}{8\pi G\rho_\Lambda}}\sinh\left(\sqrt{\frac{8\pi G\rho_\Lambda}{3}}t\right) & t \geq 0 \\ \sqrt{\frac{3}{8\pi G\rho_\Lambda}}\sinh\left(-\sqrt{\frac{8\pi G\rho_\Lambda}{3}}t\right) & t \leq 0 \end{cases} \\
& H(t) = \sqrt{\frac{8\pi G\rho_\Lambda}{3}}\coth\left(\sqrt{\frac{8\pi G\rho_\Lambda}{3}}t\right)
\end{aligned} \tag{2.307}$$

In the case of flat FLRW, the scale factor is non-zero for finite t, and goes to zero as $t \to \infty$ (in the expanding $a = e^{Ht}$ case) and is increasing exponentially with coordinate time. Similarly in the case of closed, the scale factor is also non zero and increasing exponentially with time. Indeed this is not a coincidence. One can define

a larger 5-dimensional space $\mathbb{R}^5$ with Lorentzian metric

$$ds^2 = -dv^2 + dw^2 + dx^2 + dy^2 + dz^2 \tag{2.308}$$

and embed into it the hyperboloid defined by

$$-v^2 + w^2 + x^2 + y^2 + z^2 = \frac{3}{8\pi G\rho_\Lambda} \tag{2.309}$$

which has constant positive scalar curvature $R = 16\pi G\rho_\Lambda$

New coordinates (t, ψ, θ, ϕ) can be defined on the hyperboloid

$$v = \sqrt{\frac{3}{8\pi G\rho_\Lambda}} \sinh\left(\sqrt{\frac{3}{8\pi G\rho_\Lambda}} t\right), \quad w = \sqrt{\frac{3}{8\pi G\rho_\Lambda}} \cosh\left(\sqrt{\frac{3}{8\pi G\rho_\Lambda}} t\right) \cos\psi$$

$$x = \sqrt{\frac{3}{8\pi G\rho_\Lambda}} \cosh\left(\sqrt{\frac{3}{8\pi G\rho_\Lambda}} t\right) \sin\psi\cos\theta \quad y = \sqrt{\frac{3}{8\pi G\rho_\Lambda}} \cosh\left(\sqrt{\frac{3}{8\pi G\rho_\Lambda}} t\right) \sin\psi\sin\theta\cos\phi$$
$$z = \sqrt{\frac{3}{8\pi G\rho_\Lambda}} \cosh\left(\sqrt{\frac{3}{8\pi G\rho_\Lambda}} t\right) \sin\psi\sin\theta\sin\phi \tag{2.310}$$

In these coordinates the induced metric on the hyperboloid takes the form

$$ds^2 = -dt^2 + \frac{3}{8\pi G\rho_\Lambda} \cosh^2\left(\sqrt{\frac{8\pi G\rho_\Lambda}{3}} t\right) \left(d\psi^2 + \sin^2\psi d\theta^2 + \sin^2\psi\sin\theta d\phi^2\right) \tag{2.311}$$

The entire sub manifold is covered by the new coordinates $-\infty < t < \infty$, $0 \leq \psi \leq \pi$, $0 \leq \theta \leq \pi$, $0 \leq \phi \leq 2\pi$, except where the metric is degenerate $\psi, \theta = 0, \pi$. The induced metric in equation 2.311 we recognise as the vacuum dominated closed solution to the Friedmann equations 2.307. The spatial slices with constant t are submanifolds of $\mathbb{R}^5$ with constant positive curvature. A different set of coordinates

on the hyperbolid

$$\begin{aligned} t' &= \sqrt{\frac{3}{8\pi G\rho_\Lambda}} \ln\left[(v+w)\sqrt{\frac{8\pi G\rho_\Lambda}{3}}\right] \\ x' &= \frac{x}{v+w}\sqrt{\frac{3}{8\pi G\rho_\Lambda}}, \quad y' = \frac{y}{v+w}\sqrt{\frac{3}{8\pi G\rho_\Lambda}}, \quad z' = \frac{z}{v+w}\sqrt{\frac{3}{8\pi G\rho_\Lambda}} \end{aligned} \tag{2.312}$$

yields the induced metric

$$ds^2 = -dt'^2 + e^{2\sqrt{\frac{8\pi G\rho_\Lambda}{3}}t'}\left(dx'^2 + dy'^2 + dz'^2\right) \tag{2.313}$$

The timelike coordinate is defined for $v + w > 0$ only and the spatial coordinates are undefined for $w + v = 0$, so this chart covers only half of the higher dimensional $\mathbb{R}^5$ manifold, excluding the line $w + v = 0$. The constant t' hypersurfaces are ones of constant zero curvature. We recognise this metric again as the vacuum dominated flat space solution to the Friedmann Equations 2.307.

A third set of coordinates can be defined on the submanifold

$$\begin{aligned} v &= \sqrt{\frac{3}{8\pi G\rho_\Lambda}}\sinh\left(\sqrt{\frac{8\pi G\rho_\Lambda}{3}}t\right)\cosh\psi, \quad w = \sqrt{\frac{3}{8\pi G\rho_\Lambda}}\cosh\left(\sqrt{\frac{8\pi G\rho_\Lambda}{3}}t\right) \\ x &= \sqrt{\frac{3}{8\pi G\rho_\Lambda}}\sinh\left(\sqrt{\frac{8\pi G\rho_\Lambda}{3}}t\right)\cos\theta, \quad y = \sqrt{\frac{3}{8\pi G\rho_\Lambda}}\sinh\left(\sqrt{\frac{8\pi G\rho_\Lambda}{3}}t\right)\sin\theta\cos\phi \\ z &= \sqrt{\frac{3}{8\pi G\rho_\Lambda}}\sinh\left(\sqrt{\frac{8\pi G\rho_\Lambda}{3}}t\right)\sin\theta\sin\phi \end{aligned} \tag{2.314}$$

which cover only the $w > 0$ part of the manifold. The metric in these coordinates is

$$ds^2 = -dt^2 + \frac{3}{8\pi G\rho_\Lambda}\sinh^2\left(\sqrt{\frac{8\pi G\rho_\Lambda}{3}}t\right)\left(d\psi^2 + \sinh^2\psi d\theta^2 + \sinh^2\psi\sin^2\theta d\phi^2\right) \tag{2.315}$$

Equation 2.315 is the metric of the vacuum dominated open FLRW spacetime. We see clearly now that each of the three cases represent flat, closed and open slicing

of the same underlying spacetime manifold of constant positive scalar curvature $R = 16\pi G\rho_\Lambda$, which is referred to as de Sitter space. Each case is a particular coordinated choice on the manifold. The choices of coordinates for the flat and open spatial slicing are not fully extendable and are incapable of describing the entire spacetime, where as the closed spatial slicing can describe the entirety of de Sitter space. Furthermore, from the fact that the scalar curvature is well defined everywhere and the fact that the closed slicing, which described all of de Sitter space, has $a > 0$, it is clear that when $a \to 0$ in the flat and open slicing this represents a coordinate singularity.

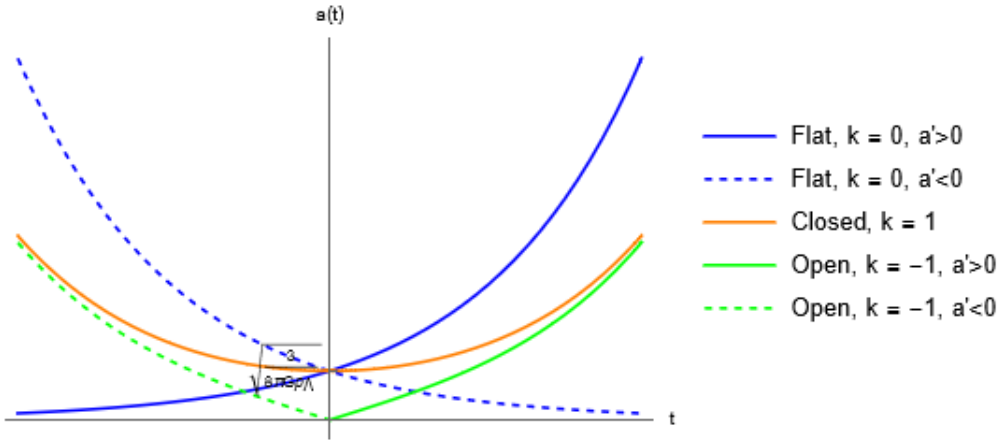

Figure 2.5: Plots of the scale factor solutions to the Friedmann Equations for a vacuum dominated universe given by eq. 2.307. In blue, the spatially flat $k = 0$, where we have chosen $a(0) = \sqrt{3/8\pi G\rho_\Lambda}$. In orange, the closed $k = 1$ solution. In green, the open $k = -1$ solution. The contracting branches of the flat and open solutions have been displayed in dashed to emphasise that they are separate solutions, defined on a different domain than the expanding solutions.

In figure 2.5 we plot the solutions to the vacuum dominated Friedmann Equations given in eq. 2.307, choosing to set $a(0) = \sqrt{3/8\pi G\rho_\Lambda}$ which we may do arbitrarily as the Friedmann equations are insensitive to an overall scaling of $a(t)$ by a positive non-zero factor. Likewise this does not affect the Hubble parameter $H = \dot{a}/a$. In the radiation and vacuum dominated cases, the closed solutions were convex functions with the scale factor shrinking to zero at the boundaries and as such, the closed universes can exist only for finite amounts of time. In the vacuum dominated case,

we see that the scale factor is a concave function, reaching a global minimum at $a(0) = \sqrt{3/8\pi G\rho_\Lambda}$.

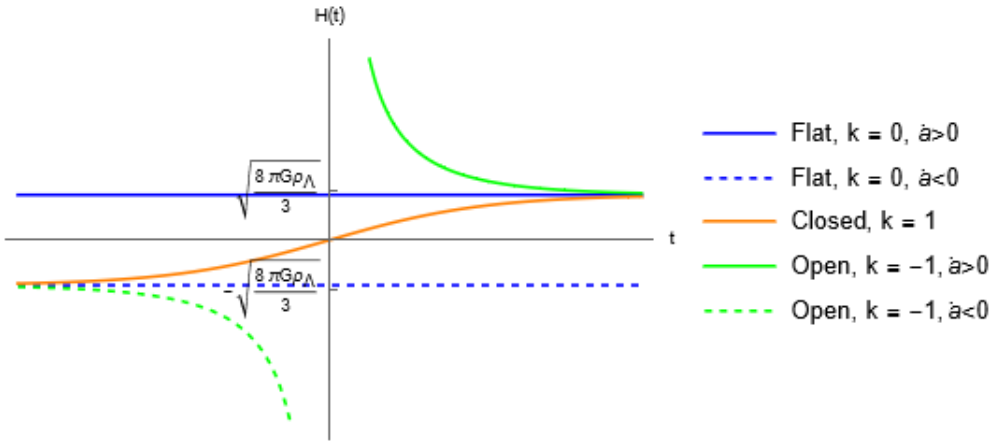

Figure 2.6: Plots of the Hubble parameters for a vacuum dominated universe, given in equation 2.307. In blue, the spatially flat $k = 0$ solution. In orange, the closed $k = 1$ solution. In green, the open $k = -1$ solution. The contracting branches of the flat and open solutions are displayed in dashed.

Figure 2.6 shows the Hubble parameter functions for a vacuum dominated universe for the three distinct spatial topologies. As we would have expected, for the flat and closed universe, the Hubble parameter is well defined everywhere as the scale factor is non-zero for all time, and in the case of open spatial slices, the scale factor goes to zero as $t \to 0$ and thus the Hubble factor diverges as $t \to 0$ from either side. In all three cases, the scale factor is exponential $a \sim e^{\sqrt{8\pi G\rho_\Lambda/3}t}$ for large t and so the Hubble parameters converge as $t \to \pm\infty$ to a constant value $\pm\sqrt{8\pi G\rho_\Lambda/3}$.

2.2.2.5 Curvature Dominated Solution

We now turn briefly to the final case of curvature domination, we consider the energy density of matter in the universe to be negligible in comparison to the contribution of the curvature term in the Friedmann Equations. The Friedmann Equations in such as case reduce to

$$\left(\frac{\dot{a}}{a}\right)^2 = -\frac{k}{a^2} \tag{2.316}$$

The left hand side of eq. 2.316 is strictly greater than or equal to zero, and we

therefore must have $k \leq 0$. The $k = 0$ case results in the trivial static solution $\dot{a} = 0$ where the scale of the spatial slices is constant for all time. The non-trivial solution requires negative spatial curvature and it is restricted to the open geometry with $k = -1$. The equation of motion is easily solved in this case with $a(t) = t$ and $H(t) = t^{-1}$.

2.2.3 Cosmological Observables and Thermal History of the Universe

We now understand the behaviour of the scale factor and Hubble parameters in the approximations where the matter content of the universe is dominated particular kinds of perfect fluids, the energy density of each scaling with $a(t)$ as $\rho_i(t) \sim a(t)^{-n_i}$ for some $n \geq 0$. But in reality, the universe does not contain only one type of matter we know that there exist high energy relativistic particles as well as cold, non-relativistic matter. There is also no apriori reason to rule out a contribution from a vacuum energy and potential spatial curvature. Generally, we should include all the kinds o matter we have discussed in the Friedmann equations

$$H^2 + \frac{k}{a^2} = \frac{8\pi G}{3} \sum_i \rho_i(t) \tag{2.317}$$

where the index i runs over the vacuum, matter and radiation energy densities respectively. Recalling the scaling of each energy density with the scale factor, and that the curvature term can be thought of as equivalent to an energy density we may write

$$H^2 = \frac{8\pi G}{3} \left(\rho_\Lambda + \rho_k a^{-2} + \rho_m a^{-3} + \rho_r a^{-4} \right) \tag{2.318}$$

where $\rho_\Lambda, \rho_k, \rho_m$ and ρ_r are the vacuum, curvature, matter and radiation densities observed today ($a = 1$).

Equation 2.318 can equivalently be written in terms of the Hubble and density parameters observed when at the present time, which we denote H_0 & Ω_i.

$$\left(\frac{H}{H_0}\right)^2 = \Omega_\Lambda + \Omega_k a^{-2} + \Omega_m a^{-3} + \Omega_r a^{-4} \tag{2.319}$$

In the literature, it is conventional to work in terms of a variable z, rather than the scale factor which we define by

$$a(t) = \frac{1}{1+z} \tag{2.320}$$

z is called the redshift and acts as a physical measure of cosmological time. It derives its name from one of the most fundamental pieces of observational evidence for an expanding universe, the cosmological redshifting of light.

2.2.3.1 Horizons

Simply by inspecting the units of the Hubble parameter we can see that it has units of inverse time and so the Hubble constant H_0 defines a length scale (in units where $c = 1$) and $1/H_0$ defines a time scale. This is even more apparent when using the Hubble parameter to compute the age of the universe. Using equation 2.319 and the definition of redshift z one can write

$$H(z) = H_0\sqrt{E(z)}, \quad E(z) = \Omega_\Lambda + \Omega_k(1+z)^2 + \Omega_m(1+z)^3 + \Omega_r(1+z)^4 \tag{2.321}$$

The Hubble factor in terms of redshift is

$$H = \frac{da}{dt} = -\frac{1}{(1+z)^2}\frac{dz}{dt} \tag{2.322}$$

Thus equation 2.321 can be integrated from $t = 0, z = \infty$ to the present day $t, z = 0$.

$$t = \frac{1}{H_0}\int_0^\infty \frac{1}{(1+z)^2\sqrt{E(z)}}dz \tag{2.323}$$

This calculation is of course model dependant as one needs to know the density parameters Ω_i. However we can see that generically $t \sim H_0^{-1}$ and so the inverse Hubble parameter truly represents a cosmological time scale.

It is useful at this point to discuss two physical length scales that are defined using the Hubble parameter. The first is the notion of a ***Particle Horizon***. The particle horizon is the maximum comoving distance a light signal can reach between being emitted at the Big Bang t_0 and some later time t when we observe it. In calculating this, we may always choose our frame such that the light travels on a radial null geodesic and thus the line element reads

$$dt^2 = \frac{a^2(t)}{1-kr^2}dr^2 \tag{2.324}$$

And thus the comoving distance is

$$\chi_p(t) = \int_{t_0}^{t} \frac{1}{a}dt = \int_{\ln a_0}^{\ln a} \frac{1}{aH} d\ln a = \eta - \eta_0 \tag{2.325}$$

where η is conformal time. The proper horizon, which is the manifold distance is then $d_p(t) = a(t)\chi_p(t)$. The term "horizon" derives from the fact that the particle horizon tells us the maximum distance light could have travelled to us have travelled to us if it were emitted at the Big Bang. Anything at distances larger than the particle horizon would lie outside out past light cone and so the particle horizon represents a boundary between the observable and observable universe.

Just as the particle horizon of an observer defines the boundary between past events that they could and could not have been in casual contact with, it is also possible to define the boundary between future events that they could and could not be in causal contact with. Consider an observer at $r = 0$ who emits a light signal along a radial null geodesic at time t, then the maximum comoving distance of an observer who can receive the signal is

$$\chi_e(t) = \int_t^\infty \frac{1}{a} dt = \int_{\ln a}^{\ln a_\infty} \frac{1}{aH} d\ln a = \eta_\infty - \eta = \int_0^R \frac{1}{\sqrt{1-kr^2}} dr \tag{2.326}$$

Any observer at a comoving distance $r > R$ will not be able to receive the signal and is this out of future causal contact. Provided that the integral

$$\chi_e(t) = \int_t^\infty \frac{1}{a} dt \tag{2.327}$$

converges, the comoving distance χ_e is called the ***event horizon*** of the observer at $(t, r = 0)$. It also may not be the case that $a(t)$ is globally monotonic, and that there exists a global maximum $a(t_{\max}) = a_{\max}$ and that the universe undergoes a recollapse, in which case the event horizon is defined analogously as

$$\chi_e(t) = \int_t^{t_{\max}} \frac{1}{a} dt \tag{2.328}$$

It is important to note that the horizons $\chi_p(t)$ and $\chi_e(t)$ defined here are different from the casual horizons defined in the context of the Hawking-Penrose singularity theorems [29] as $\chi_p(t)$ and $\chi_p(t)$ are explicitly observer-dependant.

The particle and event horizon may or may not exist depending on the choice of model and observer. In the case of an FLRW cosmology, the conditions for the existence of horizons can be easily investigated. As an example we may show this for the flat spatial slices $k = 0$, although horizons exist in all three constant curvature regimes. Consider again the perfect fluid, for which we have already derived the scaling of the energy density with the scale factor in eq 2.264 $\rho = \rho_0 a^{-3(1+w)}$. The 1st Friedmann equation then becomes

$$H^2 = H_0^2 a^{-3(1+w)} \quad H_0^2 = \frac{8\pi G}{3}\rho_0 \tag{2.329}$$

Recalling the definition of the Hubble parameter $H = \dot{a}/a$, equation 2.329 can be

integrated to obtain

$$\frac{2}{3(1+w)}a^{\frac{3}{2}(1+w)} = H_0 t \tag{2.330}$$

for $w \neq 1$, where we have assumed an expanding universe and thus taken the positive square root and set the integration constant to zero. The Hubble parameter associated with the solution 2.330 is

$$H = \frac{2}{3(1+w)t} \tag{2.331}$$

We can thus calculate the particle horizon of an observer at time t using he integral definition 2.325

$$\begin{aligned}\chi_p(t) &= \int_0^t \frac{1}{a} dt \\ &= \left[\frac{3(1+w)}{2}H_0\right]^{-\frac{2}{3(1+w)}} \int_0^t t^{-\frac{2}{3(1+w)}}\, dt \\ &\sim \left[t^{\frac{1+3w}{3(1+w)}}\right]_0^t\end{aligned} \tag{2.332}$$

In order for the lower limit of the integral to converge we require

$$\frac{1+3w}{3(1+w)} > 0 \implies w > -\frac{1}{3} \text{ or } w < -1 \tag{2.333}$$

Indeed the bound of $w > -1/3$ is satisfied by the dust and radiation classifications of matter that we explored in section 2.2.2.1. This condition for the existence of a particle horizon also imposes that the universe is accelerating, one can see this through the second Friedmann equation 2.255

$$\begin{aligned}\frac{\ddot{a}}{a} &= -\frac{4\pi G}{3}(\rho + 3p) \\ &= -\frac{4\pi G}{3}\rho(1+3w)\end{aligned} \tag{2.334}$$

since $w > -1/3$ enforces $\ddot{a} > 0$ and therefore the universe is accelerating. However the conditions for the existence of a particle horizon are not necessarily the same as

those for the existence of an event horizon. From the definition of the event horizon $\chi_e(t)$ in equation 2.328, which is essentially the same as the particle horizon but with different limits of integration, we have

$$\chi_e(t) \sim \left[t^{\frac{1+3w}{3(1+w)}} \right]_t^\infty \tag{2.335}$$

The upper limit of integration will converge for $-1 < w < -1/3$, and so for the same observer, we cannot have the existence of both a particle horizon and an event horizon simultaneously.

2.2.3.2 Cosmological Redshift

In this section we will derive the redshifting of light due to FLRW expansion of the universe through Killing vector field arguments. For the sake of demonstration we will first consider the simplest case of flat spatial slices, the metric is thus

$$ds^2 = -dt^2 + a^2(t)(dx^2 + dy^2 + dz^2) \tag{2.336}$$

but we need not specify the matter content filling the spacetime. The metric is obviously independent of all spatial coordinates and thus ∂_x, ∂_y & ∂_z are Killing vector fields on the spacetime. Consider now a light signal emitted at a point p_1 on the manifold and then received by a stationary comoving observer at a point p_2 with 4-velocity u^μ. The light signal emitted at p_1 will follow a null geodesic to p_2 with tangent vector k^μ. Without loss of generality we may choose the projection of k^μ into the spatial slice at p_1, Σ_1 to be in the ∂_x direction. Since the projection is entirely in the ∂_x direction at p_1 we have $(k \cdot \partial_y)_{p_1} = (k \cdot \partial_z)_{p_1} = 0$. From our discussion of Killing vector field in section 2.2.1.1 we may use the fact that the inner products are conserved along geodesics, and thus at the observation point p_2, the projection of k^μ into the spatial slice Σ_2 is in the ∂_x direction, which is a Killing vector field $\xi = \partial_x$. Since the tangent vector is null, its projection onto the observers 4-velocity is equal in magnitude and opposite in sign as its projection into the spatial

slice Σ which is in the direction of the Killing vector field $\xi = \partial_x$ and we therefore have

$$k^\mu u_\mu = -k^\mu \frac{\xi_\mu}{|\xi|} \tag{2.337}$$

The frequency of the light as measured by the stationary comoving observer is $\omega = -k \cdot u$ and so the frequencies measured at p_1 and p_2 are

$$\omega_1 = -(k^\mu u_\mu)_{p_1} = \frac{(k^\mu \xi_\mu)_{p_1}}{|\xi|_{p_1}} \tag{2.338}$$

$$\omega_2 = -(k^\mu u_\mu)_{p_2} = \frac{(k^\mu \xi_\mu)_{p_2}}{|\xi|_{p_2}} \tag{2.339}$$

The norm of the Killing vector field $\xi = \partial_x$ at a point p is given by $|\xi|^2 = g_{\mu\nu}\xi^\mu\xi^\nu = a^2(t)$, so the norms at p_1 and p_2 compare as

$$\frac{|\xi|_{p_1}}{|\xi|_{p_2}} = \frac{a_1}{a_2} \tag{2.340}$$

Since ξ is a Killing vector field the inner product $k^\mu\xi_\mu$ is conserved along the geodesic so we have $(k^\mu\xi_\mu)_{p_1} = (k^\mu\xi_\mu)_{p_2}$. Thus the ratio of the frequencies is

$$\frac{\omega_2}{\omega_2} = \frac{a_1}{a_2} \tag{2.341}$$

Written in terms of the redshift variables this is

$$\frac{\omega_2}{\omega_1} = \frac{1+z_2}{1+z_1} \tag{2.342}$$

The scale factor at the present time in the earths frame is always taken to be unity,as we have mentioned we are free to choose this arbitrarily, which corresponds to a redshift of $z = 0$. Thus light reaching us emitted from a source in the past at redshift $z > 0$ is observed at a frequency

$$\omega_{\text{obs}} = \frac{\omega_{\text{emitted}}}{1+z} < \omega_{\text{emitted}} \tag{2.343}$$

Contextualising this result with the scaling of radiation energy density with the scale factor given in eq. 2.267, there is a clear interpretation that electromagnetic radiation emitted in the early universe cools as the universe expands due to the gravitational fields capacity to do work on it, and thus the spectrum of light that we observe emitted from distant astrophysical objects is shifted to a lower temperature than when it was originally produced. This can be seen explicitly when considering blackbody radiation. A blackbody spectrum observed today at a temperature T_o will have the spectrum [56]

$$B(\omega_o, T_o) = \frac{\hbar\omega_o^3}{2\pi^2 c^2} \frac{1}{e^{\frac{\hbar\omega_o}{k_B T_o}} - 1} \tag{2.344}$$

If the blackbody radiation is emitted from a source at redshift z, then each frequency ω_o will have been redshifted by $\omega_o = \omega_e/(1+z)$ and thus the source blackbody spectrum is

$$B_z(\omega_e, T_o) = \frac{\hbar\omega_e^3}{2\pi^2 c^2 (1+z)^3} \left(e^{\frac{\hbar\omega_e}{k_B T_o (1+z)}} - 1\right)^{-1} \tag{2.345}$$

The blackbody spectrum of equation 2.345 can be interpreted as having a temperature $T_e = T_o(1+z)$, thus the temperature of the blackbody spectrum observed today is cooler than an emitter in the past.

2.2.3.3 Thermal Evolution of The Universe; ΛCDM, HBB Theory

So far we have equipped ourselves with enough tools to understand that to understand some of the generic dynamics of the universe as we trace it's evolution back in time. In section 2.2.2.1 we derived solutions of the Friedmann Equations which gave a scale factor $a(t)$. We saw that quite generically, going backwards in coordinate time from the present day, the scale factor gets smaller and smaller, equivalent to a larger redshift value.

We derived scalings of the energy densities of different kinds of matter contributions with the scale factor and when written in terms of the density parameters observed in the present day, the Hubble parameter is

$$H^2 = H_0^2 \left[\Omega_\Lambda + \Omega_k a^{-2} + \Omega_m a^{-3} + \Omega_r a^{-4}\right] \tag{2.346}$$

Early in the universe when the scale factor is small, the dominant term in equation 2.346 will be the contribution from relativistic matter and the universe will be in a radiation dominated era, at later times the cold matter term will contribute more significantly and the universe will be matter dominated. After matter domination, there could be a period of curvature domination before finally all contributions are beaten out by the vacuum energy Ω_Λ. In section 2.2.3.2 we showed how as the universe expands, radiation becomes redshifted and cools, so conversely, at earlier times close to $a = 0$, the universe was much hotter and packed into a smaller length scale. Broadly speaking, the idea that the early universe was in a hot dense state that the cooled as it expanded and allowed for the formation familiar matter that we see today is known as the Hot Big Bang theory. We not here a subtle distinction in what we identify at the big bang, where the scale factor of the universe $a(t) \to 0$, and the HBB. When the scale factor reaches zero, the mathematical description of General Relativity fails to remain predictive and is considered to have broken down. However even before this point, around the scale of the Planck time t_p or equivalently at energy scales above the Planck mass M_{pl}, it is conventionally assumed that our classical description of gravity is no longer valid and that quantum gravity effects must be accounted for, in order to continue to describe the evolution of spacetime and matter dynamics beyond this point In section 5 we will show that it is possible to continue cosmological dynamical systems through the Big Bang in an entirely classical description. The HBB really regards thermal physics of the universe some short time after the universe exits this energy scale and our current understanding of gravity and the standard model of particle physics becomes accurate.

The first major event in the cosmological calendar is that of baryogensis. We observe today, thankfully, that there is a vast over abundance of matter compared to antimatter, thus at some point in the early universe matter and anti matter must have entered a state of asymmetry which resulted in a huge suppression in the amount of available antimatter in the universe. Very little is known about what time or temperature this happened, except that the universe exited baryogensis with an overabundence of matter. At energies above 100GeV the matter content of the universe would have consisted of a hot, dense plasma of fundamental particles, mainly electrons, positrons, photons, neutrinos, and asymptotically free quarks, with heavier species in negligible quantities. At around 100GeV electroweak symmetry breaking kicks in, particles gain mass through the Higgs mechanism and the electromagnetic and weak force become distinct. As the universe cools even further the universe undergoes a QCD phase transition as quark interactions begin to become dominated by the strong force at around 150MeV. The strong force interactions allow quarks to form protons and neutron bound states.

By this point in the evolution of the universe, it is far enough away from the gravitational extreme conditions of the Big Bang to assume that General Relativity is an appropriate description of gravity. Imposing the conditions of the cosmological principle, spacetime must follow the dynamics of an FLRW model. All particles in the primordial "soup" will be undergoing complicated interaction, at an interaction rate $\Gamma \sim n\sigma(T)$ where $n \sim a^{-3}$ is the number density of a given particle species and $\sigma(T)$ is the cross section of the leading order interaction at temperature T. The interaction rate defines an interaction time scale $\tau_I \sim a^3/\sigma(T)$. This interaction time tells us roughly the time scale that is needed for local thermalisation inside the particle horizon. The Hubble parameter also defines a natural characteristic time scale for the expansion of the universe $\tau_E \sim 1/H$. Thus if the interaction time (for a given particle species) is much shorter than the characteristic expansion time $\tau_I << \tau_E$, then particles will remain in equilibrium with the thermal bath. When the characteristic interaction and expansion times are on roughly the same

order $\tau_I \sim \tau_E$ the particle species begin to "***Freeze-Out***" as for $\tau_I >> \tau_E$ they cannot locally thermalise within the particle horizon. At freeze-out, the interactions of a given particle species essentially switch off and they exit equilibrium with the thermal bath and begin to travel through the universe relatively unimpeded on geodesic motion. Taking the $k = 0$ scale factor for a generic perfect fluid in equation 2.330 we have

$$\tau_I \sim \frac{t^{\frac{2}{1+w}}}{\sigma(T)}, \quad \tau_E \sim t \tag{2.347}$$

and thus assuming a sufficiently high cross section $\sigma(T)$ for high temperatures in the early universe, $\tau_I >> \tau_E$ and local thermalisation is possible. As the universe expands and cools, the cross sections for leading order processes get smaller and the particle species will eventually freeze-out. Different particle species will of course have different dominant interaction rates and thus we can expect them to freeze-out at different times.

The first particle species to freeze out are neutrinos, when the weak interaction rate falls below the expansion rate at a temperature $T \sim 1$MeV, around 1 second after the Big Bang. After the neutrinos freeze out and decouple from the thermal bath, the universe is left with a relic of cosmic background neutrinos. At around 1.5 second the proton $\leftrightarrow$ neutron interactions freeze out. The neutron mass is approximately 939MeV whereas the proton mass is about 1MeV lighter and are thus more abundant that neutrons at freeze out, resulting in a number density ratio of $n_n/n_p \sim 1/6$. When the temperature drops to the scale of the electron mass $T \sim$ 0.5MeV there is a significant cross section for electron-positron annihilation which produces photons (and the converse interaction, although this is less energetically favourable and thus has a smaller cross section). This interaction dumps energy into the photon bath, heating it above the temperature of the cosmic neutrino background. As the temperature of the thermal baths continues to drop below the scale of the electron mass, all of the positrons are annihilated, since there is already an overabundance of matter compared to antimatter, leaving behind an excess of electrons.

At around 3 minutes into the evolution of the universe and a temperature of $T \sim 10^9$K, the universe undergoes a period of Big Bang Nucleosynthesis in which the first light nuclei are formed. This comprises mainly of helium-4, about 25% by mass with small abundances of hydrogen and lithium and with higher mass elements in practically negligible amounts. Since these nuclei form in low amounts, there still exists a bath of free electrons present in the universe. It is not until the temperature of the universe drops by around 6 orders of magnitude to around 0.3eV or 4000K that the next significant event occurs at a time of approximately 10^5 years after the big bang. Below this temperature the cross section for Coulomb scattering of electrons and protons becomes less significant than that of hydrogen formation and photo disintegration of hydrogen nuclei becomes energetically disfavoured. This allows for the creation of much more neutral hydrogen by "***recombination***" of electrons and protons[3]. Before recombination, photons in the thermal bath were strongly coupled to free electrons through Thompson scattering, but recombination causes a rapid and significant drop in the number density of free electrons after which photons are frozen out and decouple from the thermal bath. This last scattering event happens at a redshift of around $z \sim 1100$ and leaves behind a cosmic background of photons that simply become redshifted as they travel through the universe. We observe these photons today as the CMB at a temperature of around 3K. The CMB represents the furthest back in time we can see the universe through the lens of electromagnetic radiation, since before it's formation any information becomes scrambled through many Thompson scattering events.

Our understanding of the CMB represents a hallmark of modern cosmology and it forms a crucial test for the predictions of General Relativity. The CMB is a blackbody thermal spectrum and so measurements of the spectrum allow us to determine its present day temperature of around $T = 2.7$K. From standard results in statistical thermodynamics we know that the energy density of a photon blackbody is proportional to T^4, specifically

[3]The name recombination is slightly misleading as electrons and protons involved in these reactions were not somehow previously combined.

$$\rho_\gamma = \frac{\pi^2}{15\hbar c^3}(k_B T)^4 \tag{2.348}$$

Thus CMB temperature measurements allow us to determine the energy density of the photon background. In order to determine the associated density parameter Ω_γ one also needs to know the Hubble constant H_0 in order to determine the critical density $\rho_c = 3H_0^2/8\pi G$. Measurements of the Hubble constant come primarily from two sources, type Ia supernovae ("standard candles") and Baryon Acoustic Oscillations (BAO) of the CMB. Current measurements of the Hubble constant from the Planck collaboration provide a value of $H_0 = 67.4 \pm 0.5 \text{kms}^{-1}\text{Mpc}^{-1}$ [4]. As we would expect, the photon density today is incredibly small $\Omega_\gamma \sim 10^{-5}$. This comprises most of the radiation density, but it is not the only contribution, the neutrino background also contributes to the overall radiation density. Measurements of the CMB and its anisotropies infact allow us to determine all of the present day density parameters, the collection of density parameters [4, 57, 58]

$$\Omega_\Lambda = 0.6847 \pm 0.0073,\ \Omega_k = 0.001 \pm 0.002,\ \Omega_m = 0.3153 \pm 0.0073,\ \Omega_r \sim 10^{-5} \tag{2.349}$$

essentially defines the Lambda-Cold Dark Matter (ΛCDM). The energy content of the present day universe is primarily dominated by a large vacuum energy density presence Ω_Λ. Radiation energy density has been diluted by the expansion of the universe to the point where it becomes a negligible contribution. The idea of "cold dark matter" is related to the matter density parameter Ω_m. Measurements of the universes baryon density parameter put it at $\Omega_b 0.0486 \pm 0.001$ [4]. Therefore there is a large missing contribution to the overall non-relativistic matter component Ω_m. This, combined with observations such as spiral galaxy rotation curves [59] has lead to the consideration that there must be some other form non relativistic, gravitationally interacting matter that contributes to the majority matter content of the universe, known as "Dark Matter".

2.2.3.4 The Flatness Problem

In the set of observed present day density parameters 2.349, the curvature component is incredibly small, to the point where curvature is practically negligible. In fact one can show that however small the density parameter is today, it must have been even smaller in the past. The first Friedmann equation when written in terms of the total density parameter Ω and spatial curvature k is

$$1 + \frac{k}{a^2 H^2} = \Omega \tag{2.350}$$

we can therefore track the evolution of Ω with the growth of the scale factor a, or in practise with the natural log of a, which turns out to be computationally more convenient and grows monotonically with a.

$$\begin{aligned} \frac{d\Omega}{d\ln a} &= a\frac{d\Omega}{da} \\ &= \frac{1}{H}\frac{d\Omega}{dt} \\ &= -\frac{2k}{\dot{a}^2 H^2}\frac{\ddot{a}}{a} \end{aligned} \tag{2.351}$$

For a universe dominated by a perfect fluid, the second Friedmann equation 2.255 gives the acceleration parameter

$$\begin{aligned} \frac{\ddot{a}}{a} &= -4\pi G\rho(1+3w) \\ &= -\frac{1}{2}H^2\Omega(1+3w) \end{aligned} \tag{2.352}$$

And so we have

$$\frac{d\Omega}{d\ln a} = (1+3w)\Omega(\Omega - 1) \tag{2.353}$$

From equation 2.353 it is clear that there are two fixed-point solutions, $\Omega = 0$ and $\Omega = 1$. The $\Omega = 0$ solution is the fully curvature dominated solution, which corresponds to a universe with no matter or vacuum energy content, only curvature. On the other hand the $\Omega = 1$ solution describes a universe with flat spatial slices.

Since we observe a universe today with almost no curvature, it's quite reasonable to investigate small perturbations around the $\Omega = 1$ solution. Considering such a small perturbation $\Omega(a) = 1 + \omega(a)$, we have the following equation of motion to first order in $\omega(a)$

$$\frac{d\omega}{d\ln a} = (1 + 3w)\omega \tag{2.354}$$

which is separable and has the solution

$$\omega(a) = \omega_0 a^{1+3w} \tag{2.355}$$

It is clear from equation 2.355 that the stability is of the $\Omega = 1$ fixed-point solution depends on the value of the state parameter w. For $1 + 3w < 0$, $\omega \to 0$ and $a \to \infty$, so the perturbations are killed off with the expansion of the universe and $\Omega = 1$ is a stable fixed point, however all ordinary matter that we know of, satisfying the strong energy condition has $1 + 3w > 0$, for which the perturbations grow with the scale factor. Assuming that the early universe could be accurately approximated as having gone through periods of radiation and matter domination, we would then expect that during these periods curvature perturbations should have grown. Because of these periods of presumed growth in curvature perturbations, however small we observe Ω_k to be today, it must have been even smaller in the past, somewhere close to, if not exactly zero. This situation is known as the "***Flatness Problem***", to observe such a small density parameter today, the universes initial density parameter at the time of the big bang must have been fine tuned to an incredible degree. There currently does not exist a particularly compelling argument as to why the universe should be fine tuned in such a way, and we will see in the following section that the dilution of the universes curvature can be explained without imposing such a fine tuning of its initial conditions.

2.2.3.5 The Horizon Problem

In section 2.2.3.1 we showed that for FLRW universes dominated by SEC satisfying matter, there exists a particle horizon for matter satisfying the SEC. The particle horizon which we calculated in eq 2.332 in terms of cosmic time t can also be written in terms of the scale factor a, which turns out to be more convenient for the purposes of considering the "***Horizon Problem***". We have the definition of the comoving particle horizon as

$$\chi_p(a) = \int_{\ln a_i}^{\ln a} \frac{1}{aH} d\ln a \tag{2.356}$$

The quantity $(aH)^{-1}$ is known as the Hubble radius, this represents roughly the comoving radius of spherical volume of spacetime that the cosmic observer is in causal contact with at time t. Taking the perfect fluid dominated FLRW spacetime, the first Friedmann equation is

$$H^2 = H_0^2 a^{-3(1+w)} \tag{2.357}$$

and thus the integral 2.356 can be calculated as

$$\begin{aligned} \chi_p(a) &= \frac{1}{H_0} \frac{2}{1+3w} \left[a^{\frac{1+3w}{2}} - a_i^{\frac{1+3w}{2}} \right] \\ &= \frac{2}{1+3w} \left[(aH)^{-1} - (aH)_i^{-1} \right] \end{aligned} \tag{2.358}$$

Taking the initial scale factor as $a_i = 0$, the particle horizon only exists for matter satisfying the SEC, and is dominated by the contribution from late times, as the Hubble radius grows with the scale factor.

$$\frac{d(aH)^{-1}}{da} = \frac{1+3w}{2} H_0^{-1} a^{\frac{-1+3w}{2}} \tag{2.359}$$

The growing Hubble sphere means that the comoving particle horizon today would be larger than the particle horizon at the time of recombination when the CMB is formed.

Another way of looking at this is that there must be a finite amount of conformal time between the big bang and the formation of the CMB since one has $\chi_p = \eta - \eta_i$. This finite amount of conformal time and the fact that the horizon would be bigger today than it was at the formation of the CMB, means that there should be patches of the CMB which have never been in causal contact. A detailed calculation can be performed with the measured density parameters 2.349, which allow us to write $H(z) = H_0\sqrt{E(z)}$ where

$$E(z) = \Omega_\Lambda + \Omega_k(1+z)^2 + \Omega_m(1+z)^3 + \Omega_r(1+z)^4 \tag{2.360}$$

The Horizon can be calculated in terms of redshift z

$$\chi_p(z, z_i) = \int_{a_i}^{a} \frac{1}{aH} da = \frac{1}{H_0} \int_{\frac{1}{1+z}}^{\frac{1}{1+z_i}} \frac{1}{(1+z)\sqrt{E(z)}} dz \tag{2.361}$$

Recombination occurred around a redshift of $z \sim 1100$, we can compare how the size of the horizon has changed from the Big Bang to the formation of the CMB and from the formation of the CMB to the present day. These horizons are $\chi_p(\text{CMB}) = \chi_p(1100, \infty)$ and $\chi_p(t_0) = \chi_p(0, 1100)$ respectively, and the integrals can be calculated numerically since the density parameters are known. One finds that we have

$$\chi_p(\text{CMB}) \approx \frac{0.06}{H_0}, \quad \chi_p(t_0) \approx \frac{3.1}{H_0} \tag{2.362}$$

In the small angle approximation, the causally disconnected patches should then be separated by a small angle such that $\chi_p(\text{CMB}) = \theta\chi_p(t_0)$, given the calculations of 2.362, $\theta \sim 1.1$ degrees. Therefore when looking at the CMB, we should expect that patches separated by more than about 1 degree should never have been in causal contact with each other. However observations of the CMB show that its temperature is uniform to about 1 part in 10^5 [4, 42, 60].

This outlines the Horizon Problem, the fact that the CMB appears to be in thermal equilibrium at scales well beyond what should be possible if the Hubble has been growing from the Big Bang onwards. The reader is referred to [61] for a more detailed overview of CMB temperature anisotropies.

2.2.4 Inflation

In sections 2.2.3.4 & 2.2.3.5 we showed that the CMB, whilst being a cornerstone of modern cosmology, also suggests some fundamental problems about our understanding of the universes history and evolution. In particular we saw that because the Hubble radius is increasing in the early universe, during periods of radiation and matter domination, patches of the CMB observed today at angles more than about 1 degree should never have been in causal contact. Yet they appear to be in thermal equilibrium with very small temperature fluctuations $\Delta T/T \sim 10^{-5}$. In the Horizon problem, we saw that due to the growing Hubble radius the dominant contribution to the particle horizon was from late times. This mean that there was a finite amount of conformal time between the Big Bang and the formation of the CMB, leading to patches with non-overlapping past light cones. This problem could be alleviated if there existed some period of time in the early universe for which the Hubble radius was shrinking for a sufficient amount of time. Simply through observing equation 2.359 we see that this is possible if the universe is dominated by and SEC violating fluid which has $w < -1/3$. Such a fluid would cause the expansion of the universe to accelerate, since Friedmann's second equation tells us that

$$\frac{\ddot{a}}{a} = -\frac{4\pi G}{3}\rho(1+3w) \tag{2.363}$$

Conveniently, this also provides a way to tackle the Flatness Problem. In our discussion of the Flatness Problem, we saw that early time perturbations in the density parameter would grow unless there was a period of domination by an SEC violating fluid, in which case these perturbations would get smaller as the scale factor

grows. This period of accelerated expansion is called "***Inflation***", a sufficient period of inflation could provide an explanation of the observed smallness of the density parameter and the homogeneity of the CMB.

To see how we might obtain such a period of inflation, consider the following time derivative of the Hubble radius

$$\frac{d(aH)^{-1}}{dt} = -\frac{1}{a}\left(1 - \varepsilon_H\right) \tag{2.364}$$

where

$$\varepsilon_H = -\frac{\dot{H}}{H^2} \tag{2.365}$$

is the first Hubble slow roll parameter. For the Hubble sphere to be shrinking i.e. a period of inflation, we require $\varepsilon_H < 1$. Recall in section 2.2.2.1, we discussed vacuum dominated solutions to the Friedmann equations and saw that a perfect fluid with negative pressure was able to produce and exponentially increasing scale factor $a \sim e^{Ht}$ with constant Hubble parameter H. Such a fluid could then produce the require inflationary effects, and would correspond to $\varepsilon_H = 0$, since $\dot{H} = 0$. This is referred to as quasi-de Sitter inflation, during inflation the spacetime is approximately de Sitter, however it cannot be perfectly de Sitter otherwise there would be no end to inflation and we would still be experiencing it today. Thus more realistically, the universe would require some period of quasi-de Sitter inflation where $H \approx$ constant for some finite amount of time. The amount of inflation experienced by the universe is usually discussed in terms of e-folds N, defined by $a = e^N$, rather than the amount of coordinate time that has passed. In order to resolve the Horizon and Flatness problem, one typically needs around 60 e-folds of inflation [30,62]. The first Hubble slow roll parameter can be written in terms of the e-folds of inflation simply as

$$\varepsilon_H = -\frac{d\ln H}{dN} \tag{2.366}$$

Inflation will end when the first Hubble slow roll parameter reaches unity, so in order to have a sufficient amount of inflation, one requires the fractional change in ε_H per Hubble time to be small, hence we define the second Hubble slow roll parameter as

$$\eta_H = \frac{d \ln \varepsilon}{dN} = \frac{\dot{\varepsilon}}{H\varepsilon} \tag{2.367}$$

For $|\eta_H| < 1$ the fractional change in ε_H is sufficiently small over the course of one inflation time that we remain in a quasi-de Sitter expansion. Thus for inflation to occur, and be sustained for a sufficiently long period of time, we have two conditions that must be satisfied

$$\varepsilon_H < 1, \quad |\eta_H| < 1 \tag{2.368}$$

The universe will start to exit quasi-de Sitter expansion when $|\eta_H| \sim 1$ and inflation will fully stop when $\varepsilon_H = 1$.

2.2.4.1 Slow Roll Inflation

The simplest possible mechanism by which we can establish the conditions required for an inflationary phase in the early universe is that of "***Slow Roll***" inflation [63]. In the slow roll regime, we consider the energy density of the universe to be dominated by that of a scalar field ϕ, often called the inflaton field, minimally coupled to the Einstein Hilbert action. Recalling equation 2.188, the action is then

$$S = \int d^4x \sqrt{-g} \, (R + \mathcal{L}_m) \tag{2.369}$$

where $g_{\mu\nu}$ is the FLRW metric and the matter Lagrangian is

$$\mathcal{L}_m = \frac{1}{2}\dot{\phi}^2 - V(\phi) \tag{2.370}$$

Note that the conditions of homogeneity and isotropy mean that the scalar field must be a function of time only.

Recalling the definition of the matter stress-energy tensor 2.191, one can easily calculate the pressure and energy density of the scalar field

$$p_\phi = \frac{1}{2}\dot{\phi}^2 - V(\phi), \quad \rho_\phi = \frac{1}{2}\dot{\phi} + V(\phi) \tag{2.371}$$

We therefore have the state-parameter associated with the scalar field

$$w_\phi = \frac{p_\phi}{\rho_\phi} = \frac{\frac{1}{2}\dot{\phi}^2 - V(\phi)}{\frac{1}{2}\dot{\phi} + V(\phi)} \tag{2.372}$$

If the kinetic term $\dot{\phi}^2/2$ is sufficiently small compared to the potential, then the state parameter is approximately constant

$$w_\phi \approx -1 \tag{2.373}$$

and satisfied the bound required for inflation $w < -1/3$. The slow roll regime is an approximation, part of which assumes the aforementioned condition $\dot{\phi}^2 \ll V(\phi)$, but this is not the only condition. The first Friedmann equation during the inflationary phase is

$$H^2 = \frac{1}{3M_{pl}^2}\left(\frac{1}{2}\dot{\phi}^2 + V\right) \tag{2.374}$$

from which we have the time derivative

$$\dot{H} = -\frac{1}{2}\frac{\dot{\phi}^2}{M_{pl}^2} \tag{2.375}$$

where M_{pl} is the Planck mass. The minimally coupled scalar field also has a Klein-Gordon equation of motion

$$\ddot{\phi} + 3H\dot{\phi} = -V'(\phi) \tag{2.376}$$

where $V' = dV/d\phi$. Note that the expansion of the universe enters into the equation of motion for the scalar field as a frictional term $3H\dot{\phi}$. The equations of motion for the Hubble parameter and scalar field can be used to investigate the Hubble slow roll parameters further and eventually, define a second set of parameters which are

dependant entirely on the field potential $V(\phi)$. Given equations 2.374 & 2.375, the first Hubble slow roll parameter is simply

$$\varepsilon_H = -\frac{\dot{H}}{H^2} = \frac{\dot{\phi}^2}{2M_{pl}^2 H^2} \tag{2.377}$$

From this we may calculate the second Hubble slow roll parameter, recalling $\eta_H = \dot{\varepsilon_H}/H\varepsilon_H$

$$\eta_H = 2\left(\frac{\ddot{\phi}}{\phi H} - \frac{\dot{H}}{H^2}\right) \tag{2.378}$$

Defining $\delta = -\ddot{\phi}/H\dot{\phi}$, the second Hubble slow roll parameter can be written as

$$\eta_H = 2(\varepsilon_H - \delta) \tag{2.379}$$

Thus the two conditions $\varepsilon_H, |\delta| \ll 1$ are sufficient for the required inflationary regime to occur and sustain itself. In the slow roll approximation, the scalar field kinetic term is negligible compared to its potential, and thus equation 2.374 becomes

$$H^2 \approx \frac{1}{3M_{pl}^2} V(\phi) \tag{2.380}$$

The condition that the acceleration parameter δ be small means that we can approximate the equation of motion of the scalar field 2.376 as

$$3H\dot{\phi} \approx V' \tag{2.381}$$

In this approximation, the first Hubble slow parameter becomes

$$\varepsilon = \frac{\dot{\phi}}{2M_{pl}^2 H^2} \approx \frac{1}{2} M_{pl}^2 \left(\frac{V'}{V}\right)^2 \tag{2.382}$$

We can also calculate the combination

$$\delta + \varepsilon \approx M_{pl}^2 \frac{V''}{V} \tag{2.383}$$

The parameters

$$\varepsilon = \frac{1}{2} M_{pl}^2 \left(\frac{V'}{V} \right)^2 \tag{2.384}$$

and

$$\eta = M_{pl}^2 \frac{V''}{V} \tag{2.385}$$

are called the first and second potential slow roll parameters respectively. The conditions $\varepsilon(\phi) < 1$ and $|\eta(\phi)| \ll 1$ tell us if the shape of the scalar field potential can create the conditions required for a quasi-de Sitter inflationary period. Tracking these two slow roll parameters is important as they have significant implications for observational tests of slow roll inflation. Quantum fluctuations in the scalar field ϕ during inflation result in perturbations to the intrinsic curvature of the spacetime manifolds spatial slices Σ_t. The deviation of the power spectrum of scalar fluctuations $\Delta^2_{\mathcal{R}}(k)$ from scale independence is measured by the spectral index n_s

$$n_s - 1 = \left. \frac{d \ln \Delta^2_{\mathcal{R}}}{d \ln k} \right|_{k=aH} \tag{2.386}$$

Likewise there also tensor fluctuations in the metric, which have an associated power spectrum $\Delta^2_t(k)$. The spectral index and the ratio of tensor-to-scalar fluctuations $r = \Delta^2_t / \Delta^2_{\mathcal{R}}$ are both related to the potential slow roll parameters. To first order the expressions are [62]

$$\begin{aligned} n_s &= 1 - 6\varepsilon + 2\eta \\ r &= 16\varepsilon \end{aligned} \tag{2.387}$$

The spectral index and tensor-to-scalar ratio can be constrained by measurements of the CMB temperature anisotropies, since they are inherently related to stochastic fluctuations of the inflaton field ϕ. They therefore form a set of important cosmological observable which can be used to test the validity of proposed inflationary models.

To give more context to figure 2.7, we could consider the simple toy model of ϕ^2 inflation, where the inflationary potential is a harmonic one $V(\phi) = \frac{1}{2} m^2 \phi^2$. In

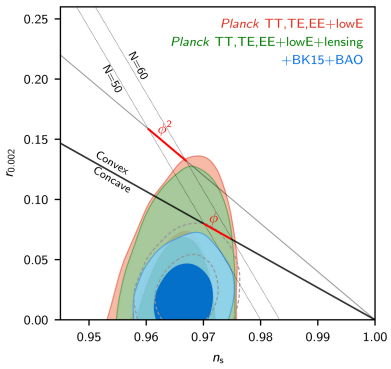

Figure 2.7: The constrained (r, n_s) parameter space from the Planck 2018 data release, assuming a the ΛCDM model. The dotted diagonal lines represent the analytical predictions of inflationary potentials of the form $V(\phi) \sim (\frac{\phi}{m_{pl}})^p$ at $N = 50, 60$ e-folds of inflation. The linear $(p = 1)$ and quadratic $(p = 2)$ predictions are highlighted in red. Figure obtained from [4]

.

this case one may easily find analytical predictions of the spectral index and tensor-scalar ratio in the slow roll regime. Given the harmonic potential, the potential slow parameters are

$$\begin{aligned} \varepsilon(\phi) &= \frac{2m_{pl}^2}{\phi^2} \\ \eta(\phi) &= \frac{2m_{pl}^2}{\phi^2} \end{aligned} \tag{2.388}$$

Thus the spectral index and tensor-scalar ratio which are defined in terms of the slow roll parameters in equations 2.387 are

$$n_s = 1 - \frac{8m_{pl}^2}{\phi^2} \tag{2.389}$$

$$r = \frac{32m_{pl}^2}{\phi^2} \tag{2.390}$$

It is more common to parameterise n_s and r in terms of the efolds of inflation N. the number of efolds of inflation can be written as an integral

$$N = \int_{a_I}^{a_E} d\ln a = \int_{t_I}^{t_E} H dt \tag{2.391}$$

where $a_I(t_I)$ is the scale factor at the start of inflation and $a_E(t_E)$ is the scale factor

at the end of inflation. the integral in equation 2.391 can be converted to an integral over the inflation field as follows. One has $dt = \dot{H} dH$ and thus

$$N = \int_{H_I}^{H_E} \frac{H}{\dot{H}} dH = -\int_{H_I}^{H_E} \frac{1}{H\varepsilon_H} dH \tag{2.392}$$

In the slow roll regime one has $\varepsilon_H \approx \varepsilon(\phi)$ and well as $H^2 \approx V(\phi)/3m_{pl}^2$ thus $dH = \frac{1}{2\sqrt{3}m_{pl}} V^{-\frac{1}{2}} V' d\phi$. We arrive at the number of efolds of inflation as a function of the inflaton field

$$N = \frac{1}{m_{pl}^2} \int_{\phi_{\text{end}}}^{\phi} \frac{V}{V'} d\phi \tag{2.393}$$

In the case of the harmonic potential one had $V/V' = \phi/2$ and therefore

$$N = \frac{1}{4m_{pl}^2} \left[\phi^2 - \phi_{\text{end}}^2\right] \tag{2.394}$$

Recalling that we consider slow roll inflation to end when $\varepsilon(\phi) = 1$, we have

$$\varepsilon(\phi_{\text{end}}) = \frac{2m_{pl^2}}{\phi_{\text{end}}^2} = 1 \tag{2.395}$$

which may be solved for the value of the inflaton field at the end of inflation $\phi_{\text{end}}^2 = 2m_{pl}^2$. Thus at a given field values ϕ we have the remaining number of efolds of inflation

$$N + \frac{1}{2} = \frac{1}{4m_{pl}^2} \phi^2 \tag{2.396}$$

The spectral index and tensor-scalar ratio in equations 2.389 & 2.390 can then be written as functions of the remaining efolds of inflation

$$n_s = 1 - \frac{4}{2N+1} \tag{2.397}$$

$$r = \frac{16}{2N+1} \tag{2.398}$$

We thus have a simple linear relationship in the $n_s - r$ plane

$$r = 4(1 - n_s) \tag{2.399}$$

The straight line described by eq. 2.399 is precisely that highlighted in red in figure 2.7. One can see in figure 2.7 that the predictions of the ϕ^2 inflationary model pass through the least constrained region of parameter space only slightly. Furthermore, the predicted relationship between r and n_s alone is not enough to determine the suitability of a slow roll inflation model, one must also take into account its reheating dynamics.

As the process of inflation ends, the universe is still dominated by an inflation field ϕ. But the observable universe today is made up of standard model particles, the process by which the inflaton field transfers energy to standard model particle fields at the end of inflation is known as "***Reheating***". Slow roll inflation ends when the particle potential $V(\phi)$ starts to become too steep, so one might generally expect that as inflation ends, the scalar field enters a local minima of the potential where it is approximately harmonic $V(\phi) \sim \frac{1}{2}\phi^2$. Thus the inflation field will execute approximately damped oscillations according to the equation of motion

$$\ddot{\phi} + 3H\dot{\phi} \simeq -m^2\phi \tag{2.400}$$

and begin to dump energy into standard model fields, leaving the universe at a temperature T_{re} at the end of reheating, after which conventional HBB and FLRW dynamics ensue. The specific dynamics of reheating are highly model dependant, the amount of reheating e-folds and the exact temperature at the end of reheating will depend on the specific reheating mechanism and couplings of the inflaton field. Detailed analysis can be found in [64–67].

The reheating dynamics ϕ^2 inflation have been explored extensively, and detailed calculations can be found in [68–70]. Generally speaking, the relationship between r and n_s alone is insufficient since the temperature of the universe at the end of

reheating is model dependant, and depends on the number of efolds of inflation. The number of efolds of inflation required to produce and (n_s, r) prediction that lies within an acceptable region of the constrained parameter space, may not produce a sufficient reheating of the universe. This will be explored further shorty.

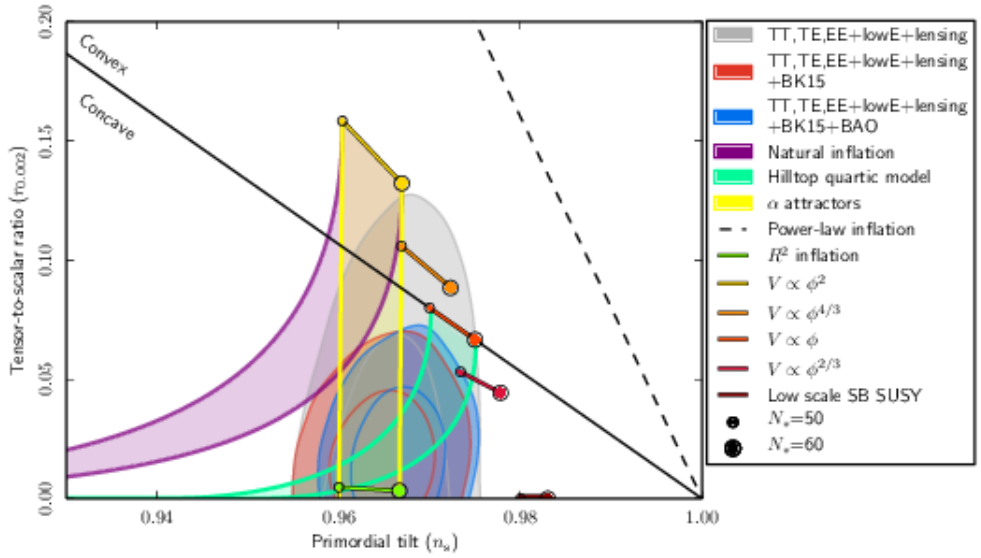

Figure 2.8: The (n_s, r) predictions from a collection of candidate inflationary models compared to the marginalised distributions from the Planck 2018 data release. Figure taken from [4].

Data collected from the Planck satellite constrains the spectral index to $n_s = 0.9649 \pm 0.0042$ and the tensor-to-scalar ratio to $r < 0.1$ [71]. When combining data from Planck with data from BICEP2/Keck Array this the constraint on r is further reduced to $r < 0.056$. In practise, there exist a great many proposed models for inflation within the slow roll regime. We required only that field potential has a suitable shape for inflation. There are many such potentials that can provide the conditions necessary for slow roll inflation. There are also more complicated models that contain multiple fields, rather than just a single scalar field [72, 73]. Figure 2.8 shows the predictions of a number of inflationary models compared to the constrained parameter space derived from the Planck 2018 data release [4, 71].

Chapter 3

Quartic Hilltop Inflation

This section is based on research published by the author and David Sloan, contained in Physical Review D [1].

With the release of the Planck 2018 data it has been possible to accurately test a variety of candidate inflationary models [74]. Noe particular class of models that has recieved attention is that of Hilltop models. This class of inflationary models is defined by potentials of the form [75]

$$V(\phi) = \Lambda \left[1 - \lambda \left(\frac{\phi}{m_{\rm pl}} \right)^q + ... \right] \tag{3.1}$$

where ... indicates higher order terms. Hilltop models are characterised by inflation occurring near the maxima of the potential on a broad, flat plateau or "hilltop". This feature makes Hilltop models attractive for slow roll inflation as the conditions are easy for such a model to fulfil. Furthermore, simple potentials such as these are easier to understand from a particle physics and QFT perspective and do occur in symmetry breaking theories [76], supergravity [77–85], supersymmetry [86, 87] and superstring theory models [88]. Broadly speaking, inflation models can be divided into two categories [89]. These are large field models, where inflation starts with the field at a large value $\phi > m_{\rm pl}$, and small field models for which the inflation starts with the field at a small value $\phi < m_{\rm pl}$.

Hilltop models encompass both small and large field inflation, but one particular small field hilltop model, "***Quartic Hilltop Inflation***" is among the models that are most consistent with the Planck 2018 constraints on the (n_s, r) parameter space. Small field models are a widely studied class of models that are easily viewed from the perspective of an effective field theory in particle physics, particularly because the field varies on a scale less than $m_{\rm pl}$, which should be the cutoff of such a theory. They are also good at accommodating slow-roll inflation [63, 89–91], making calculations tractable enough for comparison with observational data.

In slow roll inflation, the potential energy of the inflaton field $V(\phi)$ dominates over its kinetic energy and the field evolves slowly. To provide a sufficient amount of slow-roll inflation, potentials which are close to being flat are advantageous. This is well accommodated by small and large field models, whose potentials can be constructed to feature long, flat plateaus for the field to evolve through whilst the universe expands rapidly.

Hilltop models thus have many attractive features for an inflationary model. In Hilltop models, when the parameter is large enough, $\lambda \gtrsim 1$ inflation occurs at a small value of the field $\phi/m_{\rm pl} \ll \lambda$ and thus the higher order terms in the potential are heavily suppressed and are conventionally considered not to affect inflationary predictions of the model. For this reason, Hilltop models containing only the lowest order terms have usually been considered in previous studies.

The Quartic Hilltop (QH) model invokes a simple potential consisting of a constant term and a quartic term in the field ϕ. The plateau-like shape of the potential is demonstrated in figure 3.1.

$$V(\phi) = \Lambda \left[1 - \lambda \left(\frac{\phi}{m_{\rm pl}} \right)^4 \right] \tag{3.2}$$

The QH model has recently received more attention in light of the Planck 2018 data, to which it showed a satisfactory fit under a numerical analysis [92], whereas earlier attempts at an analytical treatment had ruled QH out on the basis that the

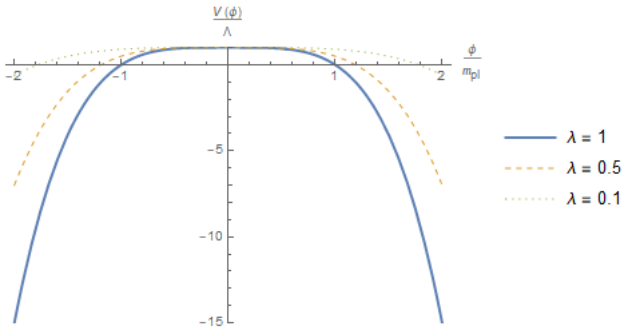

Figure 3.1: The Quartic Hilltop potential 3.2 of the inflation field ϕ at various values of λ. The numerical values of λ chosen for this figure best illustrate the shape of the potential, but the physically interesting values will be for $\lambda \ll 1$.

predictions for the spectral index n_s as a function of the number of remaining e-folds N of inflation after the scale k_* exits the horizon [93]

$$n_s = 1 - \frac{3}{N} \tag{3.3}$$

was too small at $N = 50$ & 60 to fit within the bounds of the Planck 2018 data, as this places n_s between 0.94 and 0.95. To align with the Planck data we require $n_s \gtrsim 0.96$.

Numerical treatments indicate that the QH model does achieve this, so there is an apparent discrepancy between the results of numerical and analytic investigations. The reason is that in the earlier attempts at solving the model analytically, it was assumed that the physically relevant parameter space has $\lambda \sim 1$. In [5], it is shown that this is in fact not the case and that the parameter λ is actually very small. This allows for a more detailed analytic investigation of the QH model, by revising two key assumptions used in deriving the result 3.3.

1. The value of the inflation field $\phi(N)$ at a given N is much smaller than its vacuum expectation value (VEV) i.e. $\phi(N) \ll \langle\phi\rangle \sim m_{\rm pl}/\lambda^{1/4}$.

2. The contribution of the value of the inflation field at the end of inflation $\phi_{\rm end}$ to the calculation of $N(\phi)$ is negligible.

By relaxing both of these assumptions it is possible to derive a theoretical prediction for the $r - n_s$ curve which is in close agreement with numerical analysis and thus better fits the Planck 2018 data. In the small λ regime, the higher order terms become of greater importance and as we will show in this work, accounting for such terms leads to distinct results when compared to the QH model in the (n_s, r) parameter space favoured by the Planck 2018 survey. Ultimately what is derived in [5] is a relationship between the scalar tensor ratio r and the spectral index n_s at a given number of e-folds before the end of inflation N.

$$r(n_s, N) = \frac{8}{3}(1 - n_s)\left[1 - \frac{\sqrt{3[2(1 - n_s)N - 3]}}{(1 - n_s)N}\right] \tag{3.4}$$

Whilst this treatment of the QH models yields a result that is much more satisfactory due to being a better fit to the Planck data, the model is not without its issues as discussed in [94]. Namely, that the QH potential turns negative shortly after inflation ends and is unbounded from below [94]. This is clearly unsatisfactory as such a theory, when quantised would posses arbitrarily low energy states. The potential needs to be stabilised by the higher order terms that have been neglected in 3.2.

We will take the investigation of the QH model in [5] as a guide for investigating a model which accounts for the higher order terms.

That is, we will follow steps analogous to those for investigating the QH model

i Compute the number of e-folds, $N(\phi)$, of inflation after the cosmological scale leaves the horizon

ii Derive the contribution to N from the inflaton at the end of slow-roll in terms of λ, $N_{\rm end}(\lambda)$ by solving the conditions $\varepsilon(\phi_{\rm end}) = 1$ & $|\eta(\phi_{\rm end})| = 1$

iii Express the spectral index n_s in terms of N and λ through our solution for $N_{\rm end}(\lambda)$

iv Invert the expression for $n_s(\lambda, N)$ to find $\lambda(n_s, N)$ and use this to derive the relationship between r and n_s for $N = 50$ and $N = 60$

Although the general method for the QH model and the model containing higher order terms will be the same, a major difference comes in the final step when deriving the relationship between the spectral index and tensor-scalar ratio in which we find that, unlike in the QH case, we find a one-to-many mapping of n_s to r for given values of N.

Whilst we will derive analytical results for the relationship between the tensor-scalar ratio and spectral index at a given number of remaining efolds of inflation N which allows accurate comparison of the predictions of the two models. However, this does not necessarily allow us to evaluate how well the Quartic Hilltop model or its corrected version explain the data collected by Planck and other such surveys of the CMB. The $r - n_s$ relationship is only really one half of the picture since, given some model defined by a potential $V(\phi)$ as we are considering here, one may fix any arbitrary (n_s, r) by simply choosing an appropriate time at which the scale k exits the horizon, which translates into an amount of remaining efolds N. There are of course some a priori restrictions on N as it is well established that approximately 50 efolds of inflation are required to solve the horizon problem. However as we show in section 4, by considering the reheating dynamics of the corrected model, which one cannot do for the UV-incomplete QH model, it is possible to place further

restrictions on the possible values of N so that the resulting temperature of the universe at the end of reheating is consistent with standard cosmology, which may not be the case if one simply chooses N to get a desired (n_s, r) pair.

3.1 The Quartic Hilltop Squared Model

As noted in [5], the Quartic Hilltop (QH) model[1]

$$V(\phi) = \Lambda \left[1 - 2\lambda \left(\frac{\phi}{m_{\rm pl}} \right)^4 \right] \tag{3.5}$$

approximates a linear potential near $V(\phi) = 0$ which will become negative for $\phi > m_{\rm pl}$ shortly before the end of inflation, and needs to be stabilised by higher order terms. The shape of this potential is demonstrated in figure 3.2. This can be achieved by working with the Quartic Hilltop Squared Model (QHS) as suggested in [94] for which $V(\phi) \geq 0$.

$$V(\phi) = \Lambda \left[1 - \lambda \left(\frac{\phi}{m_{\rm pl}} \right)^4 \right]^2 \tag{3.6}$$

The approach of squaring the Hilltop potential to investigate the effects of accounting for stabilising terms has previously been investigated in the case of the Quadratic Hilltop potential [95] (its corrected form known as Double Well Inflation) and in [96] where the authors discuss different aspects of the same corrected Quartic Hilltop potential. As such, it is known that such models, whilst agreeing closely with the uncorrected versions at small field values as one would expect from Taylor expanding the potential, still produce substantially different predictions for the tensor-scalar ratio and spectral index when the VEV is in the super-Planckian regime.

[1]The parameter in the QH model is taken to be 2λ to keep the form consistent with the series expansion of 3.6.

Hilltop models generally require a super-Planckian VEV for their predictions of r and n_s to be in lie with current measurements and this is shown for both the Quadratic [95] and Quartic Hilltop models [5].

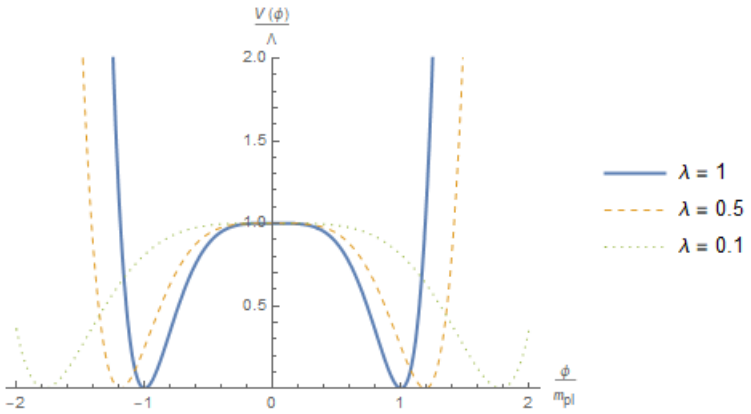

Figure 3.2: The Quartic Hilltop-Squared potential 3.6 at various values of λ. The values of λ are chosen to illustrate the shape of the potential, which unlike the QH potential, is bounded from below and gains a local minima from the higher order terms but retains a flat plateau needed for slow-roll inflation.

We will calculate analytically the spectral index n_s and tensor-scalar ratio r. The analytic calculations can be compared to the detailed data collected by the Planck satellite. Just as the QH model is investigated analytically in [5], analogous steps can be performed for the QHS model. The spectral index and tensor-scalar ratio can be written in terms of the potential slow roll parameters ε & η.

$$n_s = 1 - 6\varepsilon + 2\eta \tag{3.7}$$

$$r = 16\varepsilon \tag{3.8}$$

where the slow roll parameters are

$$\begin{aligned} \varepsilon(\phi) &= \frac{1}{2} m_{\rm pl}^2 \left(\frac{V'(\phi)}{V(\phi)} \right)^2 \\ &= 32\lambda^2 \left(\frac{\phi}{m_{\rm pl}} \right)^6 \frac{1}{\left[1 - \lambda \left(\frac{\phi}{m_{\rm pl}} \right)^4 \right]^2} \end{aligned} \tag{3.9}$$

$$\begin{aligned}\eta(\phi) &= m_{\rm pl}^2 \frac{V''(\phi)}{V(\phi)} \\ &= \varepsilon(\phi) - 24\lambda \left(\frac{\phi}{m_{\rm pl}}\right)^2 \frac{1}{\left[1 - \lambda\left(\frac{\phi}{m_{\rm pl}}\right)^4\right]}\end{aligned} \tag{3.10}$$

Just as in [5], it is easiest to work with the spectral index and tensor-scalar ratio in terms of a parameter Z which will be defined shortly and N, the remaining number of e-folds until the end of inflation after the cosmological scale has exited the horizon. This is calculated as

$$\begin{aligned}N &= \frac{1}{m_{\rm pl}^2} \int_{\phi_{\rm end}}^{\phi(N)} \frac{V}{V'} d\phi \\ &= \frac{1}{16}\left(\frac{\phi}{m_{\rm pl}}\right)^2 + \frac{1}{16\lambda}\left(\frac{\phi}{m_{\rm pl}}\right)^{-2} - N_{\rm end}\end{aligned} \tag{3.11}$$

where the value of the scalar field at the end of inflation is $\phi_{\rm end}$ and

$$N_{\rm end} = \frac{1}{16}\left(\frac{\phi_{\rm end}}{m_{\rm pl}}\right)^2 + \frac{1}{16\lambda}\left(\frac{\phi_{\rm end}}{m_{\rm pl}}\right)^{-2} \tag{3.12}$$

By defining

$$\bar{N} \equiv N + N_{\rm end} = \frac{1}{16}\left(\frac{\phi}{m_{\rm pl}}\right)^2 + \frac{1}{16\lambda}\left(\frac{\phi}{m_{\rm pl}}\right)^{-2} \tag{3.13}$$

and $Z = 64\lambda\bar{N}^2$, equation 3.11 may be solved for $\left(\frac{\phi}{m_{\rm pl}}\right)^2$ as

$$\left(\frac{\phi}{m_{\rm pl}}\right)^2 = 8\bar{N}[Z] \tag{3.14}$$

The function $[Z]$ is defined as

$$[Z] = 1 - \sqrt{1 - \frac{1}{Z}} \tag{3.15}$$

A property of this function that we will make use of later is that it satisfies $[Z]^2 = 2[Z] - 1/Z$. The appearance of this function $[Z]$ sets a constraint $Z > 1$.

Since the Z parameter is defined as $Z = 64\lambda\bar{N}^2$, this constraint is saying that for a given value of λ, which is a free parameter in the model, there will always be a minimum amount of inflation given by

$$\bar{N} > \frac{1}{8\sqrt{\lambda}} \tag{3.16}$$

In the QH model there is an analogous bound $\bar{N}_{\rm QH} > 1/4\sqrt{\lambda}$, in fact it is shown that in the small λ regime $\bar{N}_{\rm QH} \simeq N + 1/4\sqrt{\lambda}$. This suggests that for the QHS model we should expect $\bar{N} \simeq N + 1/8\sqrt{\lambda}$, and in fact we will later show that this is indeed the case.

Using equation 3.14, the slow roll parameters can be written as

$$\varepsilon = \frac{4}{\bar{N}} \frac{Z^2[Z]^3}{\left(1 - Z[Z]^2\right)^2} \tag{3.17}$$

$$\eta = \varepsilon - \frac{3}{\bar{N}} \frac{Z[Z]}{1 - Z[Z]^2} \tag{3.18}$$

which allows a calculation of the spectral index and tensor-scalar ratio as

$$n_s = 1 - \frac{6}{\bar{N}} \frac{Z[Z]}{1 - Z[Z]^2} - \frac{16}{\bar{N}} \frac{Z^2[Z]^3}{\left(1 - Z[Z]^2\right)^2} \tag{3.19}$$

$$r = \frac{64}{\bar{N}} \frac{Z^2[Z]^3}{\left(1 - Z[Z]^2\right)^2} \tag{3.20}$$

Equation 3.19 can be written as a quadratic in $F(Z) = \sqrt{Z/(Z-1)}$ by virtue of the purely algebraic relations

$$1 - Z[Z]^2 = 2\left(1 - Z[Z]\right) \tag{3.21}$$

$$\left(\frac{Z[Z]}{1 - Z[Z]}\right)^2 = \frac{Z}{Z-1} \tag{3.22}$$

Thus we have

$$n_s = 1 + \frac{1}{\bar{N}}\sqrt{\frac{Z}{Z-1}} - \frac{4}{\bar{N}}\left(\frac{Z}{Z-1}\right) \tag{3.23}$$

with the solution

$$\sqrt{\frac{Z}{Z-1}} = \frac{1+\sqrt{1+16\bar{N}\tilde{n}_s}}{8} \tag{3.24}$$

where $\tilde{n}_s = 1 - n_s$.

The goal of this investigation is to produce an analytic relationship between the tensor-scalar ratio r and spectral index n_s at a given number of e-folds before the end of inflation N for $\lambda \ll 1$. Recalling the definitions $Z = 64\lambda\bar{N}^2$ and $\bar{N} = N + N_{\rm end}$, to produce such a function $r(n_s, N)$, we are required to eliminate λ & $\bar{N}$ from the equations.

$N_{\rm end}$ is the contribution of the value of the inflation field at the end of inflation to the total number of e-folds, which as noted in [5] can be large for the QH model at small λ. Investigation of this $N_{\rm end}$ term results in the approximation $\bar{N}_{\rm QH} \simeq N + 1/4\sqrt{\lambda}$, so we are motivated to find an analogous approximation for the QHS model.

Thus far we have extracted both the spectral index and tensor-scalar ratio in terms of two newly defined parameters Z and $\bar{N}$. The end goal of this analysis is to produce a closed form expression for the tensor-scalar ratio in terms of only the spectral index n_s and remaining number of e-folds N. A strategy for proceeding can the be devised as follows: An explicit expression for $N_{\rm end}(\lambda)$ will be derived in the small λ limit. This allows for the total number of e-folds $\bar{N}$ to be written only in terms of N and λ and hence also the Z parameter and spectral index. The resulting expression for $n_s(N, \lambda)$ is invertible for $\lambda(N, n_s)$. The expressions for $\bar{N}(N, \lambda)$ and $\lambda(N, n_s)$ can then be substituted into the definition of Z which is used in equation 3.20 to find the target closed form relationship between r and n_s for a given N.

3.2 Small λ behaviour of $N_{\rm end}$

Guided by the QH model and Planck data, we are mainly interested in the region of parameter space where λ is very small, roughly $\lambda \lesssim 10^{-4}$. The small λ behaviour of $N_{\rm end}$ can be investigated by considering separately the cases where inflation is ended by the slow roll parameters ε and η.

3.2.1 $\varepsilon(\phi_{\rm end}) = 1$

Consider first the case where slow roll inflation is ended by ε reaching unity before η. In this case equation 3.9 becomes

$$\frac{1}{\lambda} = \left(\frac{\phi_{\rm end}}{m_{\rm pl}}\right)^3 \left(\frac{\phi_{\rm end}}{m_{\rm pl}} + 4\sqrt{2}\right) \tag{3.25}$$

For $\lambda \ll 1$, we have $\phi_{\rm end} \gg m_{\rm pl}$ and thus one has approximately

$$\left(\frac{\phi_{\rm end}}{m_{\rm pl}}\right)^2 \simeq \frac{1}{\sqrt{\lambda}} \tag{3.26}$$

This result may be substituted into equation (3.12) to get an approximate expression for $N_{\rm end}$ in the $\lambda \ll 1$ limit.

$$N_{\rm end} \simeq \frac{1}{8\sqrt{\lambda}} \tag{3.27}$$

3.2.2 $|\eta(\phi_{\rm end})| = 1$

Consider now the second case where the end of slow roll is characterised by $|\eta(\phi_{\rm end})| = 1$, which of course has two sub cases $\eta(\phi_{\rm end}) = 1$ & $\eta(\phi_{\rm end}) = -1$. starting with the $\eta(\phi_{\rm end}) = 1$ case we have

$$\left(\frac{\phi_{\rm end}}{m_{\rm pl}}\right)^8 - 56\left(\frac{\phi_{\rm end}}{m_{\rm pl}}\right)^6 - \frac{2}{\lambda}\left(\frac{\phi_{\rm end}}{m_{\rm pl}}\right)^4 + \frac{24}{\lambda}\left(\frac{\phi_{\rm end}}{m_{\rm pl}}\right)^2 + \frac{1}{\lambda^2} = 0 \tag{3.28}$$

Again, for $\lambda \ll 1$, $(\phi_{\rm end}/m_{\rm pl}) \gg 1$ and 3.28 is approximately

$$\left(\frac{\phi_{\rm end}}{m_{\rm pl}}\right)^8 + \frac{1}{\lambda^2} \simeq 0 \tag{3.29}$$

which has no real solutions. In second sub case $\eta(\phi_{\rm end}) = -1$ we come to the same conclusion. For $\lambda \ll 1$, there are no real, positive solutions. From these cases we conclude that, to a first approximation, for small λ the end of slow-roll inflation is marked only by $\varepsilon(\phi) \geq 1$.

3.2.3 Small λ Relationship Between r and n_s

Given the results of section 2, for small λ we can use the approximation

$$\bar{N} \simeq N + \frac{1}{8\sqrt{\lambda}} \tag{3.30}$$

which should come as no surprise given the earlier bound derived on $\bar{N}$ in equation (3.16). We see that just as in the case of the QH model, the term contributed by $\phi_{\rm end}$ is proportional to $\lambda^{-\frac{1}{2}}$ so this term certainly cannot be neglected when $\lambda \ll 1$. With this expression we can now write equation 3.24 in terms of λ, n_s and N.

$$\sqrt{1 + \frac{1}{16N\sqrt{\lambda} + 64N^2\lambda}} = \frac{1}{8}\left[1 + \sqrt{1 + 16\tilde{n}_s\left(N + \frac{1}{8\sqrt{\lambda}}\right)}\right] \tag{3.31}$$

Equation 3.31 can be solved as a quadratic in terms of $\sqrt{\lambda}$, and as such there will be two solutions, both of which are valid. This is of course because λ is a free parameter in the model, a given r may map to multiple values of λ.

$$\left(\sqrt{\lambda}\right)_{\pm} = \frac{12N\tilde{n}_s - 2N^2\tilde{n}_s^2 - 15 \pm \sqrt{8N\tilde{n}_s - 15}}{8N\left(15 - 8N\tilde{n}_s + N^2\tilde{n}_s^2\right)} \tag{3.32}$$

The crossover point between the two branches where $\left(\sqrt{\lambda}\right)_+ = \left(\sqrt{\lambda}\right)_- = \sqrt{\lambda_c}$ is at $\sqrt{8N\tilde{n}_s - 15} = 0 \rightarrow N\tilde{n}_s = 15/8$, this also defines the maximum possible value

of n_s at a given N

$$n_s^{\max} = 1 - \frac{15}{8N} \tag{3.33}$$

The calculated spectral index bounds $n_s^{\max}(N = 60) = 0.96875$ and $n_s^{\max}(N = 50) = 0.9625$ are consistent with the observational data provided by Planck 2018 [74]

Substituting $N\tilde{n}_s = \frac{15}{8N}$ into 3.32 one finds $\sqrt{\lambda}_c = \frac{1}{60N}$, resulting in the critical values of $\lambda_c \simeq 7.72 \times 10^{-8}$ and $\lambda_c \simeq 1.11 \times 10^{-7}$ for $N = 60$ & $N = 50$ respectively.

The tensor-scalar ratio r which we aim to calculate, can be expressed in terms of the slow-roll parameter ε as

$$\begin{aligned} r &= 16\varepsilon \\ &= \frac{16}{\bar{N}} \left(\frac{Z}{Z-1} \right) \left(1 - \sqrt{\frac{Z-1}{Z}} \right) \end{aligned} \tag{3.34}$$

Using equation 3.24 and the solutions for $\sqrt{\lambda}$ 3.32, we can calculate the quantities $\bar{N}$ and $Z/(Z-1)$ in terms of n_s and N as desired.

$$r = \begin{cases} \frac{1}{4N} \left(\frac{12N\tilde{n}_s - 2N^2\tilde{n}_s^2 - 15 + \sqrt{8N\tilde{n}_s - 15}}{4N\tilde{n}_s - N^2\tilde{n}_s^2 + \sqrt{8N\tilde{n}_s - 15}} \right) \left[1 + g_+(\tilde{n}_s, N) \right] \left[g_+(\tilde{n}_s, N) - 7 \right], & \lambda \geq \lambda_c \\ \\ \frac{1}{4N} \left(\frac{12N\tilde{n}_s - 2N^2\tilde{n}_s^2 - 15 - \sqrt{8N\tilde{n}_s - 15}}{4N\tilde{n}_s - N^2\tilde{n}_s^2 - \sqrt{8N\tilde{n}_s - 15}} \right) \left[1 + g_-(\tilde{n}_s, N) \right] \left[g_-(\tilde{n}_s, N) - 7 \right], & \lambda < \lambda_c \end{cases} \tag{3.35}$$

Where we define the function

$$g_\pm(\tilde{n}_s, N) = \sqrt{\frac{12N\tilde{n}_s + 62N^2\tilde{n}_s^2 - 16N^3\tilde{n}_s^3 - 15 \pm (1 + 16N\tilde{n}_s)\sqrt{8N\tilde{n}_s - 15}}{12N\tilde{n}_s - 2N^2\tilde{n}_s^2 - 15 \pm \sqrt{8N\tilde{n}_s - 15}}} \tag{3.36}$$

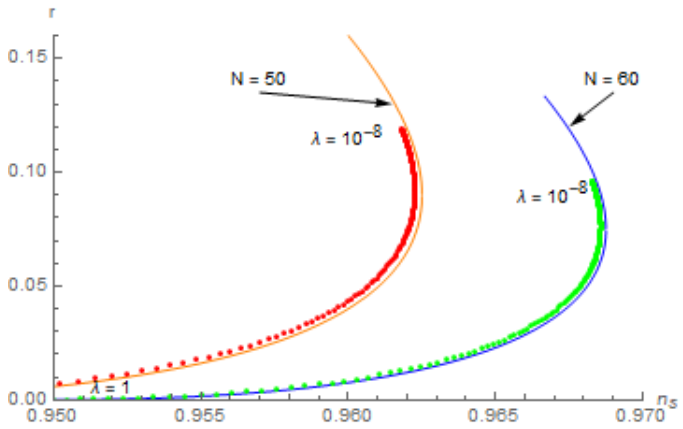

Figure 3.3: Analytical solutions (bold) for the spectral index n_s and tensor-scalar ratio r of the QHS model equation 4.3, compared with their numerical solutions (dotted) for $10^{-8} \leq \lambda \leq 1$ at $N = 50$ and $N = 60$ e-folds before the end of inflation.

By comparison to numerical solutions for a broad range of λ from $\lambda \ll 1$ to $\lambda \approx 1$ in figure 3.3 we can see that this approximation is quite accurate, even in the regime when λ is large ($\lambda \sim 1$). We can further validate the analytical solution by comparing the $N = 60$ and $N = 50$ solutions to numerical solutions calculated up to the predicted critical λ_c values. In figures 3.4a and 3.4b it can be seen that if the system is solved numerically up to the predicated λ_c values, the solution branches do indeed stop at the crossover point between the r_+ and r_- branches of the analytical solution.

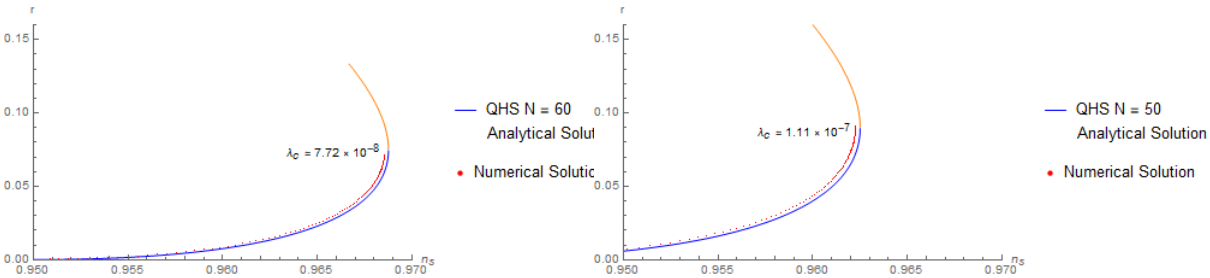

(a) QHS $N = 60$ numerical solution calculated up to the crossover point between $r_\pm$ branches at λ_c compared to analytical solution

(b) QHS $N = 50$ numerical solution calculated up to the crossover point between $r_\pm$ branches at λ_c compared to analytical solution

Figure 3.4: Comparison of QHS numerical and analytical solutions

Comparing the solution for the QH model 3.4 and QHS model 4.3 in figure 3.5, we see that the effect of including the higher order stabilising terms causes the predictions of the QHS model to diverge quite dramatically from those of the QH model. The models begin to diverge around $n_s \simeq 0.95$ which is well outside of the region expected from the Planck 2018 data making them quite distinct within the acceptable regions. This is an important result as it makes clear that different methods of stabilising the potential must be considered as distinct if we are to take Hilltop potentials as serious candidates for inflation. It is not sufficient to ignore these stabilising terms in the potential since in the small λ regime they have a dramatic effect on inflationary predictions of the theory.

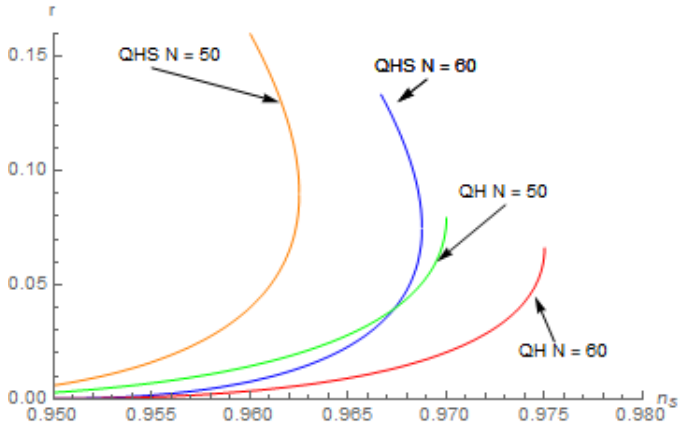

Figure 3.5: Comparisons of the analytic $r(n_s)$ solutions for Quartic Hilltop-Squared 4.3 calculated in this work and Quartic Hilltop 3.4 calculated in [5] at $N = 50$ & $N = 60$ e-folds before the end of inflation.

The result of including the stabilising terms, as shown in figure 3.6, is that the N = 50 branch has shifted out of the 1σ region whilst remaining just within the 2σ bound. In the QH model, both branches remains within the 1σ region, however this does not spell such bad news for the QHS model since $N \simeq 60$ is generally favoured by reheating constraints.

Another feature that is seen in the QHS model but not the QH model is that the solution for $r(n_s)$ is not a function, given n_s may correspond to multiples values of r. As such, the curves in figure 3.3 representing the pass vertical and. The points

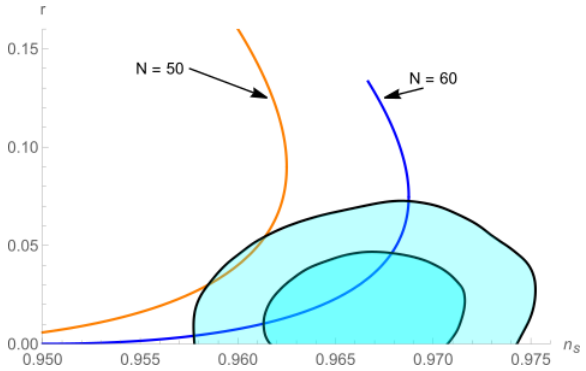

Figure 3.6: Analytical QHS solutions (bold) given by equation 4.3 at $N = 50$ & $N = 60$ e-folds before the end of inflation, compared to the Planck 2018 data bounds represented by the filled regions (2σ in lighter, 1σ in darker).

at which the curves reach their maximal values of the spectral index are indeed the bounds calculated earlier $n_s^{\max}(N = 60) = 0.96875$ and $n_s^{\max}(N = 50) = 0.9625$. This arises due to the stabilisation, and is a general feature of stabilised Hilltop models. This can be seen by considering the spectral index n_s and tensor ratio as functions of the slow roll parameters

$$\begin{aligned} n_s &= 1 - 6\varepsilon(\phi) + 2\eta(\phi) \\ r &= 16\varepsilon(\phi) \end{aligned} \tag{3.37}$$

In the QHS case, the slow roll parameters are

$$\eta(\phi) = \varepsilon(\phi) - 24\lambda \left(\frac{\phi}{m_{\rm pl}}\right)^2 \frac{1}{1 - \lambda\left(\frac{\phi}{m_{\rm pl}}\right)^4} \tag{3.38}$$

Defining

$$\Gamma(\phi, \lambda) = 24\lambda \left(\frac{\phi}{m_{\rm pl}}\right)^2 \frac{1}{1 - \lambda\left(\phi/m_{\rm pl}\right)^4} \tag{3.39}$$

the two equations in (3.38) can be combined to give

$$r = 8\left(1 - n_s\right) - 32\Gamma(\phi, \lambda) \tag{3.40}$$

From the analytical results in this work, specifically equation 3.32, for a given $n_s < n_s^{\max}$ there will be one or two corresponding values of lambda $\lambda_\pm$ (one in the case $N\tilde{n}_s = 15/8$ and two otherwise). And thus for a given n_s there will be one or two values of $\Gamma(\phi, \lambda)$ and hence one or two corresponding values of r. The QH model does not exhibit this behaviour because in this particular case $\eta(\phi)$ and $\varepsilon(\phi)$ are linearly independent. From a physical standpoint, we expect this to be a generic feature of all Hilltop models that take higher order correction terms into account. Consider the spectral index n_s written in terms of the Hilltop potential $V(\phi)$.

$$n_s = 1 - 3m_{\rm pl}^2 \left(\frac{V'(\phi)}{V(\phi)}\right)^2 + 2m_{\rm pl}^2 \frac{V''(\phi)}{V(\phi)} \tag{3.41}$$

The dependence of n_s on the ratios of the derivatives of the potential to the potential itself suggests that we should write this in terms of $W(\phi) = \ln V(\phi)$ for which

$$n_s = 1 - m_{\rm pl}^2 W'(\phi) + 2m_{\rm pl}^2 W''(\phi) \tag{3.42}$$

If one includes the stabilising terms in $V(\phi)$ then the potential will have a local minima and thus the second derivative will also have a local minima $\phi_{min} < \phi_{\rm end}$ for sufficiently small λ. Because the curvature of $V(\phi)$ has a turning point, $W''(\phi)$ will have a form such that if we fix a particular value $W''_* = W(\phi_0, \lambda_0)$, we can find another set (ϕ_1, λ_1) for which $W''_* = W(\phi_1, \lambda_1)$. Since the spectral index is just a linear combination of the first and second derivatives it will also inherit this property. So for a fixed value of the spectral index n_s^* at (ϕ_0, λ_0), we may also find another set (ϕ_1, λ_1) which corresponds to the same value of the spectral index. However the gradient term $W'(\phi)$ is not necessarily the same at (ϕ_0, λ_0) and (ϕ_1, λ_1) and since the tensor-scalar ratio is proportional to only this term, n_s^* will necessarily correspond to multiple values of r.

3.3 Reheating in QHS

3.3.1 Generic Reheating Analysis and Subsequent Bound on w_{re}

Whilst it is useful to be able to calculate (n_s, r) pairs for the Quartic Hilltop Squared model, and verify that for $50 \lesssim N \lesssim 60$ the predictions of the model lie within the parameter space determined by Planck 2018 data, this does not fully validate the model as a viable candidate for inflation. As discussed in section D of [97], given a generic potential $V(\phi)$ one may calculate and desired (n_s, r) pair by through equations 3.7 & 3.8 by choosing an appropriate time at which the scale k exits the horizon. This will correspond to a number of efolds of inflation N_k remaining when the scale exits. This however, may not result in acceptable reheating predictions of the model defined by $V(\phi)$. The number of reheating efolds and the temperature at the end of reheating T_{re} depends explicitly on N_k [66, 97]. This dependence is derived by considering the evolution of the horizon scale and the energy density throughout the evolution of the universe.

Let the comoving scale at the time it exits the horizon be $k = a_k H_k$, and consider its evolution from inflation to the present day as outlined in figure 3.7.

$$\frac{k}{a_0 H_0} = \frac{a_k}{a_{end}} \frac{a_{end}}{a_{re}} \frac{a_{re}}{a_{eq}} \frac{a_{eq}}{a_0} \frac{H_{eq}}{H_0} \frac{H_k}{H_{eq}} \tag{3.43}$$

We the write $N_k = \ln a_{end}/a_k$ for the number of remaining inflation efolds after the scale exits the horizon, $N_{re} = \ln a_{re}/a_{end}$ for the number of reheating efolds, $N_{RD} = \ln a_{eq}/a_{re}$ for the number of efolds during radiation domination.

$$\ln \frac{k}{a_0 H_0} = -N_k - N_{re} - N_{RD} - \ln \frac{a_{eq}}{a_0} + \ln \frac{H_{eq}}{H_0} + \ln \frac{H_k}{H_{eq}} \tag{3.44}$$

Assuming a constant equation of state during reheating w_{re}, we may track the evolution of the energy density from the end of inflation to the end of reheating

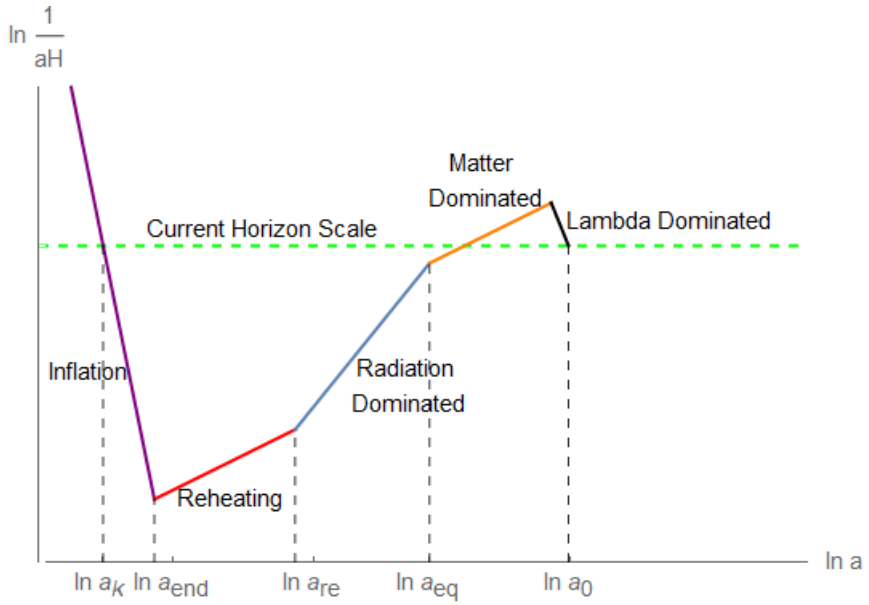

Figure 3.7: A schematic outlining the evolution of the horizon scale $(aH)^{-1}$ as a function of the (log) scale factor $a(t)$ and dominant matter source at each time from inflation to the present day at $a_0(t)$.

$$\frac{\rho_{end}}{\rho_{re}} = \left(\frac{a_{end}}{a_{re}}\right)^{-3(1+w_{re})} \tag{3.45}$$

In terms of the reheating efolds this is

$$N_{re} = \frac{1}{3(1+w_{re})} \ln \frac{\rho_{end}}{\rho_{re}} \tag{3.46}$$

where the energy densities are given by

$$\rho_{re} = \frac{\pi^2}{30} g_{re} T_{re}^4 \tag{3.47}$$

$$\rho_{end} = \frac{3}{2} V_{end} \tag{3.48}$$

where V_{end} is the value of the potential at the end of inflation (i.e. when $\varepsilon \simeq 1$), g_{re} is the effective number of relativistic species at the end of reheating.

The reheating temperature T_{re} can be written in terms of the CMB temperature today T_0

$$\frac{T_{re}}{T_0} = \left(\frac{43}{11 g_{re}}\right)^{\frac{1}{3}} \frac{a_0}{a_{eq}} \frac{a_{eq}}{a_{re}} \tag{3.49}$$

By taking the logarithm of equation 3.49 and combining with equation 3.44 we obtain the reheating efolds and temperature (Equivalently one may also consider the reheating energy density 3.48 rather than the temperature as is done in some literature [97].

$$N_{re} = \frac{4}{1-3w_{re}} \left(\frac{1}{4} \ln \frac{\pi^2 g_{re}}{45} + \frac{1}{3} \ln \frac{11}{43 g_{re}} + \ln \frac{a_0 T_0}{k} - \ln \frac{V_{end}^{\frac{1}{4}}}{H_k} - N_k \right) \tag{3.50}$$

$$T_{re} = \left[\left(\frac{43}{11 g_{re}}\right)^{\frac{1}{3}} \left(\frac{a_0 T_0}{k}\right) H_k e^{-N_k} \left[\frac{45 V_{end}}{\pi^2 g_{re}}\right]^{-\frac{1}{3(1+w_{re})}} \right]^{\frac{3(1+w_{re})}{3w_{re}-1}} \tag{3.51}$$

For the model to at least be considered as an acceptable candidate one needs both that the predicted (n_s, r) are within the bounds of current measurements and that the corresponding remaining number of inflation efolds N_k gives an acceptable reheating temperature T_{re}. We may calculate analytically the model dependant terms in equations 3.50 & 3.51. Firstly the value of the potential at the end of inflation is simply $V(\phi)$ evaluated on the solution to equation 3.25. However using just the first-order approximate solution 3.26 would result in $V_{end} = 0$. This may be sufficient for calculating N_{re} since it only depends logarithmically on V_{end}, but the reheating temperature T_{re} is sensitive to V_{end} so one needs at least the second order term in the power series solution to 3.25 to calculate the reheating temperature.

$$\left(\frac{\phi_{end}}{m_{pl}}\right) \simeq \lambda^{-\frac{1}{4}} + 3\lambda^{-\frac{7}{4}} \qquad \lambda \ll 1 \tag{3.52}$$

and thus we have the value of the potential at the end of inflation

$$V_{end} \simeq 144 \Lambda \lambda^{-3} \tag{3.53}$$

The value of the Hubble parameter H_k at the pivot scale is

$$H_k \simeq \pi m_{pl} \sqrt{\frac{A_s r}{2}} \tag{3.54}$$

Finally, given $N_{end} \simeq 1/8\sqrt{\lambda}$ and equation 3.11, the number of remaining efolds of inflation N_k may be written in terms of the field value at the pivot scale ϕ_k.

$$N_k = \frac{1}{16}\left(\frac{\phi_k}{m_{pl}}\right)^2 + \frac{1}{16\lambda}\left(\frac{\phi_k}{m_{pl}}\right)^{-2} - \frac{1}{8\sqrt{\lambda}} \tag{3.55}$$

And thus the reheating efolds and temperature are expressed as

$$N_{re} = \frac{4}{1-3w_{re}}\left[\frac{1}{4}\ln\frac{\pi^2 g_{re}}{45} + \frac{1}{3}\ln\frac{11}{43 g_{re}} + \ln\frac{a_0 T_0}{k} - \ln\left[\frac{\sqrt{2}(144\Lambda)^{\frac{1}{4}}}{\lambda^{\frac{3}{4}}\pi m_{pl}\sqrt{A_s r}}\right] + \frac{1}{8\sqrt{\lambda}} - \frac{1}{16}\left(\frac{\phi_k}{m_{pl}}\right)^2 - \frac{1}{16\lambda}\left(\frac{\phi_k}{m_{pl}}\right)^{-2}\right]$$

$$T_{re} = \left[\left(\frac{43}{11 g_{re}}\right)^{\frac{1}{3}}\left(\frac{a_0 T_0}{k}\right)\pi m_{pl}\sqrt{\frac{A_s r}{2}}e^{-N_k}\left[\frac{6480\Lambda}{\lambda^3}\pi^2 g_{re}\right]^{-\frac{1}{3(1+w_{re})}}\right]^{\frac{3(1+w_{re})}{3w_{re}-1}}$$

To investigate the reheating predictions of the model we consider $r - n_s$ curves for $50 \leq N_k \leq 65$ and their corresponding reheating efolds and temperatures.

From the plots of the reheating efolds in figure 3.9a, one sees that if there are more than approximately 55 remaining efolds of inflation when the pivot scale exits the horizon, then it it not possible to get $N_{re} > 0$. However for $N_k \leq 55$, all of the (n_s, r) predictions of the model lie outside of the 1σ bound in figure 3.8 and thus an equation of state parameter of $w_{re} = 0$ leaves the model with no acceptable predictions compared to the Planck 2018 data.

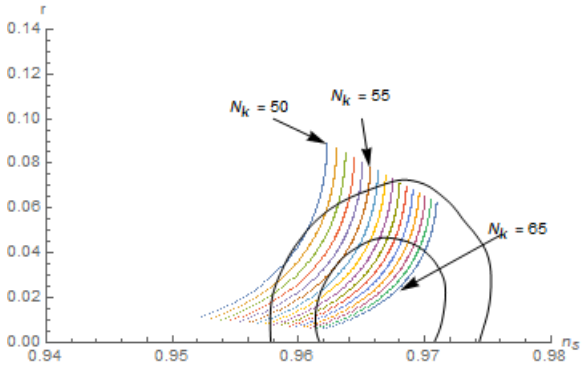

Figure 3.8: QHS numerical solutions of the tensor-scalar ratio r and spectral index n_s for $50 \leq N_k \leq 65$ over the parameter range $10^{-3} \lesssim \lambda \lesssim 10^{-7}$. The solid black lines represent the Planck 2018 bounds just as in figure 3.6

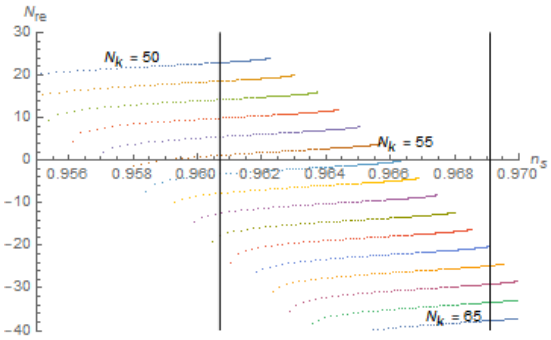

(a) Plots of the reheating efolds N_{re} corresponding to the numerical (n_s, r) solutions for the QHS model in figure 3.8 with $w_{re} = 0$. The solid vertical black lines mark the Planck 2018 1σ bound on the spectral index n_s. For $N_k > 55$ all of the constant N_k curves lie below the $N_{re} = 0$ line, thus in this case the model does not produce any reheating if there are more than 55 efolds of inflation.

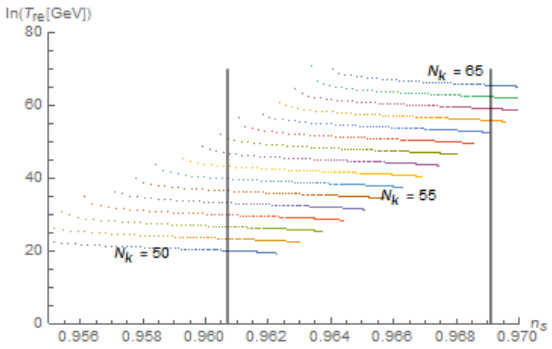

(b) Plots of the (log) reheating temperature T_{re} corresponding to the numerical (n_s, r) solutions for the QHS model in figure 3.8 with $w_{re} = 0$. The solid vertical black lines mark the Planck 2018 1σ bound on the spectral index n_s.

Figure 3.9: Reheating efolds and temperature for the QHS model with $w_{re} = 0$

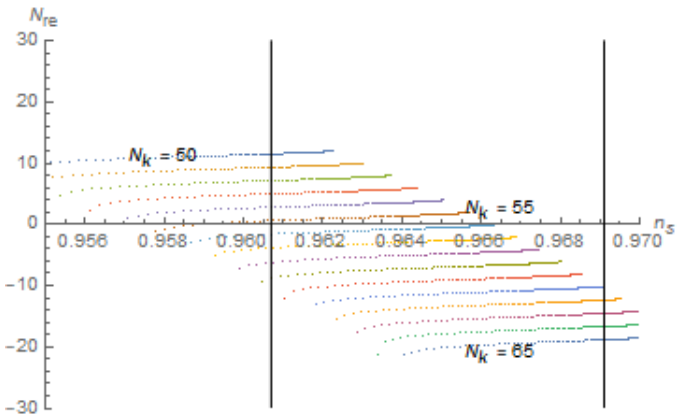

Figure 3.10: Plots of the reheating efolds N_{re} corresponding to the numerical (n_s, r) solutions for the QHS model in figure 3.8 with $w_{re} = -1/3$. The solid vertical black lines mark the Planck 2018 1σ bound on the spectral index n_s. Just as in figure 3.9a The model cannot produce any reheating efolds if there are more than 55 efolds of inflation.

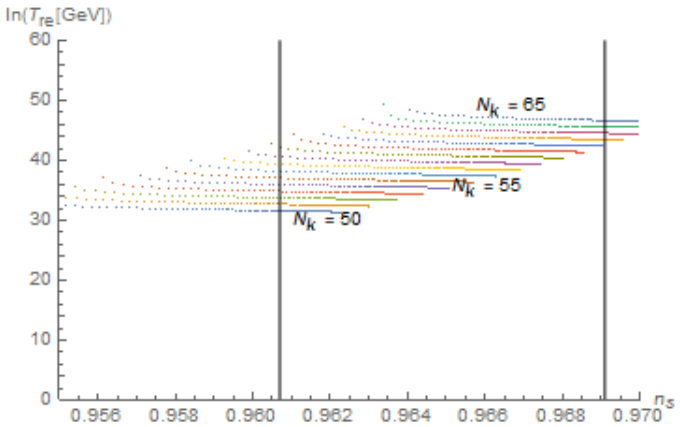

Figure 3.11: Plots of the (log) reheating temperature T_{re} corresponding to the numerical (n_s, r) solutions for the QHS model in figure 3.8 with $w_{re} = -1/3$. The solid vertical black lines mark the Planck 2018 1σ bound on the spectral index n_s.

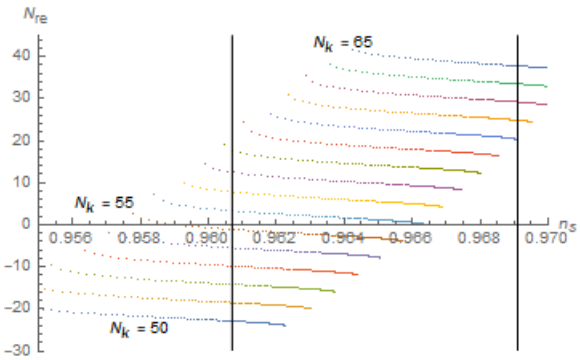

(a) Plots of the reheating efolds N_{re} corresponding to the numerical (n_s, r) solutions for the QHS model in figure 3.8 with $w_{re} = 2/3$. The solid vertical black lines mark the Planck 2018 1σ bound on the spectral index n_s. In this case the behaviour of the reheating efolds is inverted from figures 3.9a & 3.10, the model only produces non-zero reheating efolds $N_{re} \geq 0$ for $N_k \geq 55$. However, also restricting to the region of the spectral index's 1σ bound makes this inequality noninclusive $N_k > 55$.

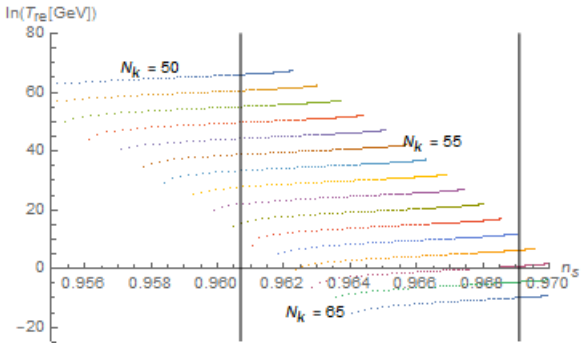

(b) Plots of the (log) reheating temperature T_{re} corresponding to the numerical (n_s, r) solutions for the QHS model in figure 3.8 with $w_{re} = 2/3$. The solid vertical black lines mark the Planck 2018 1σ bound on the spectral index n_s.

Figure 3.12: Reheating efolds and temperature for the QHS model with $w_{re} = 2/3$

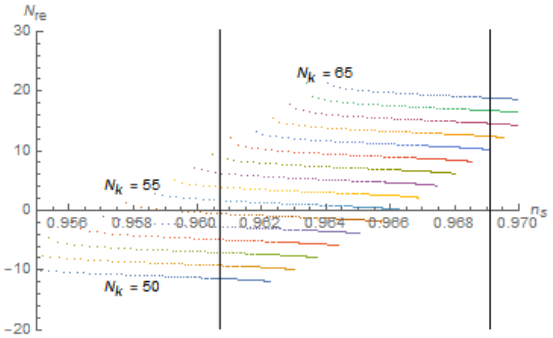

(a) Plots of the reheating efolds N_{re} corresponding to the numerical (n_s, r) solutions for the QHS model in figure 3.8 with $w_{re} = 1$. The solid vertical black lines mark the Planck 2018 1σ bound on the spectral index n_s. As in figure 3.12a, the constant N_k curves lie above the $N_{re} = 0$ line in the 1σ n_s region for $N_k > 55$.

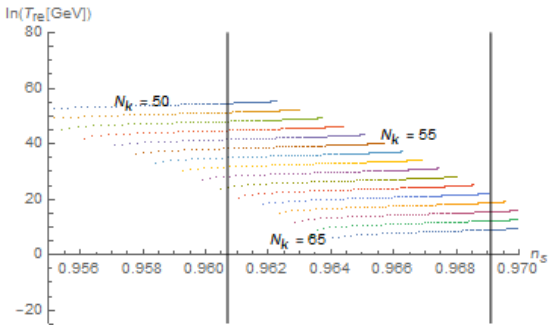

(b) Plots of the (log) reheating temperature T_{re} corresponding to the numerical (n_s, r) solutions for the QHS model in figure 3.8 with $w_{re} = 1$. The solid vertical black lines mark the Planck 2018 1σ bound on the spectral index n_s.

Figure 3.13: Reheating efolds and temperature for the QHS model with $w_{re} = 1$

Taking a negative equation of state parameter $w_{re} = -1/3$ as in figures 3.10 and 3.11 serves to push the solutions slightly tighter together compared to the $w_{re} = 0$ case, as one would expect given that the dependence of the reheating efolds N_{re} on w_{re} follows $(1 - 3w_{re})^{-1}$. In this case there are still no acceptable solutions for $N_k > 55$. We may however also try positive equation of state parameters. Using a positive equation of state parameter in figures 3.12 and 3.13 inverts the behaviour of N_{re} and T_{re} with respect to N_k so that the number of reheating efolds increases with N_k and the reheating temperature decreases for with N_k. In this case there are now solutions which lie in the 1σ region of figure 3.8 (i.e. $N_k > 55$) and have $N_{re} > 0$.

3.3.2 Reheating Temperature Restrictions On The $r - n_s$ Parameter Space.

In section 4.1 we have established that in order to get a non-zero amount of reheating efolds from the QHS model consistent with Planck measurements of the spectral index n_s, one is restricted to a positive equation of state parameter $0 < w_{re} \leq 1$. The temperature of the universe at the end of reheating is loosely bounded from below in order to be consistent with standard cosmology. If reheating is to occur before Big Bang Nucleosynethsis (BBN) then one requires $T_{re} > T_{BBN}$. BBN occurs on temperature scales of roughly $T_{BBN} \lesssim 10\text{MeV}$ [98] so the reheating temperature is constrained to be at least larger than 0.01GeV. The reheating temperature is also loosely bounded from above by the fact that it should not exceed the energy scale of inflation $T_{re} \lesssim 10^{16}\text{GeV}$ [99], but this bound may be further restricted if one accepts supersymmetry and considers the effects of gravitino production during inflation on BBN [100–103]. This restricts the reheating temperature to much smaller range $0.01\text{GeV} \lesssim T_{re} \lesssim 10^{8}\text{GeV}$.

Considering the extremal case where the equation of state parameter $w_{re} = 1$, the reheating temperature bounds can be used to restrict the QHS model to a much tighter region of the $r - n_s$ parameter space, whose reheating efolds are non-zero and reheating temperature is compatible with standard cosmology.

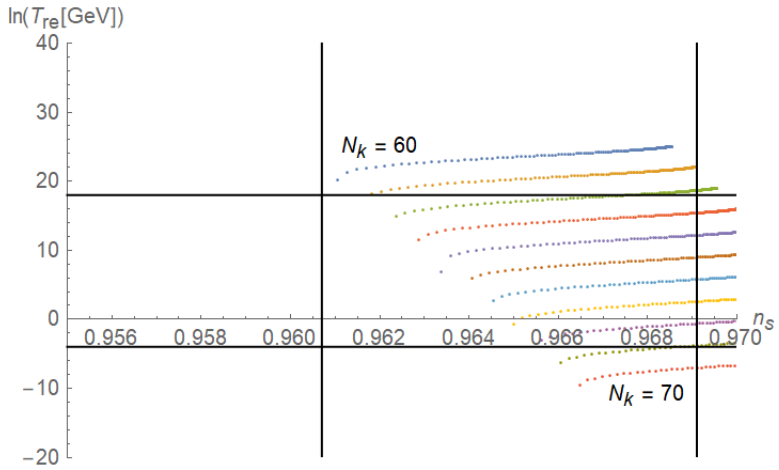

Figure 3.14: We plot the (log) reheating temperature of the QHS model over the range $60 \leq N_k \leq 70$ where as in previous figures the vertical black lines mark the 1σ Planck 2018 bounds on the spectral index n_s. The horizontal black lines mark the reheating temperature bounds $0.01\text{GeV} \lesssim T_{re} \lesssim 10^8\text{GeV}$. The range of the parameter λ is the same as in the figure 3.8.

If we consider the fixed N_k curves in figure 3.14 who lie within the reheating temperature bounds for all values of λ within the 1σ region, one is restricted to the range $63 \leq N_k \leq 68$ of remaining efolds of inflation. In figure 3.15 we plot the $r - n_s$ curves for $N_k = 63$ and $N_k = 68$. These curves bound a region of parameter space that is both compatible with the Planck 2018 measurements and such that the model produces reheating temperatures within the range $0.01\text{GeV} \lesssim T_{re} \lesssim 10^8\text{GeV}$.

3.4 Disscusion

We have derived analytical predictions for the cosmological parameters n_s and r in a Quartic Hilltop Squared model. This model accounts for a higher order correction term which stabilises the potential in [5], such that it is nowhere negative. The

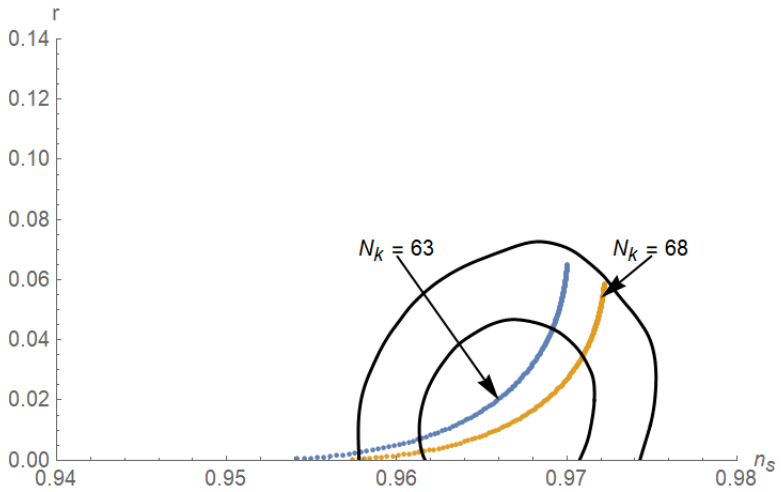

Figure 3.15: The reheating temperature limits restrict us to the area bounded by the $N_k = 63$ and $N_k = 68$ curves in the $r - n_s$ parameter space which is considerably smaller than just the Planck 2018 bounds.

work of [5] makes it clear that when working with Hilltop models in the small λ regime (the one in which they best fit observational data), one cannot assume that when calculating the remaining number of e-folds of inflation, the contribution of the inflaton field at the end of inflation will be small enough to be negligible. In fact one find that the contribution is $N_{\rm end} \propto \lambda^{-1/2}$. Clearly this will be large for small λ. In the case of the Quartic Hilltop model the relevant range of values of λ are $\lambda \leq 10^{-4}$, yet one only needs $\lambda = 4 \times 10^{-4}$ for the $\lambda^{-1/2}$ contribution to be as large as 50 e-folds. In this paper we find that the same relationship exists when accounting for the higher order terms in the Quartic Hilltop Squared model. The only difference is that the constant of proportionality is smaller. For the QH model $N_{\rm end}^{\rm QH}/\lambda^{-1/2} = 1/4$ and for the QHS model $N_{\rm end}^{\rm QHS}/\lambda^{-1/2} = 1/8$. Because $N_{\rm end}$ and λ follow the same relationship in the QHS model studied in this paper we also conclude that one cannot assume this contribution to be small in the calculation of the remaining number of e-folds and that it must be accounted for in order to explain why the model fits well to observational data.

When the analytical solution derived in this work is compared with that of the QH model in [5] and the Planck 2018 data there are two important observations to

be made. Firstly, both Hilltop models provide very good fits to the observational data, being within the 1σ region with the exception only of the QHS $N = 50$ branch. The QH model was already known to be a good candidate inflationary model and we show here that whilst accounting for the higher order terms does shift the positions of the N-branches quite dramatically, the model still remains within a region of the parameter space that makes it an attractive inflationary model. In addition to both models being favourable with respect to the Planck 2018 data, it is clear from comparing the two solutions, such as in figure (3.5), that the two solutions deviate quite dramatically long before either model enters the region of parameter space favoured by the Planck 2018 data. This is because the higher order terms actually become large during inflation and are therefore relevant to the calculation of observables and dramatically change the inflationary predictions of the model by shifting the $r - n_s$ spectrum far to the left. Clearly the QH and QHS models need to be treated distinctly in the context of inflation, and that one cannot simply take the Quartic Hilltop model as an accurate approximation of Quartic Hilltop Squared.

Throughout this work frequent references and comparisons are made to numerical solutions for the Hilltop models in question. The numerical solutions help evaluate the validity of the results and form part of ongoing work by the author to develop numerical solutions for a wide range of inflationary models. The ability to solve models numerically will aid in investigating the generic features of Hilltop models. For example whether or not the $N_{\text{end}} \propto \lambda^{-1/2}$ relationship holds for other Hilltop models or if there is some other power law. Furthermore, the numerical solutions also make it possible to investigate how dramatically the $r - n_s$ changes in other Hilltop models, say for example quintic models as opposed to quartic and whether or not those models require us to account for the higher order correction terms.

At a first glance, the fact that both the QH and QHS model predictions for the tensor-scalar ratio and spectral index fit nicely into the Planck 2018 bounds seems encouraging, however as we note, and has already been discussed at length in the literature, this does not necessarily mean the model goes a long way in helping

explain the data that has been presented since we may generate any (n_s, r) pair by appropriate choice of N_k, that may or may not correspond to reheating predictions that are consistent with standard cosmology.

Correcting the models UV behaviour allows us to explore the reheating dynamics of the QHS model through the numerical solutions and further constrain its $r - n_s$ parameter space to the region bounded by $63 \leq N_k \leq 68$, by considering Big Bang Nucleosynthesis limits on the reheating temperature. Whilst this does not drastically reduce the range of allowed values of n_s and r, the area of (n_s, r) pairs is significantly smaller than if one were to just consider the bounds derived by the Planck 2018 survey.

Chapter 4

Regularisation of Single Field Inflation Models

This section is based on research published by the author and David Sloan, contained in Physical Review D [2].

A number of the single scalar field models analysed in [95], including some of those most favoured by the Planck survey, involve potentials which are unbounded from below after the end of inflation. Such models may be able to provide satisfactory inflationary dynamics, however if they are taken to be valid beyond inflation the potentials quickly become negative and due to their unboundedness, lead to universes that collapse on a time scale $\tau \sim H^{-1}$. Clearly this is not the cosmology we observe today, so such behaviour must be corrected by regularizing the potentials to introduce a local minima shortly after inflation ends. Naturally one may ask if modifying the behaviour after the end of inflation significantly changes the models predictions of inflationary observables such as the tensor fraction and spectral index, even 50-60 efolds before the end of inflation.

In this section we explore the effect of generic correction terms on a collection of inflationary models. The correction terms are designed only to be the simplest possible options that prevent collapse of the universe after the end of inflation. Such terms which stabilise the inflaton VEV may, and do, appear in in more physically

motivated in other physically motivated models. Although in this work we do not attempt to explain the physical origin of such terms. We show that such corrections will have an effect on the inflationary predictions of the model. Thus, regardless of how corrections of these forms may appear, they do indeed need to be accounted for before the inflationary predictions of the model can be trusted.

We show that the addition of correction terms designed to stabilise the inflaton VEV affect the reheating temperature T_{re} predicted by the model as a function of the spectral index n_s at a given number of efolds before the end of inflation N_k. Therefore by requiring that the predicted reheating temperature stays within the loose bounds set by the big bang nucleosynthesis scale and the energy scale of inflation, $0.01\text{GeV} \leq T_{re} \leq 10^{16}\text{GeV}$, the model under consideration may fall into a further restricted region of $r-n_s$ space that is acceptable under the Planck 2018 results. Thus we arrive at a key result of our analysis: In considering models which require regularization, it is insufficient to examine their predictions without taking such regularization into account. We have chosen to remain agnostic on the form that such regularization should take, motivating the correction terms solely by their role in ensuring that the potential remain positive with zero minimum. This allows us to demonstrate that generic regularizations should be taken into account regardless of their physical origins. In specific cases there are good physical reasons which inform the precise nature of the regularization, such as the contribution of higher loop corrections to the radiatively corrected Higgs inflation from the Jordan frame. However our goal is not simply to test specific models and regularizations but to make the broader point that since regularizations do make an impact on physical observables for such models, a wide range of potentials requiring regularization should only have their observational consequences examined with such regularizations in place.

In the work of [1], detailed in section 3, we addressed for the case of quartic hilltop inflation, a model well favoured by Planck, corrected by one particular modification scheme which involves squaring the potential. It is shown that modifying the quartic hilltop potential in this way does have a significant effect on the final (r, n_s)

parameter space that is consistent with the Planck 2018 results. In this paper, we explore several different modification types for quartic hilltop, radiatively corrected Higgs inflation and Exponential SUSY inflation. These are all single field inflation models featured in [95] which all suffer from the same issue of unboundedness. We consider generic corrections to these models, motivated only by preventing collapse of the universe after the end of inflation, but we show that should such correction terms arise from physical motivations, they may have significant effects on the inflationary predictions of the models. Therefore one must carefully consider exactly how a candidate potential exits inflation. As we will show in this section, it can have a significant effect on the inflationary predictions. Models that produce such a collapsing universe, must be corrected before calculations of r and n_s are compared to data. In all three models we explore the effects of simply squaring the potential to form a potential that is bounded below. We then explore the simplest possible correction terms that may be used to extend the models, these are polynomial and inverse polynomial terms for QH and RCHI respectively.

4.1 Corrected Hilltop Models

While the predictions of the tensor fraction and spectral index for the QHS model are consistent with the Planck 2018 bounds, the numerical analysis that these results are derived from still acts in an opaque manner. It tells us only the results that we should expect for $r(n_s)$ and not precisely why the model behaves in a certain way. Further more, this analysis is incomplete with regards to reheating after inflation. Since the QHS potential is UV regulated, there exists a local minima of the potential just after inflation ends around which the inflaton oscillate. The damped oscillations cause the inflaton field to dump it's energy into the thermal bath of the universe, leading eventually the production of ordinary matter. The temperature of the universe at the end of reheating T_{re} and the number of reheating efolds N_{re} depend explicitly on the number of efolds of inflation after the scale exits N_k.

$$T_{re} = V_0 \left[\left(\frac{43}{g_{re}} \right)^{\frac{1}{3}} \left(\frac{a_0 T_0}{k} \right) H_k e^{-N_k} \left(\frac{45}{\pi^2 g_{re}} \right)^{-\frac{1}{3(1+w_{re})}} \right]^{\frac{3(1+w_{re})}{3w_{re}-1}} \tag{4.1}$$

$$N_{re} = \frac{4}{1-3w_{re}} \left(\frac{1}{4} \ln \frac{\pi^2 g_{re}}{45} + \frac{1}{3} \ln \frac{11}{43 g_{re}} + \ln \frac{a_0 T_0}{k} - \ln \frac{V_{end}^{\frac{1}{4}}}{H_k} - N_k \right) \tag{4.2}$$

where g_{re} is the effective number of relativistic species at the end of reheating, T_0 is the present day CMB temperature, V_{end} is the value of the inflaton potential at the end of inflation, H_k is the value of the Hubble parameter when the scale exits and w_{re} is the effective equation of state parameter of the inflaton during reheating. Throughout this paper we will assume a mean reheating parameter of $w_{re} = 1$ as this providers the most conservative estimates on the predictions of reheating [104].

For a fixed value of N_k, we have seen in section 3 that the (r, n_s) predictions of the QH model differ quite drastically from the QHS model. In that analysis we derive a closed form expression for $r(n_s)$

$$r = \begin{cases} \frac{1}{4N} \left(\frac{12N\tilde{n}_s - 2N^2\tilde{n}_s^2 - 15 + \sqrt{8N\tilde{n}_s - 15}}{4N\tilde{n}_s - N^2\tilde{n}_s^2 + \sqrt{8N\tilde{n}_s - 15}} \right) \left[1 + g_+(\tilde{n}_s, N) \right] \left[g_+(\tilde{n}_s, N) - 7 \right], & \lambda \geq \lambda_c \\ \\ \frac{1}{4N} \left(\frac{12N\tilde{n}_s - 2N^2\tilde{n}_s^2 - 15 - \sqrt{8N\tilde{n}_s - 15}}{4N\tilde{n}_s - N^2\tilde{n}_s^2 - \sqrt{8N\tilde{n}_s - 15}} \right) \left[1 + g_-(\tilde{n}_s, N) \right] \left[g_-(\tilde{n}_s, N) - 7 \right], & \lambda < \lambda_c \end{cases} \tag{4.3}$$

where

$$g_\pm(\tilde{n}_s, N) = \sqrt{\frac{12N\tilde{n}_s + 62N^2\tilde{n}_s^2 - 16N^3\tilde{n}_s^3 - 15 \pm (1 + 16N\tilde{n}_s)\sqrt{8N\tilde{n}_s - 15}}{12N\tilde{n}_s - 2N^2\tilde{n}_s^2 - 15 \pm \sqrt{8N\tilde{n}_s - 15}}} \tag{4.4}$$

and the critical parameter value is $\lambda_c = (60N)^{-\frac{1}{2}}$. As noted previously, in the QH model, there is a contribution $N_{end}^{QH} = 1/4\sqrt{\lambda}$ to the total efolds of inflation coming from the value of the field at the end of inflation ϕ_{end}. In the QHS model this contribution is found to be $N_{end}^{QHS} = 1/8\sqrt{\lambda}$ (when $\lambda \ll 1$) the contribution is half as small as in the QHS model, for small λ the higher order terms begin to contribute significantly, and push the field out of slow roll inflation sooner than in

QH. For all of the corrected quartic hilltop models in this paper, we work in the small λ regime, where the symmetry breaking scale $\mu = m_{pl}(4\lambda)^{-1/4}$ is large [105], thus avoiding the region of parameter space that is not compatible with the Planck results.

Furthermore, the we completed the analysis of QHS model by computing it's reheating temperature and efolds. Computing the reheating parameters allows us to further constrain the parameter space for QHS by demanding that the reheating temperature be bounded below by the Big Bang Nucleosynthesis scale $T_{BBN} \lesssim 0.01\text{GeV} \lesssim T_{re}$ and bounded above by the energy scale of inflation $T_{re} \lesssim 10^{16}\text{GeV}$. In fact, the size of the acceptable region in (r, n_s) space of the QHS model reduces significantly after reheating consistency is taken into account. Before reheating, whilst only bounded by the Planck 2018 data, the QHS model was constrained to the region defined by

$$\begin{aligned} 0.9607 \lesssim & n_s \lesssim 0.9691 \\ 55 \lesssim & N_k \end{aligned} \tag{4.5}$$

whereas after taking into account reheating consistency, this is reduced to

$$\begin{aligned} 0.9607 \lesssim & n_s \lesssim 0.9691 \\ 63 \lesssim & N_k \lesssim 68 \end{aligned} \tag{4.6}$$

The fact that the inflationary potential must be UV regularised and that the models predictions of the tensor fraction and spectral index must be consistent with reheating bounds significantly constrains the models parameter space which is in agreement with the Planck 2018 bounds.

Choosing to regularise the potential by squaring it, is simply one possibility out of a great many. In this work, we show that how one chooses the regularise the shape of the potential near the end of inflation can have an important and quantifiable effect on the models predictions of n_s and r.

The QHS potential essentially amounts to adding a $(\phi/m_{pl})^8$ correction term to the original QH potential, which is seen simply by expanding out the potential and rescaling the coupling parameter λ.

$$V_{\mathrm{QH}}(\phi) = V_0 \left[1 - \lambda \left(\frac{\phi}{m_{pl}}\right)^4\right]^2 \tag{4.7}$$

$$\begin{aligned} V_{\mathrm{QHS}}(\phi) &= V_0 \left[1 - 2\lambda \left(\frac{\phi}{m_{pl}}\right)^4 + \lambda^2 \left(\frac{\phi}{m_{pl}}\right)^8\right] \\ &= V_0 \left[1 - \tilde{\lambda} \left(\frac{\phi}{m_{pl}}\right)^4 + \frac{1}{4}\tilde{\lambda}^2 \left(\frac{\phi}{m_{pl}}\right)^8\right] \end{aligned} \tag{4.8}$$

As well as squaring the potential, one may also consider what the effect of adding single polynomial terms ϕ^p to the potential are. We only wish to correct the behaviour of the potential for large ϕ, so we look at positive values of p. Furthermore, the coefficient of the ϕ^p term must be fine-tuned to ensure that the VEV remains at $V(\phi_0) = 0$ so that inflation ends in a finite time. Therefore consider potentials of the form

$$V(\phi) = V_0 \left[1 - \lambda \left(\frac{\phi}{m_{pl}}\right)^4 + \alpha_p \left(\frac{\phi}{m_{pl}}\right)^p\right], \quad p > 4 \tag{4.9}$$

The potential has stationary points at

$$\phi^3 \left(p\alpha_p \phi^{p-4} - 4\lambda\right) = 0 \tag{4.10}$$

and thus the VEV is located at

$$\phi_0 = \left(\frac{4\lambda}{p\alpha_p}\right)^{\frac{1}{p-4}} \tag{4.11}$$

Requiring that $V(\phi_0) = 0$ allows us to solve for the fine-tuning of the coefficient α_p

$$\alpha_p = 4\lambda^{\frac{p}{4}} p^{-\frac{p}{4}} (p-4)^{\frac{p-4}{4}} \tag{4.12}$$

So to add polynomial corrections to the Quartic Hilltop model, we work with potentials of the form

$$V(\phi) = V_0 \left[1 - \lambda \left(\frac{\phi}{m_{pl}} \right)^4 + 4\lambda^{\frac{p}{4}} p^{-\frac{p}{4}} (p-4)^{\frac{p-4}{4}} \left(\frac{\phi}{m_{pl}} \right)^p \right] \tag{4.13}$$

Henceforth we will refer to such models as QH_p, with the Quartic Hilltop Squared model being equivalent to QH_8 as per equation 4.8.

The lowest order term that we can add to modify the small-field behaviour of the potential but retain its plateau and large-field shape is $p = 5$ since the QH model already contains a ϕ^4 term. As we shall see from the results later in this section, there is no need to investigate larger than $p = 10$, so we consider only terms in this range. Starting from $p = 5$ through to $p = 10$ we have calculated the tensor ratio r as a function of the spectral index n_s and the temperature at the end of reheating T_{re} as a function of the spectral index between $50 \leq N_k \leq N_k = 70$. We then determine which of these curves are reheating-consistent by demanding that they lie within the rectangle on the $T_{re} - n_s$ plots. The horizontal bounds on the reheating temperature plots are $0.01\mathrm{GeV} \lesssim T_{re} \lesssim 10^{16}\mathrm{GeV}$. The reheating temperature is bounded below by the energy scale of Big Bang Nucleosynthesis (BBN) [66, 106] $T_{BBN} \sim 10\mathrm{MeV}$. Measurements of the CMB anisotropies constraining the tensor fraction r are equivalent to upper bounds on the energy scale of inflation [43, 71, 106] since

$$V_*^{\frac{1}{4}} = \left(\frac{3\pi^2 A_s}{2} r m_{pl} \right)^{\frac{1}{4}} \lesssim 10^{16}\mathrm{GeV} \tag{4.14}$$

where V_* is the energy scale of inflation and A_s is the amplitude of scalar perturbations. This bounds T_{re} from above.

In all of the following $r - n_s$ plots, we produce results from numerical solutions of the tensor fraction and spectral index and the corresponding temperature at the end of reheating for QH_p models with $p = 5, 10$. Figures for $p = 6, 7, 9$ are contained in appendix A.1 (omitting $\mathrm{QH}_8 \equiv \mathrm{QHS}$). The solid and dashed black curves are

the Planck 2018 1σ and 2σ bounds respectively. The horizontal black line is the BICEP/Keck Array bound on the tensor fraction $r < 0.036$ [43]. Similarly, in all following $T_{re} - n_s$ plots, the upper horizontal line is the energy scale of inflation bound $T_{re} \lesssim 10^{16}$GeV and the lower horizontal line is the BBN bound $0.01\text{GeV} \lesssim T_{re}$. The vertical solid lines represent the Planck 2018 bounds $0.9607 \lesssim n_s \lesssim 0.9691$.

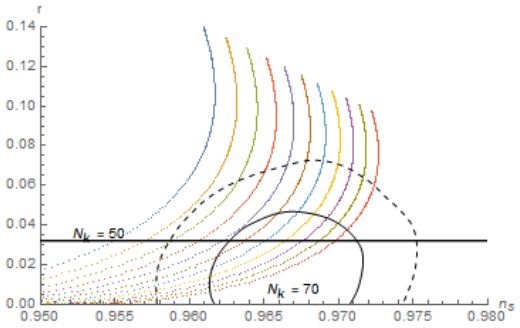

(a) Numerical solutions of the tensor-scalar ratio r and spectral index n_s for the QH_5 model over the $50 \leq N_k \leq 70$.

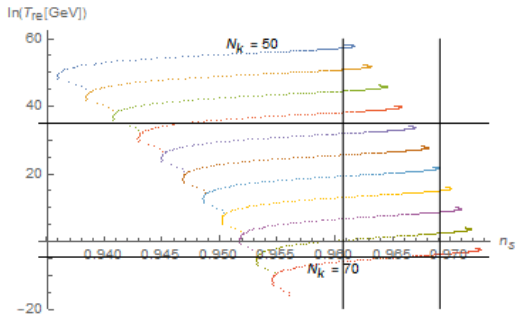

(b) The (log) reheating temperature of the QH_5 model against the spectral index n_s over $50 \leq N_k \leq 70$.

Figure 4.1: Numerical solutions of (n_s, r) and reheating temperature for the QH_5 model.

Starting with the QH_5 model, only those curves with $58 \lesssim N_k \lesssim 68$ are within the acceptable region of reheating temperate and spectral index in figure 4.1b. However when one also takes into account the 1σ region in figure 4.1a this is further reduced to $60 \lesssim N_k \lesssim 68$. Requiring that we consider both the Planck-consistent and reheating-consistent curves thus drastically reduces the acceptable region of $r - n_s$ parameter space for the corrected quartic hilltop model. This is significant as the corrections themselves are required for such models to even be taken seriously as candidates for single-field slow-roll inflation as without regularizing the potentials they produce a cosmology entirely incompatible with a universe that does not immediately collapse after inflation ends.

For QH_5, the resulting acceptable region on the $r - n_s$ plot lies in the mid to upper-left corner of the 1σ bound. If further, more precise measurements were to constrain the tensor fraction and spectral index away from this region, QH_5 would quickly become untenable.

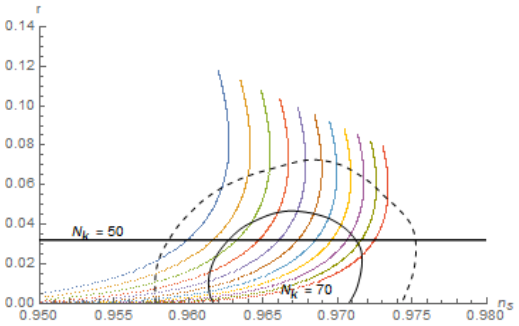

(a) Numerical solutions of the tensor-scalar ratio r and spectral index n_s for the QH_{10} model over the $50 \leq N_k \leq 70$.

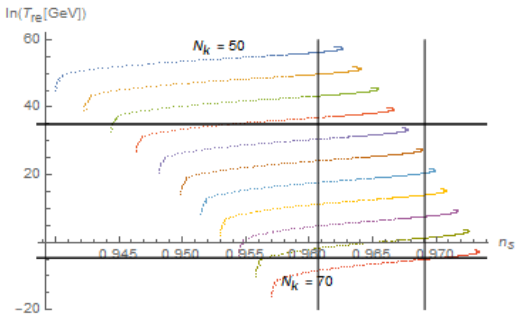

(b) The (log) reheating temperature of the QH_{10} model against the spectral index n_s over $50 \leq N_k \leq 70$.

Figure 4.2: Numerical solutions of (n_s, r) and reheating temperature for the QH_10 model.

Considering the QH_{10} in figure 4.2a, we see that increasing p causes more curves to enter the 1σ region of the $r - n_s$ plot. If one were to not consider reheating consistency this would place a lower bound of $56 \lesssim N_k$ on the number of efolds of inflation after the scale exits. However as we increase the power of the correction term, the curves in the (log) reheating temperature plot move very slowly and by $p = 10$ no new curves have entered or left the acceptable region in figure 4.2b. Reheating consistency of QH_{10} thus still requires $60 \lesssim N_k \lesssim 68$ just as with the lowest order correction QH_5. In contrast to QH_5 we see that now the curves for which $54 \lesssim N_k \lesssim 58$ have now entered the 1σ region in figure 4.2a however must still reject these as they remain outside the acceptable region of the reheating plot.

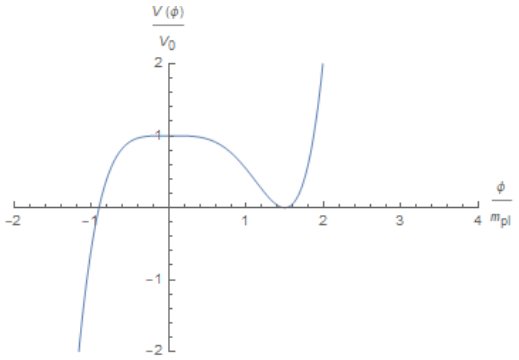

(a) The QH_5 potential at $\lambda = 1$

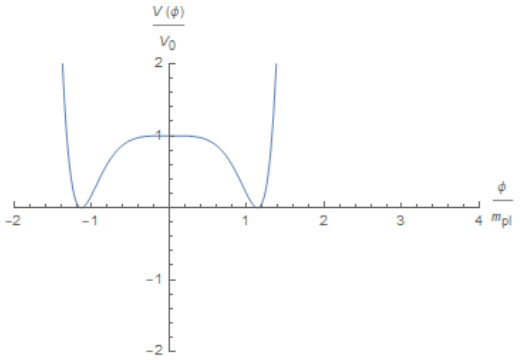

(b) The QH_{10} potential at $\lambda = 1$

Figure 4.3: Plots of the QH_5 and QH_{10} potentials.

Overall, the region of reheating-consistent parameter space in the $r - n_s$ plot actually increases with increasing p, as the distance between the curves remains relatively constant and they are only shifted along laterally. Initially it may then seem that one could simply add arbitrarily high powers to the Quartic Hillop model in order to increase the region of validity.

4.2 Radiatively Corrected Higgs Inflation

The case of the quartic hilltop model demonstrates clearly that we must only consider those potentials that are regularised and will not collapse the universe immediately after exiting inflation. How one regularises the potential is important if the model is to be compared to measurements. A huge number of candidate single field inflation models are analysed in [95]. Out of these models there are two which suffer from the same vacuum stabilisation as quartic hilltop. The first of these is the Radiatively Corrected Higgs Inflation (RCHI) model. This model derives from taking into account 1-loop corrections to the Higgs inflation model, in which the inflaton is a Higgs particle [107–111]. If one considers the standard model with the Higgs non-minimally coupled to classical gravity, the simplest such action in the Jordan frame is

$$S_T = \int d^4x\sqrt{-g}\left[\frac{1}{2}m_{pl}^2 R + \xi H^\dagger H R + \mathcal{L}_{SM}\right] \tag{4.15}$$

where $H^\dagger$ is the Higgs doublet and $\xi > 0$ is a dimensionless coupling parameter.

If we consider only the gravi-scalar sector of the theory and make use of the unitary gauge for which $H = (0, h/\sqrt{2})$ where h is a real scalar field, then the action of interest is

$$S = \int d^4x\sqrt{-g}\left[\frac{1}{2}F(h)R - \frac{1}{2}\partial_\mu h\partial^\mu h - W(h)\right] \tag{4.16}$$

the functions $F(h)$ and $W(h)$ which we define now for later convenience are

$$F_1(h) = (m_{pl}^2 + \xi h^2), \quad W(h) = \frac{\lambda}{4}(h^2 - \nu^2) \tag{4.17}$$

where ν is the electroweak symmetry breaking scale. After a conformal transformation of the metric

$$g_{\mu\nu} \to \theta(x) g_{\mu\nu}, \quad \theta(x) = \frac{m_{pl}^2}{m_{pl}^2 + \xi h^2} \tag{4.18}$$

we obtain the Einstein frame action

$$S = \int d^4x \sqrt{-g} \left[\frac{1}{2} m_{pl}^2 R - \frac{1}{2} m_{pl}^2 K(\theta) \partial_\mu \theta \partial^\mu \theta - V(\theta) \right] \tag{4.19}$$

in which the scalar field θ has a non-trivial kinetic term

$$K(\theta) = \frac{1}{4|a|\theta^2} \left(\frac{1 - 6|a|\theta}{1 - \theta} \right), \quad a = -\frac{\xi}{1 + 6\xi} \tag{4.20}$$

After rescaling to a canonically normalised field the action becomes

$$S = \int d^4x \sqrt{-g} \left[\frac{1}{2} m_{pl}^2 R - \frac{1}{2} \partial_\mu \phi \partial^\mu \phi - V(\phi) \right] \tag{4.21}$$

where the field ϕ satisfied the differential equation

$$\frac{1}{M_{pl}^2} \left(\frac{d\phi}{d\theta} \right)^2 = K(\theta) \tag{4.22}$$

The exact solution, which we omit here for brevity, is given in [107]. At tree level, where the coupling in the Jordan frame ξ is large and $a \simeq 1/6$ the Einstein frame potential is approximately

$$V(\phi) = \frac{M_{pl}^4 \lambda}{4\xi^2} \left(1 - e^{-\sqrt{\frac{2}{3}} \frac{\phi}{m_{pl}}} \right)^2 \tag{4.23}$$

We see from equation 4.23 that the Higgs self coupling λ and coupling to gravity ξ only enter the potential through it's overall normalisation so the ratio $\sqrt{\lambda}/\xi$ is completely determined from the CMB normalisation. However, the 1-loop radiative corrections to the effective action 4.16 in the Jordan frame contribute more significantly at large values of ξ, so it is not sufficient to consider only the tree

level approximation [112]. The radiative corrections modify the functions $F(h)$ and $W(h)$. To first order these corrections are

$$F(h) = m_{pl}^2 + \xi h^2 + \frac{C}{16\pi^2} h^2 \ln\left(\frac{m_{pl}^2 h^2}{\mu^2}\right) \tag{4.24}$$

$$W(h) = \frac{1}{4}\lambda\left(h^2 - \nu^2\right)^2 + \frac{\lambda A}{128\pi^2} h^4 \ln(\frac{h^2}{\mu^2}) \tag{4.25}$$

The modifications to these functions change the resulting Einstein frame potential from which we compute the inflationary observable n_s and r. The Radiatively Corrected Higgs Inflation (RCHI) potential is thus

$$V(\phi) \simeq V_0\left(1 - 2e^{-\frac{2\phi}{\sqrt{6}m_{pl}}} + \frac{A_I}{16\pi^2}\frac{\phi}{\sqrt{6}m_{pl}}\right) \tag{4.26}$$

where A_I is a free parameter as given in eq 4.12 of [95].

Before moving on to calculating corrections terms to the RCHI model we take note that there exists in the literature a modification to the Higgs inflation model that produces a regularized potential (as opposed to equation 4.26) which is unbounded from below. Firstly, in the literature there has been debate over the validity of the Higgs inflation model due to it's UV cutoff being very close to the energy scale of inflation $H \sim \sqrt{\lambda} m_{pl}/\xi$ [113–117] The cutoff scale, at which unitarity is broken for tree-level amplitudes, is calculated in [114] as $\Lambda \sim m_{pl}/\xi$ in the Einstein frame. For non-minimal coupling ξ and $\lambda \sim O(1)$ the effective field theory may not be a valid description of inflationary dynamics. In [113] the authors point out that these calculations of the cutoff scale are performed in the small field approximation $\phi \approx h$. However the we note that the inflationary regime has $\phi \gg 1$, in which the Einstein frame potential is

$$\begin{aligned} V(\phi) &\approx \frac{\lambda}{4\xi^2}\left(1 + e^{-\frac{2\phi}{\sqrt{6}}}\right)^2 \\ &\approx \frac{\lambda}{4\xi^2}\left(1 + 2e^{-\frac{2\phi}{\sqrt{6}}}\right) \end{aligned} \tag{4.27}$$

If one considers the series expansion of the potential in powers of ϕ, the result is quite different to what would have been obtained in the small field approximation

$$V(\phi) \approx \frac{3\lambda}{4\xi^2} - \frac{\lambda}{\xi^2\sqrt{6}}\phi + \frac{\lambda}{6\xi^2}\phi^2 - \frac{\lambda}{9\sqrt{6}\xi^2}\phi^3 + ... \tag{4.28}$$

thus the one-loop quantum corrections will contribute a cutoff

$$\Lambda \sim \frac{\xi^2}{\lambda} m_{pl} \tag{4.29}$$

This unitarity bound is well above the energy scale of inflation and so the effective field theory remains a safe description of inflationary physics with a regularized potential given by equation 4.27. In this paper however we focus only on the RCHI model featured in [95] as a means of demonstrating the effect of correction terms required by such unregularized potentials.

The Radiatively Corrected Higgs Inflation model shares similarities to Quartic Hilltop in that it also fits within the 1σ region of the Planck 2018 data over a given range of it's free parameter A_I, but does not produce a cosmology consistent with a universe that does not collapse.

In figure 4.4a there are indeed a few curves that fit well within the 1σ region provided by the Planck 2018 data, specifically those with $50 \lesssim N_k \lesssim 60$. When we take into account reheating consistency over the same parameter range in figure 4.4b we see that lie within the acceptable region formed by the rectangular bounds, essentially ruling out this model as a possibility. Like the quartic hilltop model, this potential also fails to produce a cosmology compatible with what we observe today. In the RCHI model, we exit inflation at small ϕ and shortly after the potential becomes negative. This behaviour of the potential needs to be corrected. There are a variety of ways one may correct the behaviour of this potential, as we did to form the QHS model. As such we could first consider simply squaring the potential to produce one which is regularised. However for RCHI, the potential only needs to be corrected at small field values as we would like to retain the flatness of the potential

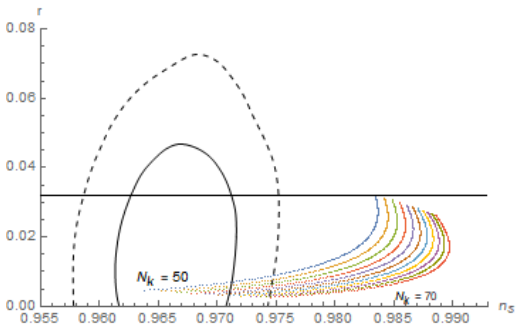

(a) Numerical solutions for tensor fraction r and spectral index n_s of the RCHI model over the range $1 \leq A_I \leq 40$ for $50 \leq N_k \leq 70$. The solid and dashed curves represent the Planck 2018 1σ and 2σ bounds respectively. The horizontal black line is the BICEP tensor fraction bound $r \lesssim 0.032$.

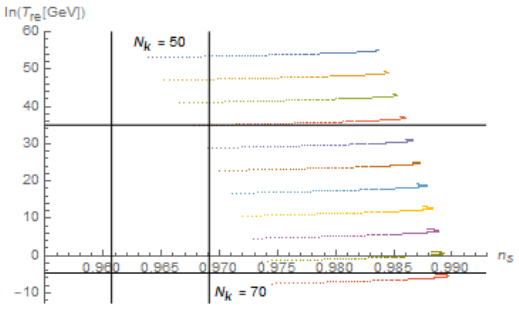

(b) Numerical solutions for reheating temperature T_{re} and spectral index n_s of the RCHI model over the range $1 \leq A_I \leq 40$ for $50 \leq N_k \leq 70$. The vertical solid lines represent the Planck 2018 spectral index bounds $0.9607 \lesssim n_s \lesssim 0.9691$ and the horizontal solid lines represent the reheating temperature bounds $0.01\text{GeV} \lesssim T_{re} \lesssim 10^{16}\text{GeV}$.

Figure 4.4: Numerical solutions of (n_s, r) and the reheating temperature of the RHCI model.

during slow-roll. Squaring the potential does not achieve this very well as it makes the potential very steep at large ϕ.

Compared to the standard RCHI model, the $r - n_s$ curves in figure 4.5a are elongated and far more dramatically curved outside of the 2σ region. Whilst the curves with $50 \lesssim N_k \lesssim 58$ lie within the 1σ region, it still remains the case that none of the curves are able to be made reheating-consistent. Furthermore, it is also worth noting that one needs at least 60 efolds of inflation to solve the horizon problem, making a squared version of the RCHI potential even less favourable.

The simplest such terms that one could add the only modify the potential at small ϕ are inverse powers of the form ϕ^{-p} where $p > 0$. Henceforth we refer to such models as RCHI$_p$. Just as we did when adding polynomial correction to the quartic hilltop model, we must ensure that the coefficient of the correction term keeps the scalar fields VEV at zero in order for inflation to end in a finite time. That is,

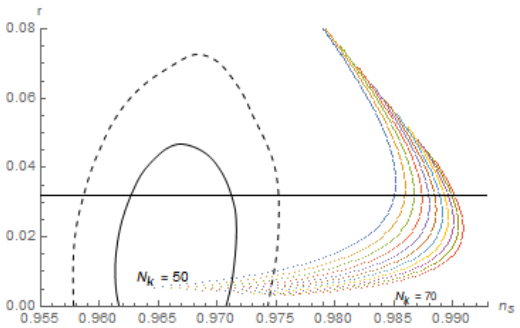

(a) Numerical solutions for tensor fraction r and spectral index n_s of the RCHI-Squared model over the range $1 \leq A_I \leq 40$ for $50 \leq N_k \leq 70$. The solid and dashed curves represent the Planck 2018 1σ and 2σ bounds respectively. The horizontal black line is the BICEP tensor fraction bound $r \lesssim 0.032$

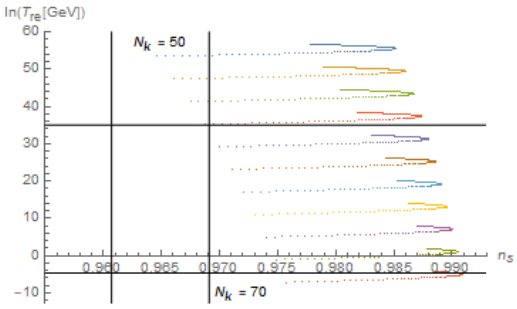

(b) Numerical solutions for reheating temperature T_{re} and spectral index n_s of the RCHI model over the range $1 \leq A_I \leq 40$ for $50 \leq N_k \leq 70$. The vertical solid lines represent the Planck 2018 spectral index bounds $0.9607 \lesssim n_s \lesssim 0.9691$ and the horizontal solid lines represent the reheating temperature bounds $0.01\text{GeV} \lesssim T_{re} \lesssim 10^{16}\text{GeV}$.

Figure 4.5: Numerical solutions of (n_s, r) and the reheating temperature of the RCHI-Squared model.

consider a potential of the form

$$V(\phi) = 1 - 2e^{-\frac{2\phi}{\sqrt{6}m_{pl}}} + \frac{A_I}{16\pi^2}\frac{\phi}{\sqrt{6}m_{pl}} + \alpha_p 6^{\frac{p}{2}}\phi^{-p} \tag{4.30}$$

The coefficient α_p must be such that $V(\phi_0) = 0$, where ϕ_0 is the field value at the minimum of the potential and therefore satisfies $V'(\phi_0) = 0$

$$\frac{4\phi_0}{\sqrt{6}m_{pl}}e^{-\frac{2\phi_0}{\sqrt{6}m_{pl}}} + \frac{A_I}{16\pi^2\sqrt{6}m_{pl}} - p\alpha_p 6^{\frac{p}{2}}\phi_0^{-(p+1)} = 0 \tag{4.31}$$

Equation 4.31 cannot be solved analytically for ϕ_0 but we may make use of an approximation. The minima of the potential is at small field values $\phi_0/m_{pl} \lesssim 1$ and thus

$$e^{-\frac{2\phi_0}{\sqrt{6}m_{pl}}} \approx 1 - \frac{2\phi_0}{\sqrt{6}m_{pl}} \tag{4.32}$$

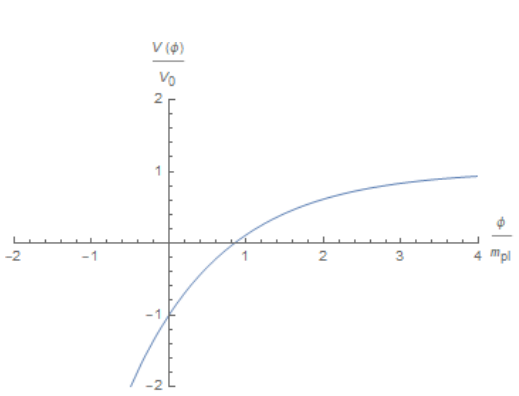

(a) The RCHI potential at $A_I = 1$

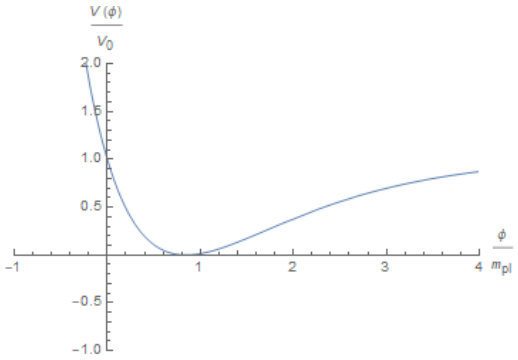

(b) The RCHI-Squared potential at $A_I = 1$.

Figure 4.6: Plots of the RCHI and RCHI-Squared potentials.

The $\phi_0^{-(p+1)}$ term will dominate the expression and thus we may solve for $\phi_0(\alpha_p)$

$$\phi_0 \simeq \sqrt{6}\left(\frac{16\pi^2 p\alpha_p m_{pl}}{A_I + 64\pi^2}\right)^{\frac{1}{p+1}} \tag{4.33}$$

Now substituting approximate solution 4.33 into $V(\phi_0) = 0$ allows us to solve for the coefficient

$$\alpha_p = \left(\frac{16\pi^2 m_{pl}}{A_I + 64\pi^2}\right)^p p^p (1+p)^{-(p+1)} \tag{4.34}$$

and so we work with an approximate potential

$$V(\phi) = 1 - 2e^{-\frac{2\phi}{\sqrt{6}m_{pl}}} + \frac{A_I}{16\pi^2}\frac{\phi}{\sqrt{6}m_{pl}} + \left(\frac{16\pi^2 m_{pl}}{A_I + 64\pi^2}\right)^p p^p (1+p)^{-(p+1)} 6^{\frac{p}{2}} \phi^{-p} \tag{4.35}$$

In the following figures we display the $r - n_s$ and $T_{re} - n_s$ plots for RCHI$_p$ with $1 \leq p \leq 10$. The bounds on the parameter spaces are the same as in all previous figures.

Starting with the RCHI$_1$ model which contains a ϕ^{-1} correction term, it can be seen in figure 4.7a, that the 1σ region contains those curves with $50 \lesssim N_k \lesssim 62$. Taking into account reheating consistency in figure 4.7b, we see that the reheating-consistent curves are those with $58 \lesssim N_k \lesssim 62$. However, these curves only slightly fit into the acceptable region of the $T_{re} - n_s$ plot over the parameter range $1 \leq A_I \leq 40$, so the likelihood that they would survive any further constraining by more

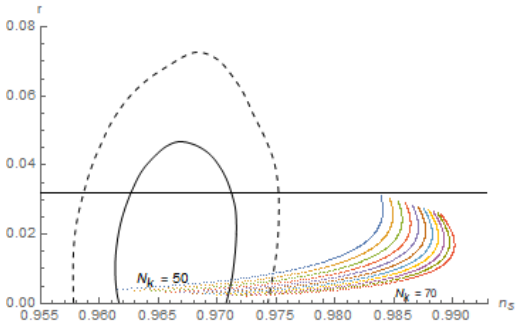

(a) Numerical solutions of the tensor-scalar ratio r and spectral index n_s for the RCHI$_1$ model over the $50 \leq N_k \leq 70$.

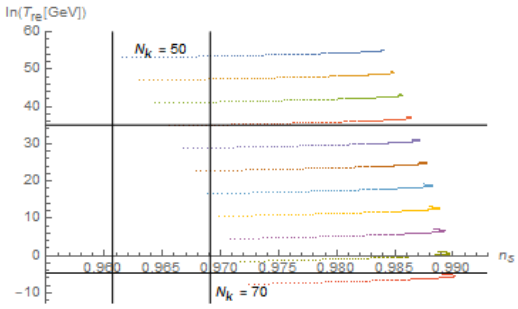

(b) The (log) reheating temperature of the RCHI$_1$ model against the spectral index n_s over $50 \leq N_k \leq 70$.

Figure 4.7: Numerical solutions of (n_s, r) and the reheating temperature of the $RCHI_1$ model.

precise measurements of n_s is low.

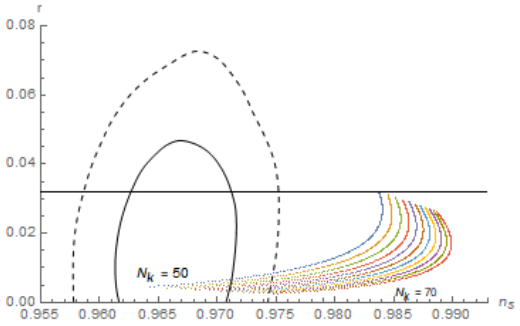

(a) Numerical solutions of the tensor-scalar ratio r and spectral index n_s for the RCHI$_{10}$ model over the $50 \leq N_k \leq 70$.

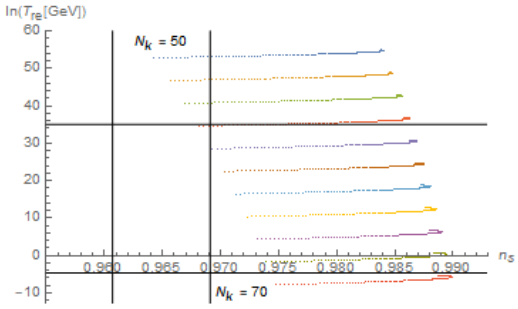

(b) The (log) reheating temperature of the RCHI$_{10}$ model against the spectral index n_s over $50 \leq N_k \leq 70$.

Figure 4.8: Numerical solutions of (n_s, r) and the reheating temperature of the $RCHI_{10}$ model.

As we increase the power of the correction term through to $p = 10$, the effect of this term in the potential is of course much stronger at small ϕ where the model exits inflation, and much weaker at large ϕ where it starts. Figures for $2 \leq p \leq 9$ are given in Appendix C. The effect on the $r - n_s$ plot compared to that of RCHI$_1$ is to push out of a few of the curves, leaving those with $50 \lesssim N_k \lesssim 60$ in the 1σ region. This is a relatively small change in the $r - n_s$ parameter space. Conversely,

in figure 4.8b we see that all of the curves have been pushed out of the acceptable in the reheating plot, leaving none that are reheating consistent over this parameter range.

Clearly the models become less viable as one increases the strength of the correction term. We also see from figures 4.9a and 4.9b that as the the power of the correction term increases the approximation for the coefficient α_p given in equation 4.34 becomes less accurate and the local minima is displaced from $V(\phi_0) \simeq 0$. Given that the RCHI_1 model only just survives reheating-consistency, it's likely that RCHI and corrections thereof will not fair well under any future, more precise measurements.

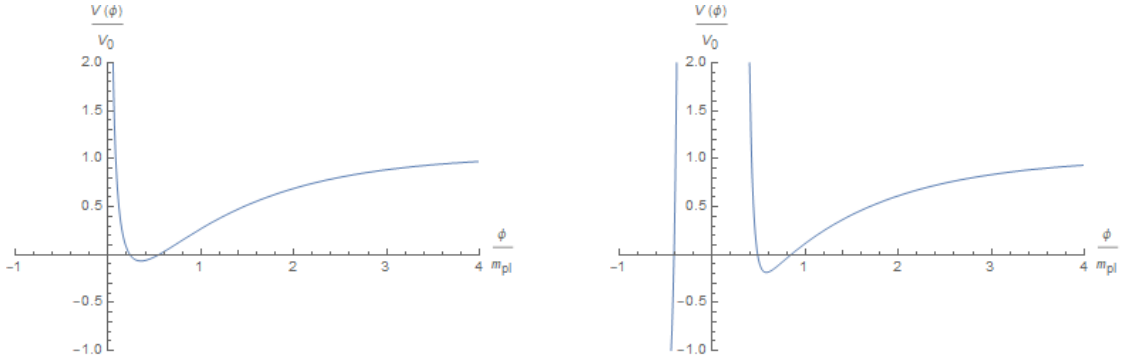

(a) The RCHI_1 potential at $A_I = 1$ (b) The RCHI_{10} potential at $A_I = 1$.

Figure 4.9: Plots of the $RCHI_1$ and $RCHI_{10}$ potentials.

4.3 Exponential SUSY Inflation

The final model we will investigate is that of Exponential SUSY Inflation (ESI). ESI models are governed by potentials of the form

$$V(\phi) - V_0 \left(1 - e^{-q\frac{\phi}{m_{pl}}}\right) \tag{4.36}$$

where q is the free parameter of order 1.

Potentials of this form appear in a broad range of literature [118–122], so we will not discuss the precise nature in which they occur in detail and only focus on the

inflationary predictions of the potential 4.36 and modifications thereof. Exponential SUSY inflation is a large field inflation model, one can calculate exactly the field value when slow roll inflation ends [95].

$$\frac{\phi_{\text{end}}}{m_{pl}} = \frac{1}{q} \ln\left(1 + \frac{q}{\sqrt{2}}\right) \tag{4.37}$$

For $q \sim \mathcal{O}(1)$, inflation ends at small field values $\phi_{end}/m_{pl} \lesssim 1$, after which the potential becomes negative. The ESI model is another of the single field inflation models featured in [95] which fits well within the Planck 2018 bounds. However like RCHI and QH, the potential remains unregularized and thus the model cannot lead to any physically realised cosmology.

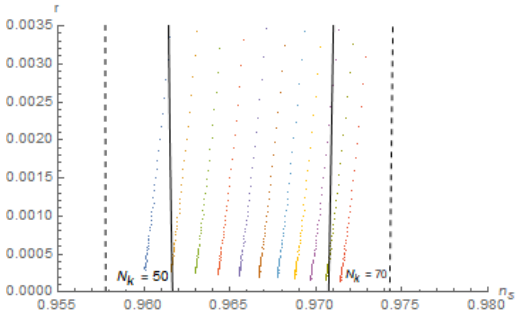

(a) Numerical solutions of the tensor-scalar ratio r and spectral index n_s for the ESI model with $0 < q < 10$ over $50 \leq N_k \leq 70$. The solid and dashed curves represent the Planck 2018 1σ and 2σ bounds respectively.

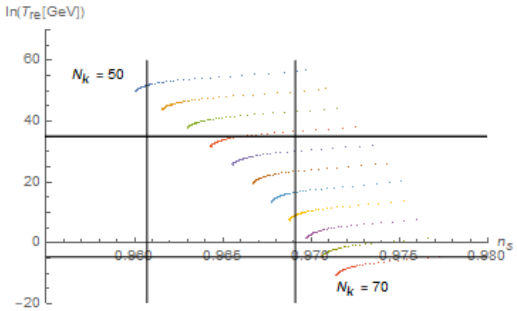

(b) The (log) reheating temperature of the ESI model with against the spectral index n_s with $0 < q < 10$ over $50 \leq N_k \leq 70$. The vertical solid lines represent the Planck 2018 spectral index bounds $0.9607 \lesssim n_s \lesssim 0.9691$ and the horizontal solid lines represent the reheating temperature bounds $0.01\text{GeV} \lesssim T_{re} \lesssim 10^{16}\text{GeV}$

Figure 4.10: Numerical solutions of (n_s, r) and the reheating temperature of the *ESI* model.

If one considers only the $r - n_s$ plot in figure 4.10a, ESI is among the most promising of the three models investigated in this paper, with all curves between $52 \lesssim N_k \lesssim 68$ lying within the 1σ region. In figure 4.10b however, only the curves for $56 \lesssim N_k \lesssim 64$ lie withing the acceptable region, and much like for the RCHI$_p$ models, only a small proportion of the curves fit within the Planck 2018 n_s bounds,

particularly for larger N_k, making it difficult for this model to remain viable if the parameter space were to be further constrained towards the centre of the rectangular bound. Of course we argue that these results are of little significance due to the unregularized behaviour of the potential. Just as with QH and RCHI this can be corrected by taking the square of the potential and calculating the resulting spectral index, tensor fraction and temperature at the end of reheating.

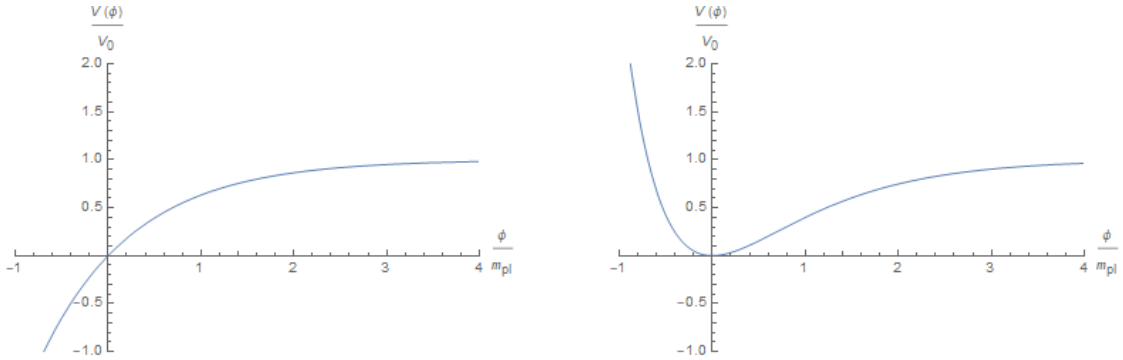

(a) The ESI potential at $q = 1$ (b) The ESI-Squared potential at $q = 1$.

Figure 4.11: Plots of the ESI and ESI-Squared potentials.

Just as with quartic hilltop and RCHI, one may try simply squaring the ESI potential to obtain a new potential that is bounded below. The squaring of the potential is motivated simply as a means of obtaining a new potential which behaves similarly to the original potential during inflation but has modified behaviour as the inflaton exits inflation. Namely that the potential is bounded from below and has a stable vacuum. From both figures 4.12a & 4.12b we see that squaring the potential does little to change the inflationary predictions of the model but gives allows the potential to produce a cosmology compatible with a universe that does not immediately collapse after inflation. The reheating-consistent curves remain those with $56 \lesssim N_k \lesssim 64$, although they still cover only a small fraction of the parameter space in figure 4.12b.

Unlike QH, we cannot add polynomial terms as an option to correct the ESI model at the end of inflation, since the exponential function will dominate over any ϕ^p term we can add towards the end of inflation. We could however, consider adding

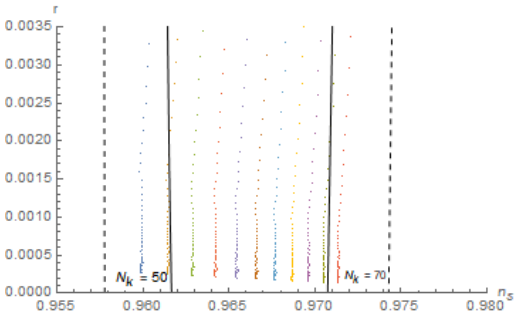

(a) Numerical solutions of the tensor-scalar ratio r and spectral index n_s for the ESI-Squared model with $0 < q < 10$ over $50 \leq N_k \leq 70$. The solid and dashed curves represent the Planck 2018 1σ and 2σ bounds respectively.

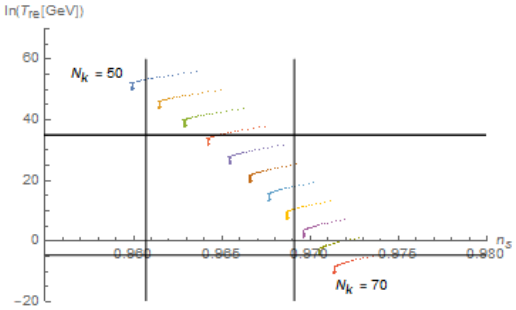

(b) The (log) reheating temperature of the ESI-Squared model with against the spectral index n_s with $0 < q < 10$ over $50 \leq N_k \leq 70$. The vertical solid lines represent the Planck 2018 spectral index bounds $0.9607 \lesssim n_s \lesssim 0.9691$ and the horizontal solid lines represent the reheating temperature bounds $0.01\text{GeV} \lesssim T_{re} \lesssim 10^{16}\text{GeV}$

Figure 4.12: Numerical solutions of (n_s, r) and the reheating temperature of the ESI-Squared model.

an inverse power correction of the form ϕ^{-p} as we did with RCHI to form the family of RCHI$_p$ models.

Consider a potential of the form

$$V(\phi) = 1 - e^{-q\frac{\phi}{m_{pl}}} + \alpha_p \phi^{-p} \tag{4.38}$$

Just as with the QH$_p$ and RCHI$_p$ models, we must adjust the coefficient α_p to ensure that the potentials at the VEV remains at $V(\phi_0) \simeq 0$ to first order so that inflation ends in a finite time. The VEV ϕ_0 satisfies $V'(\phi) = 0$ and thus

$$\frac{q}{m_{pl}} e^{-q\frac{\phi_0}{m_{pl}}} - p\alpha_p \phi_0^{-(p+1)} = 0 \tag{4.39}$$

For sufficiently small ϕ_0 equation 4.39 is dominated by the $\phi_0^{-(p+1)}$ term and thus to first order

$$\phi_0^{p+1} \simeq \frac{p\alpha_p m_{pl}}{q} \tag{4.40}$$

Demanding that the potential at the VEV is zero, one arrives at the equation

$$\phi_0 \left(1 + \frac{1}{p}\right) = 0 \tag{4.41}$$

for generic p this would require $\alpha_p = 0$,thus to a first approximation in the methods used here, there are no such correction terms that we can find for ESI. There may be other regularization methods outside the scope of this analysis which could perform this role.

4.4 Discussion

In this section we have investigated three promising candidate single field inflation models. These models all belong to the subset of candidate inflation models that are capable of producing acceptable an acceptable spectral index and tensor fraction in light of the Planck 2018 data, but do not predict any kind of sensible cosmology that is consistent with what we are simply around to observe the universe today. The issue lies in the unstabilized nature of the potentials after inflation ends. The Quartic Hilltop, radiatively corrected Higgs and exponential SUSY potentials do not posses local minima and so there is no stable vacuum about which the inflaton may oscillate and reheat the universe after expansion. In fact, since the potentials are unbounded from below, if the energy density of the universe continues to be dominated by the inflaton it will collapse on a time scale $t = H^{-1}$ after the end of inflation. This is a generic feature of any such potential that is not stabilized after inflation. The question remains as to whether regularizing the behaviour of these potentials has a significant effect on the inflationary predictions of the models, which indeed it does.

The corrections that are made to the inflationary potentials in this model are not motivated by a particular physical principle, however such potentials do indeed have to be corrected, otherwise the resulting cosmology is simply not compatible with the cosmology we observe today. We show that any such correction terms are significant

in terms of their effect on the inflationary predictions of the model. There are of course examples of more physically motivated corrections to inflationary models that previously suffered from the same issue of unboundedness. Brane inflation models featured in [95] can be consistently modified in a way that does not introduce new fine tuning parameters, to fit the Planck 2018 data in KKTLI inflation [123]. Likewise, the Higgs inflation model featured also has a physically motivated modification scheme that is consistent with Planck [113,114]. In this approach, the corrections to the functions $F(h)$ and $W(h)$ in equations 4.24 & 4.25 are calculated in the Einstein frame, giving an inflationary potential 4.27 that is everywhere positive with a local minima.

Potentials with regularized behaviour may undergo the reheating period after inflation without the universe collapsing in the process. The reheating temperature must at least as large as the BBN energy scale, and no greater than the energy scale of inflation, and so is loosely bounded by $0.01\text{GeV} \lesssim T_{re} \lesssim 10^{16}\text{GeV}$. Since T_{re} depends explicitly on the amount of inflation that has occurred, through N_k and H_k. Demanding reheating-consistency further constrains the acceptable region of the $r - n_s$ parameter space when combined with the Planck 2018 and BICEP/Keck Array measurements. Furthermore, at least approximately 60 efolds of inflation are required to solve the horizon problem [124], this consideration also allows us to pinpoint the regions of $r - n_s$ and $T_{re} - n_s$ inhabited by these regularized models.

For the Quartic Hilltop model investigated in [1], before taking into account reheating consistency, one may fit all curves with $53 \lesssim N_k$ into the acceptable region of $r - n_s$ parameter space, however after regularizing to form the QHS model, reheating consistency reduces this to only the curves with $63 \lesssim N_k \lesssim 68$ corresponding to reheating temperatures $1.8 \times 10^{-2}\text{GeV} \lesssim T_{re} \lesssim 6.0 \times 10^{4}\text{GeV}$. In this paper we investigate further options for correcting the behaviour of QH by adding polynomial terms ϕ^p forming the class of QH_p models for $5 \leq p \leq 10$. The lowest order corrected model QH_5 has reheating consistent curves $60 \lesssim N_k \lesssim 68$ corresponding to reheating temperatures $1\text{GeV} \lesssim T_{re} \lesssim 7.2 \times 10^{10}\text{GeV}$. As

we increase the strength of the correction term through to QH_{10}, the reheating-consistent curves in the $r - n_s$ parameter space still remain only those with $60 \lesssim N_k \lesssim 68$ as the spectral index and tensor fraction N_k efolds before the end of inflation are not particularly sensitive to the strength of the correction term which kicks in towards the end of inflation. However the reheating temperature is sensitive to this change and for QH_{10} these curves correspond to reheating temperatures of $8.2 \times 10^{-2}\text{GeV} \lesssim T_{re} \lesssim 1.1 \times 10^{13}\text{GeV}$

The next model in our discussion is that of Radiatively Corrected Higgs Inflation. Out of the three models considered in this paper, RCHI appears to be the least favourable, having already started in a precarious position even before regularization. Un-regularized RCHI potential allows only those curves with $50 \lesssim N_k \lesssim 60$ in the acceptable region of $r - n_s$ parameter space, considering that we require at least 60 efolds for the horizon problem that leaves only a singular curve $N_k \simeq 60$ as a potential candidate. However, none of the curves enter the region of reheating-consistency in the $T_{re} - n_s$ space. As we did with quartic hilltop, we may attempt to regularize this model by simply squaring the potential. The RCHI-Squared potential however only admits curves with $50 \lesssim N_k \lesssim 58$ in the acceptable region of $r - n_s$ space, so it does not address the horizon problem, which is an important corner stone of scalar field inflation models. Squaring the RCHI potential significantly alters the shape of the potential during inflation, so we may look for options that only affect the potential towards the end of inflation when the inflation field ϕ is small. The simplest such choices would be inverse power corrections of the form ϕ^{-p}, forming a family of RCHI_p models. We investigate these for $1 \leq p \leq 10$. RCHI_1 admits curves with $58 \lesssim N_k \lesssim 62$ in the acceptable region of $r - n_s$ space, further constrained to $60 \lesssim N_k \lesssim 62$ to be consistent with the horizon problem, corresponding to reheating temperatures $2.4 \times 10^{7}\text{GeV} \lesssim T_{re} \lesssim 3.6 \times 10^{9}\text{GeV}$. This simple correction makes the model very tightly bound and ideal for further analysis under more precise measurements of the spectral index and tensor fraction. As we increase the power of the correction term, there are less reheating-consistent curves

available in the $r - n_s$ parameter space. The highest order corrected model we look at, RCHI_{10} contains no reheating-consistent curves at all.

The final model discussed in this paper is that of exponential SUSY inflation. This potential in its un-regulairzed form already inhabits promising regions of the $r - n_s$ and $T_{re} - n_s$ parameter spaces. When squared to form a regularized ESI-squared model, the reheating consistent curves are those with $56 \lesssim N_k \lesssim 64$. Taking into account the horizon problem this is further reduced to $60 \lesssim N_k \lesssim 64$, a corresponding bound on the reheating temperature of $1.5 \times 10^2\text{GeV} \lesssim T_{re} \lesssim 4.9 \times 10^8\text{GeV}$. Unlike QH, adding polynomial corrections to ESI does not stabilise the potential as the exponential function dominates any such term that we could add. We show also that is it not possible to add inverse power terms that can be investigated analytically to first order.

Single field inflation models provide a versatile landscape of models to approach the problem of explaining cosmological inflation, but one must take great care that any model under consideration produces a cosmology after inflation that is consistent with what we observe today. In particular, it is important that the inflationary models we consider in this paper have stable vacuums which prevent the universe from collapsing shortly after inflation ends. This is an important consideration for as we have shown in the cases of Quartic Hilltop and radiatively corrected Higgs inflation, how one decides to regularise the potential can have significant effects on the observable that we measure today and may determine the viability of a given model when compared to observational data. In this work we make use of polynomial and inverse power correction terms, it is certainly worth noting that for a scalar field theory in $d = 4$ dimensions, only ϕ^4 interaction terms are renormalizable [125, 126]. So even models such as these with corrected potentials cannot be quantised to form self-consistent QFT's, they can only be considered as classical effective field theories for computing inflationary observables.

Chapter 5

Continuation of Bianchi Spacetimes Through The Big Bang

] *This section is based on research by the author and David Sloan published in Physical Review D [127]. It also contains an expanded upon discussion of the ADM formalism and homogeneous spacetimes, closely following references cited where relevant.*

One of the biggest conceptual and practical problems in contemporary cosmology is that of singularities in General Relativity (GR). The Hawking-Penrose theorems [128] establish that a wide class of spacetimes are geodesically incomplete. Without going into the details of measures on a space of theories, this is generally taken to mean that maximally extended space-times without any singularities are a set of measure zero. Solutions to the Einstein Field Equations (EFE) provide the metric structure and manifold geometry at each point in spacetime, when the EFE become indeterminate, the spacetime structure cannot be defined. In this sense there is a boundary beyond which physics cannot be deterministically continued which we know as a singularity. Typically this is characterised by some component of the Ricci tensor growing arbitrarily large [129], although this is not always the case. The most comprehensive understanding of singularities is provided by the Hawking-Penrose theorems, in which geodesic incompleteness necessitates a spacetime singularity,

there will be a boundary beyond which a null or timelike geodesic terminates after finite affine length [29, 128]. This poses a problem for General Relativity. Many physical solutions are bound to contain a point region beyond which physics cannot be continued in a deterministic manner. In particular, cosmological solutions to GR contain a Big Bang singularity, characterised by the vanishing of the scale factor and the infinite growth of the Hubble parameter. Study of the Big Bang has been at the centre of contemporary cosmology research [130]. In most modern literature, attempts to resolve spacetime singularities invoke a quantisation of gravity, be it perturbatively through string theory [131–133] or non-perturbatively through Loop Quantum Gravity [134–139].

These resolutions can be broadly fit into two camps. In the first camp the singularity is avoided dynamically through, e.g. the introduction of a new type of matter, or repulsive force at small scales. In the second, the space-time geometry is replaced by a quantum counterpart such as a quantum foam. In both cases the resolution requires that GR be 'corrected' in the neighbourhood of the singularity. The need for these corrections informs two key aspects in the study of quantum gravity. In the first the necessity of replacing GR by a quantum counterpart is underlined by the presence of singular points at which the theory needs to be corrected. In turn this means that that such points are the focus of where quantum theories of gravity should provide observable deviations from GR.

In this work, we present an approach to the resolution of spacetime singularities in an entirely classical manner, appealing to the relationalist framework of Shape Dynamics (SD) [140, 141]. A key dynamical variable in the cosmological sector of GR is the scale factor a. The scale factor however, is not a physical observable. One never measures (or more precisely, is not able to measure) the size of the universe a, only the size compared to some reference scale a/a_{ref}. Any measurement of the size of universe is a relative one, as our measuring apparatus is indeed part of the system we are attempting to measure. The relationalist framework laid out by Barbour and Bertotti [142] seeks to track only the intrinsic change of a dynamical

system. This has formed the foundation of the Shape Space, and recently, Dynamical Similarity [143] approach to cosmology. In this work, we synthesise recent work on the Shape Dynamics formalism [144, 145] and Dynamical Similarity to show how, starting with the ADM description of Hamiltonian GR, one can move formally to a description of cosmology with equivalent physical dynamics that never makes reference to a notion of absolute scale. In this description the dynamical system of physical observables defined on the phase space manifold remains well defined through the initial cosmological singularity and in this sense it is resolved classically. In this description the principle mathematical objects, namely the Hamiltonian and contact structure, remain finite and well defined, which hints at a rigorous route to quantisation.

This classical resolution is possible because we relax the requirement that our physical system consists of a pseudo-Riemannian geometry at all times. With the elimination of scale from our system we form a physical entity which, away from the singularity, can always be embedded within a pseudo-Riemannian framework through the additional assignment of scale. However, while this assignment breaks down at the singularity, crucially the integrability of the equations of motion does not. Therefore within this framework the singularity is not an endpoint of physics, but rather a point at which the pseudo-Riemannian description in terms of a three dimensional spatial manifold with volume is no longer appropriate.

5.1 Dynamical Similarity

Here we present how scale invariance can be used to reduce a theory from a symplectic manifold to a contact manifold. For a formal mathematical exposition see [146]. Scale invariance is an important aspect of the analysis of dynamical systems in cosmology. In any cosmological measurement, the scale factor is never directly observable as we are only able to infer relative changes. We shall start by reviewing some foundational results in the study of dynamical similarities presented

by Sloan in [147], in particular the fact that quotient out a dynamical similarity from a symplectic system leaves behind a symmetry reduced contact system. This is an autonomous dynamical system defined entirely in terms of dimensionless relational variables, and describes the same physics as the symplectic system. Consider for example the Kepler problem as in [148]. We consider the Lagrangian of two unit mass particles interacting through Newtonian gravity

$$L = \frac{1}{2}\dot{r}^2 + \frac{1}{2}r^2\dot{\theta}^2 + \frac{G}{r} \tag{5.1}$$

where r is the separation in the centre of mass frame. There exists a coordinate transformation that moves between indistinguishable solutions of the equations of motion. In particular this coordinate transformation is a multiplicative rescaling by a non-zero constant λ

$$r \to \lambda r, \quad t \to \lambda^{\frac{3}{2}} t \tag{5.2}$$

Under this rescaling, the action

$$S = \int L(r, \dot{r}, \dot{\theta}) dt \tag{5.3}$$

transforms also by a multiplicative rescaling $S \to \lambda^{\frac{1}{2}} S$ and hence the equations of motion whose solutions are critical paths of the action $\delta S = 0$, remain unchanged. This is an example of a dynamical similarity [143], which is a scaling symmetry of the dynamical system. As we will see in sections 2.2 and 2.3, Lagrangians of relevant cosmological models exhibit a dynamical similarity associated with the scale factor. In this section (2.1) we show how the identification of a dynamical similarity can be used to quotient out a redundant symmetry of the symplectic phase space, and define a system with equivalent dynamics on a contact manifold phase space.

Consider a symplectic system with Lagrangian $L(q_i, \dot{q}_i) : TQ \to \mathbb{R}$ and action

$$S = \int L(q_i, \dot{q}_i) dt \tag{5.4}$$

integrated over physical paths γ of the tangent bundle manifold TQ of a configuration space Q, parameterised by time over some interval $I \subseteq \mathbb{R}$. The physical curves γ on TQ are tangent lifts of curves $\bar{\gamma}$ on the configuration space. In this paper we will consider Lagrangians that have a configuration space scaling symmetry (CSSS). We define a CSSS to be a vector field $\bar{\mathbf{D}}$ on $Q \times I$ such that

i For all curves $\bar{\gamma} : I \to Q$ whose tangent lifts are stationary paths of the action 5.4, $\bar{\mathbf{D}}\bar{\gamma}$ are also stationary paths of the action.

ii $\mathbf{D}L = \Lambda L$, where $\Lambda \in \mathbb{R}$ and $\mathbf{D}$ is the tangent lift of the CSSS

The scaling symmetry $\bar{\mathbf{D}}$ moves between curves on configuration space Q, which represent indistinguishable solutions of the equations of motion as the Lagrangian scales by a multiplicative constant Λ which we call the degree of the CSSS. The CSSS is defined only up to a non-zero scalar factor, which we may fix by demanding that $\mathbf{D}$ preserves the Lie drag of the Lagrange one-form

$$\mathcal{L}_{\mathbf{D}}\mu_L = \mu_L, \quad \mu_L = \frac{\partial L}{\partial \dot{q}_i} dq_i \tag{5.5}$$

Consider a scaling symmetry of one of the configuration space variables $x \in Q$ and possibly of the time coordinate $t \in I$ and write the new coordinates under the scaling symmetry as

$$(\bar{x}, \bar{t}) = (Ax, Bt) = (\bar{\mathbf{D}}x, \bar{\mathbf{D}}t), \quad \bar{\mathbf{D}} = D_x\partial_x + D_t\partial_t \tag{5.6}$$

Thus the CSSS can be written locally w.l.o.g. as

$$\bar{\mathbf{D}} = Ax\frac{\partial}{\partial x} + Bt\frac{\partial}{\partial t} \tag{5.7}$$

which has tangent lift acting on the Lagrangian $\mathbf{D}L = \Lambda L$

$$\mathbf{D} = Ax\frac{\partial}{\partial x} + (A - B)\dot{x}\frac{\partial}{\partial \dot{x}} - B\dot{q}_i\frac{\partial}{\partial \dot{q}_i} + Bt\frac{\partial}{\partial t} \tag{5.8}$$

where $q_i \in Q$ are the configuration space coordinates unaffected by the scaling symmetry. We next make a coordinate and lapse transformation

$$\rho = x^{\frac{1}{A}}, \quad d\tau = \rho^{-B} dt \tag{5.9}$$

under which the CSSS is isochronal ($B = 0$) and has tangent lift

$$\mathbf{D} = A\left(x\frac{\partial}{\partial x} + x'\frac{\partial}{\partial x'}\right) \sim x\frac{\partial}{\partial x} + x'\frac{\partial}{\partial x'}, \quad \text{Normalising } A = 1 \tag{5.10}$$

where $'$ denotes derivatives w.r.t. the new time coordinate τ. We know show that given a Lagrangian function $L : TQ \to \mathbb{R}$ with a CSSS $\mathbf{D}$ of degree 1, it is possible to construct a Herglotz Lagrangian $L^H : TQ \times \mathbb{R} \to \mathbb{R}$ that describes the same dynamics on $TQ/\mathbf{D}$. Firstly, consider the converse. Let $L^H(q, \dot{q}, S)$ be a Herglotz Lagrangian, and define

$$L = e^{\rho}\left(L^H + \dot{\rho}S\right), \quad \rho = -\frac{\partial L^H}{\partial S} \tag{5.11}$$

Since L^H is a Herglotz Lagrangian, the physical paths on the manifold satisfy the Herglotz-Lagrange equations of motion 2.147. Thus one can show that the original tangent bundle coordinates $(q, \dot{q})$ satisfy the Euler-Lagrange equations generated by L.

$$\begin{aligned} \frac{d}{dt}\left(\frac{\partial L}{\partial \dot{q}}\right) - \frac{\partial L}{\partial q} &= \frac{d}{dt}\left(\frac{\partial L^H}{\partial \dot{q}}\right) - \frac{\partial L^H}{\partial q} + \dot{\rho}\frac{\partial L^H}{\partial \dot{q}} \\ &= \frac{d}{dt}\left(\frac{\partial L}{\partial \dot{q}} - \frac{\partial L^H}{\partial q}\right) - \frac{\partial L^H}{\partial S}\frac{\partial L^H}{\partial \dot{q}} = 0 \end{aligned} \tag{5.12}$$

Thus the dynamics of all $(q, \dot{q}) \in TQ$ generated by L and L^H are equivalent. Lastly make a change of coordinate $x = e^{\rho}$, under which the Lagrangian becomes

$$L = xL^H + \dot{x}S \tag{5.13}$$

The Lagrangian 5.13 clearly has a scaling symmetry of degree 1 given by

$$\mathbf{D} = x\partial_x + \dot{x}\partial_{\dot{x}} \tag{5.14}$$

Now consider the converse, let $L : TQ \to \mathbb{R}$ be a Lagrangian with the scaling symmetry 5.14 of degree 1. By the definition of $\mathbf{D}$ we have $\mathbf{D}L = L$ thus

$$x\frac{\partial L}{\partial x} + \dot{x}\frac{\partial L}{\partial \dot{x}} = L \tag{5.15}$$

We identify the partial derivatives as

$$L^H = \frac{\partial L}{\partial x}, \quad S = \frac{1}{x} i_{\mathbf{D}} \mu_L = \frac{\partial L}{\partial \dot{x}} \tag{5.16}$$

where $L^H(q, \dot{q}, S) : TQ \times \mathbb{R}$ can be shown to be a Herglotz Lagrangian with equivalent dynamics to L. The physical paths satisfy the Euler-Lagrange equations generated by L, which can be written in terms of L^H.

$$\begin{aligned} &\frac{d}{dt}\left(\frac{\partial L}{\partial \dot{q}}\right) - \frac{\partial L}{\partial q} = 0 \\ &\implies x\frac{d}{dt}\left(\frac{\partial L^H}{\partial \dot{q}}\right) - x\frac{\partial L^H}{\partial x} - L^H\delta_{x,q} + \dot{S}\delta_{\dot{x},\dot{q}} - x\frac{\partial L^H}{\partial S}\frac{\partial L^H}{\partial \dot{q}} = 0 \\ &\implies \frac{d}{dt}\left(\frac{\partial L^H}{\partial \dot{q}}\right) - \frac{\partial L^H}{\partial q} - \frac{\partial L^H}{\partial S}\frac{\partial L^H}{\partial \dot{q}} = 0 \end{aligned} \tag{5.17}$$

Thus the physical paths also satisfy the Herglotz equations of motion generated by L^H on the symmetry reduced manifold $TQ/\mathbf{D}$.

5.2 The ADM Formalism

In this section we present a brief review of the ADM formalism of General Relativity and cosmological spacetimes of interest in this section, namely Bianchi (I and IX) and flat FLRW. In particular we closely follow the approaches of [28, 149], which can be consulted for additional detail.

Within the framework of General Relativity, spacetime is assumed to be a 4-dimensional Lorentzian differentiable manifold $\mathcal{M}$ with metric $g_{\mu\nu}$. The manifold is assumed to be globally hyperbolic, so that it has the topological structure of $\mathbb{R} \times \Sigma$ where Σ is a spatial 3-manifold. Since $\mathcal{M}$ is globally hyperbolic, it can be foliated by such spacelike hypersurfaces. The full spacetime metric may be decomposed as

$$g_{\mu\nu} = \begin{pmatrix} N_i N^i - N^2 & N_j \\ N_i & \gamma_{ij} \end{pmatrix} \tag{5.18}$$

where the shift vector N^i, lapse function N and spatial 3-metric γ_{ij} fully determine the 4-dimensional spacetime metric $g_{\mu\nu}$.

With the 3+1 foliation of spacetime described above, one may start with the Einstein-Hilbert action and decompose it into dynamical variables defined on the 3-geometry

$$\begin{aligned} S &= \int d^4x \sqrt{-g} R \\ &= \int d^4x N \sqrt{\gamma} \left({}^3R(\gamma) + K^2 + K_{ij}K^{ij} - 2\nabla_n K - \frac{2}{N} D^i D_i N \right) \end{aligned} \tag{5.19}$$

where ${}^3R$ is the Ricci scalar associated with the spatial 3-metric γ_{ij}, K_{ij} is the extrinsic curvature of the spatial spatial slice Σ_t given by

$$K_{ij} = -\gamma_i^\sigma \gamma_j^\rho \nabla_\sigma n_\rho = \frac{1}{2N} \left(D_i N_j + D_j N_i - \dot{\gamma}_{ij} \right) \tag{5.20}$$

$K = \gamma_{ij} K^{ij}$ is the extrinsic curvature scalar, D_i are the spatial covariant derivatives and $\nabla_n K$ is the covariant derivative along the normal vector to the spatial 3-manifold n^μ, normalised to $n^\mu n_\mu = -1$. It is important to note that the objects γ_{ij}, K_{ij} and D_i are non-zero only on the spatial 3-manifold and therefore only have Latin subscripts. The action in eq. 5.19 is equivalent to

$$S = \int d^4x N\sqrt{\gamma}\left[{}^3R(\gamma) + K_{ij}K^{ij} - K^2\right] \tag{5.21}$$

up to boundary terms that have no effect on the equations of motion as their variation can be set to zero. Thus we have the Einstein-Hilbert Lagrangian

$$\mathcal{L} = N\sqrt{\gamma}\left[{}^3R(\gamma) + K_{ij}K^{ij} - K^2\right] \tag{5.22}$$

from which we may find the conjugate momenta of the dynamical variables $\{N, N^i, \gamma_{ij}\}$.Firstly one sees immediately that the lapse N and shift vector N^i have no conjugate momenta as their velocities do not enter into the Lagrangian. We will see that the lapse and shift vector actually turn out to be non-dynamical variables, as variation of the action with respect to them results in constraint relations which are fundamental to the Hamiltonian description of GR. On the other hand, the conjugate momenta to the spatial 3-metric is given by

$$\pi^{ij} = \frac{\partial\mathcal{L}}{\partial\dot{\gamma}_{ij}} = \sqrt{\gamma}\left(K\gamma^{ij} - K^{ij}\right) \tag{5.23}$$

The Hamiltonian density can then be obtained from a Legendre transform $\mathcal{H} = \pi^{ij}\dot{\gamma}_{ij} - \mathcal{L}$, giving the Hamiltonian

$$H = \int_{\Sigma_t} d^3x\,\mathcal{H} = \int_{\Sigma_t} d^3x\,N\left[\frac{1}{\sqrt{\gamma}}\left(\pi^{ij}\pi_{ij} - \frac{1}{2}\pi^2\right) - \sqrt{\gamma}^3R(\gamma)\right] + 2\int_{\Sigma_t} d^3x\,\pi^{ij}D_iN_j \tag{5.24}$$

The term in the second integral of eq 5.24 can be written in terms of a spatial covariant derivative of π^{ij} up to a boundary term which we may neglect. Thus the Hamiltonian that is conventionally presented in the ADM literature is

$$H = \int_{\Sigma_t} d^3x\,N\left[\frac{1}{\sqrt{\gamma}}\left(\pi^{ij}\pi_{ij} - \frac{1}{2}\pi^2\right) - \sqrt{\gamma}^3R(\gamma)\right] - 2\int_{\Sigma_t} d^3x\,N^iD^j\pi_{ij} \tag{5.25}$$

As usual, the physical paths on the solution space are the stationary paths of the action. Requiring the variation of the action 5.21 with respect to the lapse and

shift vector produces

$$\sqrt{\gamma}^3 R(\gamma) = K_{ij}K^{ij} - K^2 = \frac{1}{\sqrt{\gamma}}\left(\pi^{ij}\pi_{ij} - \frac{1}{2}\pi^2\right) = 0 \tag{5.26}$$

$$D^i \pi_{ij} = 0 \tag{5.27}$$

respectively. These are constraint equations which must be satisfied by solutions to the equations of motion. The first constraint in equation 5.26 is known as the Hamiltonian constraint and equation 5.27 is the diffeomorphism constraint. The expression of the ADM Hamiltonian 5.24 can be written in terms of the constraints by defining

$$\mathbb{H}[N] = \int_{\Sigma_t} d^3x\, N \left[\frac{1}{\sqrt{\gamma}}\left(\pi^{ij}\pi_{ij} - \frac{1}{2}\pi^2\right) - \sqrt{\gamma}^3 R(\gamma)\right] \approx 0 \tag{5.28}$$

$$\mathbb{D}[N^i] = -2\int_{\Sigma_t} d^3x\, N^i D^j \pi_{ij} \approx 0 \tag{5.29}$$

Where ≈ 0 denotes zero for solutions of the equations of motion which lie on the spacelike hypersurfaces Σ_t. Thus the Hamiltonian is written as

$$H = \mathbb{H}[N] + \mathbb{D}[N^i] \approx 0 \tag{5.30}$$

The Hamiltonian and diffeomorphism constraints form a set of *first class constraints*. A first class constraint f, as defined in Diracs treatment of constrained Hamiltonian systems [150] is a constraint whose Poisson bracket vanishes weakly with all other constraints of the system ϕ_i

$$\{f, \phi_i\} \approx 0 \tag{5.31}$$

The Hamiltonian and diffeomorphism constraints form a closed algebra under Poisson brackets, known as the "***Hypersurface Deformation Algebra***", and thus they vanish on spatial hypersurfaces.

$$\begin{aligned}\{\mathbb{D}[N^i], \mathbb{D}[M^j]\} &= \mathbb{D}\left[[N, M]\right] \\ \{\mathbb{D}[N^i], \mathbb{H}[N]\} &= \mathbb{H}\left[N^i \partial_i N\right] \\ \{\mathbb{H}[N], \mathbb{H}[M]\} &= \mathbb{D}\left[\gamma^{ij}\left(N\partial_i M - M\partial_k N\right)\right]\end{aligned} \tag{5.32}$$

The detail of deriving this algebra may be found in appendix H of [149] or Diracs original work [150]. The Hamiltonian and diffeomorphism constraints restrict physical paths to a subset of the GR phase space admitted by Hamiltons equations of motion. The Hamiltonian and diffeomprhism constraints must be zero on shell for arbitrary N and N^i, in this sense the lapse function and shift vector are non-dynamical Lagrange multipliers. The spatial 3-metric γ_{ij} and conjugate momentum π^{ij} satisfy Hamiltons equations of motion

$$\dot{\gamma}_{ij} = \frac{\partial \mathcal{H}}{\partial \pi^{ij}}, \quad \pi^{ij} = -\frac{\partial \mathcal{H}}{\partial \gamma^{ij}} \tag{5.33}$$

5.3 The Bianchi Classification and Homogeneous Cosmologies

In section 2.2.2 we reviewed homogeneous and isotropic solutions to the Einstein Field Equations. In this section we will be concerned with spatially homogeneous, but not necessarily isotropic cosmological spacetimes. The isomotries of such spacetimes are captured by the "***Bianchi Classification***", which we will describe here following along the lines of [149, 151, 152]. A spatially homogeneous spacetime $M = \mathbb{R} \times \Sigma$ is one for which there exists a Lie group G such that for any point p on the spatial 3-manifold, every point $q \in \Sigma_t$ lies in the group orbit of p. In other words, $\forall p, q \in \Sigma_t$ there exists a unique $g \in G$ such that $q = g(p)$. In this case the group G is said to act "simply transitively" on Σ_t. Since g is unique, the dimension of the group G must be equal to the dimension of the spatial slice Σ_t, thus the group isometries on the spatial manifold have 3-independent Killing vector fields ξ_a as their infinitesimal generators.

We saw in section 2.2.1.1 that a Lie algebra of Killing vector fields satisfies the commutation relation

$$[\xi_a, \xi_b] = C^c_{ab}\xi_c \tag{5.34}$$

where C^c_{ab} are the structure constants of the Lie group G. Here we will consider the group to be simply transitive, in the only case where there is a group that does not act simply transitively, or have a sub group that acts as such is $SO(3) \times \mathbb{R}$ acting on $M = S^2 \times \mathbb{R}$ which results in the Kantowski-Sachs model [153].

Up until this point we have worked in a coordinate basis $e_i = \partial_i$, $e^i = dx^i$. In general, the coordinate basis we are used to working in may not be invariant under the isometries generated by the three independent Killing vector field. However the existence of the Killing vector fields means that it is always possible to construct an invariant basis e_a, even if it does not coincide with the coordinate basis.

$$[e_a, e_b] = C^c_{ab}e_c \tag{5.35}$$

Associated with the invariant basis vectors, there will exist a dual basis of invariant 1-forms $\omega^a = e^a_\alpha dx^\alpha$ which satisfy the Maurer-Cartan equation

$$d\omega^c = \frac{1}{2}C^c_{ab}\omega^a \wedge \omega^b \tag{5.36}$$

The triads e^a_α satisfy orthogonality relations $e^a_\alpha e^\alpha_b = \delta^a_b$ & $e^a_\alpha e^\beta_a = \delta^\alpha_\beta$. On the spatial hypersurfaces, one can construct a metric which is the Cartan-Killing form [149, 154, 155]

$$\gamma_{ab} = C^c_{ad}C^d_{bc} = \gamma_{ba} = \gamma(e_a, e_b) \tag{5.37}$$

The Cartan-Killing form is symmetric by definition, and is non-degenerate for Lie algebras of semi-simple groups, which we shall assume here.

Any two Lie algebras with the same structure constant are isomorphic and thus describe the same topological structure, and so to determine the distinct homogeneous cosmologies, one must identify all inequivalent (real) 3 dimensional

Lie algebras. This is the Bianchi classification which we will outline here. First, we will show that given a vector X, its components in the invariant basis satisfy the same commutation relation as the basis vectors 5.35. Consider writing the induced line element on the spatial hypersurfaces Σ_t in terms of the invariant dual basis

$$dl^2 = \gamma_{ab}(x)\omega^a(x)\omega^b(x) \tag{5.38}$$

The line element must be invariant under a change of coordinates $x^\alpha \to x'^\alpha(x)$ which means we must have $\omega^a(x') = \omega^a(x)$. In terms of the triads and the dual coordinate basis we have

$$e^a_\alpha(x')dx'^\alpha = e^a_\alpha(x)dx^\alpha \tag{5.39}$$

Recall that the triads satisfy orthogonality conditions, thus we have

$$\begin{aligned} e^\beta_a(x')e^a_\alpha(x')dx'^a &= e^\beta_a(x')e^a_\alpha(x)dx^\alpha \\ \delta^\beta_\alpha dx'^\alpha &= e^\beta_a(x')e^a_\alpha(x)dx^\alpha \\ dx'^\beta &= e^\beta_a(x')e^a_\alpha(x)dx^\alpha \end{aligned} \tag{5.40}$$

Since $x' = x'(x)$, the exterior derivative can be written as

$$dx'^\beta = \frac{\partial x'^\beta}{\partial x^\alpha}dx^\alpha \tag{5.41}$$

We may then identify

$$\frac{\partial x'^\beta}{\partial x^\alpha} = e^\beta_a(x')e^a_\alpha(x) \tag{5.42}$$

This is a set of coupled partial differential equations. In order for these to be integrable, they must satisfy the Schwarz condition, that the Hessian of x'^β be symmetric

$$\frac{\partial^2 x'^\beta}{\partial x^\gamma \partial x^\alpha} = \frac{\partial^2 x'^\beta}{\partial x^\alpha \partial x^\gamma} \tag{5.43}$$

Using equation 5.42, we have the following second partial derivative

$$\begin{aligned}\frac{\partial^2 x'^\beta}{\partial x^\gamma \partial x^\alpha} &= \frac{\partial}{\partial x^\gamma}\left(e^\beta_a(x')e^a_\alpha(x)\right) \\ &= \frac{\partial e^\beta_a(x')}{\partial x^\gamma}e^a_\alpha(x) + e^\beta_a(x')\frac{\partial e^a_\alpha(x)}{\partial \gamma} \\ &= \frac{\partial e^\beta_a(x')}{\partial x'^\rho}\frac{\partial x'^\rho}{\partial x^\gamma}e^a_\alpha(x) + e^\beta_a(x')\frac{\partial e^a_\alpha(x)}{\partial \gamma} \\ &= \frac{\partial e^\beta_a(x')}{\partial x'^\rho}e^\rho_k(x')e^k_\gamma(x)e^a_\alpha(x) + e^\beta_a(x')\frac{\partial e^a_\alpha(x)}{\partial \gamma}\end{aligned} \tag{5.44}$$

After exchanging derivatives between terms using the triad orthogonality relations, the integrability condition reads

$$e^\beta_c(x')e^\rho_d(x')\left[\frac{\partial e^k_\beta(x')}{\partial x'^\rho} - \frac{e^k_\rho(x')}{\partial x'^\beta}\right] = e^\beta_c(x)e^\rho_d(x)\left[\frac{\partial e^k_\beta(x)}{\partial x^\rho} - \frac{e^k_\rho(x)}{\partial x^\beta}\right] \tag{5.45}$$

Since x and x' are arbitrary, the equality of equation 5.45 can be true if and only if both sides are constant. We are free to choose these constants to be the structure constants of the Lie algebra

$$e^\beta_c(x)e^\rho_d(x)\left[\frac{\partial e^k_\beta(x)}{\partial x^\rho} - \frac{e^k_\rho(x)}{\partial x^\sigma}\right] = C^k_{cd} \tag{5.46}$$

Multiplying by e^γ_k gives

$$\begin{aligned}e^\beta_c(x)e^\rho_d(x)\left[e^k_\rho\frac{\partial e^\gamma_k}{\partial x^\beta} - e^k_\beta\frac{e^\gamma_k}{x^\beta}\right] &= C^k_{cd}e^\gamma \\ \implies e^\beta_c\frac{\partial e^\gamma_d}{\partial x^\beta} - e^\rho_d\frac{\partial e^\gamma_c}{\partial x^\rho} &= C^k_{cd}e^\gamma_k\end{aligned} \tag{5.47}$$

The components of a vector X in the invariant basis are related to the coordinate basis by $X_a = e^\alpha_a\partial_\alpha$. The commutator can then be written as

$$\begin{aligned}[X_a, X_b] &= e^\alpha_a\partial_\alpha(e^\beta_b\partial_\beta) - e^\beta_b\partial_\beta(e^\alpha_a\partial_\alpha) \\ &= e^\alpha_a(\partial_\alpha e^\beta_b)\partial_\beta - e^\beta_b(\partial_\beta e^\alpha_a)\partial_\alpha\end{aligned} \tag{5.48}$$

From equation 5.47 we may write

$$\begin{aligned} e_a^\alpha \frac{\partial e_b^\beta}{\partial x^\alpha} - e_b^\rho \frac{\partial e_a^\beta}{\partial x^\rho} &= C_{ab}^c e_c^\beta \\ \implies e_a^\alpha (\partial_\alpha e_b^\beta)\partial_\beta &= e_b^\rho (\partial_\rho e_a^\beta)\partial_\beta + C_{ab}^c e_c^\beta \partial_\beta \\ e_a^\alpha (\partial_\alpha e_b^\beta)\partial_\beta &= e_b^\rho (\partial_\rho e_a^\beta)\partial_\beta + C_{ab}^c X_c \end{aligned} \tag{5.49}$$

where in the final line we have identified $X_k = e_k^\beta \partial_\beta$. Equation 5.49 may be substituted into equation 5.48, with a relabelling of the dummy indices $\rho \to \beta$, $\beta \to \alpha$ to give the required result

$$[X_a, X_b] = C_{ab}^c X_c \tag{5.50}$$

The commutator $[X_a, X_b]$ satisfies the Jacobi identity

$$[X_a, [X_b, X_c]] + [X_b, [X_c, X_a]] + [X_c, [X_a, X_b]] = 0 \tag{5.51}$$

Or equivalently in terms of the structure constants

$$C_{bc}^d C_{ad}^f + C_{ca}^d C_{bd}^f + C_{ab}^d C_{cd}^f = 0 \tag{5.52}$$

In order to determine the different isomotries, and hence distinct Bianchi cosmologies, we must determine all the inequivalent sets of structure constants. The first step in this process is to decompose the structure constants as follows. Let $a_a = C_{ba}^b$ and define

$$C^{ab} = \frac{1}{2}\epsilon^{acd}\left(C_{cd}^b - \delta_c^b a_d\right) \tag{5.53}$$

Contracting with the Levi-Civita symbol ϵ_{aef} one has

$$\begin{aligned}\epsilon_{aef}C^{ab} &= \frac{1}{2}\epsilon_{aef}\epsilon^{acd}\left(C^b_{cd} - \delta^b_c a_d\right) \\ &= \frac{1}{2}\left(\delta_{ec}\delta_{fd} - \delta_{ed}\delta_{fc}\right)\left(C^b_{cd} - \delta^b_c a_d\right) \\ &= C^b_{ef} + \frac{1}{2}\left(\delta^b_f a_e - \delta^b_e a_f\right)\end{aligned} \tag{5.54}$$

Contracting over the e and b indices we have

$$\begin{aligned}\epsilon_{ebf}C^{ab} &= C^b_{bf} + \frac{1}{2}\left(\delta^b_f a_b - \delta^b_b a_f\right) \\ &= a_f + \frac{1}{2}(a_f - 3a_f) \\ &= 0\end{aligned} \tag{5.55}$$

Equation 5.55 is the statement that C^{ab} is a symmetric matrix, to see this more clearly we may write the summation explicitly

$$\begin{aligned}&\epsilon_{abf}C^{ab} = \epsilon_{12f}C^{12} + \epsilon_{13f}C^{13} + \epsilon_{21f}C^{21} + \epsilon_{23f}C^{23} + \epsilon_{31f}C^{31} + \epsilon_{32f}C^{32} = 0 \\ &f = 1 \implies C^{32} - C^{32} = 0 \\ &f = 2 \implies C^{31} - C^{13} = 0 \\ &f = 3 \implies C^{12} - C^{21} = 0\end{aligned} \tag{5.56}$$

Thus any structure constant can be decomposed as

$$C^c_{ab} = \epsilon_{abd}C^{dc} + \delta^c_b a_a - \delta^c_a a_b \tag{5.57}$$

where $C^{ab} = C^{ba}$. with this decomposition of the structure constant, the Jacobi identity 5.52 is

$$C^{ab}a_b = 0 \tag{5.58}$$

Without loss of generality, the invariant basis can be chosen such that the symmetric matrix C^{ab} can be taken to be diagonal, with principle eigenvalues (n_1, n_2, n_3) and $a_a = (a, 0, 0)$. The Jacobi identity then reduces to

$$n_1 a = 0 \tag{5.59}$$

This splits the Bianchi classification into two classes. Class A models are those for which $a = 0$, and class B models are those for which $a \neq 0$. The distinct Bianchi models are therefore classified by all possible choices of $n_i \in \{-1, 0, 1\}$ and a satisfying 5.59 [149]. The commutator structure is explicitly

Classification	a	n_1	n_2	n_3
I	0	0	0	0
II	0	1	0	0
III	1	0	1	-1
IV	1	0	0	1
V	1	0	0	0
VI_a	a	0	1	-1
VI_0	0	1	-1	0
VII_a	a	0	1	1
VII_0	0	1	1	0
VIII	0	1	1	-1
IX	0	1	1	1

Figure 5.1: The Bianchi classification of real 3 dimensional Lie algebras and the associated values of a parameter and principle eigenvalues n_i of the symmetric matrix C^{ab}.

$$\begin{aligned} [X_1, X_2] &= -aX_2 + n_3 X_3 \\ [X_2, X_3] &= n_1 X_1 \\ [X_3, X_1] &= n_2 X_2 + aX_3 \end{aligned} \tag{5.60}$$

5.3.1 A Brief Aside: The Principle of Symmetric Criticality

At this point we may discuss an important subtlety which has gone unmentioned so far. When looking at a dynamical system from the variational perspective, one often starts with an action functional S and insists that the physical paths are the stationary points of the action. These are curves that satisfy the equations of motion resulting from the infinitesimal first order variation of the action. Sometimes however the physical system under consideration may be quite complicated, and we may only wish to look for solutions who are invariant under the action of some symmetry group G. For example spherically symmetric solutions which are invariant under the group of rotations in the relevant number of dimensions. In which case, we may first form the symmetry reduced action $S|_G$ and then try to solve the equations of motion resulting from its variational principle.

Much of the time we naively assume that the critical points of the symmetry reduced action $S|_G$ will also be critical points of the full action S. This is the "***Principle of Symmetric Criticality*** (PSC). The PSC was first considered by Palais in [156]. More formally, Palais defines the PSC as such: Let M be a C^∞ smooth manifold and let G be a group of diffeomorphisms acting on M. Let $f : M \to \mathbb{R}$ be a $C^\infty(M)$ smooth function on M that is G-invariant. Then define a critical point p of f and a point $p \in M$ such that $df|_p = 0$. Define a symmetric point $p \in M$ as an element of the set of points in M that are invariant under the group action i.e. $p \in \Sigma$, where $\Sigma - \{p \in M | g(p) = p \, \forall g \in G\}$. Then given a symmetric point p of M, for p to be a critical point of M it is sufficient for it to be a critical point of $f|_\Sigma$ where $f|_\Sigma$ denotes the restriction of f to Σ. Palais notes that the PSC need not always be valid nor well defined. When the PSC is well defined, a sufficient condition for it to be valid is that M is Riemannian and G is an isometry of M. The PSC is particularly important when studying homogeneous spacetimes in General Relativity. As Fels & Torre write in [157], typically in GR we start with a fixed spacetime (M, g) and try to determine its group of isometries by identifying a set of Killing vector fields, however in the ADM approach to Bianchi Cosmologies,

we look for a restriction of all possible spacetimes to a class of spacetimes with a chosen isometry. We therefore want to be sure that critical points the symmetry reduced Einstein-Hilbert action are in fact critical point of the general Einstein-Hilbert action. It was Hawking who noted in [158] that the PSC is valid if and only if the Bianchi spacetime is of class A. For class B isometry groups, the variation of the symmetry reduced action produces a non-trivial boundary term and hence the equations of motion do not coincide with those derived from the variation of the general Einstein-Hilbert action. In this work we will be concerned only with Bianchi type A cosmologies, and henceforth we will assume $a = 0$. In particular, we will look at the Bianchi I and Bianchi IX models. For both cosmological models, we will want to determine the Hamiltonian and diffeomorphism constraints 5.28 & 5.29 in the invariant basis and determine what we may about solutions to Hamiltons equations of motion for the dynamical variables. More detail on the PSC can be found in [159, 160].

5.4 Bianchi I

The Bianchi I cosmology 5.1 has $n_1 = n_2 = n_3 = 0$ and so the structure constants are all identically zero C^c_{ab}. This admits the simple Lie bracket structure

$$[X_1, X_2] = [X_2, X_3] = [X_3, X_1] = 0 \tag{5.61}$$

and its symmetry group is the Abelian group of translations in three dimensions $\mathbb{R}^3$. In this case the invariant basis coincides with the coordinate basis $e_\alpha = \partial_\alpha$ and the triads are simply Kronecker deltas $e^\alpha_a = \delta^\alpha_a$. Recall that in a coordinate basis, variation of the action with respect to the non-dynamical shift vector results in 5.27 $D^i \pi_{ij} = 0$, and so the diffeomorphism is satisfied trivially when our invariant basis which coincides with the coordinate basis. The Hamiltonian constraint 5.28 is

$$\mathbb{H}[N] = \int_{\Sigma_t} d^3x \, \frac{N}{\sqrt{\gamma}} \left(\pi^{\alpha\beta}\pi_{\alpha\beta} - \frac{1}{2}\pi^2 \right) \tag{5.62}$$

Thus the Bianchi I Hamiltonian can be written as

$$H_{BI} = \frac{n}{\sqrt{\gamma}} \left(\frac{1}{2} \pi^{ab} \pi_{ab} - \frac{1}{2} \pi^2 \right) \tag{5.63}$$

where $n = \int_{\Sigma_t} d^3x N$ is the lapse function spatially integrated over the fiducial cell. This is a non-dynamical Lagrange multiplier and so can be set to unity without loss of generality. The integration over the fiducial cell takes us from field theory of GR with an infinite number of degrees of freedom (although a finite number per point), to a particle theory with a finite number of degrees of freedom. Note here that While the ADM Hamiltonian of equation 5.62 describes the dynamics of general spacetimes, the Bianchi I Hamiltonian 5.63 is a symmetry reduced Hamiltonian.

We now continue to determine Hamiltons equations of motion for the Bianchi I Hamiltonian. For the following partial derivatives we have

$$\begin{aligned} \frac{\partial H_{BI}}{\partial \pi^{\alpha\beta}} &= \frac{n}{\sqrt{\gamma}} \left(\frac{\partial}{\partial \pi^{\alpha\beta}} \left(\pi^{\rho\sigma} \pi_{\rho\sigma} \right) - \pi \frac{\partial \pi}{\partial \pi^{\alpha\beta}} \right) \\ &= \frac{n}{\sqrt{\gamma}} \left(\pi_{\alpha\beta} + \pi^{\rho\sigma} \frac{\partial \pi_{\rho\sigma}}{\partial \pi^{\alpha\beta}} - \pi \gamma_{\alpha\beta} \right) \\ &= \frac{n}{\sqrt{\gamma}} \left(\pi_{\alpha\beta} + \frac{\partial}{\partial \pi^{\alpha\beta}} \left(\gamma_{\alpha\rho} \gamma_{\sigma\beta} \pi^{\alpha\beta} \right) - \pi \gamma_{\alpha\beta} \right) \\ &= \frac{n}{\sqrt{\gamma}} \left(\pi_{\alpha\beta} + \pi^{\rho\sigma} \gamma_{\alpha\rho} \gamma_{\sigma\beta} - \pi \gamma_{\alpha\beta} \right) \\ &= \frac{n}{\sqrt{\gamma}} \left(2\pi_{\alpha\beta} - \pi \gamma_{\alpha\beta} \right) \end{aligned} \tag{5.64}$$

$$\frac{\partial H_{BI}}{\partial \gamma_{\alpha\beta}} = n \left(\pi^{\rho_\sigma} \pi_{\rho_\sigma} - \frac{1}{2} \pi^2 \right) \frac{\partial \gamma^{-\frac{1}{2}}}{\partial \gamma_{\alpha\beta}} + \frac{n}{\sqrt{\gamma}} \left(\pi^{\rho\sigma} \frac{\partial \pi_{\rho\sigma}}{\partial \gamma_{\alpha\beta}} - \pi \frac{\partial \pi}{\partial \gamma_{\alpha\beta}} \right) \tag{5.65}$$

On shell, the ADM Hamiltonian must vanish for an arbitrary lapse and shift vector, so we have the constraint equation

$$\frac{1}{2} \pi^{ab} \pi_{ab} - \frac{1}{2} \pi^2 \approx 0 \tag{5.66}$$

We are only concerned with on-shell dynamics on the spatial hypersurfaces, so we

may enforce the constraint in the first term of equation 5.65 giving

$$\begin{aligned}\frac{\partial H_{BI}}{\partial \gamma_{\alpha\beta}} &= \frac{n}{\sqrt{\gamma}}\left(\pi^{\rho\sigma}\frac{\partial}{\partial\gamma_{\alpha\beta}}\left(\gamma_{\rho\delta}\gamma_{\sigma\omega}\pi^{\delta\omega}\right) - \pi\frac{\partial}{\partial\gamma_{\alpha\beta}}\left(\gamma_{\rho\sigma}\pi^{\rho\sigma}\right)\right) \\ &= \frac{n}{\sqrt{\gamma}}\left(\pi^{\alpha\sigma}\pi^{\beta\omega}\gamma_{\sigma_\omega} + \pi^{\rho\sigma}\pi^{\delta\beta}\gamma_{\rho\delta} - \pi\pi^{\alpha\beta}\right) \\ &= \frac{n}{\sqrt{\gamma}}\left(2\pi^{\alpha\sigma}\pi^{\beta}_{\sigma} - \pi\pi^{\alpha\beta}\right)\end{aligned} \tag{5.67}$$

Thus we have Hamiltons equations of motion for the metric and its conjugate momentum

$$\dot{\gamma}_{\alpha\beta} = \frac{n}{\sqrt{\gamma}}\left(2\pi_{\alpha\beta} - \pi\gamma_{\alpha\beta}\right), \quad \dot{\pi}^{\alpha\beta} = -\frac{n}{\sqrt{\gamma}}\left(2\pi^{\alpha\sigma}\pi^{\beta}_{\sigma} - \pi\pi^{\alpha\beta}\right) \tag{5.68}$$

As one would expect the spatial curvature invariant for the Bianchi I cosmology is exactly zero, and thus it describes geometries with flat spatial hypersurfaces.

We will now proceed to derive solutions to the vacuum equations of motion, by first making a series of canonical transformations and taking $n = 1$. The metric and momentum can always be chosen to be diagonal through a linear transformation of the coordinate basis and we choose to work in Ashtekar-Henderson-Sloan variables [161] where $\gamma_{\alpha\beta}$ and $\pi^{\alpha\beta}$ take the form

$$\gamma_{\alpha\beta} = (Q_1, Q_2, Q_3) \tag{5.69}$$

$$\pi^{\alpha\beta} = \left(\frac{P_1}{Q_1}, \frac{P_2}{Q_2}, \frac{P_3}{Q_3}\right) \tag{5.70}$$

in which the Hamiltonian is

$$H_{BI} = \frac{1}{\sqrt{Q_1Q_2Q_3}}\left[P_1^2 + P_2^2 + P_3^2 - \frac{1}{2}\left(P_1 + P_2 + P_3\right)^2\right] \tag{5.71}$$

We then make a further transformation of (canonical) variables

$$Q_1 = \nu^{\frac{2}{3}}e^{-\frac{x}{\sqrt{2}}+\frac{y}{\sqrt{6}}}, \quad Q_2 = \nu^{\frac{2}{3}}e^{\frac{x}{\sqrt{2}}+\frac{y}{\sqrt{6}}}, \quad Q_3 = \nu^{\frac{2}{3}}e^{-\sqrt{\frac{2}{3}}y} \tag{5.72}$$

$$P_1 = -\frac{k_x}{\sqrt{2}} + \frac{k_y}{\sqrt{2}} + \frac{\nu\tau}{2}, \quad P_2 = \frac{k_x}{\sqrt{2}} + \frac{k_y}{\sqrt{2}} + \frac{\nu\tau}{2}, \quad P_3 = -\sqrt{\frac{2}{3}k_y} + \frac{\nu\tau}{2} \tag{5.73}$$

The variables (x, y) are called the Misner anisotropy parameters [162] which measure the deviation from homogeneity, since when $x, y = 0$ the spacetime is both homogeneous and isotropic. The Misner variables have conjugate momenta (k_x, k_y) and ν is the volume factor which describes the overall scale of the fiducial cell and conjugate momenta τ, known as the York time. The Bianchi I Hamiltonian in this set of variables takes the form

$$H_{BI} = \nu^{-1}\left(-\frac{3}{8}\nu^2\tau^2 + k_x^2 + k_y^2\right) \tag{5.74}$$

From the form of the Hamiltonian in equation 5.76, particularly from the overall factor of ν^{-1}, we can see intuitively that there will be a singularity at $\nu \to 0$, in the sense that the Hamiltonian flow becomes ill-defined and therefore the Hamiltonian description of this dynamical system ceases to become predictive. We make one final transformation of variables

$$\begin{aligned} \nu &= \nu_0 e^{-\frac{\sqrt{3}}{2}x_0}, \quad \tau = -\frac{2}{\sqrt{3}}\nu_0^{-1}e^{\frac{\sqrt{3}}{2}x_0}p_0 \\ x &= \sqrt{2}x_1, \quad k_x = \frac{1}{\sqrt{2}}p_1 \\ y &= \sqrt{2}x_2, \quad k_y = \frac{1}{\sqrt{2}}p_2 \end{aligned} \tag{5.75}$$

where ν_0 is a constant scale. This gives a Hamiltonian of the form

$$H_{BI} = \frac{1}{2}\nu_0^{-1}e^{\frac{\sqrt{3}}{2}x_0}\left(-p_0^2 + p_1^2 + p_2^2\right) \tag{5.76}$$

The Bianchi I Hamiltonian 5.76 is independent of x_1 and x_2, consequently the conjugate momenta p_1 and p_2 are conserved along its flow. There are two more

equations of motion for x_0 and p_0 which read

$$\dot{x}_0 = \frac{\partial H_{BI}}{\partial p_0} = -\nu_0^{-1} p_0 e^{\frac{\sqrt{3}}{2}x_0} \tag{5.77}$$

$$\dot{p}_0 = -\frac{\partial H_{BI}}{\partial x_0} = -\sqrt{3}\nu_0^{-1} e^{\frac{\sqrt{3}}{2}x_0}\left(-p_0^2 + p_1^2 + p_2^2\right) \tag{5.78}$$

For the Hamiltonian constraint to be satisfied at all points along the flow, we require

$$-p_0^2 + p_1^2 + p_2^2 \approx 0 \tag{5.79}$$

and thus p_0 is also a conserved momentum and equation 5.77 admits the simple solution

$$e^{-\frac{\sqrt{3}}{2}x_0} = C_0 + \frac{\sqrt{3}}{2}\nu_0^{-1} p_0 t \tag{5.80}$$

where C_0 is a constant of integration. Hamiltons equations for x_1 and x_2 read

$$\dot{x}_i = \frac{\partial H_{BI}}{\partial p_i} = \nu_0^{-1} e^{\frac{\sqrt{3}}{2}x_0} p_i, \quad i = 1, 2. \tag{5.81}$$

Having already solved for $x_0(t)$ we may simply integrate for $x_i(t)$

$$\begin{aligned} x_i(t) &= C_i + \nu_0^{-1} p_i \int e^{\frac{\sqrt{3}}{2}x_0}\, dt \\ &= C_i + 2p_i \int \frac{1}{2\nu_0 C_0 + \sqrt{3}p_0 t}\, dt \\ &= C_i + \frac{2p_i}{\sqrt{3}p_0} \ln\left(2\nu_0 C_0 + \sqrt{3}p_0 t\right) \end{aligned} \tag{5.82}$$

Having solved the Hamiltons equations of motion for the vacuum Bianchi I cosmology, known as the "***Kasner Solution***, we are interested in analysing the dynamics of the metric components Before proceeding, we set all integration constants to zero, noting that we may do so without loss of generality, as they amount to a simply translation of our coordinate system. We will now trace back our step through the coordinate transformations and determine the spatial metric

components $\gamma_{\alpha\beta}(t)$. Recall that the volume factor is related to x_0 by 5.75

$$\nu(t) = \nu_0 e^{-\frac{\sqrt{3}}{2}x_0(t)} = \frac{\sqrt{3}}{2}p_0 t \tag{5.83}$$

and the Misner anisotropy parameters are

$$\begin{aligned} x(t) &= \sqrt{2}x_1 = 2\sqrt{\frac{2}{3}}\frac{p_1}{p_0}\ln\left(\sqrt{3}p_0 t\right) \\ y(t) &= \sqrt{2}x_2 = 2\sqrt{\frac{2}{3}}\frac{p_2}{p_0}\ln\left(\sqrt{3}p_0 t\right) \end{aligned} \tag{5.84}$$

The constant momentum p_0 can be set to unity by a rescaling of the time coordinate, after which we have the spatial metric

$$\gamma_{\alpha\beta}(t) = \left(t^{2q_1}, t^{2q_2}, t^{2q_3}\right) \tag{5.85}$$

where

$$\begin{aligned} q_1 &= \frac{1}{3} + \frac{1}{\sqrt{3}}p_2 - p_1 \\ q_2 &= \frac{1}{3} + \frac{1}{\sqrt{3}}p_2 + p_1 \\ q_3 &= \frac{1}{3} - \frac{2}{3}p_2 \end{aligned} \tag{5.86}$$

The parameters q_i are known as the "***Kasner Exponents***", by simply inspection we can see that they must satisfy

$$q_1 + q_2 + q_3 = 1 \tag{5.87}$$

Considering also the Hamiltonian constraint (remembering that we have effectively p_0 to unity through a rescaling of the time coordinate) $1 = p_1^2 + p_2^2$ we see that

$$q_1^2 + q_2^2 + q_3^2 = 1 \tag{5.88}$$

These two constraints mean that there is only one free Kasner exponent, and thus we have a 1-parameter family of solutions, described by the intersection of the "Kasner plane" $\sum_i q_i = 1$ with the "Kasner sphere" $\sum_i q_i^2 = 1$, which is just the unit 2-sphere. Without loss of generality we may choose an ordering of the Kasner exponents $q_1 \leq q_2 \leq q_3$ and parameterise the exponents by letting $u = q_2/q_3$ for $q_3 \neq 0$. Equation which defines the Kasner plane 5.87 then gives

$$q_1 = 1 - q_3(1+u) \tag{5.89}$$

Substituting this into the equation 5.88 for the Kasner sphere gives

$$\begin{aligned} &[1 - q_3(1+u)]^2 + u^2 q_3^3 + q_3^2 = 1 \\ \implies\ &q_3\left[q_3(u^2+u+1) - (1+u)\right] = 0 \end{aligned} \tag{5.90}$$

Since we have $q_3 \neq 0$ the only valid solution is

$$q_1(u) = -\frac{u}{u^2+u+1}, \quad q_2(u) = \frac{u(1+u)}{u^2+u+1}, \quad q_3(u) = \frac{1+u}{u^2+u+1} \tag{5.91}$$

There exist only two non-degenerate solutions to equations 5.87 & 5.88 which are $(0,0,1)$ and $(-\frac{1}{3}, \frac{2}{3}, \frac{2}{3})$. Otherwise, no two Kasner exponents are equal. All solutions other than $(0,0,1)$ must have one negative Kasner exponent and two positive ones, and so there is always one contracting spatial dimension as $t \to \infty$. In converse, as $t \to -\infty$, two of the spatial dimensions are contracting whilst one is expanding, squashing the spacetime into a pancake-like shape!

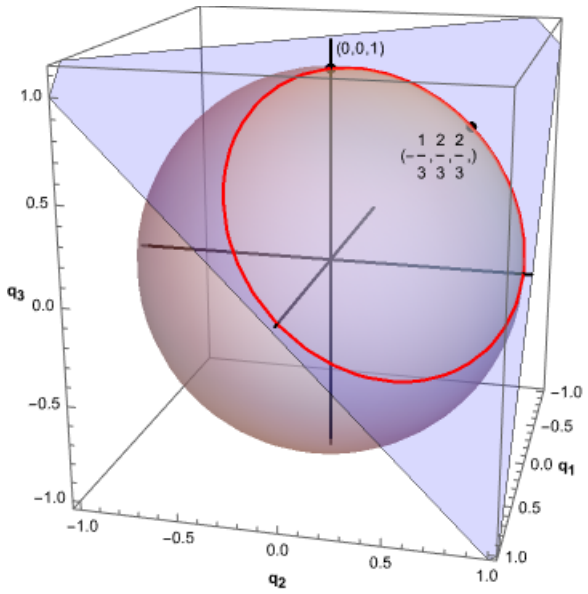

Figure 5.2: Figure showing the intersection of the Kasner plane $\sum_i q_i = 1$ (light blue) with the Kasner sphere $\sum_i q_i^2 = 1$ (light red). The solutions lie on the Kasner circle (bold red). The only two degenerate solutions $(0, 0, 1)$, $(-\frac{1}{2}, \frac{2}{3}, \frac{2}{3})$ are both labelled. Apart from where it passes through the north pole of the Kasner sphere, the Kasner circle always lies in a quadrant where one of the Kasner exponents is negative.

The intersection between the Kasner plane and the Kasner sphere is plotted in figure 5.2, the resulting set of solutions lie on the "Kasner circle". In figure 5.3 we plot the solutions for the Kasner exponents as functions of the free parameter u, highlighting the degenerate solutions.

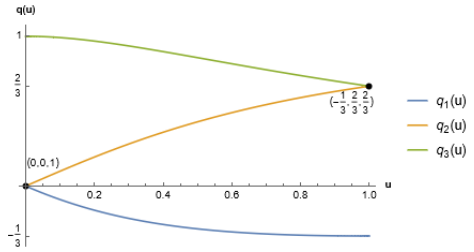

Figure 5.3: Plots of the constrained Kasner exponents which lie on the Kasner circle, in terms of the free parameter $q(u)$. The degenerate solutions $(0, 0, 1)$ and $(-\frac{1}{2}, \frac{2}{3}, \frac{2}{3})$ are highlighted.

The curvature invariant has a genuine singularity at $t = 0$ in all solutions except the degenerate $(0, 0, 1)$ solution. In this case the spacetime metric can be shown to

be flat 1+1 dimensional Minkowski metric through a coordinate transformation

$$\tau = t\cosh z, \quad \psi = t\sinh z \tag{5.92}$$

for which we have

$$\begin{aligned} d\tau^2 - d\psi^2 &= \left(\cosh z dt + t\sinh z dz\right)^2 - \left(\sinh z dt + t\cosh z dz\right)^2 \\ &= \left(\cosh^2 z - \sinh^2 z\right) dt^2 + t^2\left(\sinh^2 z - \cosh^2 z\right) dz^2 \\ &= dt^2 - t^2 dz^2 \end{aligned} \tag{5.93}$$

The invariant metric line element is then

$$\begin{aligned} ds^2 &= -dt^2 + \gamma_{ab}\omega^a\omega^b \\ &= -dt^2 + \gamma_{ab}dx^a dx^b \\ &= -dt^2 + t^2 dz \\ &= -d\tau^2 + d\phi^2 \end{aligned} \tag{5.94}$$

5.5 Bianchi IX

We now move on to determining the Bianchi IX Hamiltonian. Recall from the table in figure 5.1, that the Bianchi IX Lie algebra has $n_1 = n_2 = n_3 = 1$, which admits the Lie bracket structure

$$\begin{aligned} [X_1, X_2] &= X_3 \\ [X_2, X_3] &= X_1 \\ [X_3, X_1] &= X_2 \end{aligned} \tag{5.95}$$

The structure constants are simply Levi-Civita symbols $C^c_{ab} = \epsilon_{abc}$. Unlike the Bianchi I cosmology, the invariant basis does not coincide with a coordinate basis for Bianchi IX. A choice of the invariant 1-form basis in terms of the coordinate

basis is given by [147, 149, 155]

$$\begin{aligned}\omega^1 &= -\sin r\, d\theta + \cos r \sin\theta\, d\phi \\ \omega^2 &= -\cos r\, d\theta - \sin r \sin\theta\ \ d\phi \\ \omega^3 &= dr + \cos\theta\, d\phi\end{aligned} \tag{5.96}$$

Where (r, θ, ϕ) are spherical coordinates. These 1-forms are invariant under the group rotations in three dimensions, and thus the Bianchi IX Lie algebra is $\mathfrak{so}(3)$.

The Hamiltonian and diffeomorphism constraints from equations 5.28 and 5.29 in the invariant basis become

$$\mathbb{H}[N] = \int_{\Sigma_t} d^3x \frac{N\sin\theta}{\sqrt{\gamma}} \left[\mathrm{Tr}\gamma^2 - \frac{1}{2}\left(\mathrm{Tr}\gamma\right)^2 + \pi^{ab}\pi_{ab} - \frac{1}{2}\pi^2\right] \tag{5.97}$$

$$\mathbb{D}[N^a] = -2\int_{\Sigma_t} d^3x N^a \sin\theta \epsilon^c_{ab}\pi^{bc}\gamma_{bc} \tag{5.98}$$

Just as in the Bianchi I case, the spatially integrated lapse function can be packaged into a variable n

$$n = \int_{\Sigma_t} d^3x\, N\sin\theta \tag{5.99}$$

which enters as a Lagrange multiplier, and thus the overall factor of n can be set to unity in both the Hamiltonian and diffeomorphism constraint giving

$$\mathbb{H} = \frac{1}{\sqrt{\gamma}}\left(\mathrm{Tr}\gamma^2 - \frac{1}{2}\left(\mathrm{Tr}\gamma\right)^2 + \pi^{ab}\pi_{ab} - \frac{1}{2}\pi^2\right) \approx 0 \tag{5.100}$$

$$\mathbb{D}_a = -2\epsilon^c_{ab}\pi^{bd}\gamma_{dc} \approx 0 \tag{5.101}$$

The diffeomorphism constraint can be written in terms of a commutator that strongly suggests the same gauge fixing used in the Bianchi I case should be used here

$$[\pi^{ac}, \gamma_{cb}] \approx 0 \tag{5.102}$$

To this end we impose the Taub gauge where the 3-metric and conjugate momentum

are diagonal and choose the same Misner anisotropy parameter variables as in eq's 5.72 and 5.73. Following the same transformation of variables as in section 5.4 one arrives at the Bianchi IX ADM Hamiltonian

$$H_{BIX} = \nu^{-1}\left[-\frac{3}{8}\nu^2\tau^2 + \frac{1}{2}(p_x^2 + p_y^2) + \nu^{\frac{4}{3}}V_s(x,y)\right] \tag{5.103}$$

where the function $V_s(x,y)$ is the "shape potential" given by

$$\begin{aligned} V_s(x,y) &= f(-\sqrt{3}x + y) + f(\sqrt{3}x + y) + f(-2y) \\ f(z) &= \frac{1}{2}e^{\sqrt{\frac{2}{3}}z} - e^{-\frac{z}{\sqrt{6}}} \end{aligned} \tag{5.104}$$

The shape potential originates from the 3-Ricci scalar on the spatial hypersurface, which in the chosen coordinates is simply the volume factor multiplied by a "scale-free" part ${}^3R(\gamma) = \nu^{-\frac{2}{3}}V_s(x,y)$. There is an important comparison between the Bianchi IX and Bianchi I Hamiltonian. The Hamiltonian describing the Bianchi IX dynamical system can be likened to that of a free point particle acting under a potential term $\nu^{\frac{4}{3}V_s(x,y)}$ (we may ignore the ν^{-1} pre-factor here as the lapse can always be chosen to scale with ν such that the resulting pre-factor is constant.) In the case where $V_s(x,y) = 0$, we are left with the Bianchi I dynamical system in which the point particle simply moves along straight lines in the (x,y) plane. From this perspective we can see that Bianchi IX solutions pass through points where the geometry is that of Bianchi I.

In figure 5.4a we plot the shape potential (in log scale) and in figure 5.4b we plot its heat map and equipotential lines, as a functions of the anisotropy parameters. The potential has exponentially steep walls with a triangular shape. The exponential steepness of the shape potential means that in the regions between the walls, the potential is approximately zero, and thus the solution to the equations of motion are approximately Kasner. The Bianchi IX dynamics can be described from the perspective of a particle which travels freely along straight lines until it suddenly collides with the potential wall. Shape potential couples directly to the volume factor

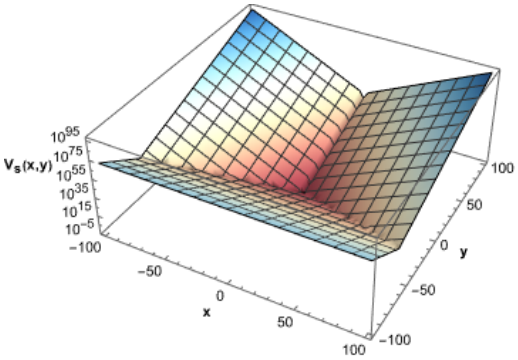

(a) Plot in log scale of the shape potential $V_s(x, y)$ defined in equation 5.104 as a function of the anisotropy parameters (x, y). The shape potential exhibits exponentially steep walls with a triangular symmetry around about the origin.

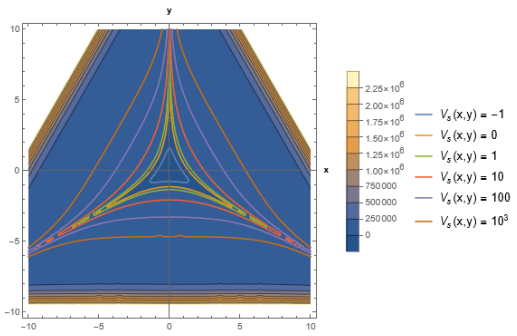

(b) A heat map plot of shape potential $V_s(x, y)$. In particular we highlight the equipotential lines $V_s(x, y) = (-1, 0, 1, 10, 100, 10^3)$

Figure 5.4: Plots of the shape potential $V_s(x, y)$.

which increases monotonically with time, and therefore the walls of the potential are receding from the "particle" and the collisions are inelastic. After each collision the Bianchi IX dynamical system sets off on a new approximate Kasner trajectory with decreased momentum $\sqrt{p_x^2 + p_y^2}$. These transitions between quasi-Kasner states are known as Taub transitions. Detailed explanations of these transitions can be found in section 4.3.2 of [149] and section 13.1 of [140]. A natural question arises from consideration of Taub transitions of the Bianchi IX system. Since the potential walls are receding away from the particle, are there configurations for which there are a finite number of bounces off the potential walls before the dynamical system is left in a final quasi-Kasner state? Such a condition is called "***Quiescence***", and the answer is that Quiescence is not possible in vacuum Bianchi IX cosmologies. Here we will outline the arguments given in [140, 149] from the perspective of the ADM Hamiltonian. In section 4.3.2 of [149] one can also find an argument from the perspective of the Einstein field equations. The end result from both approaches is the same: quasi-Kasner solutions in the vacuum Bianchi IX dynamical system are never stable, and there will be an infinite number of Taub transitions before the

spacetime singularity is reached in finite proper time. The argument is as follows. We start with the ADM Hamiltonian, where we have chosen the lapse to scale with $\sqrt{\gamma}$ for which

$$H_{BIX} = \mathrm{Tr}\gamma^2 - \frac{1}{2}\left(\mathrm{Tr}\gamma\right)^2 + \pi^{ab}\pi_{ab} - \frac{1}{2}\pi^2 \tag{5.105}$$

Following the same steps as before, gauge fixing the metric and momentum to be diagonal we have

$$H_{BIX} = -\frac{3}{8}\nu^2\tau^2 + k_x^2 + k_y^2 + \nu^{\frac{4}{3}}V_s(x,y) \tag{5.106}$$

Then making the canonical transformation

$$\begin{aligned} \nu &= \nu_0 e^{-\frac{3}{2}x_0}, \quad \tau = -\frac{2}{\sqrt{3}}\nu_0^{-2}e^{\frac{3}{2}x_0}p_0 \\ x &= \sqrt{2}x_1, \quad k_x = \frac{1}{\sqrt{2}}p_1 \\ y &= \sqrt{2}x_2, \quad k_y = \frac{1}{\sqrt{2}}p_2 \end{aligned} \tag{5.107}$$

The Hamiltonian is then

$$H_{BIX} = \frac{1}{2}\left(-p_0^2 + p_1^2 + p_2^2\right) + W(x_0, x_1, x_2) \tag{5.108}$$

Where the potential function $W(x_0, x_1, x_2)$ is given by

$$W(x_0, x_1, x_2) = \nu_0^{\frac{4}{2}} e^{-\frac{2}{\sqrt{3}}x_0} V_s(x_1, x_2) \tag{5.109}$$

Consider the dynamical system during a Kasner epoch, where the potential term is negligible in comparison to the kinetic term $-p_0^2 + p_1^2 + p_2^2$, then the Hamiltonian is

$$H \sim \frac{1}{2}\left(-p_0^2 + p_1^2 + p_2^2\right) \approx 0 \tag{5.110}$$

where all momenta are constant. To clarify the notation here we use $\sim$ to denote "approximately equal to" and $\approx$ to denote on-shell equality. The equations of motion

during this Kasner epoch are simply

$$x_0 = -p_0 t, \quad x_i = p_i t, \quad i = 1, 2 \tag{5.111}$$

where we have set the integration constants to zero. The Hamiltonian constraint during a Kasner epoch sets $p_0 = -\sqrt{p_1^2 + p_2^2}$, where have chosen the $p_0 \leq 0$ solution, since we are interested in cases where $\nu_0 \to x_0$ as $x_0 \to \infty$. We next make a coordinate transformation of (x_1, x_2) to polar coordinates

$$x_1 = r\cos\phi, \quad x_2 = r\sin\phi \tag{5.112}$$

The potential function felt by the particle during a Kasner epoch is then

$$\begin{aligned} W(x_0, x_1, x_2) &= \nu_0^{\frac{4}{3}} e^{-\frac{2}{\sqrt{3}}x_0} V_s(r, \phi) \\ &= \nu_0^{\frac{4}{3}} \sum_i c_i e^{r f_i(\phi) - \frac{2}{\sqrt{3}}x_0} \\ &= \nu_0^{\frac{4}{3}} \sum_i c_i e^{\left(f_i(\phi) - \frac{2}{\sqrt{3}}\right)\sqrt{p_1^2+p_2^2}\,t} \end{aligned} \tag{5.113}$$

The functions $f_i(\phi)$ and their coefficients are given by

$$\begin{aligned} &f_1(\phi) = \frac{2}{\sqrt{3}}\sin\phi + 2\cos\phi, \quad c_1 = \frac{1}{2}, \quad f_2(\phi) = \frac{2}{\sqrt{3}}\sin\phi - 2\cos\phi, \quad c_2 = \frac{1}{2} \\ &f_3(\phi) = -\frac{1}{\sqrt{3}}\sin\phi + \cos\phi, \quad c_3 = -1, \quad f_4(\phi) = -\frac{1}{\sqrt{3}}\sin\phi - \cos\phi, \quad c_4 = -1 \\ &f_5(\phi) = -\frac{4}{\sqrt{3}}\sin\phi, \quad c_5 = \frac{1}{2}, \quad f_6(\phi) = \frac{2}{\sqrt{3}}\sin\phi, \quad c_6 = -1 \end{aligned} \tag{5.114}$$

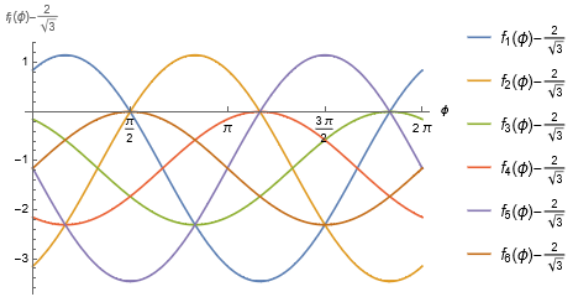

Figure 5.5: Plots of the exponents $f_i(\phi) - \frac{2}{\sqrt{3}}$ in the potential function $W(x, r, \phi)$ as given in equation 5.113

The functions $f_i(\phi) - \frac{2}{\sqrt{3}}$ appearing in the exponents of the potential 5.113 are plotted in figure 5.5. One can see clearly that all functions $f_i(\phi)$ are bounded below and for any given ϕ, there is always at least one function satisfying $f_i(\phi) - \frac{2}{\sqrt{3}} \geq 0$. Therefore during any Kasner epoch, the potential term will eventually grow to dominate the kinetic term, even if it is initially negligibly small in comparison. Any Kasner epoch is thus unstable and cannot persist indefinitely. The particle is guaranteed to catch up with the receding potential wall resulting in another inelastic collision. Since this carries on indefinitely, there will be an infinite number of bounces from any given time until the particle reaches the singularity at $\nu, \to 0$. Quiescence therefore cannot be achieved in vacuum Bianchi IX. The behaviour in which the particle undergoes an infinite number of Taub transitions before reaching the singularity is known as the Mixmaster behaviour [163]. The Mixmaster behaviour is opaque to its initial conditions in that by the time the particle has reached the singularity, it has gone through infinitely many Taub transitions scrambling any information that could have been inferred about its initial configuration.

Whilst quiescence cannot be attained in vacuum solutions, the introduction of a minimally coupled homogeneous scalar field eliminates the Mixmaster behaviour. Through the same procedure in which we derived the vacuum ADM Hamiltonian, it can be easily shown that the introduction of such a scalar field $\phi(t)$ simply introduces an additional kinetic term into the Bianchi IX Hamiltonian in the way that we could intuitively suspect and a potential term should we choose to include it. The details

of this can be found in section 5.3 of [149].

$$H_{BIX} = -\frac{3}{8}\nu^2\tau^2 + k_x^2 + k_y^2 + \frac{1}{2}p_\phi^2 + \nu^{\frac{4}{3}}V_s(x,y) + \nu^2 V(\phi) \tag{5.115}$$

The key differences in this model that allow for quiescence are that the scalar field is not coupled to the shape potential, and therefore does not feel the effect of its bounces, consequently its momentum is conserved through Taub transitions. Secondly the field potential has a different coupling to the volume factor than the shape potential, we will see that there are restrictions on how fast the field potential may grow if quiescence is to be achieved. Following the same canonical coordinate transformation we are now used to 5.107, the Bianchi IX Hamiltonian 5.115 becomes

$$\begin{aligned} H_{BIX} &= \frac{1}{2}\left(-p_0^2 + p_1^2 + p_2^2 + p_\phi^2\right) + W(x_0, x_1, x_2, \phi) \\ W(x_0, x_1, x_2, \phi) &= \nu_0^{\frac{4}{3}} e^{-\frac{2}{\sqrt{3}}x_0} V_s(x_1, x_2) + v_0^2 e^{-\sqrt{3}x_0} V(\phi) \end{aligned} \tag{5.116}$$

During Kasner epochs we have the familiar solutions to the approximate equations of motion Firstly we require that

$$\lim_{t\to\infty}\left[e^{-\sqrt{3}x_0(t)}V(\phi(t))\right] = 0 \tag{5.117}$$

so that the field potential term cannot dominate over the shape potential term after a sufficient amount of time. Provided that this is satisfied, then during a Kasner epoch the solutions to the approximate equations of motion are the familiar

$$\begin{aligned} x_0 &= -p_0 t, \quad x_i = p_i t, \quad i = 1, 2 \\ \phi &= p_\phi t \end{aligned} \tag{5.118}$$

with all momenta constant.

The Hamiltonian constraint now reads $p_0 = -\sqrt{p_1^2 + p_2^2 + p_3^2}$. Writing (x_1, x_2) in polar coordinates (r, θ), the potential function during a Kasner epoch is

$$W(r,\theta,\phi) = \nu_0^{\frac{4}{3}} \sum_i c_i e^{\sqrt{p_1^2+p_2^2}\left(f_i(\theta) - \frac{2}{\sqrt{3}}\sqrt{1+\frac{p_\phi^2}{p_1^2+p_2^2}}\right)t} + \nu_0^2 e^{-\sqrt{p_1^2+p_2^2+p_\phi^2}t} V(p_\phi t) \quad (5.119)$$

As mentioned, the scalar field does not interact with the shape potential, as so inelastic collisions with the potential wall reduce $p_1^2+p_2^2$ and not p_ϕ^2. After a sufficient number of Taub transitions the dynamical system will reach a point where

$$f_i(\phi) < \frac{2}{\sqrt{3}}\sqrt{1 + \frac{p_\phi^2}{p_1^2 + p_2^2}}, \quad \forall i \quad (5.120)$$

Since the momentum $p_1^2 + p_2^2$ decreases for every bounce, there will no longer be any positive exponent in the potential function and the shape potential term will begin to exponentially decay. We thus reach a state where the dynamical system undergoes one final Taub transition and continues on its final quasi-Kasner trajectory.

5.6 Contact Reduction of Cosmological Dynamical Systems

5.6.1 FLRW

Having now reviewed the ADM formulation of Hamiltonian General Relativity, subsequently determining the Bianchi I & IX Hamiltonians we will now apply the mathematical framework of dynamical similarities outlined in section 5.1 to reduce the symplectic Hamiltonian systems to contact ones. In particular, in section 5.1 we established that it is possible to reduce the standard symplectic description of a system to a contact one when there exists a scaling symmetry $\mathbf{D}$ such that the Lie drag of the Lagrangian moves between indistinguishable solutions $L_{\mathbf{D}_\Lambda}\mathcal{L} = \Lambda\mathcal{L}$.

Before diving straight into the Bianchi cosmologies, we will first describe the process of contact-reducing the flat ($k = 0$) FLRW (+ free massless scalar field) Lagrangian as a toy model. The process of contact reduction will involve removing a redundant, non-physical degree of freedom, the volume factor ν leaving a dynamical system which is described in therms of the physical relational quantities such as the Hubble factor ν'/ν. We start by considering the action of a scalar field minimally coupled to the FLRW metric

$$S = \int_{\mathbb{R}} \int_{\Sigma_t} d^4x \sqrt{-g} \left(R + \frac{1}{2}\dot{\phi}^2 - V(\phi) \right) \tag{5.121}$$

where the spacetime $\mathcal{M} = \mathbb{R} \times \Sigma_t$ is foliated by spacelike hypersurfaces Σ_t. The metric $g_{\mu\nu}$ is the FLRW metric with line element $ds^2 = -dt^2 + a(t)^2(dx^2 + dy^2 + dz^2)$. The Ricci scalar associated with the FLRW metric is

$$R = 6 \left[\frac{\ddot{a}}{a} + \left(\frac{\dot{a}}{a} \right)^2 \right] \tag{5.122}$$

In terms of the volume factor $\nu(t) = a(t)^3$ the action is

$$S = \int d^4x \, \nu \left[-\frac{2}{3} \left(\frac{\dot{\nu}}{\nu} \right)^2 + \frac{1}{2}\dot{\phi}^2 - V(\phi) \right] \tag{5.123}$$

The Lagrangian

$$\mathcal{L} = \nu \left[-\frac{2}{3} \left(\frac{\dot{\nu}}{\nu} \right)^2 + \frac{1}{2}\dot{\phi}^2 - V(\phi) \right] \tag{5.124}$$

exhibits an isochronal scaling symmetry of the volume factor

$$\nu = \lambda\bar{\nu} \implies \mathcal{L} = \lambda\bar{\nu} \left[-\frac{2}{3} \left(\frac{\dot{\bar{\nu}}}{\bar{\nu}} \right) + \frac{1}{2}\dot{\phi}^2 - V(\phi) \right] = \lambda\bar{\mathcal{L}}, \quad \lambda \in \mathbb{R}/\{0\} \tag{5.125}$$

The CSSS that generates this scaling symmetry is $\bar{\mathbf{D}} = \nu\partial_\nu$ with tangent lift $\mathbf{D} = \nu\partial_\nu + \dot{\nu}\partial_{\dot{\nu}}$ By acting on the Lagrangian with $\mathbf{D}$ one sees clearly that this is already a scaling symmetry of degree 1 (therefore no coordinate transformations are

required before forming the Herglotz Lagrangian). As per section 2.1, there exits a Herglotz Lagrangian $\mathcal{L}^H$ given by equation 5.16 which describes the same physics as $\mathcal{L}$ on the symmetry-reduced contact manifold $TQ/\mathbf{D}$. In the following sections we will switch notation from $S \to h$ to describe the global coordinate on the contact manifold.

$$\begin{aligned} h &= \frac{1}{\nu} i_{\mathbf{D}} \mu_L = -\frac{4\dot{\nu}}{3\nu} \\ \mathcal{L}^H(q, \dot{q}, h) &= \frac{\partial \mathcal{L}}{\partial \nu} = \frac{3}{8}h^2 + \frac{1}{2}\dot{\phi}^2 - V(\phi) \end{aligned} \tag{5.126}$$

The contact Hamiltonian given by the Legendre transformation and contact form are

$$\mathcal{H}^c = -\frac{3}{8}h^2 + \frac{1}{2}p_\phi^2 + V(\phi), \quad \eta = -dh + p_\phi d\phi \tag{5.127}$$

In the contact formalism, scalar field has been decoupled from the redundant scale factor variable in the symplectic system, however this still does not make (h, ϕ) the correct choice of coordinates to describe the manifold geometry near the Big Bang singularity. These variables still diverge as we approach the Big Bang. We will show in section 5.7 that making a compactification onto shape space provides a suitable description in which the dynamical variables, contact form and Hamiltonian are well defined through the Big Bang. The Herglotz equations of motion for the Lagrangian 5.126 are

$$\frac{d}{dt}\left(\frac{\partial \mathcal{L}^H}{\partial \dot{\phi}}\right) - \frac{\partial \mathcal{L}^H}{\partial \phi} = \frac{\partial \mathcal{L}^H}{\partial h}\frac{\partial \mathcal{L}^H}{\partial \dot{\phi}} \implies \ddot{\phi} + \partial_\phi V = \frac{3}{4}h\dot{\phi} \tag{5.128}$$

$$\dot{h} = \mathcal{L}^H \implies \dot{h} = \frac{3}{8}h^2 + \frac{1}{2}\dot{\phi}^2 - V(\phi) \tag{5.129}$$

n this example it's quite clear how a contact manifold is a useful description of frictional systems. The equation of motion for $\phi(t)$ 5.128 can be seen as a driven harmonic oscillator with a time dependant frictional term $h(t)$. In this case the oscillator is being driven by its potential $V(\phi)$ with friction generated by the Hubble factor $h(t)$.

In the potential-free case these equations can be solved exactly, with solution

$$h(t) = -\frac{4}{3t}, \quad \phi(t) = \phi_0 + \frac{2}{\sqrt{3}} \ln |t| \tag{5.130}$$

It is explicitly clear that there still exits a divergence of the dynamical variables as we reach the big bang at $t \to 0$. In the shape space representation, the dynamical variables of the contact Hamiltonian/Herglotz Lagrangian and Hamiltonian flow will remain well defined.

5.6.2 Vacuum Bianchi

In section 5.5, we showed that the ADM Hamiltonian of a type A Bianchi cosmology with shape potential $V_s(x, y)$ is given by

$$\mathcal{H}_B = \nu^{-1} \left[-\frac{3}{8}\nu^2\tau^2 + \frac{1}{2}\left(p_x^2 + p_y^2\right) + \nu^{\frac{4}{3}} V_s(x, y) \right] \tag{5.131}$$

where (x, y) are the anisotropy parameters with conjugate momenta k_i, ν is the scale factor with conjugate τ (York time). For Bianchi I the shape potential is everywhere zero and for Bianchi IX it is given by

$$\begin{aligned} V_s(x, y) &= f(-\sqrt{3}x + y) + f(\sqrt{3}x + y) + f(-2y) \\ f(z) &= \frac{1}{2} e^{\sqrt{\frac{2}{3}}z} - e^{-\frac{z}{\sqrt{6}}} \end{aligned} \tag{5.132}$$

whilst Bianchi cosmologies are most easily studied in the Hamiltonian/ADM formalism, for the purpose of applying the contact-reduction scheme outlined in section 5.1 we will use Lagrangian given by the Legendre transformation

$$\mathcal{L} = \nu \left[-\frac{2}{3}\left(\frac{\dot{\nu}}{\nu}\right)^2 + \frac{1}{2}\left(\dot{x}^2 + \dot{y}^2\right) - \nu^{-\frac{2}{3}} V_s(x, y) \right] \tag{5.133}$$

In the Bianchi I case $V_s = 0$ the Lagrangian reduces to

$$\mathcal{L} = \nu \left[-\frac{2}{3} \left(\frac{\dot{\nu}}{\nu} \right)^2 + \frac{1}{2} \left(\dot{x}^2 + \dot{y}^2 \right) \right] \tag{5.134}$$

which is identical in form to the FLRW Lagrangian except we have the anisotropy parameters as our dynamical variables rather than a scalar field. For this section we will show the contact-reduction with the general non-zero shape potential. starting with the Bianchi Lagrangian eq 5.133, we see that there is a scaling symmetry $\nu = \lambda\bar{\nu}$, $t = \lambda^{\beta}\bar{t}$ under which the Lagrangian transforms as

$$\mathcal{L} = \lambda\bar{\nu} \left[-\frac{2}{3}\lambda^{-2\beta} \left(\frac{\bar{\nu}'}{\bar{\nu}} \right)^2 + \frac{1}{2}\lambda^{-2\beta}(x'^2 + y'^2) - \lambda^{-\frac{2}{3}}\bar{\nu}V_s(x,y) \right], \quad q' = \frac{dq}{d\bar{t}} \tag{5.135}$$

We require $\beta = 1/3$ in order for the shape potential term to scale the same with λ as the other two terms in the brackets. Making the CSSS vector field

$$\bar{\mathbf{D}} = \nu\frac{\partial}{\partial\nu} + \frac{1}{3}t\frac{\partial}{\partial t} \tag{5.136}$$

The CSSS is only defined up to a non-zero constant factor, so with foresight we will choose to work with

$$\bar{\mathbf{D}} = \frac{3}{2}\nu\frac{\partial}{\partial\nu} + \frac{1}{2}t\frac{\partial}{\partial t} \tag{5.137}$$

which has tangent lift

$$\mathbf{D} = \frac{3}{2}\nu\frac{\partial}{\partial\nu} + \dot{\nu}\frac{\partial}{\partial\dot{\nu}} - \frac{1}{2}\dot{x}\frac{\partial}{\partial\dot{x}} - \frac{1}{2}\dot{y}\frac{\partial}{\partial\dot{y}} + \frac{1}{2}t\frac{\partial}{\partial t} \tag{5.138}$$

This is a non-isochronal scaling symmetry with degree 1/2, therefore we require a coordinate transformation and reparameterisation of the time variable in order to form an isochornal, degree 1 scaling symmetry. Consider the transformation $\rho = \nu^{\frac{2}{3}}$,

$d\tau = \rho^{-\frac{1}{2}} dt$ under which the action becomes

$$S = \int \mathcal{L}(\nu, \dot{\nu}, \mathbf{x}, \dot{\mathbf{x}}) dt = \int \rho \left[-\frac{3}{2} \left(\frac{\rho'}{\rho} \right)^2 + \frac{1}{2}(x'^2 + y'^2) - V_s(x, y) \right] d\tau, \quad q' = \frac{dq}{d\tau} \tag{5.139}$$

We identify the transformed Lagrangian

$$\mathcal{L} = \rho \left[-\frac{3}{2} \left(\frac{\rho'}{\rho} \right)^2 + \frac{1}{2}(x'^2 + y'^2) - V_s(x, y) \right] \tag{5.140}$$

which clearly has a scaling symmetry $\mathbf{D} = \rho \partial_\rho + \rho' \partial_{\rho'}$ of degree 1. Thus there is a Herglotz Lagrangian $\mathcal{L}^H$ on $TQ/\mathbf{D}$ given by

$$\begin{aligned} h &= \frac{1}{\rho} i_{\mathbf{D}} \mu_L = \frac{\partial \mathcal{L}}{\partial \rho'} = -3 \frac{\rho'}{\rho} \\ \mathcal{L}^H(\mathbf{x}, \dot{\mathbf{x}}, h) &= \frac{\partial \mathcal{L}}{\partial \rho} = \frac{1}{6} h^2 + \frac{1}{2}(x'^2 + y'^2) - V_s(x, y) \end{aligned} \tag{5.141}$$

In this contact manifold description, the volume factor of the universe becomes decoupled in the Lagrangian from the anisotropy parameters and shape potential. Herglotz equations of motion for this system are similar in form to those of the FLRW with scalar field in section 5.6.1, but with a shape potential of the anisotropy parameters rather than a scalar field potential. The Kasner universe is the vacuum Bianchi I cosmology, which corresponds to the potential-free case $V_s = 0$ for which the equations of motion reduce to (we now use the ordinary $\dot{q}$ to denote time derivatives rather than q')

$$\begin{aligned} \dot{h} &= \frac{1}{6} h^2 + \frac{1}{2} \left(\dot{x}^2 + \dot{y}^2 \right) \\ \ddot{q} &= \frac{1}{3} h \dot{q}, \quad q = x, y \end{aligned} \tag{5.142}$$

These equations can be solved analytically, with solutions

$$h(t) = -\frac{3}{t} \tag{5.143}$$

$$q(t) = q_0 + C_q \ln|t|, \quad \sum_q C_q^2 = 3 \tag{5.144}$$

At this point we note that, whilst the quantities $h(t), x(t), y(t)$ may diverge as $t \to 0$, relational quantities like $x(t)/y(t)$ remain finite, as well as

$$h(t)e^{-\frac{1}{2}\sum_q \frac{q(t)}{C_q}} \tag{5.145}$$

This will motivate our choice of variables when we project the system onto shape space in section 5.7.

Once the Herglotz Lagrangian has been obtained it is possible to move to the contact Hamiltonian representation by a Legendre transformation

$$\mathcal{H}^c = -\frac{1}{6}h^2 + \frac{1}{2}\left(p_x^2 + p_y^2\right) + V_s(x, y) \tag{5.146}$$

with contact form

$$\eta = -dh + p_x dx + p_y dy \tag{5.147}$$

The Hamiltonian representation will be used in making the projection to shape space in section 5.7.

5.6.3 Minimally Coupled Scalar Field

The case of a scalar field minimally coupled to a Bianchi cosmology changes the procedure slightly, since the scalar field potential $V(\phi)$ couples to the scale factor differently to the shape potential $V_s(x, y)$

$$\mathcal{L} = \nu\left[-\frac{2}{3}\left(\frac{\dot{\nu}}{\nu}\right)^2 + \frac{1}{2}\dot{\phi}^2 + \frac{1}{2}\left(\dot{x}^2 + \dot{y}^2\right) - \nu^{-\frac{2}{3}}V_s(x, y) - V(\phi)\right] \tag{5.148}$$

In the case of Bianchi I, the shape potential is everywhere zero and thus the Lagrangian reduces to a form that immediately has a scaling symmetry of degree 1 associated with the scale factor ν. Therefore the exact same procedure may be

followed in section 5.6.1, whereby the contact Hamiltonian for Bianchi I + matter is given by

$$\mathcal{H}^c_{BI} = -\frac{1}{6}h^2 + \frac{1}{2}(p_x^2 + p_y^2) + \frac{1}{2}p_\phi^2 + V(\phi) \tag{5.149}$$

For Bianchi cosmologies with a shape potential that is not everywhere zero, the scaling symmetry we previously identified in section 5.6.2 $\nu = \lambda\bar{\nu}$, $t = \lambda^{\frac{1}{3}}\bar{t}$ is not a symmetry for this Lagrangian in equation 5.148. However, the scaling symmetry can be restored by introducing a velocity term $\dot{k}$ and forming a new Lagrangian

$$\mathcal{L}_* = \nu\left[-\frac{2}{3}\left(\frac{\dot{\nu}}{\nu}\right)^2 + \frac{1}{2}\dot{\phi}^2 + \frac{1}{2}\left(\dot{x}^2 + \dot{y}^2\right) - \nu^{-\frac{2}{3}}V_s(x,y)\right] - \sqrt{\nu\dot{k}V(\phi)} \tag{5.150}$$

The new variable k is a cyclic coordinate with constant momentum, it is possible to choose an appropriate boundary condition for $\dot{k}$ such that the equations of motion generated by $\mathcal{L}$ coincide with those generated by the new Lagrangian $\mathcal{L}_*$. The advantage of working with $\mathcal{L}_*$ is that it has the scaling symmetry we require in order to make a contact-reduction. The equations of motion generated by the original Lagrangian 5.148 are

$$\begin{aligned}
-\frac{4}{3}\frac{d}{dt}\left(\frac{\dot{\nu}}{\nu}\right) &= \frac{2}{3}\left(\frac{\dot{\nu}}{\nu}\right)^2 + \frac{1}{2}\left(\dot{x}^2 + \dot{y}^2\right) + \frac{1}{2}\dot{\phi}^2 - \frac{1}{3}\nu^{\frac{1}{3}}V_s - V(\phi) \\
\frac{d}{dt}\left(\nu\dot{q}\right) &= -\nu^{\frac{1}{3}}\partial_q V_s, \quad q = x, y \\
\frac{d}{dt}\left(\nu\dot{\phi}\right) &= -\nu\partial_\phi V(\phi)
\end{aligned} \tag{5.151}$$

and the equations of motion generated by the new Lagrangian $\mathcal{L}_*$ are

$$\begin{aligned}
-\frac{4}{3}\frac{d}{dt}\left(\frac{\dot{\nu}}{\nu}\right) &= \frac{2}{3}\left(\frac{\dot{\nu}}{\nu}\right)^2 + \frac{1}{2}\left(\dot{x}^2+\dot{y}^2\right) + \frac{1}{2}\dot{\phi}^2 - \frac{1}{3}\nu^{\frac{1}{3}}V_s \\
\frac{d}{dt}\left(\nu\dot{q}\right) &= -\nu^{\frac{1}{3}}\partial_q V_s, \quad q = x, y \\
\frac{d}{dt}\left(\nu\dot{\phi}\right) &= -\frac{1}{2}\sqrt{\frac{\nu\dot{k}}{V(\phi)}}\partial_\phi V(\phi) \\
C &= -\frac{1}{2}\sqrt{\frac{\nu V(\phi)}{\dot{k}}}, \quad C = \text{constant}
\end{aligned} \tag{5.152}$$

One can see that choosing the boundary condition $C = -\frac{1}{4}$ restores the original equations of motion. Choosing a boundary condition on $4\dot{k} = C^{-2}V(\phi)\nu$ is equivalent to choosing an overall scale of the potential field potential $V(\phi)$, which would have to be chosen in order to specify a solution. So while it may appear at first that the new Lagrangian $\mathcal{L}_*$ requires additional information to specify a solution compared to $\mathcal{L}$, in in fact does not, only the choice in scale of the potential is made explicit through $\dot{k}$, rather than implicit in the definition of $V(\phi)$. The new Lagrangian $\mathcal{L}_*$ now generates the same dynamics as the original in eq 5.148 whilst retaining the desired scaling symmetry $\nu = \lambda\bar{\nu}$, $t = \lambda^{\frac{1}{3}}\bar{t}$. Choosing to work with the CSSS

$$\bar{\mathbf{D}} = \frac{3}{2}\nu\frac{\partial}{\partial\nu} + \frac{1}{2}t\frac{\partial}{\partial t} \tag{5.153}$$

we have the tangent lift

$$\mathbf{D} = \frac{3}{2}\nu\frac{\partial}{\partial\nu} + \dot{\nu}\frac{\partial}{\partial\dot{\nu}} - \frac{1}{2}\dot{x}\frac{\partial}{\partial\dot{x}} - \frac{1}{2}\dot{y}\frac{\partial}{\partial\dot{y}} - \frac{1}{2}\dot{\phi}\frac{\partial}{\partial\dot{\phi}} - \frac{1}{2}\dot{k}\frac{\partial}{\partial\dot{k}} + \frac{1}{2}t\frac{\partial}{\partial t} \tag{5.154}$$

We again make a coordinate transformation and reparameterisation of the time coordinate under

$$\rho = \nu^{\frac{2}{3}}, \quad dt = \rho^{-\frac{1}{2}}d\tau \tag{5.155}$$

under which the action transforms as

$$S = \int \mathcal{L}_* dt = \int \rho \left[-\frac{3}{2}\left(\frac{\rho'}{\rho}\right)^2 + \frac{1}{2}\left(x'^2 + y'^2\right) + \frac{1}{2}\phi'^2 - V_s(x,y) - \sqrt{k'V(\phi)} \right] d\tau \tag{5.156}$$

and identify the transformed Lagrangian as

$$\mathcal{L} = \rho \left[-\frac{3}{2}\left(\frac{\rho'}{\rho}\right)^2 + \frac{1}{2}\left(x'^2 + y'^2\right) + \frac{1}{2}\phi'^2 - V_s(x,y) - \sqrt{k'V(\phi)} \right] \tag{5.157}$$

This has scaling symmetry $\mathbf{D} = \rho\partial_\rho + \rho'\partial_{\rho'}$ of degree 1, hence there is a Herglotz Lagrangian given by

$$\begin{aligned} h &= \frac{1}{\rho} i_{\mathbf{D}} \mu_L = -3\frac{\rho'}{\rho} \\ \mathcal{L}^H &= \frac{\partial \mathcal{L}}{\partial \rho} = \frac{1}{6}h^2 + \frac{1}{2}\left(x'^2 + y'^2\right) + \frac{1}{2}\phi'^2 - V_s(x,y) - \sqrt{k'V(\phi)} \end{aligned} \tag{5.158}$$

The contact Hamiltonian obtained from a Legendre transformation and contact form are

$$\begin{aligned} \mathcal{H}^c &= -\frac{1}{6}h^2 + \frac{1}{2}\left(p_x^2 + p_y^2\right) + \frac{1}{2}p_\phi^2 + V_s(x,y) - \frac{V(\phi)}{4p_k} \\ \eta &= -dh + p_k dk + p_\phi d\phi + p_x dx + p_y dy \end{aligned} \tag{5.159}$$

The cast the Hamiltonian into the form that will be used for the shape space projection, we make one last parity transformation of the p_k momentum and absorb the factor constant factor $4p_k \to -p_k$ so that we may work with a positive p_k. Thus we arrive at

$$\begin{aligned} \mathcal{H}^c &= -\frac{1}{6}h^2 + \frac{1}{2}\left(p_x^2 + p_y^2\right) + \frac{1}{2}p_\phi^2 + V_s(x,y) + \frac{V(\phi)}{p_k} \\ \eta &= -dh - \frac{1}{4}p_k dk + p_\phi d\phi + p_x dx + p_y dy \end{aligned} \tag{5.160}$$

We now have contact Hamiltonians for FLRW + scalar field, vacuum Bianchi and Bianchi + scalar field cosmologies. Although the overall scale factor of the universe $\nu(t)$ is decoupled from the dynamical variables in the contact description,

as demonstrated through the cases of potential-free FLRW and Kasner solutions, the dynamical variables still diverge at the initial singularity. There is no apriori reason why this choice of coordinates on the contact manifold should be a suitable one for describing the universe at the Big Bang. In section 5.7 we will outline a procedure that projects the system onto shape space. We will then prove that the equations of motion have unique solutions in a neighbourhood of the initial singularity via the Picard-Lindelöf theorem.

5.7 Shape Space Projection and Proof of Existence and Uniqueness Through $\beta = \pi/2$

In the following section we will take the symmetry-reduced models of FLRW and Bianchi I and IX on contact manifolds, and describe the procedure for projecting them onto shape space. The configuration space coordinates of the symplectic systems that one starts with have as their spatial manifolds, n-dimensional real space $\mathbb{R}^n$. In forming the contact system, this space is quotiented by a scaling symmetry resulting in n-dimensional real-projective space $\mathbb{RP}^n$. An important property of the gnomonic projection is that it maps straight lines in the plane to great circles on the sphere. Thus we see the geodesic motion of a free particle in the plane represented by a great circle in shape space coordinates. For a concrete example of this, we refer the reader to appendix B.2.

The projection onto shape space of the contact Hamiltonian systems under consideration is a gnomonic projection of the dynamical variables in $\mathbb{RP}^n$ onto the unit sphere S^n. The dimensionality n will depend on the number of dynamical variables. The gnomonic projection constitutes of a compactification of $\mathbb{RP}^n$ onto an n sphere. In choosing the sign of the triads used to describe the geometry, we implicitly decide on an orientation of the manifold, which does not affect the physical dynamics. The gnomonic projection maps points on the surface of an n-sphere to a tangent plane at one of the poles by drawing a straight line from the centre of the

sphere through the surface point and intersects it with the plane. We must form a double cover in order to describe both orientations of the real projective space. In $n = 2$ dimensions, this consists of two distinctly oriented tangent planes at antipodal points of an S^2 surface. The gnomonic projection maps the asymptotic boundaries of the planes to the equator of the sphere, forming a border between the two planes.

We first consider the cases of FLRW with one and then two scalar fields and show how the compactification to shape space works in the simplest cases. Once the Hamiltonian has been written in shape space variables, we show that there exist unique, smooth solutions to the equations of motion at the big bang, which is mapped to the equator of S^n under the gnomonic projection. We then progress to the Bianchi I and IX cosmologies at show the same result.

5.7.1 FLRW + 1 scalar field

We start with the contact Hamiltonian and contact form derived in eq 5.127 for FLRW + a minimally coupled scalar field

$$\begin{aligned} \mathcal{H}^c &= -\frac{3}{8}h^2 + \frac{1}{2}p_\phi^2 + V(\phi) \\ \eta &= -dh + p_\phi d\phi \end{aligned} \tag{5.161}$$

Consider the mapping of ϕ on the real line onto S^1 through a gnomonic projection

$$\phi = |\tan\beta| \tag{5.162}$$

Under the gnomonic projection, the initial singularity is mapped to $|\beta| = \pi/2$. We will also make a transformation of the Hubble factor $h(t)$.

$$h = se^{m+a|\tan\beta|}, \quad s = \text{Sign}(\tan\beta), \quad a = \text{constant} \tag{5.163}$$

Although we expect $h(t)$ to diverge as we approach the singularity, the global coordinate $m(t)$ will tend to a finite value. Next we compute the transformed contact

form

$$\eta = -h\left(dm + sa\sec^2\beta d\beta\right) + sp_\phi \sec^2\beta d\beta \tag{5.164}$$

We may divide both the contact form, and shortly the Hamiltonian by a non-zero factor, as this is equivalent to making a change of lapse. In particular we choose

$$\begin{aligned}\eta \to \frac{\eta}{sh} &= -sdm + \left(\frac{p_\phi}{h} - a\right)\sec^2\beta d\beta \\ &= -sdm + (s\chi - a)\sec^2\beta d\beta\end{aligned} \tag{5.165}$$

where we have defined $\chi = p_\phi/|h|$. From the contact form 5.165, the p_β momentum associated with β can be identified as

$$p_\beta\,(s\chi - a)\sec^2\beta \tag{5.166}$$

In these new variables the contact Hamiltonian is

$$\mathcal{H}^c = \frac{1}{2}h^2\left(p_\beta^2\cos^4\beta + 2ap_\beta\cos^2\beta + a^2 - \frac{3}{4}\right) + V(\phi) \tag{5.167}$$

The constant a may be set freely, a convenient choice of $a = \sqrt{3}/2$ cancels the constant term in eq 5.167 which diverges like h^2. Finally, choosing to divide the contact Hamiltonian by a factor of $h^2\cos^2\beta$ (equivalent to a change of lapse) we arrive at the shape space Hamiltonian for FLRW + a minimally coupled scalar field

$$\begin{aligned}\mathcal{H} = \frac{\mathcal{H}^c}{h^2\cos^2\beta} &= \frac{1}{2}p_\beta^2\cos^2\beta + \frac{\sqrt{3}}{2}p_\beta + U(\beta)e^{-2m} \\ U(\beta) &= V(\beta)e^{-\sqrt{3}|\tan\beta|}\sec^2\beta\end{aligned} \tag{5.168}$$

Heuristically, we see that provided the potential $V(\beta)$ does not grow faster than the exponential factor $e^{-\sqrt{3}|\tan\beta|}$, any divergence from the potential and the $\sec^2\beta$ factor as $\beta \to \pi/2$ will be exponentially suppressed, keeping $U(\beta)$ finite at the initial

singularity. The contact Hamiltonian equations of motion for this system **??** are

$$\begin{aligned}\dot{\beta} &= p_\beta \cos^2\beta + \frac{\sqrt{3}}{2} \\ \dot{p}_\beta &= p_\beta^2 \cos\beta \sin\beta + (2sUp_\beta - \partial_\beta U)\, e^{-2m} \\ \dot{m} &= -s\left(\frac{\sqrt{3}}{2}p_\beta + 2Ue^{-2m}\right)\end{aligned} \tag{5.169}$$

Where in the last line we have used the fact that the ADM Hamiltonian of general relativity satisfies the constraint $\mathcal{H} := 0$ on the spacial hypersurfaces Σ_t. In the potential free-case this system of ODE's can be solved exactly. Firstly the Hamiltonian constraint must be satisfied at all times.

$$\frac{1}{2}p_\beta^2\left(p_\beta \cos^2\beta + \sqrt{3}\right) = 0 \tag{5.170}$$

Thus there is one non-physical diverging solution $p_\beta = -\sqrt{3}\sec^2\beta$ and one that remains finite at the initial singularity $p_\beta = 0$. Although in this case the finite solution is a constant $p_\beta = 0$, we will show shortly that this not need the case, one may have a finite solution with non-zero potential and momentum. The $p_\beta = 0$ solution gives

$$\begin{aligned}\dot{\beta} = \frac{\sqrt{3}}{2}, \implies \beta(t) = \beta_0 + \frac{\sqrt{3}}{2}t \\ \dot{m} = 0 \implies m(t) = m_0\end{aligned} \tag{5.171}$$

Thus we reach the initial singularity at $\beta = \pi/2$ in finite proper time. At this point the dynamical variables, Hamiltonian and contact form remain finite and well defined..

5.7.2 FLRW + 2 Scalar Fields

In anticipation of projecting the vacuum Bianchi contact Hamiltonian, which contains two dynamical fields $x(t)$ and $y(t)$, we shall first show how the projection to S^2 works with a contact FLRW + 2 scalar fields cosmology. The contact-reduction

results of section 5.7.1 can be easily extended to n scalar fields in the usual way. The field ϕ is simply replaced with a vector of fields $\underline{\phi}$ and $\dot{\phi}^2$ becomes the Euclidean norm squared of $\underline{\dot{\phi}}$. The contact Hamiltonian for FLRW + 2 scalar fields is thus

$$\mathcal{H}^c = -\frac{3}{8}h^2 + \frac{1}{2}\left(p_1^2 + p_2^2\right) + V(\phi_1, \phi_2) \tag{5.172}$$

In section 5.7.1 we had a single field and made a gnomonic projection of the real (projective) line onto S^1, here there are two fields and thus it required a gnomonic projection of $\mathbb{RP}^2$ to S^2 given by

$$\begin{pmatrix}\phi_1\\ \phi_2\end{pmatrix} = |\tan\beta| \begin{pmatrix}\cos\alpha\\ \sin\alpha\end{pmatrix} \tag{5.173}$$

and a projection of the momenta into polar coordinates

$$\begin{pmatrix}p_1\\ p_2\end{pmatrix} = p \begin{pmatrix}\cos\theta\\ \sin\theta\end{pmatrix} \tag{5.174}$$

We make the same transformation of the Hubble factor as in eq 5.163, but now with the foresight to fix $a = \sqrt{3}/2$

$$h = se^{m+\frac{\sqrt{3}}{2}|\tan\beta|}, \quad s = \text{Sign}(\tan\beta) \tag{5.175}$$

The contact form under this transformation becomes

$$\eta = -h\left(dm + s\frac{\sqrt{3}}{2}\sec^2\beta\right) + sp\cos(\theta-\alpha)\sec^2\beta d\beta + p\sin(\theta-\alpha)|\tan\beta| d\alpha \tag{5.176}$$

again defining the variable ratio $\chi = p/|h|$ and scaling the contact form by the non-zero factor $\frac{1}{sh}$ gives

$$\eta \to \frac{\eta}{sh} = -sdm + \left[s\chi\cos(\theta-\alpha) - \frac{\sqrt{3}}{2}\right]\sec^2\beta d\beta + \chi|\tan\beta|\sin(\theta-\alpha)d\alpha \tag{5.177}$$

and identify the momenta

$$p_\beta = \left[s\chi \cos(\theta - \alpha) - \frac{\sqrt{3}}{2} \right] \sec^2 \beta \tag{5.178}$$

$$p_\alpha = \chi |\tan \beta| \sin(\theta - \alpha) \tag{5.179}$$

Returning to the contact Hamiltonian, it is written in terms of the new variables as

$$\mathcal{H}^c = -\frac{1}{2} h^2 \left(\chi^2 - \frac{3}{4} \right) + V(\alpha, \beta) \tag{5.180}$$

Once more, rescaling by the non-zero factor $h^{-2} \sec^2 \beta$, we arrive at the shape space Hamiltonian for FLRW + 2 scalar fields

$$\begin{aligned} \mathcal{H} &= \frac{\mathcal{H}^c}{h^2 \cos^2 \beta} = \frac{1}{2} p_\beta^2 \cos^2 \beta + \frac{\sqrt{3}}{2} p_\beta + \frac{p_\alpha^2}{2 \sin^2 \beta} + U(\alpha, \beta) e^{-2m} \\ U(\alpha, \beta) &= V(\alpha, \beta) e^{-\sqrt{3} |\tan \beta|} \sec^2 \beta \end{aligned} \tag{5.181}$$

With equations of motion

$$\begin{aligned} \dot{\alpha} &= \frac{p_\alpha}{\sin^2 \beta} \\ \dot{\beta} &= p_\beta \cos^2 \beta + \frac{\sqrt{3}}{2} \\ \dot{p}_\alpha &= \left(2sUp_\alpha - \partial_\alpha U \right) e^{-2m} \\ \dot{p}_\beta &= p_\beta^2 \cos \beta \sin \beta + \left(2sUp_\beta - \partial_\beta U \right) e^{-2m} \\ \dot{m} &= -s \left(\frac{\sqrt{3}}{2} p_\beta + 2U e^{-2m} \right) \end{aligned} \tag{5.182}$$

Just as with the single field case in section 5.7.1, we can analyse the potential-free cosmology analytically. In this case the equations of motion reduce to

$$\begin{aligned}
\dot{\alpha} &= \frac{p_\alpha}{\sin^2\beta} \\
\dot{\beta} &= p_\beta \cos^2\beta + \frac{\sqrt{3}}{2} \\
p_\alpha &= \text{constant} \\
\dot{p}_\beta &= p_\beta^2 \cos\beta \sin\beta \\
\dot{m} &= -s\frac{\sqrt{3}}{2} p_\beta
\end{aligned} \tag{5.183}$$

The Hamiltonian constraint $\mathcal{H} := 0$ must also be enforced. For the shape space Hamiltonian 5.181, we can think of the constraint as a quadratic equation in p_β

$$\sin^2\beta\cos^2\beta p_\beta^2 + \sqrt{3}\sin^2\beta p_\beta + p_\alpha^2 = 0 \tag{5.184}$$

with solutions

$$p_\beta^\pm = \frac{\sqrt{3}}{2}\sec^2\beta\left(-1 \pm \sqrt{1 - \frac{4}{3}p_\alpha^2\cot^2\beta}\right) \tag{5.185}$$

At a first glance it may seem that both solutions become undefined at $\beta = \pi/2$ due to the factor of $\sec^2\beta$, but if one considers the series expansion of the p_β^+ solutions, valid for $\tan^2\beta \geq 4p_\alpha^2/3$

$$\begin{aligned}
p_\beta^+ &= \frac{\sqrt{3}}{2}\sec^2\beta\left[-1 + \left(1 - 2p_\alpha^2\cot^2\beta - \frac{1}{2}\cot^4\beta + \mathcal{O}(\cot^6\beta)\right)\right] \\
&= -\frac{p_\alpha^2}{2\sqrt{3}\sin^2\beta}\left[2 + \frac{1}{2}p_\alpha^2\cot^2\beta + \mathcal{O}(\cot^4\beta)\right]
\end{aligned} \tag{5.186}$$

In the series expansion it is clear that p_β^+ is finite through the initial singularity at $\beta = \pi/2$. Just as p_β has been parameterised in terms of β in equation 5.186, we may also look for the solution $\alpha(\beta)$.

$$\frac{d\alpha}{d\beta} = \frac{\dot{\alpha}}{\dot{\beta}} = \frac{2p_\alpha}{\sin^2\beta\sqrt{3 - 4p_\alpha^2\cot^2\beta}} \tag{5.187}$$

Equation 5.187 has the solution

$$\frac{2p_\alpha}{\sqrt{3}}\cot\beta = \sin[\sqrt{2}(\alpha_0 - \alpha)] \tag{5.188}$$

Thus we have a solution of dynamical variables, Hamiltonian and contact form that remain well defined through the initial singularity. Furthermore, equation 5.188 is the equation of a great circle on shape space. This is to be expected since the potential-free motion corresponds to a straight line in the (ϕ_1, ϕ_2) plane and gnomonic projections map straight lines in the plane to great circles on the sphere.

5.7.3 Vacuum Bianchi

We know turn to the case of a contact-reduced vacuum Bianchi spacetime with shape potential $V_s(x, y)$. As shown in section 2.3, the contact Hamiltonian is given by

$$\mathcal{H}^c = -\frac{1}{6}h^2 + \frac{1}{2}\left(\dot{x}^2 + \dot{y}^2\right) + V_s(x, y) \tag{5.189}$$

By simply inspecting the Hamiltonian, it is clearly functionally the same as the FLRW + 2 scalar field Hamiltonian in eq. 5.172. The projection to shape space thus follows the exact same procedure as that described in section 3.2, setting $a = 1/\sqrt{3}$ to account for the coefficient of $-\frac{1}{6}$ on the Hubble factor. The shape space Hamiltonian for a vacuum Bianchi cosmology is thus

$$\begin{aligned} \mathcal{H} &= \frac{1}{2}p_\beta^2\cos^2\beta + \frac{1}{\sqrt{3}}p_\beta + \frac{p_\alpha^2}{2\sin^2\beta} + U(\alpha, \beta)e^{-2m} \\ U(\alpha, \beta) &= V(\alpha, \beta)e^{-\frac{2}{\sqrt{3}}|\tan\beta|}\sec^2\beta \end{aligned} \tag{5.190}$$

with equations of motion

$$\begin{aligned}
\dot{\alpha} &= \frac{p_\alpha}{\sin^2\beta} \\
\dot{\beta} &= p_\beta \cos^2\beta + \frac{1}{\sqrt{3}} \\
\dot{p}_\alpha &= (2sUp_\alpha - \partial_\alpha U)\, e^{-2m} \\
\dot{p}_\beta &= p_\beta^2 \cos\beta \sin\beta + (2sUp_\beta - \partial_\beta U)\, e^{-2m} \\
\dot{m} &= -s\left(\frac{1}{\sqrt{3}} p_\beta + 2Ue^{-2m}\right)
\end{aligned} \tag{5.191}$$

The Kasner solutions, which are exactly solvable, correspond to great circles on S^2 given by

$$\sqrt{3} p_\alpha \cot\beta = \sin[2(\alpha_0 - \alpha)] \tag{5.192}$$

For a non-zero shape potential, there is not a general solution to the system of equations and so we rely on a different method to prove existence of smooth solutions passing through the Big Bang. The Picard-Lindelöf theorem states that, given an ordinary differential equation of the form

$$r'(t) = f(t, r), \quad r(t_0) = r_0 \tag{5.193}$$

there exists a unique, local solution if $f(t, r)$ is continuous in t and locally Lipschitz continuous in r. This extends to a system of ODE's

$$r_i'(t) = f_i(t, \mathbf{r}), \quad r_i(t_0) = r_{i0} \tag{5.194}$$

where the functions $f_i(t, \mathbf{r})$ are required to be continuous in r and locally Lipschitz continuous in r_i. The Picard-Lindelöf theorem applies immediately to the equations of motion 5.191, the RHS's are not explicitly dependant on time and are locally Lipschitz around $\beta = \pi/2$ provided that the potential $U(\alpha, \beta)$ are its derivatives are locally bounded around $\beta = \pi/2$.

Assuming that the potential satisfies these conditions, there exists a unique local solution of the equations of motion that continues smoothly through the big bang. In the case of the vacuum Bianchi I cosmology, this is satisfied trivially as the shape potential is everywhere zero. However for Bianchi IX the shape potential is such that the exponential suppression in $U(\alpha, \beta)$ is killed off exactly. The shape potential is given by

$$V_s(x,y) = \frac{1}{2}e^{\frac{2}{\sqrt{3}}y}\left(e^{2x}+e^{-2x}\right) - e^{-\frac{1}{\sqrt{3}}y}\left(e^{x}+e^{-x}\right) + \frac{1}{2}e^{-\frac{4}{\sqrt{3}}y} - e^{\frac{2}{\sqrt{3}}y} \tag{5.195}$$

In terms of the shape space coordinates (α, β) this can be written as

$$V_s(\alpha,\beta) = \frac{1}{2}e^{f_1(\alpha)|\tan\beta|} + \frac{1}{2}e^{f_2(\alpha)|\tan\beta|} - e^{f_3(\alpha)|\tan\beta|} - e^{f_4(\alpha)|\tan\beta|} + \frac{1}{2}e^{f_5(\alpha)|\tan\beta|} - e^{f_6(\alpha)|\tan\beta|} \tag{5.196}$$

The functions $f_i(\alpha)$ are given by

$$\begin{aligned} f_1(\alpha) &= \frac{2}{\sqrt{3}}\sin\alpha + 2\cos\alpha, \quad f_2(\alpha) = \frac{2}{\sqrt{3}}\sin\alpha - 2\cos\alpha \\ f_3(\alpha) &= -\frac{1}{\sqrt{3}}\sin\alpha + \cos\alpha, \quad f_4(\alpha) = -\frac{1}{\sqrt{3}}\sin\alpha - \cos\alpha \\ f_5(\alpha) &= -\frac{4}{\sqrt{3}}\sin\alpha, \quad f_6(\alpha) = \frac{2}{\sqrt{3}}\sin\alpha \end{aligned} \tag{5.197}$$

One can see that clearly, some of these functions will surpass $f_i(\alpha) = 2/\sqrt{3}$, cancelling the exponential suppression of $e^{-\frac{2}{\sqrt{3}}|\tan\beta|}$ in $U(\alpha, \beta)$.

In figure 5.6 we plot the functions $f_i(\alpha)$ over the entire range $0 \leq \alpha \leq 2\pi$. Note that these are exactly the same functions we came across when showing that Bianchi IX could not achieve quiescence without the introduction of a matter field in section 5.5. For all values of α, there is at least one functions that is greater than or equal to $2/\sqrt{3}$. So it is not possible in vacuum Bianchi IX to find a subset of $\alpha \in [0, 2\pi]$ for which the exponential suppression in $U(\alpha, \beta)$ is not cancelled out.

The fact that local Lipschitz continuity is not in general satisfied for the Vacuum Bianchi IX cosmology should not come as a surprise, as it is well known that Bianchi

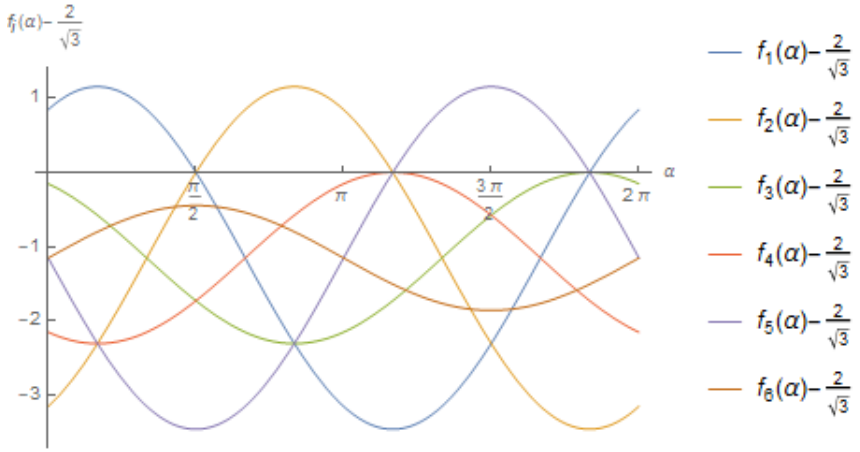

Figure 5.6: Plots of the functions $f_i(\alpha) - \frac{2}{\sqrt{3}}$ for $0 \leq \alpha \leq 2\pi$.

IX cannot achieve quiescence without the presence of a matter field [149, 161, 164]. In fact we will find that in order for Local Lipschitz continuity to hold, one needs the same essentially the same conditions on the field potential as where derived in equation 5.117 but in the shape space coordinates.

5.7.4 Bianchi + Scalar Field

Having seen in section in section 5.7.3 how Lipschitz continuity fails in the case of vacuum Bianchi IX, we are now motivated to consider the shape space projection of the contact Bianchi + scalar field Hamiltonians.

The simplest case is that of Bianchi I + scalar field, since the shape potential is everywhere zero. The contact Hamiltonian for such a system is given by eq. 5.149

$$\mathcal{H}^c_{BI} = -\frac{1}{6}h^2 + \frac{1}{2}(p_x^2 + p_y^2) + \frac{1}{2}p_\phi^2 + V(\phi) \tag{5.198}$$

with contact form

$$\eta = -dh + p_\phi d\phi + p_x dx + p_y dy \tag{5.199}$$

The configuration space variables (ϕ, x, y) are projected onto S^3 through the

gnomonic projection

$$\begin{pmatrix}\phi\\ x\\ y\end{pmatrix} = |\tan\beta| \begin{pmatrix}\cos\gamma\\ \sin\gamma\cos\alpha\\ \sin\gamma\sin\alpha\end{pmatrix}, \quad \begin{pmatrix}p_\phi\\ p_x\\ p_y\end{pmatrix} = p\begin{pmatrix}\cos\theta\\ \sin\theta\cos\psi\\ \sin\theta\sin\psi\end{pmatrix} \tag{5.200}$$

and the Hubble factor is transformed as

$$h = se^{m+\frac{1}{\sqrt{3}}|\tan\beta|}, \quad s = \text{Sign}(\tan\beta) \tag{5.201}$$

Under this set of transformations, the rescaled contact form and Hamiltonian become

$$\eta \to \frac{\eta}{sh} = -sdm + p_\alpha d\alpha + p_\beta d\beta + p_\gamma d\gamma \tag{5.202}$$

$$\begin{aligned}\mathcal{H}_{BI} &= \frac{\mathcal{H}^c_{BI}}{h^2\cos^2\beta} = \frac{1}{2}p_\beta^2\cos^2\beta + \frac{1}{\sqrt{3}}p_\beta + \frac{p_\alpha^2}{2\sin^2\beta\sin^2\gamma} + \frac{p_\gamma^2}{2\sin^2\beta} + U_\phi(\beta,\gamma)e^{-2m}\\ U_\phi(\beta,\gamma) &= V_\phi(\beta,\gamma)e^{-\frac{2}{\sqrt{3}}|\tan\beta|}\sec^2\beta\end{aligned} \tag{5.203}$$

The equations of motion generated by the shape space Bianchi I Hamiltonian 5.203 are

$$\begin{aligned}\dot{\alpha} &= \frac{p_\alpha}{\sin^2\beta\sin^2\gamma}\\ \dot{\beta} &= p_\beta\cos^2\beta + \frac{1}{\sqrt{3}}\\ \dot{\gamma} &= \frac{p_\gamma}{\sin^2\beta}\\ \dot{p}_\alpha &= \left(2sU_\phi p_\alpha - \partial_\alpha U_\phi\right)e^{-2m}\\ \dot{p}_\beta &= p_\beta^2\cos\beta\sin\beta + \frac{p_\alpha^2\cos\beta}{\sin^3\beta\sin^2\gamma} + \frac{p_\gamma^2\cos\beta}{\sin^3\beta} + \left(2sU_\phi p_\beta - \partial_\beta U_\phi\right)e^{-2m}\\ \dot{p}_\gamma &= \frac{p_\alpha^2\cos\gamma}{\sin^2\beta\sin^3\gamma} + \left(2sU_\phi p_\gamma - \partial_\gamma U_\phi\right)e^{-2m}\\ \dot{m} &= -s\left(\frac{1}{\sqrt{3}}p_\beta + 2U_\phi e^{-2m}\right)\end{aligned} \tag{5.204}$$

The right hand sides of the equations of motion 5.204 are locally Lipschitz continuous around $\beta = \pi/2$ provided that the field potential does not grow faster than the exponential suppression in $U_\phi(\beta, \gamma)$ i.e.

$$\lim_{\beta \to \frac{\pi}{2}} \left(V_\phi(\beta, \gamma) e^{-\frac{2}{\sqrt{3}} |\tan \beta|} \right) = 0 \tag{5.205}$$

Since the right hand-sides of the equations of motion are locally Lipschitz continuous, by Picard-Lindelöf there exists a unique local solution to the initial value problem.

In section 5.6.3 the contact Hamiltonian and contact form for a Bianchi cosmology with non-zero shape potential and field potential is shown to be 5.160

$$\begin{aligned} \mathcal{H}^c &= -\frac{1}{6}h^2 + \frac{1}{2}\left(p_x^2 + p_y^2\right) + \frac{1}{2}p_\phi^2 + V_s(x, y) + \frac{V(\phi)}{p_k} \\ \eta &= -dh - \frac{1}{4}p_k dk + p_\phi d\phi + p_x dx + p_y dy \end{aligned} \tag{5.206}$$

This had to be handled differently to the vacuum Bianchi case as the shape potential and field potential terms scale differently with ν. We now show the projection of this system onto shape space. In doing so, we will see how the well known conditions for Bianchi IX quiescence translate to the shape space representation. Beginning with the gnomonic projection of (ϕ, x, y) onto S^3, and writing the momenta in terms of polar coordinates

$$\begin{pmatrix} \phi \\ x \\ y \end{pmatrix} = |\tan \beta| \begin{pmatrix} \cos \gamma \\ \sin \gamma \cos \alpha \\ \sin \gamma \sin \alpha \end{pmatrix}, \quad \begin{pmatrix} p_\phi \\ p_x \\ p_y \end{pmatrix} = p \begin{pmatrix} \cos \theta \\ \sin \theta \cos \psi \\ \sin \theta \sin \psi \end{pmatrix} \tag{5.207}$$

along with the transformation

$$h = s e^{m + \frac{1}{\sqrt{3}} |\tan \beta|}, \quad s = \text{Sign}(\tan \beta) \tag{5.208}$$

and finally we define the variables χ and Ω as

$$\chi = \frac{p}{|h|}, \quad \Omega = -\frac{p_k}{4|h|} \tag{5.209}$$

the rescaled contact form then becomes

$$\begin{aligned}\frac{\eta}{sh} &= -sdm - a\sec^2\beta d\beta + \Omega dk + \chi\cos\theta d\phi + \chi\sin\theta\cos\psi dx + \chi\sin\theta\sin\psi dy \\ &= -sdm + \Omega dk + p_\alpha d\alpha + p_\beta d\beta + p_\gamma d\gamma\end{aligned} \tag{5.210}$$

We identify the shape space momenta as

$$\begin{aligned}p_\alpha &= \chi|\tan\beta|\sin\gamma\sin\theta\sin(\psi-\alpha) \\ p_\beta &= \sec^2\beta\left[s\chi\left(\cos\gamma\cos\theta + \sin\gamma\sin\theta\cos(\psi-\alpha)\right) - a\right] \\ p_\gamma &= \chi|\tan\beta|\left[-\sin\gamma\cos\theta + \cos\gamma\sin\theta\cos(\psi-\alpha)\right]\end{aligned} \tag{5.211}$$

The re-scaled shape space Hamiltonian is therefore

$$\begin{aligned}&\mathcal{H} = \frac{\mathcal{H}^c}{h^2\cos^2\beta} = \frac{1}{2}p_\beta^2\cos^2\beta + \frac{1}{\sqrt{3}}p_\beta + \frac{p_\alpha^2}{2\sin^2\beta\sin^2\gamma} + \frac{p_\gamma^2}{2\sin^2\beta} + U(\alpha,\beta,\gamma)e^{-2m} + \frac{U_\phi(\beta,\gamma)}{s\Omega}e^{-3m} \\ &U(\alpha,\beta,\gamma) = V_s(\alpha,\beta,\gamma)e^{-\frac{2}{\sqrt{3}}|\tan\beta|}\sec^2\beta \\ &U_\phi(\beta,\gamma) = V_\phi(\beta,\gamma)e^{-\sqrt{3}|\tan\beta|}\sec^2\beta\end{aligned} \tag{5.212}$$

The equations of motion generated by the shape space Hamiltonian are

$$\begin{aligned}
\dot{\alpha} &= \frac{p_\alpha}{\sin^2\beta\sin^2\gamma} \\
\dot{\beta} &= p_\beta\cos^2\beta + \frac{1}{\sqrt{3}} \\
\dot{\gamma} &= \frac{p_\gamma}{\sin^2\beta} \\
\dot{k} &= -\frac{U_\phi}{s\Omega^2}e^{-3m} \\
\dot{p}_\alpha &= \left[\left(\frac{3U_\phi}{\Omega}e^{-m} + 2sU\right)p_\alpha - \partial_\alpha U\right]e^{-2m} \\
\dot{p}_\beta &= p_\beta^2\cos\beta\sin\beta + \frac{p_\alpha^2\cos\beta}{\sin^3\beta\sin^2\gamma} + \frac{p_\gamma^2\cos\beta}{\sin^3\beta} + \left[\left(\frac{3U_\phi}{\Omega}e^{-m} + 2sU\right)p_\beta - \partial_\beta U - \frac{e^{-m}}{s\Omega}\partial_\beta U_\phi\right]e^{-2m} \\
\dot{p}_\gamma &= \frac{p_\alpha^2\cos\gamma}{\sin^2\beta\sin^3\gamma} + \left[\left(\frac{3U_\phi}{\Omega}e^{-m} + 2sU\right)p_\gamma - \partial_\gamma U - \frac{e^{-m}}{s\Omega}\partial_\gamma U_\phi\right]e^{-2m} \\
\dot{\Omega} &= \left(3U_\phi e^{-m} + 2s\Omega U\right)e^{-2m} \\
\dot{m} &= -s\left(\frac{1}{\sqrt{3}}p_\beta + 2Ue^{-2m}\right) - \frac{3U_\phi}{\Omega}e^{-3m}
\end{aligned} \tag{5.213}$$

The right-hand sides of the equations of motion 5.213 will be locally Lipschitz continuous around $\beta = \pi/2$ provided that $|\Omega| > 0$, and the potentials U and U_ϕ and their derivatives are locally bounded around $\beta = \pi/2$. The locally bounded conditions on the potentials U and U_ϕ will be satisfied if V_s and V_ϕ do not grow faster than their exponential suppression. In particular, the condition

$$\lim_{\beta\to\frac{\pi}{2}}\left(V_\phi(\beta,\gamma)e^{-\sqrt{3}|\tan\beta|}\right) = 0 \tag{5.214}$$

is the direct translation to shape space of the field potential quiescence condition for mixmaster behaviour to end in a finite number of bounces in Bianchi IX. Generically, any minimally coupled field potential that is added to the original Einstein-Hilbert action will produce a term that couples to $e^{-\sqrt{3}|\tan\beta|}$ in this way, and so all matter fields are required to become effectively massless as $\beta \to \pi/2$ in order for quiescence to be attained and for dynamical system to be able to pass smoothly through the

Big Bang. In section 5.7.3 it was established that in the vacuum Bianchi IX model, for any given value of α, there was always at least one function $f_i(\alpha)$ such that $f_i(\alpha) - 2/\sqrt{3} \geq 0$ and thus the potential

$$U(\alpha, \beta) = sec^2\beta \sum_i c_i e^{\left(f_i(\alpha) - \frac{2}{\sqrt{3}}\right)|\tan\beta|} \tag{5.215}$$

diverges at $\beta = \pi/2$. In the case of Bianchi IX + a scalar field, the anisotropy parameters are given by

$$x = |\tan\beta| \sin\gamma \cos\alpha, \quad y = |\tan\beta| \sin\gamma \sin\alpha \tag{5.216}$$

and the potential term in the shape space Hamiltonian 5.212 becomes

$$U(\alpha, \beta, \gamma) = \sec^2\beta \sum_i c_i e^{\left(f_i(\alpha)\sin\gamma - \frac{2}{\sqrt{3}}\right)|\tan\beta|} \tag{5.217}$$

where the functions $f_i(\alpha)$ as defined as they were in eq. 5.197 with coefficients c_i. One can now use the additional degree of freedom $\gamma \in [0, \pi]$ to ensure exponential suppression at $\beta = \pi/2$. Define the set

$$M = \left\{ \max_{0 \leq \alpha \leq 2\pi} f_i(\alpha) | i = 1, 2..., 6 \right\} \tag{5.218}$$

Then the exponential suppression will be retained for any $\alpha \in [0, 2\pi]$ if

$$\sin\gamma < \frac{2}{\sqrt{3}\sup(M)} \tag{5.219}$$

The form of all functions $f_i(\alpha)$ are known and the supremum of M is $\sup(M) = 4/\sqrt{3}$. Thus we have the quiescence condition

$$\sin\gamma < \frac{1}{2} \tag{5.220}$$

The conditions under which unique solutions passing through the big bang for

the various Bianchi (and FLRW) cosmologies now been established. In the next section we present numerical solutions to the equations of motion for various example models.

5.8 Numerical Simulations

In this section we will present numerical solutions to the equations of motion for a variety of the models discussed in this paper. It will be shown that there exist solutions who pass smoothly through the big bang. Under the gnomonic projection, the initial singularity of General Relativity is mapped to $\beta = \pi/2$. The contact Hamiltonians are defined on a contact manifold $T^*Q \times \mathbb{R}$ where T^*Q is an 2n-dimensional cotangent bundle. The gnomonic projection maps the dynamical variables on T^*Q to S^n.

5.8.1 FLRW + 1 Scalar Field

The simplest model we can consider is that of FLRW + 1 scalar field. The gnomonic projection in this case maps the dynamical variable ϕ onto S^1. The shape space Hamiltonian for this model is given by eq.5.168.

$$\begin{aligned} \mathcal{H} &= \frac{1}{2}p_\beta^2 \cos^2\beta + \frac{\sqrt{3}}{2}p_\beta + U(\beta)e^{-2m} \\ U(\beta) &= V_\phi(\beta)e^{-\sqrt{3}|\tan\beta|}\sec^2\beta \end{aligned} \tag{5.221}$$

In section 3.1 it was shown that the free field solution is exactly solvable, constant, everywhere-zero momentum p_β and linear solution for $\beta(t)$

$$\beta(t) = \beta_0 + \frac{\sqrt{3}}{2}t \tag{5.222}$$

The system reaches the Big Bang in finite coordinate time

$$t_s = \frac{1}{\sqrt{3}}(\pi - 2\beta_0) \tag{5.223}$$

We will consider the numerical solution for a scalar field in a harmonic potential. In the shape space representation this potential is

$$V(\phi) = \frac{1}{2}\phi^2 = \frac{1}{2}\tan^2\beta \tag{5.224}$$

The potential function $U(\beta)$ is locally Lipschitz continuous around $\beta = \pi/2$, and so Picard-Lindelöf is expected to hold here.

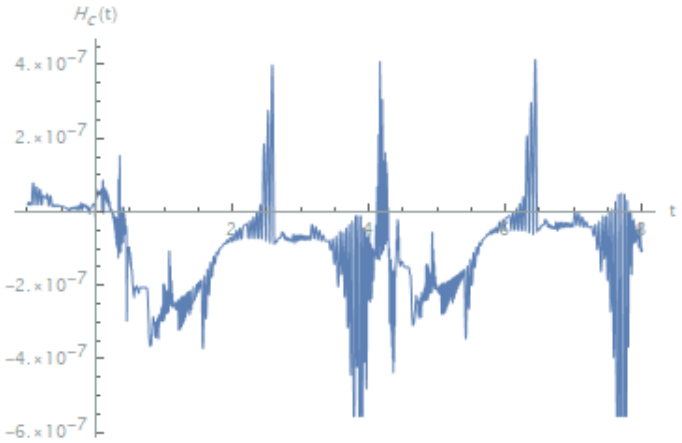

Figure 5.7: Plot of the numerical solution Hamiltonian for FLRW + Harmonic Potential over the time domain $t \in [-1, 8]$.

In figure 5.7 we plot the numerical solution Hamiltonian for the FLRW + scalar field in a harmonic potential model. The Hamiltonian constraint requires $\mathcal{H} := 0$, this is satisfied within machine precision, in this case on the order of 10^{-7}. The initial conditions are chosen at $t = 0$ as

$$\begin{aligned} &\beta(0) = \frac{\pi}{8}, \quad p_\beta = \frac{\sqrt{3}}{2}\sec^2\beta\left[-1 + \sqrt{1 - \frac{8}{3}U(\beta)e^{-2m}\cos^2\beta}\right] \\ &m(0) = 0 \end{aligned} \tag{5.225}$$

where the p_β momentum is determined by the Hamiltonian constraint $\mathcal{H} := 0$.

In figure 5.8 we plot the numerical solution of $\beta(t)$, transformed so that it intercepts the t-axis exactly when $\beta = \pi/2$. We see explicitly that the solutions pass

through $\beta = \pi/2$ in finite coordinate time. As shown in eq 5.223, the time at which the free field system passes through the big bang can be calculated analytically, as $t_s \approx 1.4$ for these particular initial conditions. The harmonic potential solutions and free field solutions lie very close together, particularly near $\beta = \pi/2$ which is to be expected as the potential becomes exponentially suppressed close to the big bang and thus the harmonic potential model becomes approximately free.

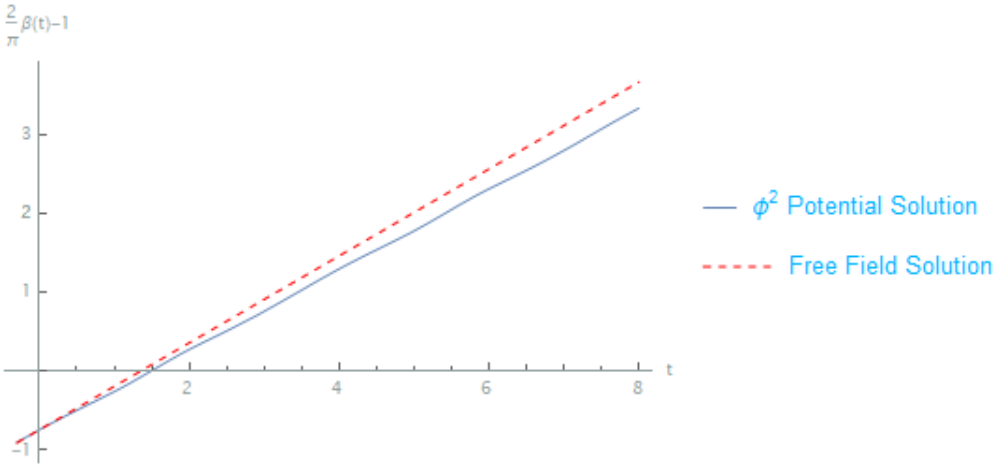

Figure 5.8: Plot of $\frac{2}{\pi}\beta(t) - 1$ for both the free field (red, dashed) and harmonic potential (blue) models. Showing explicitly that both solutions pass through $\beta = \pi/2$ at approximately $t_s = 1.5$.

The other dynamical variables for this model are the momentum p_β and frictional global coordinate $m(t)$. In the free field case the momentum is everywhere zero and $m(t)$ is a constant, which for the initial conditions 5.225 is also zero.

The phase space of the numerical solution to the harmonic potential model is plotted in figure 5.9. The numerical solution of $p_\beta(\beta)$ is π-periodic, with a cyclical structure as the spatial manifold undergoes inversions of orientation and Sign($\tan\beta$) changes between 1 and -1. The momentum also has the expected characteristic exponential suppression where $|\tan\beta| \to \infty$. Most importantly, the momentum is well defined through $\beta = \pi/2$.

Lastly, we plot in figure 5.10 the numerical solution for $m(t)$ for the harmonic potential model. This solution also displays a periodic structure and remains well defined through the big bang.

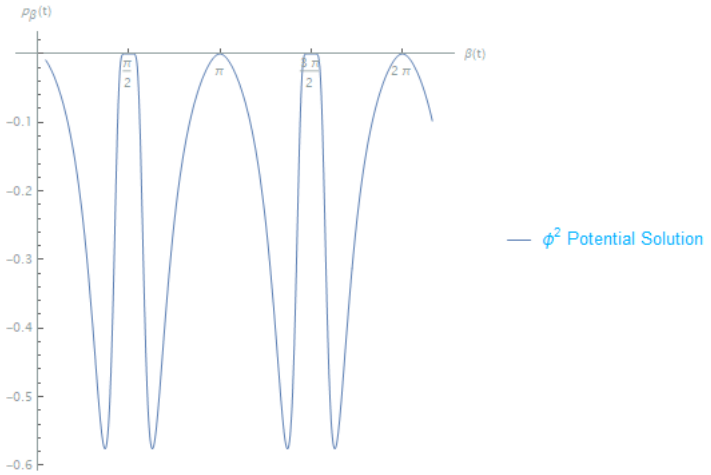

Figure 5.9: (β, p_β) phase space plot for the numerical solution of the FLRW + harmonic potential model.

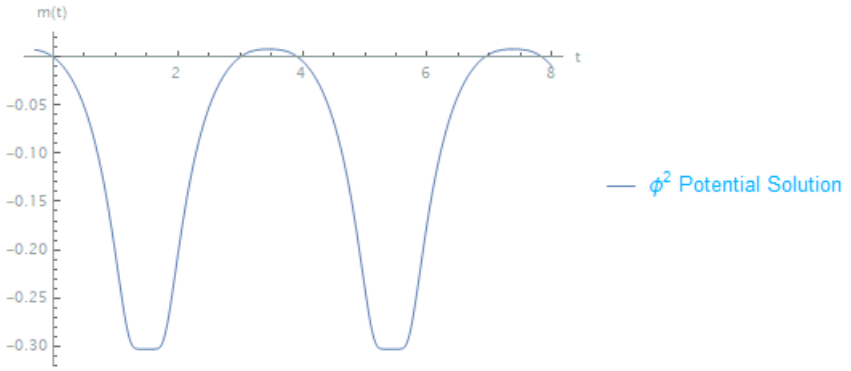

Figure 5.10: Numerical solution of $m(t)$ for the FLRW + harmonic potential model.

As well as simple toy models such as a harmonic potential, it is also possible to find numerical solutions for more complicated potentials, provided that they satisfy the conditions for Lipschitz continuity of $U(\beta)$. As an example, consider the Quartic Hilltop potential introduced in section 3

$$V_{QH}(\phi) = \Lambda \left[1 - \lambda \left(\frac{\phi}{m_{pl}} \right)^4 \right] \tag{5.226}$$

In that section, we explored corrections to the QHS model in order for it to remain valid when describing post inflationary dynamics such as reheating. In shape space

the Quartic Hilltop potential becomes (in units where $m_{pl} = 1$)

$$V_{QH}(\beta) = \Lambda(1 - \lambda \tan^4 \beta) \tag{5.227}$$

The Quartic Hilltop potential is well known to be unbounded below with no stable vacuum. One stabilised version of the potential which has been investigated in detail is the Quartic Hilltop Squared (QHS) model [1], with potential

$$\begin{aligned} V_{QHS}(\phi) &= \Lambda \left[1 - \lambda \left(\frac{\phi}{m_{pl}}\right)^4\right]^2 \\ V_{QHS}(\beta) &- \Lambda \left(1 - \lambda \tan^4 \beta\right)^2 \end{aligned} \tag{5.228}$$

Having developed the formalism of contact reduction, we may now investigate the pre-inflationary cosmological dynamics implied by the QHS potential by finding numerical solutions to the equations of motion that pass smoothly through the big bang, provided that the U_ϕ potentials are locally Lipschitz continuous around $\beta = \pi/2$. For both the Quartic Hilltop and Quartic Hilltop Squared potentials, this is indeed the case, so there will exist a unique local solution that passes through the big bang.

In figure 5.11 the numerical solution Hamiltonian for Quartic Hilltop and Quartic Hilltop Squared models, which are approximately zero to within machine precision over the time domain. The initial conditions are taken as those in eq 5.225, the energy-density scale is chosen as $\Lambda = 1/3$ and the potential parameter is $\lambda = 10^{-2}$. We have chosen a λ a few orders of magnitude larger than what is actually required for observational consistency for illustrative purposes that become apparent when one examines the numerical solutions of the dynamical variables.

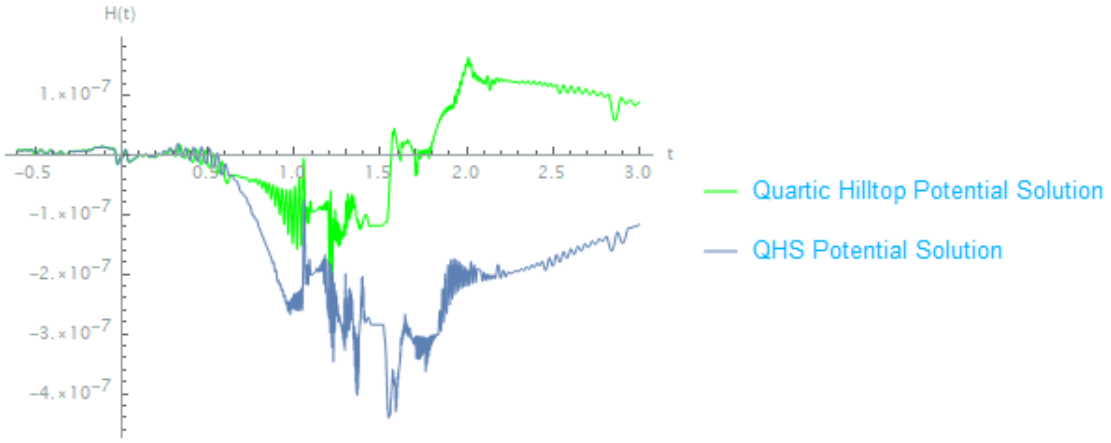

Figure 5.11: Plot of the numerical solutions Hamiltonian for the FLRW + Quartic Hilltop (green) and Quartic Hilltop Squared (blue) models with initial conditions 5.225.

In figure 5.11 the numerical solution Hamiltonian for Quartic Hilltop and Quartic Hilltop Squared models, which are approximately zero to within machine precision over the time domain. The initial conditions are taken as those in equation 5.225, the energy-density scale is chosen as $\Lambda = 1/3$ and the potential parameter is $\lambda = 10^{-2}$. We have chosen a λ a few orders of magnitude larger than what is actually required for observational consistency for illustrative purposes that become apparent when one examines the numerical solutions of the dynamical variables.

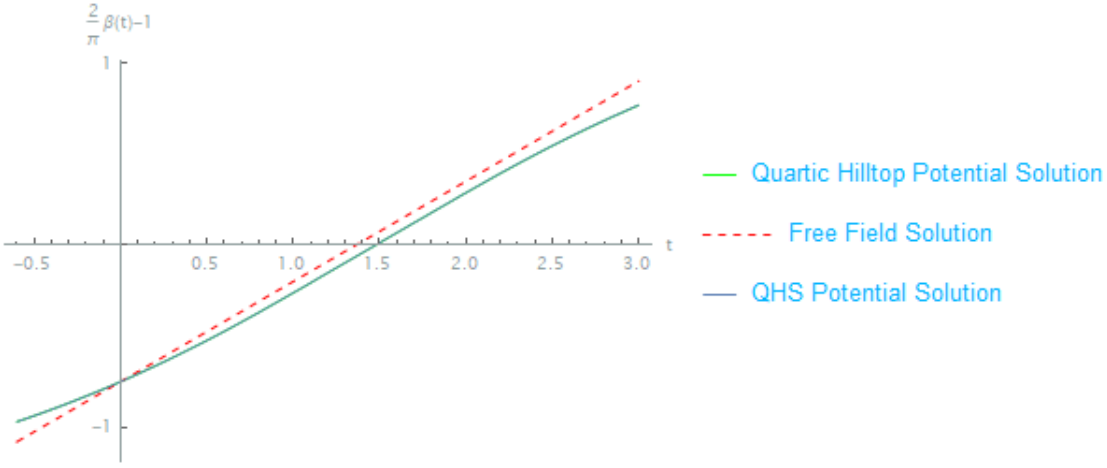

Figure 5.12: Plots of $\frac{2}{\pi}\beta(t) - 1$ for the free field (red, dashed), Quartic Hilltop (green) and Quartic Hilltop Squared (blue) models, showing explicitly that the system evolves through $\beta = \pi/2$ in finite coordinate time $t_s \approx 1.5$.

In figure 5.12 we plot the numerical solutions for the free field, Quartic Hilltop and Quartic Hilltop Squared models, again transformed so that they intercept the t-axis exactly when $\beta = \pi/2$ at $t_s \approx 1.5$. For a small potential parameter λ the QH and QHS potentials are approximately equal far from the QHS vacuum expectation value, and thus the solutions lie almost on top of each other. An even smaller value of λ closer to what is required for observational consistency with inflationary measurements would force these two solutions closer together.

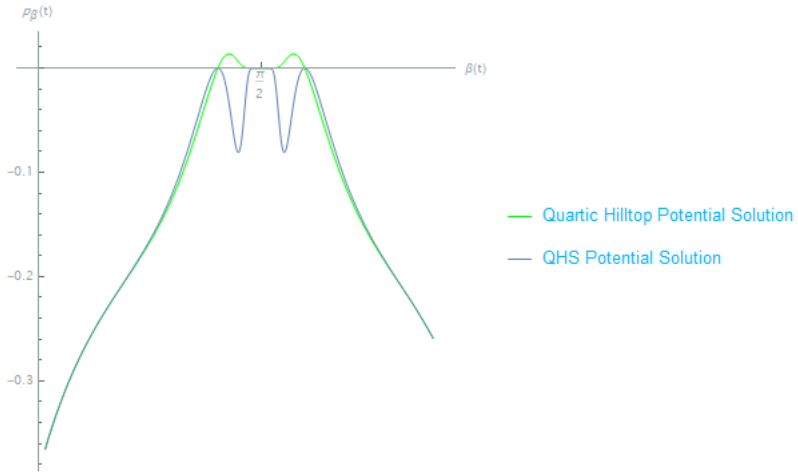

Figure 5.13: (β, p_β) phase space plot for the numerical solutions of the Quartic Hilltop (green) and Quartic Hilltop Squared (blue) models.

Although the numerical solutions for $\beta(t)$ are almost indistinguishable, the solutions of the momentum $p_\beta(t)$ displayed in the phase space diagram of figure 5.13 are quite distinct, particularly in a neighbourhood around $\beta = \pi/2$. Both momenta go to zero at the big bang as we would expect due to the exponential suppression factor and are thus well defined.

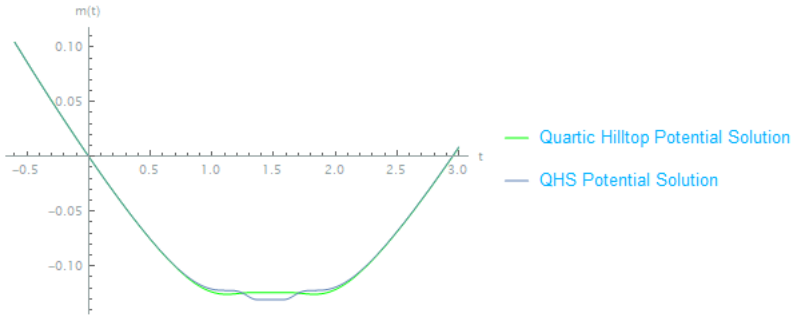

Figure 5.14: Numerical solution of $m(t)$ for the Quartic Hilltop (green) and Quartic Hilltop Squared (blue) models.

In figure 5.14 we plot the numerical solutions of the final dynamical variable, the frictional global coordinate $m(t)$ for the Quartic Hilltop and Quartic Hilltop Squared models. Just as for the other dynamical variables, the QH and QHS solutions are approximately equal far from the big bang but distinct in a neighbourhood around $t_s \approx 1.5$. For both models $m(t)$ is well defined through the big bang. Thus all dynamical variables, the Hamiltonian and contact form are well defined through the big bang.

5.8.2 FLRW + 2 Scalar Fields

In this section we present examples of a higher dimensional system than that of section 5.8.1. In the case of FLRW + 2 scalar fields, the shape space projection maps the scalar fields onto S^2. The evolution of the fields can be visualised as a path on S^2. We showed in section 3.2 that the free field case was exactly solvable, with the solutions being great circles on S^2 5.188.

The shape space Hamiltonian and equations of motion for FLRW + 2 scalar fields are

$$\begin{aligned}\mathcal{H} &= \frac{\mathcal{H}^c}{h^2\cos^2\beta} = \frac{1}{2}p_\beta^2\cos^2\beta + \frac{\sqrt{3}}{2}p_\beta + \frac{p_\alpha^2}{2\sin^2\beta} + U(\alpha,\beta)e^{-2m} \\ U(\alpha,\beta) &= V(\alpha,\beta)e^{-\sqrt{3}|\tan\beta|}\sec^2\beta\end{aligned} \tag{5.229}$$

$$\begin{aligned}\dot{\alpha} &= \frac{p_\alpha}{\sin^2\beta} \\ \dot{\beta} &= p_\beta\cos^2\beta + \frac{\sqrt{3}}{2} \\ \dot{p}_\alpha &= \left(2sUp_\alpha - \partial_\alpha U\right)e^{-2m} \\ \dot{p}_\beta &= p_\beta^2\cos\beta\sin\beta + \left(2sUp_\beta - \partial_\beta U\right)e^{-2m} \\ \dot{m} &= -s\left(\frac{\sqrt{3}}{2}p_\beta + 2Ue^{-2m}\right)\end{aligned} \tag{5.230}$$

In this example we consider a two-field harmonic potential, which has the following forms in field-space and shape shape respectively

$$\begin{aligned}V(\phi_1,\phi_2) &= \frac{1}{2}\left(\phi_1^2+\phi_2^2\right) \\ V_\phi(\alpha,\beta) &= \frac{1}{2}\tan^2\beta\end{aligned} \tag{5.231}$$

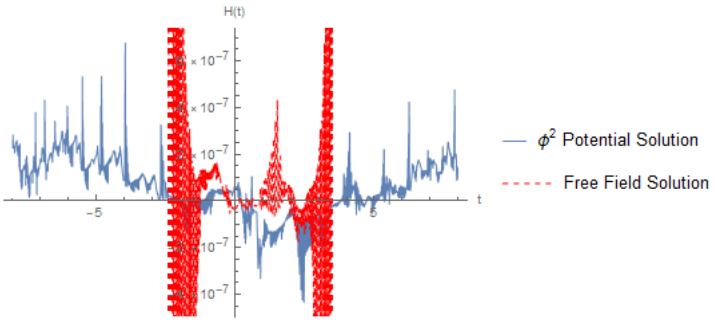

Figure 5.15: Numerical solution Hamiltonians for the free field (red, dashed) and two-field harmonic potential (blue).

In figure 5.15 we plot the numerical solution Hamiltonians for the free field and

harmonic potential models for the initial conditions at $t = 0$

$$\begin{aligned} &\beta(0) = 1, \quad p_\beta(0) = \frac{\sqrt{3}}{2}\sec^2\beta\left[-1+\sqrt{1-\frac{4}{3}\cos^2\beta\left(\frac{p_\alpha^2}{\sin^2\beta}+2Ue^{-2m}\right)}\right] \\ &\alpha(0) = \frac{\pi}{4}, \quad p_\alpha(0) = 0.5 \\ &m(0) = 0 \end{aligned} \tag{5.232}$$

Both solutions are stopped just as they become numerically unstable due to the machine precision of the discretised equations of motion becoming insufficient [165]. This point occurs at different times for each solution, with the harmonic potential solution running for much longer than the free field solution.

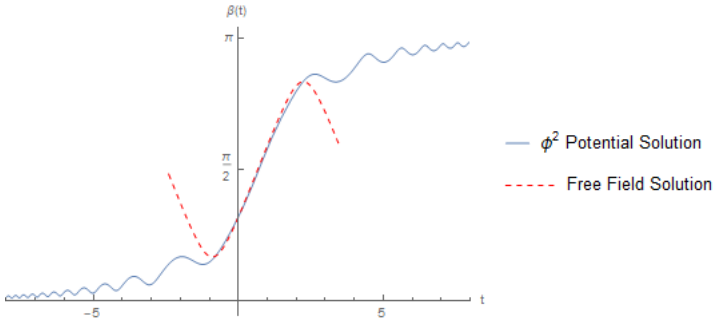

Figure 5.16: Numerical solutions of $\beta(t)$ for the free field (red, dashed) and two-field harmonic potential (blue).

In figure 5.16 we plot the numerical solutions of $\beta(t)$ for the free field (red, dashed) and harmonic potential (blue) models. Both solutions pass smoothly through $\beta = \pi/2$ in finite coordinate time. We see the characteristic exponential suppression of the potential function $U(\alpha, \beta)$ near $\beta = \pi/2$, making both solutions approximately equal near the big bang.

In figure 5.17 we plot the (β, p_β) slice of the full 4-dimensional phase space $(\alpha, \beta, p_\alpha, p_\beta)$, for the free field and harmonic potential numerical solutions. In this figure it is easier to see why the Hamiltonians are becoming numerically unstable, particularly for the harmonic potential solutions. As $\beta(t)$ approaches $0, \pi$ the momentum starts to oscillate rapidly. It is unlikely that this is the true behaviour of

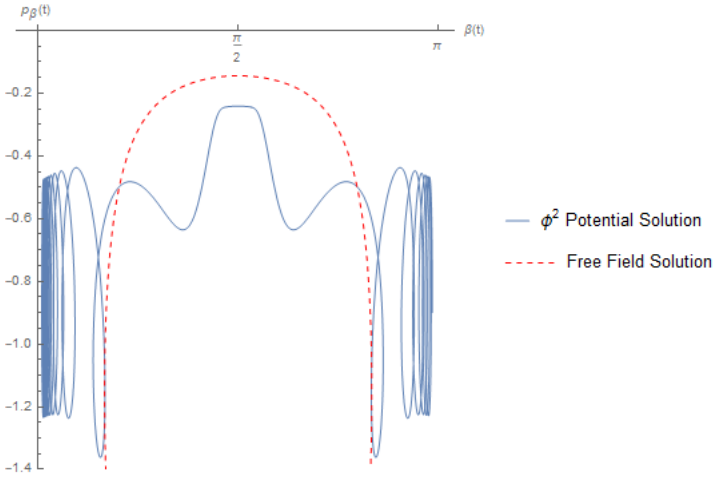

Figure 5.17: (β, p_β) phase space plot for the free field (red, dashed) and harmonic potential (blue) numerical solutions.

the system, but rather due to the numerically instability of solving a still system of coupled ODEs. Despite this, the momentum remains well defined at the big bang.

The parametric plots of $(\beta(t), \alpha(t))$ and $(\beta(t), p_\alpha(t))$ are presented in figures 5.18a and 5.18b respectively for the free field and harmonic potential numerical solutions. Both dynamical variables $\alpha(t)$ and $p_\alpha(t)$ remain well defined through $\beta = \pi/2$. In particular, in the free field case p_α is simply a constant. In figure 5.18a we see that the two solutions are approximately equal near $\beta = \pi/2$, again due to the exponential suppression of the potential close to the big bang. The potential suppression is also manifest in figure 5.18b, for the harmonic potential solutions, the p_α becomes approximately constant near $\beta = \pi/2$.

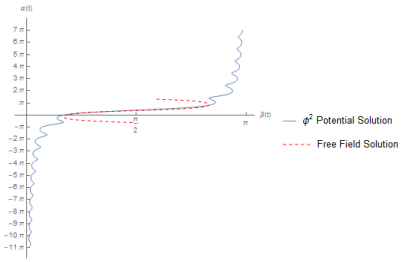

(a) Parametric plot of $(\beta(t), \alpha(t))$ for the free field (red, dashed) and harmonic potential (blue) numerical solutions.

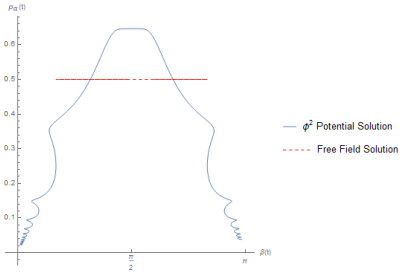

(b) Parametric plot of $(\beta(t), p_\alpha(t))$ for the free field (red, dashed) and harmonic potential (blue) numerical solutions.

Figure 5.18: Parametric numerical solutions of $(\beta(t), \alpha(t))$ and $(\beta(t), p_\alpha(t))$ for the free-field and ϕ^2 models.

Lastly in figure 5.19 we plot the global frictional variable $m(t)$ parameterised by $\beta(t)$ for the free field and harmonic potential solutions. Both solutions remain well defined through the big bang at $\beta = \pi/2$ and display the characteristic potential suppression.

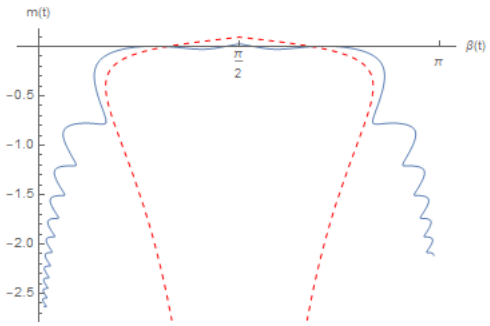

Figure 5.19: Parametric plot of $(\beta(t), m(t))$ for the free field (red, dashed) and harmonic potential (blue) numerical solutions.

In figure 5.20 we plot the free field and harmonic potential solutions (α, β) as a path on S^2, with the equator at $\beta = \pi/2$ corresponding to the big bang under the shape space gnomonic projection.

Recall that we showed explicitly in section 3.2 how the free field solution is a great circle on shape space 5.188. This can be seen clearly in figure 5.20. The great circle is incomplete due to the numerical solution being stopped just before it becomes unstable. Most importantly figure 5.20 shows clearly how the system evolves smoothly through the shape space equator.

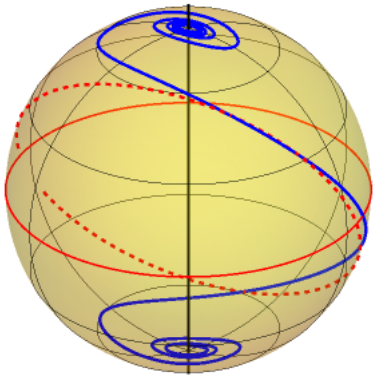

Figure 5.20: free field (red, dashed) and Harmonic potential (blue) numerical solutions of $(\alpha(t), \beta(t))$ plotted as a path on S^2. The solid red line is the shape space equator $\beta = \pi/2$, corresponding to the big bang under the gnomonic projection.

5.8.3 Bianchi I

We will now look at numerical results in the shape space representation of the Bianchi I cosmology, which contains flat FLRW geometries at the S^2 poles of shape space $\beta = 0, \pi$. The vacuum case simply corresponds to the Kasner solution. The Kasner cosmology is exactly solvable, with the solutions being great circles on S^2. In figure 5.21 below, we present the numerical solution of one such Kasner cosmology, which are parameterised by a single constant momentum p_α 5.192.

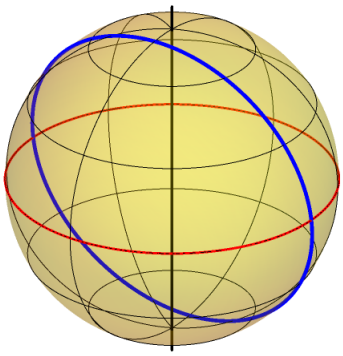

Figure 5.21: Numerical solution of $(\alpha(t), \beta(t))$ to the vacuum Bianchi I (Kasner) equations of motion 5.191, showing a great circle solution (blue) passing smoothly through the shape space equator (red) $\beta = \pi/2$.

We will now consider in more detail, the case of Bianchi I + a scalar field. In this particular case. The shape space projection now maps the dynamical variables onto S^3, as we start with the anisotropy parameters and a single scalar field. We will consider the case of a free field and harmonic potential. With the Hamiltonian and equations of motion given by eq's 5.203 and 5.204 respectively. Reproduced here for convenience.

$$\begin{aligned} \mathcal{H}_{BI} &= \frac{1}{2}p_\beta^2 \cos^2\beta + \frac{1}{\sqrt{3}}p_\beta + \frac{p_\alpha^2}{2\sin^2\beta\sin^2\gamma} + \frac{p_\gamma^2}{2\sin^2\beta} + U_\phi(\beta,\gamma)e^{-2m} \\ U_\phi(\beta,\gamma) &= V_\phi(\beta,\gamma)e^{-\frac{2}{\sqrt{3}}|\tan\beta|}\sec^2\beta \end{aligned} \tag{5.233}$$

$$
\begin{aligned}
\dot{\alpha} &= \frac{p_\alpha}{\sin^2\beta\sin^2\gamma} \\
\dot{\beta} &= p_\beta\cos^2\beta + \frac{1}{\sqrt{3}} \\
\dot{\gamma} &= \frac{p_\gamma}{\sin^2\beta} \\
\dot{p}_\alpha &= (2sU_\phi p_\alpha - \partial_\alpha U_\phi)\, e^{-2m} \\
\dot{p}_\beta &= p_\beta^2\cos\beta\sin\beta + \frac{p_\alpha^2\cos\beta}{\sin^3\beta\sin^2\gamma} + \frac{p_\gamma^2\cos\beta}{\sin^3\beta} + (2sU_\phi p_\beta - \partial_\beta U_\phi)\, e^{-2m} \\
\dot{p}_\gamma &= \frac{p_\alpha^2\cos\gamma}{\sin^2\beta\sin^3\gamma} + (2sU_\phi p_\gamma - \partial_\gamma U_\phi)\, e^{-2m} \\
\dot{m} &= -s\left(\frac{1}{\sqrt{3}}p_\beta + 2U_\phi e^{-2m}\right)
\end{aligned}
\tag{5.234}
$$

The harmonic potential in field space and shape space is given by

$$
\begin{aligned}
V(\phi) &= \frac{1}{2}\phi^2 \\
V_\phi(\beta,\gamma) &= \frac{1}{2}\tan^2\beta\cos^2\gamma
\end{aligned}
\tag{5.235}
$$

For this example, we look for a numerical solution to the equations of motion 5.234. subject to the following initial conditions at $t = 0$.

$$
\begin{aligned}
&\alpha(0) = \frac{3}{2}\pi, \quad p_\alpha(0) = 0.1 \\
&\beta(0) = 1.1, \quad p_\beta(0) = \frac{\sqrt{3}}{2}\sec^2\beta\left[-1 + \sqrt{1 - \frac{4}{3}\cos^2\beta\left(\frac{p_\alpha^2}{\sin^2\beta} + 2Ue^{-2m}\right)}\right] \\
&\gamma(0) = \frac{\pi}{4}, \quad p_\gamma(0) = 1 \\
&m(0) = 0
\end{aligned}
\tag{5.236}
$$

For this section and the following, we provide the Hamiltonian numerical solution plots in appendix B.1. In particular, one may find the numerical solution Hamiltonian for Bianchi I + free field and harmonic potential models in figure B.1.

Just as for the FLRW + 2 scalar fields model, we also see in Bianchi I + matter

that the free field solution becomes numerically unstable faster than the harmonic potential model and has to be stopped after a shorter time. We next check the numerical solutions of $\beta(t)$ to confirm that the solutions pass through the shape space equator.

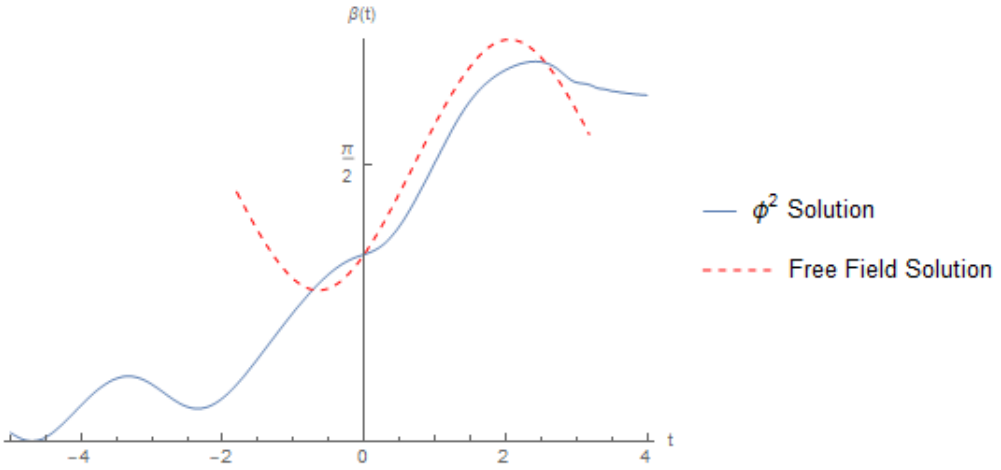

Figure 5.22: Numerical solution of $\beta(t)$ for the Bianchi I + free field (red, dashed) and harmonic potential (blue) models.

In figure 5.22 we plot the numerical solutions of $\beta(t)$ for the free field and harmonic potential model. Both solutions pass smoothly through the big bang at $\beta = \pi/2$. In this case the there is a bigger difference between the free field and harmonic potential solutions over the entire time domain. This is due to the fact that the initial conditions for each solution are slightly different. We choose p_β to be set by the Hamiltonian constraint $\mathcal{H} := 0$ (This choice is arbitrary, in principle we could have chosen any of the other dynamical variables). This means that given a set of initial $\alpha, p_\alpha, \gamma, p_\gamma$ and m, the boundary condition on p_β is determined by

$$p_\beta = \frac{\sqrt{3}}{2}\sec^2\beta\left[-1+\sqrt{1-\frac{4}{3}\cos^2\beta\left(\frac{p_\alpha^2}{\sin^2\beta}+2U(\alpha,\beta)e^{-2m}\right)}\right] \tag{5.237}$$

The potential term $U(\alpha,\beta)$ is non-zero for our chosen initial conditions in the harmonic potential case, and thus the initial p_β will be different in the free field and harmonic potential cases.

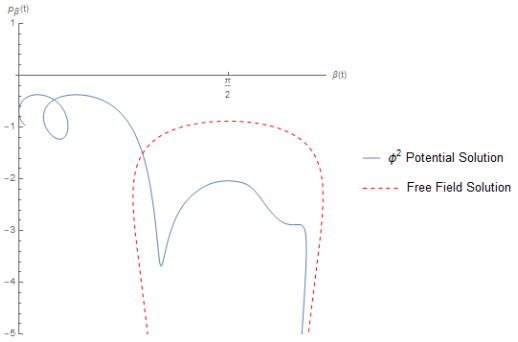

(a) Phase space plot of $(\beta(t), p_\beta(t))$ for the numerical solutions of the Bianchi I + free field (red, dashed) and harmonic potential (blue) models.

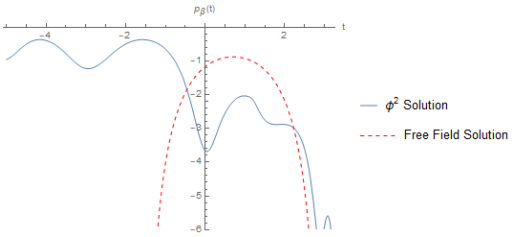

(b) Numerical solution of $p_\beta(t)$ for the numerical solutions of the Bianchi I + free field (red, dashed) and harmonic potential (blue) models.

Figure 5.23: Numerical solution of $p_\beta(t)$ for the free-field and ϕ^2 models.

In figure 5.23a the numerical solution of p_β parameterised by $\beta(t)$ ((β, p_β) slice of phase space) for the free field and harmonic potential models. Both solutions, as expected pass smoothly through the big bang at $\beta = \pi/2$. In figure 5.23b we plot $p_\beta(t)$ parameterised by the time coordinate. This plot shows explicitly that the initial p_β's at $t = 0$ are quite different for each model, so it is no surprise that the numerical solutions differ by quite a large amount as compared to some of the previous examples, even near the big bang singularity where the potential is exponentially suppressed.

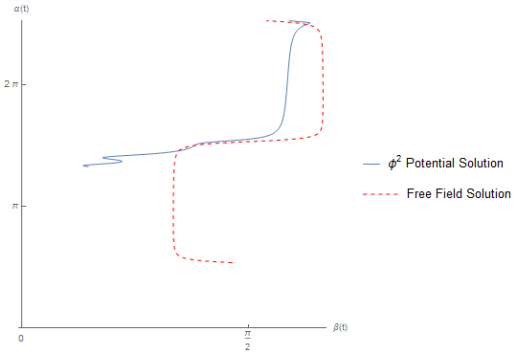

(a) Parametric plot of $(\beta(t), \alpha(t))$ for the Bianchi I + free field (red, dashed) and harmonic potential (blue) numerical solutions.

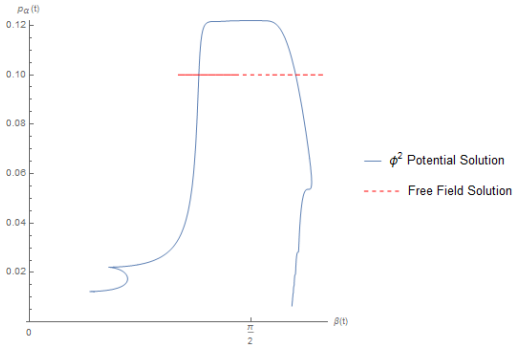

(b) Parametric plot of $(\beta(t), p_\alpha(t))$ for the Bianchi I + free field (red, dashed) and harmonic potential (blue) numerical solutions.

Figure 5.24: Parametric numerical solutions of $(\beta(t), \alpha(t))$ and $(\beta(t), p_\alpha(t))$ for the Bianchi I + free-field and ϕ^2 models.

In figures 5.24a and 5.24b we plot the numerical solutions of α and p_α respectively, parameterised by $\beta(t)$. As we expect, both solutions pass smoothly though the big bang at $\beta = \pi/2$ along with some other expected features. In figure 5.24b, we see that the free field p_α momentum is everywhere constant, as it should be since $\dot{p}_\alpha = 0$ everywhere for zero-potential. Likewise, near the big bang where the potential becomes exponentially suppressed, the harmonic potential p_α momentum becomes approximately constant.

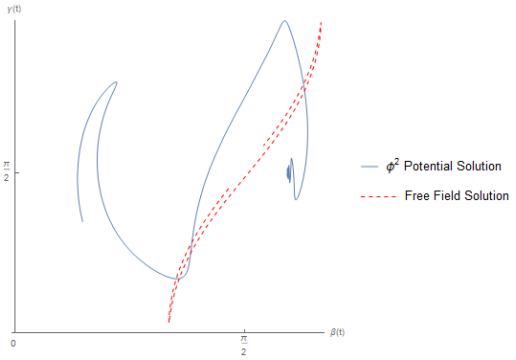

(a) Parametric plot of $(\beta(t), \gamma(t))$ for the Bianchi I + free field (red, dashed) and harmonic potential (blue) numerical solutions.

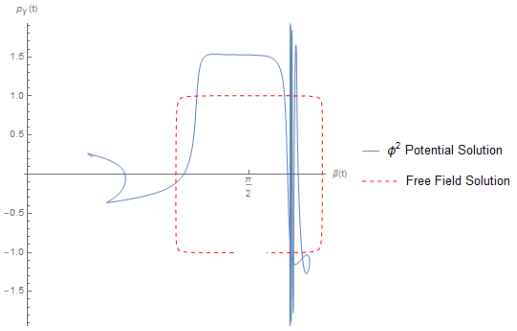

(b) Parametric plot of $(\beta(t), p_\gamma(t))$ for the Bianchi I + free field (red, dashed) and harmonic potential (blue) numerical solutions.

Figure 5.25: Parametric numerical solutions of $(\beta(t), \gamma(t))$ and $(\beta(t), p_\gamma(t))$ for the Bianchi I + free-field and ϕ^2 models.

In figures 5.25a and 5.25b we plot the numerical solutions of γ and p_γ respectively, parameterised by $\beta(t)$. We again see that the numerical solutions are well-defined through the big bang at $\beta = \pi/2$. Additionally, we see a small oscillatory behaviour in γ around $\gamma = \pi/2$. The interpretation of this will becomes clear when we look at the original configuration space variables $(\phi, x, y,)$ shortly. The last dynamical variable to check is the global frictional coordinate $m(t)$, which we plot in figure 5.26 for the free field and harmonic potential models. In both models the numerical solution is well defined through the big bang at $\beta = \pi/2$. Thus all dynamical variables, the Hamiltonian and contact form are well defined through $\beta = \pi/2$ as we expect due to the potential function $U(\alpha, \beta, \gamma)$ being locally Lipschitz continuous around $\beta = \pi/2$.

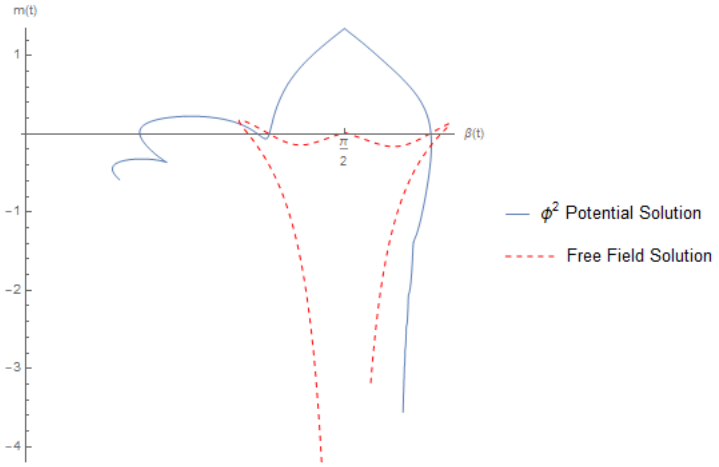

Figure 5.26: Parametric plot of $(\beta(t), m(t))$ for the Bianchi I + free field (red, dashed) and harmonic potential (blue) numerical solutions.

In the case of a Bianchi + scalar field cosmology, the shape space projection is a compactification onto S^3 (rather than S^2 as in the FLRW case), thus we can think of solutions a path on S^3. One way to visualise this is to consider constant α, β or γ slices of S^3, which are S^2 surfaces.

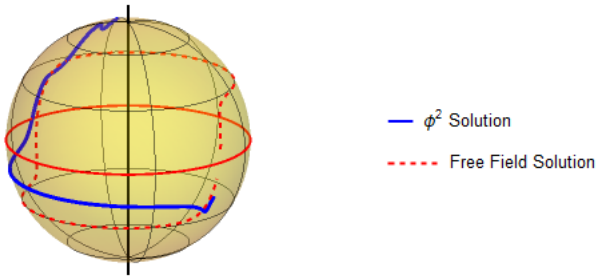

Figure 5.27: Constant γ slice of the Bianchi I + matter S^3 shape space. The (α, β) solutions for the free field (red, dashed) and harmonic potential (blue) are plotted as paths on the S^2 surface. The solid red line is the S^2 slice equator at $\beta = \pi/2$ which corresponds to the GR singularity.

In figure 5.27 we plot a constant γ slice of the full S^3 shape space with the free field and harmonic potential paths plotted on the surface. The equator is the

line $\beta = \pi/2$ which represents the big bang, both solutions pass smoothly through the shape space equator. However the paths are not symmetric on either side of the equator, despite there being a symmetric (or no) potential, since this is only a constant γ slice of the full S^3 shape space, on which the path would be symmetric either side of the big bang. Likewise we could also look at constant α and constant β slice of shape space.

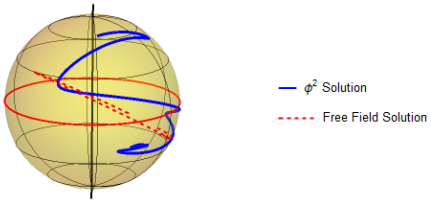

(a) Constant α slice of the Bianchi I + matter S^3 shape space. The (γ, β) solutions for the free field (red, dashed) and harmonic potential (blue) are plotted as paths on the S^2 surface. The solid red line is the S^2 slice equator at $\beta = \pi/2$ which corresponds to the GR singularity.

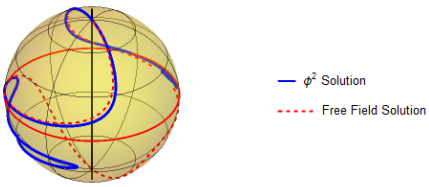

(b) Constant β slice of the Bianchi I + matter S^3 shape space. The (γ, α) solutions for the free field (red, dashed) and harmonic potential (blue) are plotted as paths on the S^2 surface. The solid red line is the S^2 slice equator at $\alpha = \pi/2$ which does not correspond to any GR singularity.

Figure 5.28: Constant α and β shape space plots for Bianchi I numerical solutions.

In figures 5.28a and 5.28b we plot constant α and β slices of the full S^3 shape space respectively. In the constant α slice, the solid red line is again the $\beta = \pi/2$ equator, representing the initial GR singularity. The solution path passes smoothly through the big bang equator for both solutions. In the constant β slice, the solid red line is the $\alpha = \pi/2$ equator, which does not correspond to any GR singularity and thus the system passing through this line is not of any particular significance in relation to GR singularities.

In this section we have seen examples of the shape pace dynamical variables and mathematical structures remain well defined through the big bang, as was to be expected from the potential function $U(\alpha, \beta, \gamma)$ satisfying the conditions for

Lipschitz continuity. It is still the case however that the original configuration space dynamical variables ϕ, x, y are ill-defined though the big bang. One may transform back to the original variables and see this explicitly for the numerical solutions.

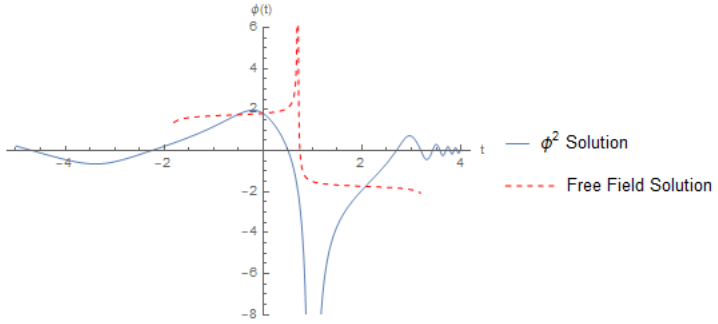

Figure 5.29: Plot of the original scalar field variable $\phi(t) = |\tan\beta(t)|\cos\gamma(t)$ for the Bianchi I + free field (red, dashed) and harmonic potential (blue) numerical solutions.

In figure 5.29 we plot the scalar field under the shape space projection 5.200 for the free field and harmonic potential numerical solutions. Since $\beta(t)$ passes smoothly through $\beta = \pi/2$, the scalar field diverges at the big bang due to the $|\tan\beta|$ factor in the gnomonic projection, but is well defined on either side of the big bang. We also see oscillations of the scalar field around the vacuum $\phi_0 = 0$ on both sides of the GR singularity, although they are more pronounced on the right-half plane. In shape space, these vacuum oscillations manifest as γ oscillating around $\gamma = \pi/2$ as seen in figure 5.25a.

In figures 5.30a and 5.30b we plot the anisotropy parameters $x(t)$ and $y(t)$ given by the shape space projection 5.200 for the free field and harmonic potential numerical solutions. The anisotropy parameters also diverge at the big bang. One would expect from solving the original configuration space equations of motion generated from the Herglotz Lagrangian

$$\mathcal{L}^H = \frac{1}{6}h^2 + \frac{1}{2}(\dot{x} + \dot{y}) + \frac{1}{2}\dot{\phi} - V(\phi) \tag{5.238}$$

that the anisotropy parameters are related to each other by a linear relationship $y(x) = y_0 + C_y x$.

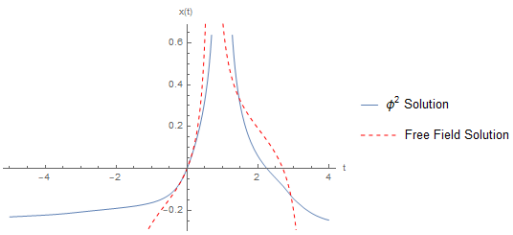

(a) Plot of the original anisotropy parameter $x(t) = |\tan\beta(t)|\sin\gamma(t)\cos\gamma(t)$ for the Bianchi I + free field (red, dashed) and harmonic potential (blue) numerical solutions.

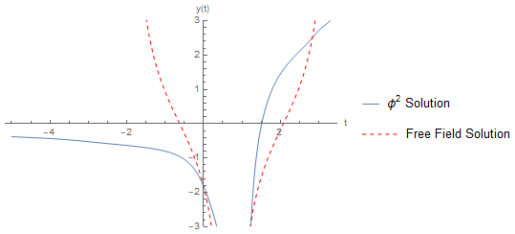

(b) Plot of the original anisotropy parameter $x(t) = |\tan\beta(t)|\sin\gamma(t)\sin\gamma(t)$ for the Bianchi I + free field (red, dashed) and harmonic potential (blue) numerical solutions.

Figure 5.30: Numerical solutions of the anisotropy parameters (x, y) for Bianchi I + free field and harmonic potential models.

In figure 5.31 we display the parametric plot $(x(t), y(t))$ and see that indeed this linear relationship is satisfied. Each solution has two straight line branches, as the system evolves through the big bang the spatial manifold undergoes an inversion of orientation and moves from one branch to the other.

5.8.4 Quiescent Bianchi IX

In this section we look at a numerical example of quiescent Bianchi IX cosmology and show that it continues smoothly through the big bang in the shape space representation. Unlike Bianchi I, the Bianchi IX cosmology has a non-trivial Lie algebra, which leads to generally non-zero shape potential and contains flat FLRW cosmologies. The shape space potential function $U(\alpha, \beta, \gamma)$ for Bianchi IX is given in equation 5.217, with the functions $f_i(\alpha)$ defined in equation 5.197. The flat FLRW-cosmologies are contained at $\beta = 0, \pi$ and $\gamma = 0, \pi$. However the time parameterisation we have chosen, implicit in the re-scaling of the contact Hamiltonian by $h^{-2}\sec^2\beta$ is not suited for investigating these sub-geometries as the Hamiltonian is undefined for $\beta, \gamma = 0, \pi$.

We will consider Bianchi IX cosmologies minimally coupled to a scalar field in the free field (massless) and harmonic potential cases. As we have already shown,

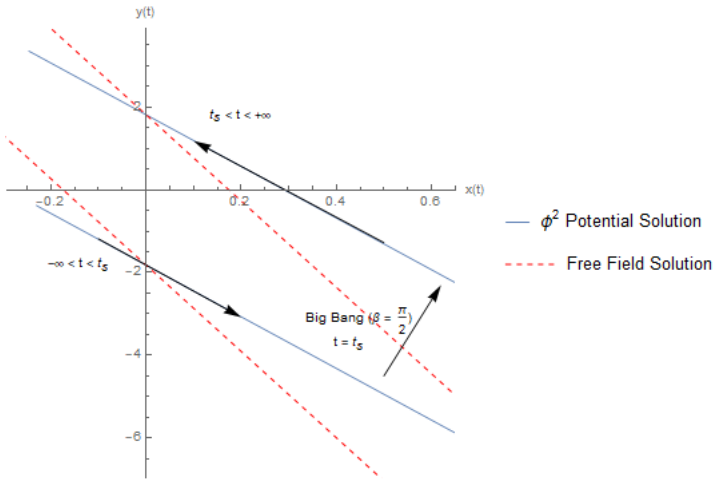

Figure 5.31: Parameteric plot of $(x(t), y(t))$ for the Bianchi I + free field (red, dashed) and harmonic potential (blue) numerical solutions. As the system evolves through the Big Bang at $\beta(t_s) = \pi/2$, the spatial manifolds orientation inverts and system moves between straight line branches.

in the case of a everywhere-zero field potential, the shape space Hamiltonian is

$$\begin{aligned}\mathcal{H} &= \frac{1}{2}p_\beta^2 \cos^2\beta + \frac{1}{\sqrt{3}}p_\beta + \frac{p_\alpha^2}{2\sin^2\beta\sin^2\gamma} + \frac{p_\gamma^2}{2\sin^2\beta} + U(\alpha,\beta,\gamma)e^{-2m} \\ U(\alpha,\beta,\gamma) &= \sec^2\beta \sum_i c_i e^{\left(f_i(\alpha)\sin\gamma - \frac{2}{\sqrt{3}}\right)|\tan\beta|}\end{aligned} \tag{5.239}$$

In section 5.7.4 we showed that, including a generally non-zero field potential changes the shape space Hamiltonian to

$$\begin{aligned}\mathcal{H} &= \frac{1}{2}p_\beta^2 \cos^2\beta + \frac{1}{\sqrt{3}}p_\beta + \frac{p_\alpha^2}{2\sin^2\beta\sin^2\gamma} + \frac{p_\gamma^2}{2\sin^2\beta} + U(\alpha,\beta,\gamma)e^{-2m} + \frac{U_\phi(\beta,\gamma)}{s\Omega}e^{-3m} \\ U(\alpha,\beta,\gamma) &= \sec^2\beta \sum_i c_i e^{\left(f_i(\alpha)\sin\gamma - \frac{2}{\sqrt{3}}\right)|\tan\beta|} \\ U_\phi(\beta,\gamma) &= V_\phi(\beta,\gamma)e^{-\sqrt{3}|\tan\beta|}\sec^2\beta\end{aligned} \tag{5.240}$$

as additional degrees of freedom (k, Ω) are required in order to retain the original scaling symmetry of the action. We consider the numerical solutions to the equations of motion 5.213 subject to the following initial conditions at $t = 0$. Simply for demonstrative purposes, we have chosen to use the Hamiltonian constraint to

determine the initial condition on p_α, rather than p_β as in previous sections.

$$\begin{aligned}
&\alpha(0) = \frac{1}{2}\pi, \quad p_\alpha(0) = |\sin\beta\sin\gamma|\sqrt{-2\left(\frac{1}{2}p_\beta^2\cos^2\beta + \frac{1}{2}\frac{p_\gamma^2}{2\sin^2\beta} + \frac{1}{\sqrt{3}}p_\beta + Ue^{-2m} + \frac{U_\phi}{s\Omega}e^{-3m}\right)} \\
&\beta(0) = \frac{1}{8}\pi, \quad p_\beta(0) - 0.5 \\
&\gamma(0) = \frac{1}{8}\pi, \quad p_\gamma(0) = 0.1 \\
&m(0) = 0 \\
&k(0) = 0, \quad \Omega(0) = -1
\end{aligned} \tag{5.241}$$

In figure 5.32 we plot $\frac{2}{\pi}\beta(t) - 1$ where $\beta(t)$ is the Bianchi IX numerical solution for the free field and Harmonic potential models, showing explicitly that the system passes through the Big Bang at $\beta = \pi/2$. In the free field case, the discretised system equations of motion become numerically unstable shortly after passing through the Big Bang.

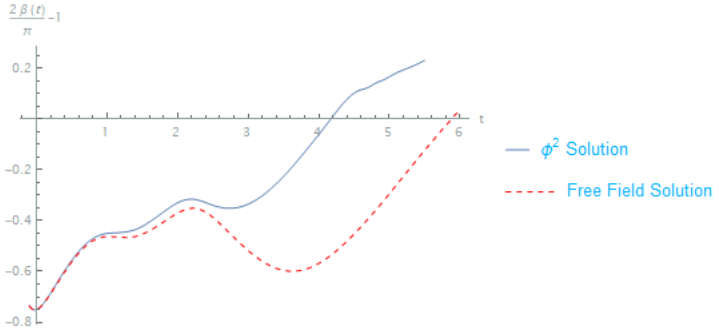

Figure 5.32: Plots of $\frac{2}{\pi}\beta(t) - 1$ for the Bianchi IX $\beta(t)$ numerical solutions, including the free field (red, dashed) and harmonic potential (blue) models.

In figure 5.33 we plot $\ln|p_\beta(t)|$ parameterised by $\beta(t)$, one can see clearly that in both cases the p_β momentum is well defined through $\beta = \pi/2$. In this particular case we choose to plot the logarithm as the free field and harmonic potential solutions of p_β differ by approximately two orders of magnitude near the big bang.

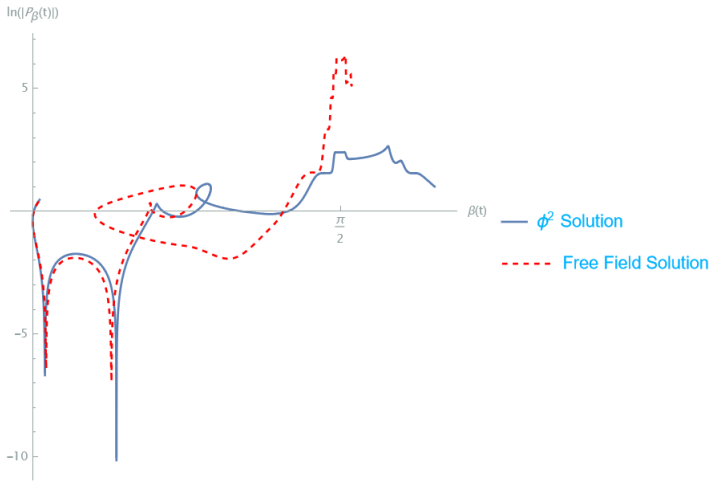

Figure 5.33: Plots of $\ln|p_\beta(t)|$ parameterised by $\beta(t)$ for the Bianchi IX $p_\beta(t)$ numerical solutions, including the free field (red, dashed) and harmonic potential (blue) models.

In figures 5.34a and 5.34b we plot the numerical solutions of the shape space coordinate α and associated momentum p_α respectively, parameterised by β. In both figures we see that the dynamical variables remain well defined through the big bang at $\beta = \pi/2$ as we expect. In the case of Bianchi I, p_α is constant for free field solutions as the equation of motion for $\dot{p}_\alpha$ contains only terms with factors of U_ϕ and ∂U_ϕ. However in the Bianchi IX case, which contains a shape potential which is not everywhere zero, the equation of motion for $\dot{p}_\alpha$ contains terms which have factors of the shape potential function U as well as the field potential U_ϕ, so even in the free field case where $U_\phi = 0$, the momentum p_α is not constant for all time as we see in the numerical solution of figure 5.34b.

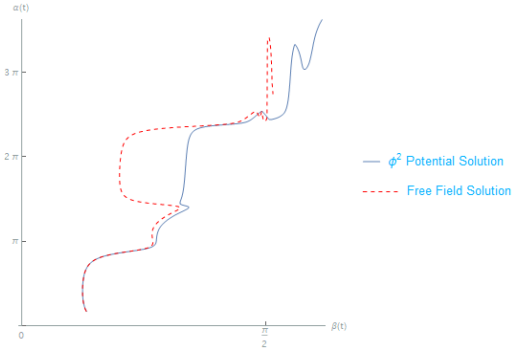

(a) Parametric plot of $(\beta(t), \alpha(t))$ for the Bianchi IX + free field (red, dashed) and harmonic potential (blue) numerical solutions.

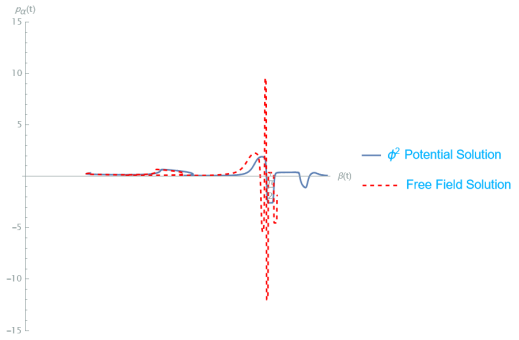

(b) Parametric plot of $(\beta(t), p_\alpha(t))$ for the Bianchi IX + free field (red, dashed) and harmonic potential (blue) numerical solutions.

Figure 5.34: Parametric plots of $(\beta(t), \alpha(t))$ and $(\beta(t), p_\alpha(t))$ for Bianchi IX + free field and harmonic potential models.

In figures 5.35a and 5.35b we plot the numerical solutions of γ and p_γ parameterised by β for the Bianchi IX + free field and harmonic potential models. Both dynamical variables remain well defined through the big bang at $\beta = \pi/2$. In addition to the shape degrees of freedom, for the Bianchi IX + matter cosmology we also have the additional degrees of freedom k and its associated momentum $\Omega(t)$ which were introduced to retain the scaling symmetry of the symplectic Lagrangian when there is a field potential present.

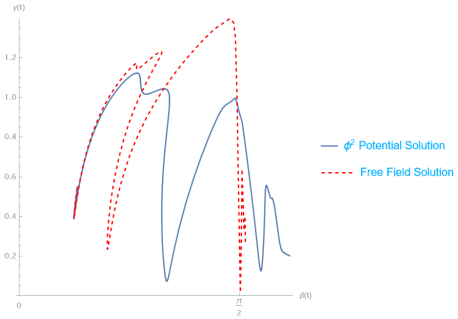

(a) Parametric plot of $(\beta(t), \gamma(t))$ for the Bianchi IX + free field (red, dashed) and harmonic potential (blue) numerical solutions.

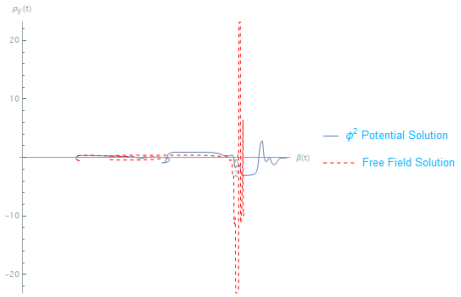

(b) Parametric plot of $(\beta(t), p_\gamma(t))$ for the Bianchi IX + free field (red, dashed) and harmonic potential (blue) numerical solutions.

Figure 5.35: Parametric plots of $(\beta(t), \gamma(t))$ and $(\beta(t), p_\gamma(t))$ for Bianchi IX + free field and harmonic potential models.

In figures 5.36a and 5.36b we plot the numerical solutions of k and Ω parameterised by $\beta(t)$ for the Bianchi IX + harmonic potential model. Both dynamical variables are well defined through the big bang at $\beta = \pi/2$. One one can see from the plot of (k, β) that the numerical solution becomes unstable shortly after passing through the big bang as $k \to \infty$.

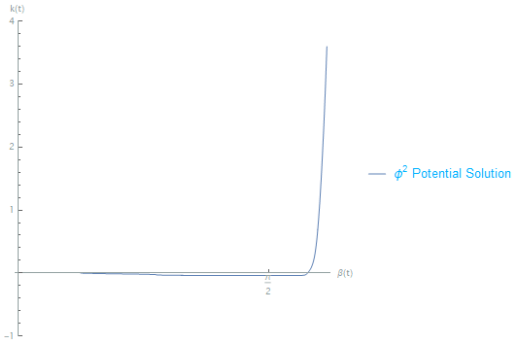

(a) Parametric plot of $(\beta(t), k(t))$ for the Bianchi IX + harmonic potential numerical solution.

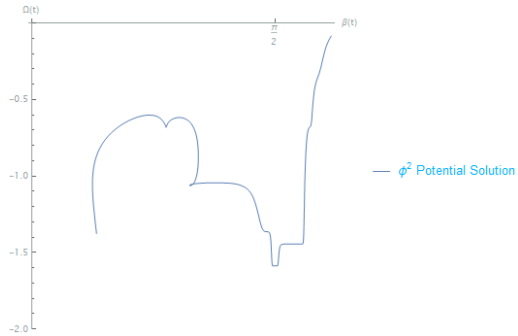

(b) Parametric plot of $(\beta(t), \Omega(t))$ for the Bianchi IX + harmonic potential numerical solutions.

Figure 5.36: Parametric plots of $(\beta(t), ka(t))$ and $(\beta(t), \Omega(t))$ for Bianchi IX + free field and harmonic potential models

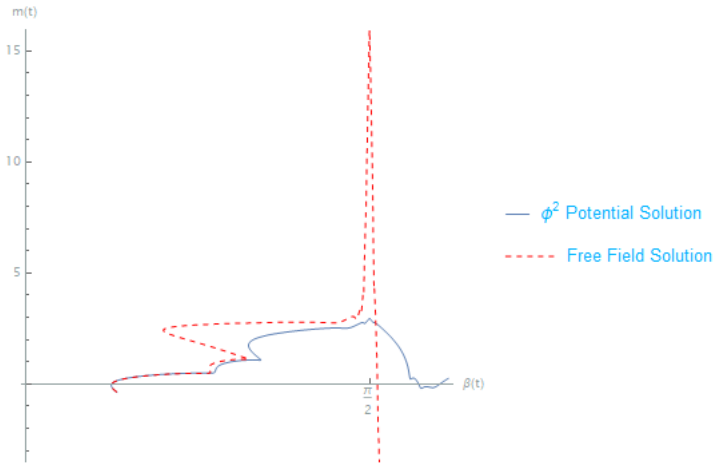

Figure 5.37: Parametric plot of $(\beta(t), m(t))$ for the Bianchi IX + harmonic potential numerical solution.

The last dynamical variable is the frictional global coordinate $m(t)$, plotted in figure 5.37. m is also well defined through the big bang and displays the characteristic "cusp" its time-derivative changes sign as the system passes through the big bang, due to the overall factor of Sign($\tan\beta$) in the equation of motion 5.213.

Thus we demonstrate that as expected, all dynamical variables, the Hamiltonian and contact form remain well defined as the system passes through the Bianchi IX big bang when the quiescence conditions are satisfied.

Once more we can visualise the evolution of the cosmology in terms of a paths on S^2 slices of the full S^3 shape space. Figure 5.38 displays a constant gamma S^2 slice of shape space. The free field and harmonic potential solutions are plotted in red/dashed and blue respectively. Both solution paths pass smoothly through the big bang, represented by the solid red equator at $\beta = \pi/2$.

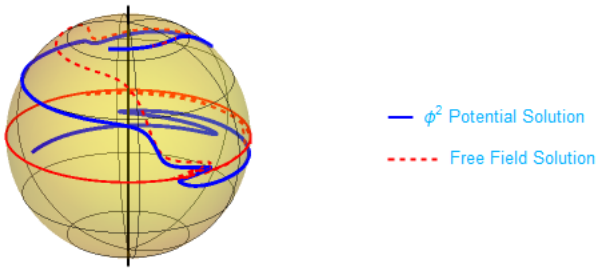

Figure 5.38: Constant γ slice of the Bianchi IX + matter S^3 shape space. The (α, β) solutions for the free field (red, dashed) and harmonic potential (blue) are plotted as paths on the S^2 surface. The solid red line is the S^2 slice equator at $\beta = \pi/2$ which corresponds to the GR singularity.

Figures 5.39a and 5.39b display constant α and constant β S^2 slices respectively. In figure 5.39a the equator is still at $\beta = \pi/2$ corresponding to the big bang, which both paths cross smoothly. However in figure 5.39a, where a constant β S^2 slice is displayed, the equator is at $\alpha = \pi/2$. which does not correspond to any GR singularity. Having numerically solved the system in the shape space representation,

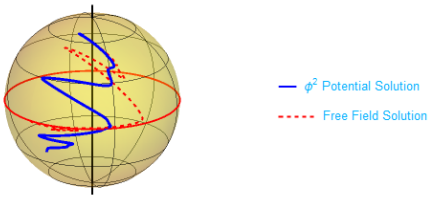

(a) Constant α slice of the Bianchi IX + matter S^3 shape space. The (γ, β) solutions for the free field (red, dashed) and harmonic potential (blue) are plotted as paths on the S^2 surface. The solid red line is the S^2 slice equator at $\beta = \pi/2$ which corresponds to the GR singularity.

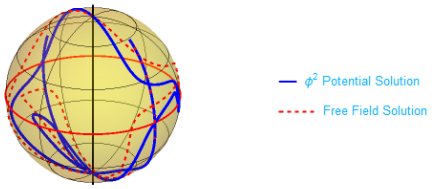

(b) Constant β slice of the Bianchi I + matter S^3 shape space. The (γ, α) solutions for the free field (red, dashed) and harmonic potential (blue) are plotted as paths on the S^2 surface. The solid red line is the S^2 slice equator at $\alpha = \pi/2$ which does not correspond to any GR singularity.

Figure 5.39: Constant α and β shape space plots of Bianchi IX + matter numerical solutions.

one can then transform back to the original configuration space dynamical variables of the scalar field ϕ and anisotropy parameters (x, y). In particular, it is much easier in this representation to see explicitly, the quiescence behaviour of the cosmology.

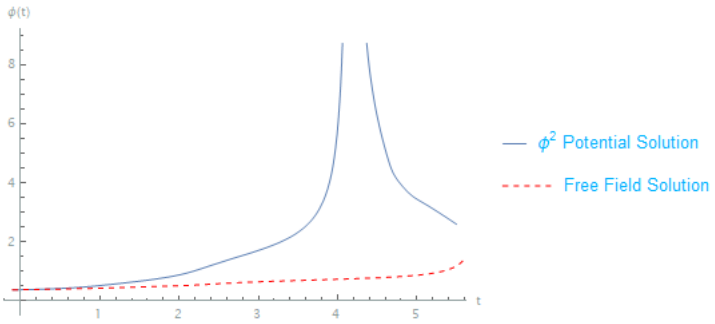

Figure 5.40: Plot of the original scalar field variable $\phi(t) = |\tan\beta(t)|\cos\gamma(t)$ for the Bianchi IX + free field (red, dashed) and harmonic potential (blue) numerical solutions.

Firstly we plot in figure 5.40 the scalar field $\phi = |\tan\beta|\cos\gamma$ for the free field and harmonic potential numerical solutions, which as expected is undefined at the big bang. Note that the free field and harmonic potential solutions pass through

the big bang at different coordinate times. From figure 5.32 one can see that the free field model passes through the big bang at approximately $t_{\text{s,free}} \approx 5.9$ and the numerical solutions becomes unstable very shortly after, so the divergence is hard to see in figure 5.40's plot of $\phi(t)$. The harmonic potential model passes through the big bang at $t_{\text{s},\phi^2} \approx 4.2$ and the numerical solution does not becomes unstable until a few coordinate time units later. Thus the divergence in $\phi(t)$ can be seen much clearer for the harmonic potential model in figure 5.40.

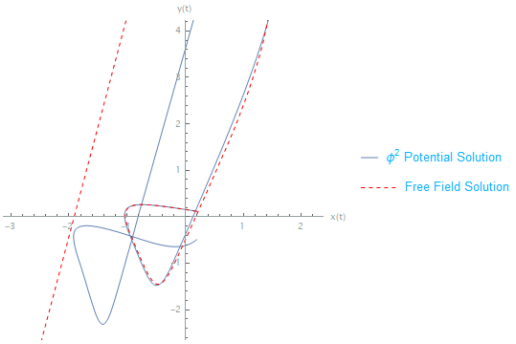

(a) Numerical solution of the anisotropy parameters $(x(t), y(t))$ for the Bianchi IX + free field (red, dashed) and harmonic potential (blue) models. With the anisotropy parameters given by $x = |\tan\beta| \sin\gamma\cos\alpha$, $y = |\tan\beta| \sin\gamma\sin\alpha$.

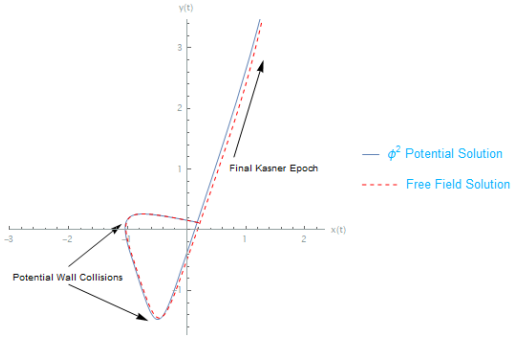

(b) Numerical solution of the anisotropy parameters $(x(t), y(t))$ for the Bianchi IX + free field (red, dashed) and harmonic potential (blue), over subset of the time domain $t \in [0, t_s]$ (t_s being the time at which each model passes through the big bang singularity). With the anisotropy parameters given by $x = |\tan\beta| \sin\gamma\cos\alpha$, $y = |\tan\beta| \sin\gamma\sin\alpha$.

Figure 5.41: Numerical solutions of the anisotropy parameters (x, y) for Bianchi IX + free field and harmonic potential models.

In figure 5.41a we plot the anisotropy parameters for the Bianchi IX + free field and harmonic potential numerical solutions, over the full time domain. Transforming back to the original configuration space variables makes it much easier to see the quiescent behaviour of the Bianchi IX cosmology. In particular, in figure 5.41b we plot the anisotropy parameter numerical solutions on a subset of the time domain, from $t = 0$ until $t = t_s$, where t_s is the time at which the models pass through the big bang singularity in shape space. Here we see explicitly Tuab transitions and the bounces of (x, y) off the shape potential wall before being set off one one final

Kasner epoch, which the cosmology remains on until it reaches the big bang and spatial contact manifold undergoes and inversion of orientation.

5.9 Discussion

The notion of a singularity in General Relativity is a subtle one. Generally speaking, in classical field theories we tend to think of singularities as points at which physical quantities become indeterminate and grow unboundedly. In GR, we solve the Einstein Field Equations for the spacetime manifold and its endowed metric structure. In this sense we can't think of a singularity in general relativity as a point on the manifold where the curvature invariant grows unboundedly, as the Einstein Field Equations need to be solved in an neighbourhood of that point in order to define the spacetime manifold and metric. Therefore the contemporary interpretation of a singularity in GR is that of a boundary to the spacetime manifold on which the curvature invariants become indeterminate [166, 167]. In this work we show how the physical quantities of the cosmological dynamical system and the mathematical structures which generate dynamics (Hamiltonian and contact form) and be smoothly continued across this boundary that stitches two identical, oppositely spatially oriented cosmologies together.

Hawking and Penrose showed that singularities in General Relativity are of a generic nature [128,166,167], the theory breaks itself with relatively lenient requirements for timelike and null geodesic incompleteness. The fact that singularities occur so generically in GR is the main motivating reason to believe that the theory is incomplete. Many hope that the key to resolving singularities in GR lies at the quantum level, and there is a large school of thought that singularities are where one should look to for effects of quantum gravity. Whilst GR is perturbatively non-renormalisable, non-perturbative approaches like loop quantum gravity [168] have been successful in resolving spacetime singularities at the quantum level [134–139]. Within the Loop Quantum Gravity framework, the singularities of FLRW (flat, open

and closed) are investigated in [137,169–171]. In much of the literature, it is assumed that quantum effects are necessary to resolve singularities in GR, particularly the initial cosmological singularity due to the small length scales involved [139, 172]. In the relational dynamics approach however, the Hamiltonian makes no reference to the overall length scale of the universe, which is not a physically observable. The shape dynamical system is subtly different from general relativity in that the fundamental gauge symmetry is that of spatial conformal invariance of the metric, rather than local diffeomorphism invariance [140,141,173] and its configuration space is an equivalence class of conformal 3-geometries, rather than the space of Riemann 3-geometries.

In this section we have shown how one may form a relational, shape space description of flat FLRW, Bianchi I and Quiescent Bianchi IX cosmologies that contains no reference to the scale factor ν, by identifying a dynamical similarity scaling symmetry associated with the scale factor in the Einstein Hilbert action. While the curvature invariant remains divergent at the initial singularity, in this relational description the system remains autonomous and well defined at the initial singularity and in this sense it is resolved at the classical level. In the literature, homogeneous and black-hole interior spacetime have been continued through their GR singularities [144, 174] by forming dimensionless dynamical variables with equations of motion generated by the usual symplectic ADM Hamiltonian. Deterministic continuation through the singularity is established by investigating integrability of the equations of motion. In this work we first form a fully relational contact system by quotienting out the scaling symmetry and forming a symmetry-reduced contact manifold with physically equivalent dynamics to the original symplectic manifold. The equations of motion in the relational system are generated directly from a contact Hamiltonian, which makes no reference to the overall scale of the universe. A gnomonic projection is performed which compactifies the phase space onto shape space, the dynamics of this contact system can thus be viewed as equivalent to the motion of a particle evolving on the surface of a

sphere. Under this gnomonic projection, the initial GR singularity is mapped to the equator. We then investigate the integrability of this system and have shown that there exist unique solutions to the contact Hamiltonian equations of motion in the shape space description which evolve smoothly through the big bang. Moreover, *the mathematical structures that generate time evolution, namely the Hamiltonian and contact form remain well defined.* This is a key development both in terms of defining the solution space, and when considering potential quantisations of the theory. In this manner we are able to define a classical Hamiltonian that is well defined across the big bang, which may be of particular interest in canonical quantisations of GR, where the Hamiltonian and symplectic structure are of fundamental importance. Similar work has also been performed in modified gravity theories, where the initial singularity in Bianchi I solutions is replaced by a bounce. In [175] the authors show that in such models the Kasner plane can be compactified onto a sphere and derive transition rules for the quasi Kasner exponents through non singular bounces.

Shape Dynamics presents a possible new path to a towards a quantum theory of gravity, in particular it offers a solution to the fundamental problem of time in the canonical approach to quantum gravity [176], in which the Hamiltonian constraint when quantised demands a stationary wavefunction. Shape Dynamics manages to decouple dynamical evolution from scale and admits unambiguous evolution in terms of the York time [177, 178].

Alongside showing analytically that cosmological dynamical system on a contact manifold may be continued uniquely through the initial singularity, in this work we have provided complete numerical solutions of the relational equations of motion for each of the cosmologies described above. These numerical solutions show the asymptotic potential-free behaviour near the big bang corresponding to great circles which continue smoothly through the shape space equator. In the case of the Bianchi spacetimes, these great circles represent Kasner solutions. As a result of the analytical treatment, we see that the Mixmaster behaviour of Bianchi IX cosmologies must be resolved to quiescence by the introduction of a suitable matter

field (in this case a scalar field) in order for the equations of motion to satisfy the Picard-Lindelöf theorem near the initial singularity. In other words, Bianchi IX quiescence must be achieved in order for the dynamical system to have a unique, smooth continuation through the big bang. In the numerical solution examples given for quiescent Bianchi IX in section 4.4, we see explicitly the final Kasner epochs and Taub transitions before the system passes through the initial singularity.

There exists in the literature a number of works on the quantisation of classical contact Hamiltonian systems from the geometric perspective. In the work of [179] the authors implement a Becchi, Rouet, Stora, and Tyutin (BRST) quantisation regime of time dependant Hamiltonian systems which are described by a contact phase space, in which general covariance is implemented from the ground up. In this quantisation regime, each point in the phase space is a fibre of an underlying vector bundle, with its own copy of canonical quantum mechanics. The operator-valued connection which allows comparison of quantum wave functions at different phase space points in the nilpotent BRST charge $\hat{Q}^2 = 0$ (up to a factor of $-i\hbar$). The nilpotency imposes a flat connection as a consequence of geometric quantisation. BRST quantisation of contact Hamiltonian systems is also explored in [180]. In [181] quantisation of contact manifolds describing thermodynamics systems, which have odd-dimensional state spaces, is studied. Quantisation is implemented through generalising the canonical commutation relations to Legendre bracket structures. The work of [182] establishes a direct contact analogue to the Kostant-Souriau quantisation of symplectic manifolds [183].

In the canonical quantisation of symplectic Hamiltonian systems, dynamical variables are promoted to operators and the natural Poisson bracket induced by the symplectic structure is replaced with a commutator structure. Within the context of GR, this means promoting dynamical elements of the metric to operators, this includes the volume factor. We present a reformulation of cosmological solutions of GR in which the scale factor has been eliminated and dynamics remain well defined at the initial GR singularity. That the scale factor can be removed at the classical

level, leaving behind a autonomous dynamical system that is well defined at points on the manifold in which GR breaks down suggests that the contact system may be a more appropriate starting point for quantisation. At this point it is an open question as to how one would implement the contact reduction of a covariant field theory exhibiting a dynamical similarity associated with the metric.

Chapter 6

Conclusion

General Relativity, whilst being one of the most successful and cohesive descriptions of nature developed within physics, is still riddled with open questions. In this thesis we address two issues that are considered of fundamental importance to our understanding of the evolution of the universe and the validity of GR, inflation and the nature of spacetime singularities. Over 100 years after Einstein first published his work on General Relativity, overwhelmingly convincing evidence has been collected indicating that the universe is expanding such as the cosmological redshifting of light from far away galaxies, the abundance of light hydrogen and helium isotopes and the rich structure of the CMB. GR provides an excellent framework for understanding and modelling this expansion. Imposing on GR the observation that the universe today seems to be homogeneous and isotropic on large scales leads to a symmetry reduced class of spacetime solutions to Einsteins Field Equations know and the Friedmann–Lemaître–Robertson–Walker solution.

The FLRW solutions are described in terms of the scale function $a(t)$ whose functional form depends on the chosen geometry of spatial hypersurfaces and the matter content in the spacetime. We saw in section 2.2.2 that assuming the matter content of the FLRW universe to be dominated by a perfect fluid leads to expanding solutions, providing an elegant and experimentally verifiable way of explaining Hubbles observation that in all direction appear to be receding away

from us at a velocity proportional to their distance from us. The Cosmic Microwave Background is arguably the cornerstone of contemporary observational cosmology and its intense scrutiny within the context of General Relativity has both provided answers to outstanding questions and opened doors to new ones. In particular, inferred measurements of the cosmological density parameters and observations of the CMB temperatures homogeneity and isotropy as have lead to the formulation of the flatness and horizon problems which were discussed in sections 2.2.3.4 & 2.2.3.5 respectively.

The leading explanation for the horizon and flatness problems is that the early universe experienced a rapid period of exponential expansion called inflation, discussed in section 2.2.4. Whilst the precise mechanism of inflation remains an open question, we discussed in section 2.2.4 that a necessary condition of inflation is the shrinking of the Hubble radius in the early universe. A shrinking Hubble radius can be achieved by means of introducing a matter field into the cosmology. This is an intuitive approach our universe is clearly filled with matter. We have seen that introducing even a simple scalar field can produce fruitful results. In section 2.2.4.1 we discussed the slow-roll regime in which a scalar field whose energy is dominated its potential is introduced generating an inflationary period. For the approximations of the slow roll regime to be valid, conditions must be placed on the shape of the field potential, these conditions essentially ensure that it is flat enough for potential dominated inflation to persist long enough to produce a sufficient "amount" of inflation, as measured by the number of e-folds.

The success of slow roll inflation is not without its problems, particularly with regard to the large number of choices one has for the field potential $V(\phi)$ that can satisfy the conditions placed on the shape of the potential. Reference [92] gives a thorough and detailed account of many of field-driven inflationary models that have been or are currently still under consideration as candidates and includes a detailed analysis of their slow roll regimes and comparison to the results from the Planck collaboration [184]. Planck observations of the CMB have been able to

place restrictions on two important cosmological observables, the spectral index n_s and ratio of tensor to scalar perturbations r, which were discussed in section 2.2.4.1. While the (n_s, r) parameter is constrained, it is not constrained enough to determine a single candidate inflationary model and there are a great many of them that are consistent with current constraints given an appropriate choice of the any free parameters in the model. In this thesis we explored work relating to a particular candidate model, Quartic Hilltop Inflation in section 3. Quartic Hilltop inflation had initially been discounted based on the fact that analytical computations of its predicted relationship spectral index at an amount of e-folds sufficient for inflation to solve the horizon and flatness problem was not consistent with observations. In particular the predicted spectral index was too small for $50 - 60$ e-folds of inflation. However this early analytical work was based on a few key assumptions about the order of magnitude of the fields vacuum expectation value, in that it was assumed to be sub-Planckian. Later numerical analysis of Quartic Hilltop performed in [92] revived interest in the model, showing that its predicted relationship between the spectral index and tensor-scalar ratio can be consistent with current observations if the assumptions about its vacuum expectation value are relaxed, allowing it to potentially be super-Planckian. A later analytical investigation of the Quartic Hilltop inflation with these assumptions was performed in [5] which shed light on the numerical treatment which is somewhat of a "black box". However the Quartic Hilltop potential as an inflationary potential suffers from a major theoretical drawback which is further amplified by dropping the assumptions on its VEV. The Quartic Hilltop model belongs to a wider class of Hilltop inflationary models whose potentials are of the form

$$V(\phi) = \Lambda \left[1 - \lambda \left(\frac{\phi}{m_{pl}} \right)^p + ... \right] \tag{6.1}$$

where "..." denotes the higher order terms which stabilise the vacuum. Typically in treatments of the Quartic Hilltop model (for which $p = 4$), the stabilising terms are assumed to be negligible and are ignored as inflation is presumed to take place far

from the VEV. This essentially means that precisely how the model exits inflation is not being considered. The exclusion of higher order terms leaves the potential with no local minimum making it unsuitable for describing post inflationary dynamics as field would be able to access an arbitrarily low energy, leading to a universe that collapses in on itself. Allowing the VEV to be super Planckian means that one now has a much harder time justifying ignoring the higher order stabilising terms as they start to become non-negligible. Furthermore, without the inclusion of such terms, the Quartic Hilltop potential would not be able to produce reheating dynamics. The reheating dynamics of a given inflationary model form an important part of connecting the model with current observations. Generally speaking, in the slow roll analysis one will derive expressions for the spectral index $n_s(N)$ and tensor-scalar ratio $r(N)$ as functions of the the number of e-folds of inflation and therefore find a bound on N in order for (n_s, r) to be consistent with the Planck data. However this is only half the story, in section 3.3 we discussed how the number of e-folds of reheating and hence the temperature of the universe at the end of reheating are dependant on the number of e-folds of inflation and the value of the potential at the end of inflation for a given model. So whilst we may be able to find n_s and r that are consistent with Planck data, it is not guaranteed that the corresponding reheating temperature and e-folds will be consistent with what we know about the thermal history of the universe. To fully consider a candidate inflationary model we must look at both its inflationary and reheating predictions and ensure that agreements with data can be found in both the (n_s, r) pair and the reheating temperature.

In section 3, based on a paper written by the Author and David Sloan [1], we argue that the inflationary predictions of the Quartic Hilltop model cannot be fully contextualised without including such stabilising terms for the reasons outlined above. We work with a previously suggested "regularisation" of the Quartic Hilltop model which involves simply squaring the potential [94] to form the Quartic Hilltop Squared model. We carry out an analytical investigation of the QHS model similar to that of the QH model in [5], deriving expressions for the spectral index and tensor-

scalar ratio in terms of the number of e-folds of inflation. We also carry out numerical simulations to solve the equations of motion of the inflaton field over a range of parameter values. We complete the analysis by computing reheating temperatures and e-folds. In this work we find that even without including the reheating analysis, the inclusion of stabilising terms in the potential significantly alters the predictions of the spectral index and tensor-scalar index, showing that how the model exits inflation has a noticeable effect on its prediction of cosmological parameters. When the reheating analysis is included, we derive bounds on the number of e-folds of inflation that are allowed within the QHS model in order for it to be consistent with Planck 2018 data, and further constrict the Planck-allowed region of parameter space that QHS falls into.

In section 4 based on the paper [2] written by the Author and David Sloan, the consideration of regularising inflationary potentials is extended to more candidate single field inflation models which also suffer from being unbounded from below. In particular, we consider higher polynomial correction terms added to the Quartic Hilltop model, forming a class of QH_p models with potentials of the form

$$V(\phi) = V_0 \left[1 - \lambda \left(\frac{\phi}{m_{pl}} \right)^4 + \alpha_p \left(\frac{\phi}{m_{pl}} \right)^p \right], \quad p > 4 \tag{6.2}$$

where we choose the coefficient α_p to be fine tuned such that the value of the potential at the fields vacuum expectation value is zero. We consider also Radiatively Corrected Higgs inflation with inverse polynomial correction terms and Exponential SUSY inflation corrected by squaring. In all cases we perform the same numerical analysis that was carried out in [1] and derive bounds on the number of e-folds of inflation that are reheating-consistent and hence bound the allowed region of (n_s, r) parameter space that each corrected model falls into.

In section 5 we develop a framework for deterministically evolving cosmological dynamical systems through spacetime singularities in the context of Bianchi IX, I, & FLRW solutions to General Relativity. We appeal to the relationalist

viewpoint developed by Barbour and Bertotti [185] and implement this within the context of contact Hamiltonain systems. The work builds off recent progress made in developing the concept of "Dynamical Similarities" and previous results by Koslowski, Mercatti & Sloan in [144] which a set of dimensionless variables can be found in (symplectic) Bianchi IX cosmologies which remain well defined through the Big Bang.

Homogeneous spacetime solutions to GR contain as a key dynamical variable a notion of absolute scale through the volume/scale factor. However no cosmological observer has access to any notion of such absolute scale. Measurements must be taken with respect to rods and clocks defined within the dynamical system itself. Indeed, physical measurements take by observers are in fact dimensionless ratios, invariant under a rescaling of the dynamical variables. If one accepts the relationlaist point of view, it is the dynamics of these dimensionless ratios that we care about, not the redundant reference scale. Barbour and Bertotti describe this through the relative "shape" configurations formed by the system. Shape dynamics is the contemporary implementation of Barbour and Bertotti's original ideas about relationalism, in the context of classical gravitational systems. Shape Dynamics, like General Relativity is a gauge theory of the metric. In General Relativity, we have an equivalence class of metrics under diffeomorphisms. In Shape Dynamics, relationalism is implemented by considering metric solutions to the equations of motion to be indistinguishable under a local rescaling, and so we have a equivalence class of metrics under Weyl transformations $g'_{\mu\nu}(x) = e^{2\phi(x)} g_{\mu\nu}(x)$. Shape Dynamics and General Relativity are distinct physical theories that live on the same phase space (γ_{ij}, ϕ^{ij}), but they admit gauge fixings in which they coincide [140].

The theory of dynamical similarities [143] formalises this notion of scale invariance within the context of classical Hamiltonian and Lagrangian systems. A key result in the study of Dynamical Similarites in symplectic Hamiltonian/Lagrangian systems is that when they exist, after quotienting out the redundancy represented by the symmetry, we are left an autonomous subsystem defined on a contact manifold.

In section 5.1 we outlined results by Sloan [147] showing that the equations of motion of this contact subsystem coincide with the symplectic system, thus they describe the same physics for the dynamical variables that remain in the contact subsystem.

The framework developed in section 5 synthesises the concepts of relationalism and dynamical similarities in the context of the ADM formalism of General Relativity. We first show that there exists a scaling symmetry of the Einstein-Hilbert action associated with the volume factor. By quotienting this dynamical similarity out of the phase space, we are left with a symmetry reduced model defined on a contact manifold. The description in terms of contact mechanics has the added benefit of being well suited to describing frictional, dissipative systems. It is well known that in expanding cosmologies such as the FLRW solution, the Hubble parameter $H(t)$ has the effect of adding friction to the evolution of matter fields present in the cosmology. In the contact system, the dynamical variables are decoupled from scale, the information left over from the volume/scale factor is present in the global coordinate on the contact manifold h. It is the contact Hamiltonians dependency on this coordinate that is precisely responsible for violating conservation of the Hamiltonian along its flow.

The contact system that remains after removing the redundancy of the scaling symmetry is defined entirely in terms of relational, dimensionless variables. This is a key distinction between the work in this thesis and the result obtained in [144]. In the latter, an appropriate set of dimensionless variables are found in the symplectic ADM Hamiltonain description which remain well defined through the Big Bang singularity. In this work, we first define a contact Hamiltonian system, whose dynamical variables are all relational. The next step in this work is to project the dynamical variables to an appropriate set of coordinates for describing the dynamical system at the initial singularity. Here we perform a gnomonic projection of the anisotropy parameters onto shape space, and describe the dynamical system in terms of the shape variables (α, β). The shape space coordinates are not chosen arbitrarily, we saw explicitly in section 5.6.2 that when solving the equations of

motion for the contact Bianchi I system, relational quantities like $x(t)/y(t) \sim \sin\alpha$ converge to a finite limit at the Big Bang. Under a rescaling of the dynamical variables, angles between tangent vectors will always be conserved so we expect these variables to appropriately encode the dynamics of the system when we make a compatification of the contact manifold onto S^n. Under the gnomonic projection, the Big Bang singularity is mapped to the $\beta = \pi/2$ equator of shape space. We show that there exist unique solutions to Hamiltons equations of motion that pass smoothly through the Big Bang by showing that the Picard-Lindelöf theorem is satisfied in the cases of FLRW, Bianchi I and Quiescent Bianchi IX cosmologies. The Hamiltonian and contact form remain well defined, thus one is able to have a well defined Hamiltonian flow at the Big Bang and be sure that the evolution of the dynamical system is deterministic. Existence and uniqueness of solutions fails in the case of vacuum Bianchi IX, for essentially the same reasons as quiescence fails in the conventional symplectic analysis of Bianchi IX. Without introducing a matter field, it is not possible to suppress exponential growth of the shape potential term in the Hamiltonian resulting in Mixmaster behaviour. The equations of motion for Kasner universes are exactly solvable and correspond to great circles on S^2. This is to be expected since Kasner solutions in the configuration space variables simply look like free particle motion in a straight line, gnomonic projections maps straight lines in the plane to great circles on the sphere.

In section 5.8 we perform numerical simulations, solving the equations of motion for a variety of FLRW, Bianchi I & Quiescent Bianchi IX models and show explicitly unique solutions passing through the Big Bang. In this section we also make contact with the work performed on Quartic Hilltop Inflation. We present numerical solutions to the contact Hamiltonian equations of motion for FLRW + a scalar field with both QH and QHS potentials. Without a regularised potential and without a way to describe near-singularity behaviour of cosmological dynamical systems, potentials like Quartic Hilltop are severally flawed in their cosmological predictions. We have already described how the post-inflationary behaviour of such potentials

needs to be accounted for as it has a significant effect on observable, the contact dynamics framework now lets us look at the pre-inflationary classical behaviour of the potential. In symplectic GR, such early-time behaviour would have been inaccessible as the Hamiltonian flow becomes ill-defined at the singularity. In section 5.8 we also transform back to the familiar configuration space dynamical variables and see explicitly the Taub transitions and final Kasner epoch in Quiescent Bianchi IX solutions.

The main success of the contact dynamics framework developed in section 5 is that we are able to define a dynamical system that resolves the singularity completely classically. Previous approaches to resolving the initial singularity have relied on invoking a quantisation of the gravitational field such as in the approaches of Loop Quantum Cosmology and String Theory. Contact manifolds have been readily used in the literature to study both classical and quantum thermodynamics due to their natural description of dissipative systems. From a speculative view, having a well defined contact Hamiltonian and contact form at the singularity could have implications in the study of statistical thermodynamics. The well defined Hamiltonian and volume measure should allow for the computation of a partition function and hence thermodynamic quantities at the Big Bang. That the mathematical structures determining evolution of the dynamical system remain well defined at the singularity, could open the door to a new approach to quantum gravity involving a quantisation of the contact dynamical system, which we have shown is already singularity free for the particular cosmologies studied. It remains an open question as to whether, and under what conditions this is a feature of generic spacetimes. To answer such questions and to set down the path of quantisation, one would need to implement the formalism of dynamical singularities into a contact field theory. Research on this procedure has only recently begun in [186].

Appendix A

A.1 QH$_p$ Correction figures

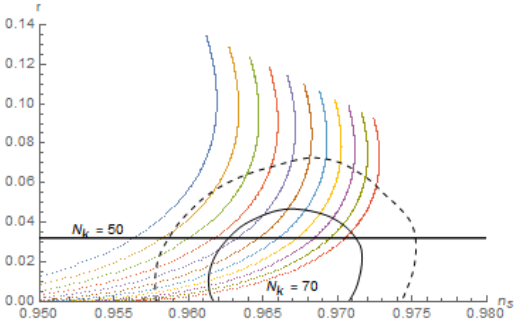

(a) Numerical solutions of the tensor-scalar ratio r and spectral index n_s for the QH$_6$ model over the $50 \leq N_k \leq 70$.

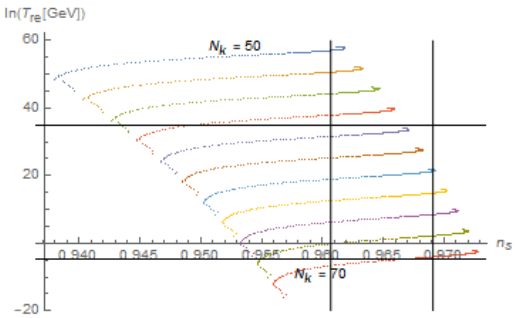

(b) The (log) reheating temperature of the QH$_6$ model against the spectral index n_s over $50 \leq N_k \leq 70$.

Figure A.1: Numerical solutions of (n_s, r) and reheating temperature for the QH_6 model.

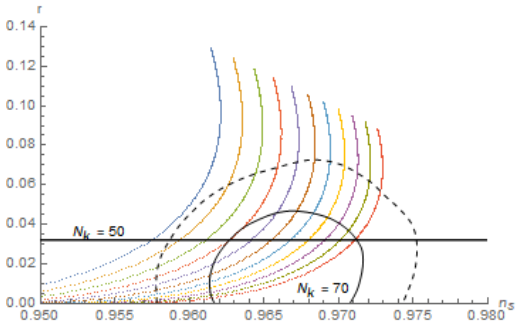

(a) Numerical solutions of the tensor-scalar ratio r and spectral index n_s for the QH_7 model over the $50 \leq N_k \leq 70$.

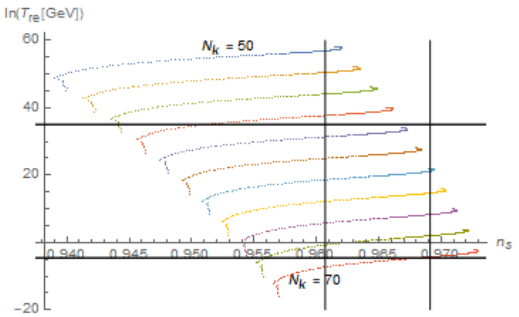

(b) The (log) reheating temperature of the QH_7 model against the spectral index n_s over $50 \leq N_k \leq 70$.

Figure A.2: Numerical solutions of (n_s, r) and reheating temperature for the QH_7 model.

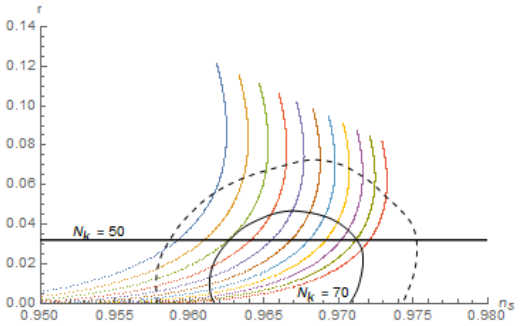

(a) Numerical solutions of the tensor-scalar ratio r and spectral index n_s for the QH_9 model over the $50 \leq N_k \leq 70$.

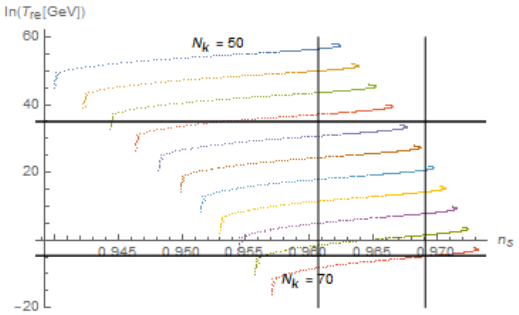

(b) The (log) reheating temperature of the QH_9 model against the spectral index n_s over $50 \leq N_k \leq 70$.

Figure A.3: Numerical solutions of (n_s, r) and reheating temperature for the QH_9 model.

A.2 RCHI$_p$ Correction Figures

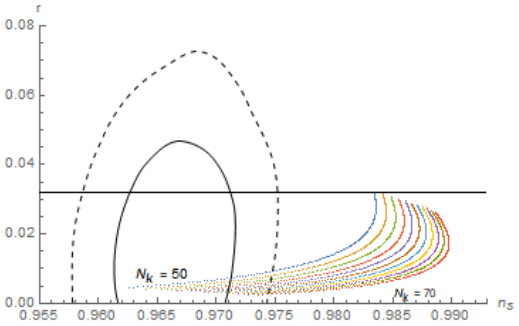

(a) Numerical solutions of the tensor-scalar ratio r and spectral index n_s for the RCHI$_2$ model over the $50 \leq N_k \leq 70$.

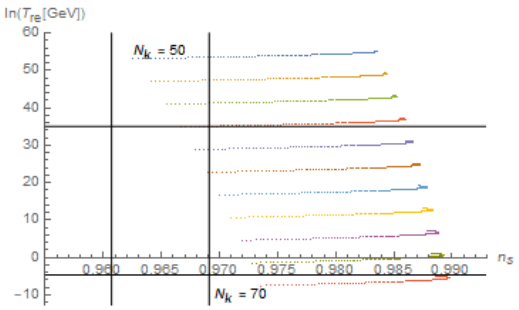

(b) The (log) reheating temperature of the RCHI$_2$ model against the spectral index n_s over $50 \leq N_k \leq 70$.

Figure A.4: Numerical solutions of (n_s, r) and the reheating temperature of the $RCHI_2$ model.

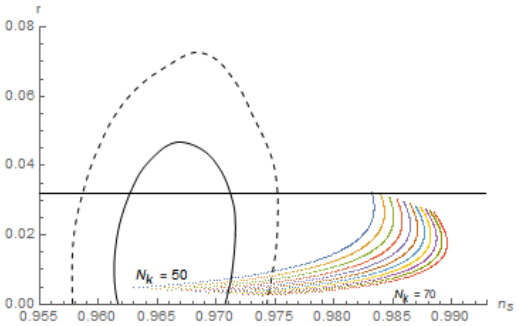

(a) Numerical solutions of the tensor-scalar ratio r and spectral index n_s for the RCHI$_3$ model over the $50 \leq N_k \leq 70$.

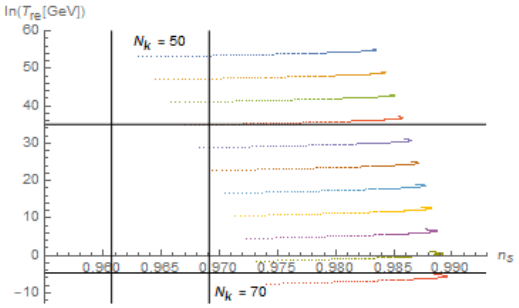

(b) The (log) reheating temperature of the RCHI$_3$ model against the spectral index n_s over $50 \leq N_k \leq 70$.

Figure A.5: Numerical solutions of (n_s, r) and the reheating temperature of the $RCHI_3$ model.

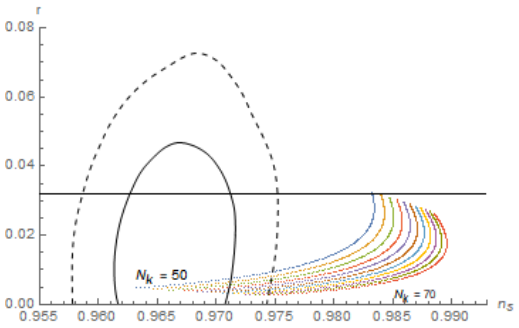

(a) Numerical solutions of the tensor-scalar ratio r and spectral index n_s for the RCHI$_4$ model over the $50 \leq N_k \leq 70$.

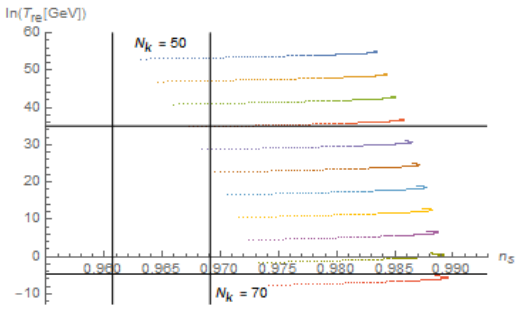

(b) The (log) reheating temperature of the RCHI$_4$ model against the spectral index n_s over $50 \leq N_k \leq 70$.

Figure A.6: Numerical solutions of (n_s, r) and the reheating temperature of the $RCHI_4$ model.

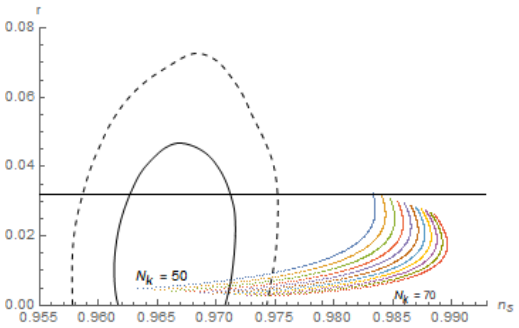

(a) Numerical solutions of the tensor-scalar ratio r and spectral index n_s for the RCHI$_5$ model over the $50 \leq N_k \leq 70$.

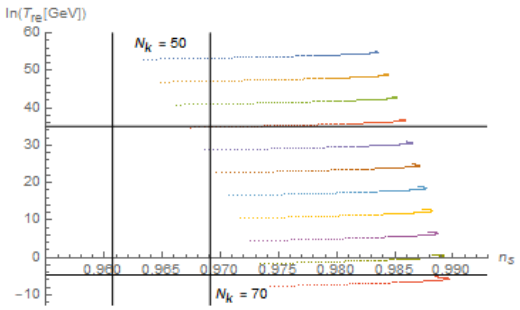

(b) The (log) reheating temperature of the RCHI$_5$ model against the spectral index n_s over $50 \leq N_k \leq 70$.

Figure A.7: Numerical solutions of (n_s, r) and the reheating temperature of the $RCHI_5$ model.

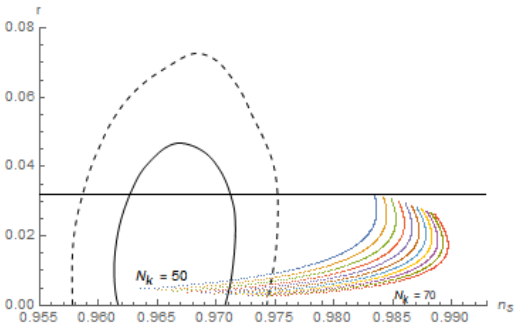

(a) Numerical solutions of the tensor-scalar ratio r and spectral index n_s for the RCHI$_6$ model over the $50 \leq N_k \leq 70$.

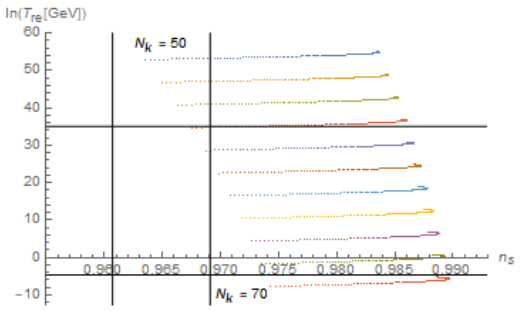

(b) The (log) reheating temperature of the RCHI$_6$ model against the spectral index n_s over $50 \leq N_k \leq 70$.

Figure A.8: Numerical solutions of (n_s, r) and the reheating temperature of the $RCHI_7$ model.

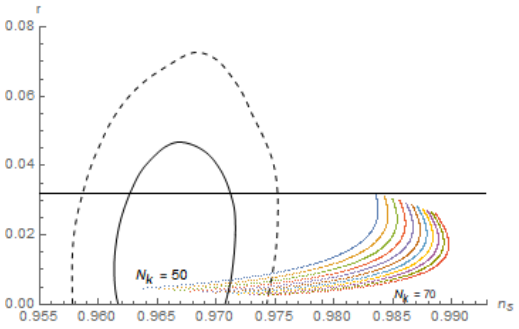

(a) Numerical solutions of the tensor-scalar ratio r and spectral index n_s for the RCHI$_7$ model over the $50 \leq N_k \leq 70$.

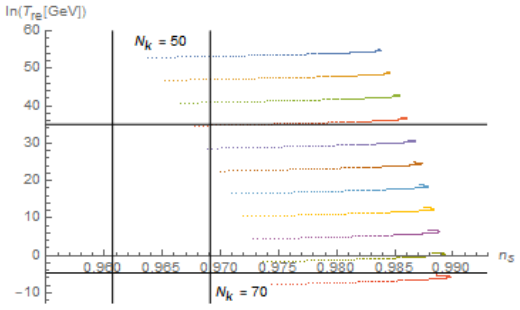

(b) The (log) reheating temperature of the RCHI$_7$ model against the spectral index n_s over $50 \leq N_k \leq 70$.

Figure A.9

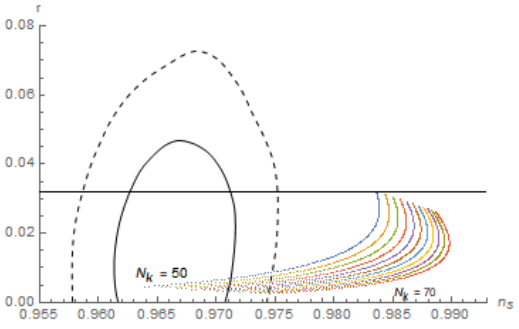

(a) Numerical solutions of the tensor-scalar ratio r and spectral index n_s for the RCHI$_8$ model over the $50 \leq N_k \leq 70$.

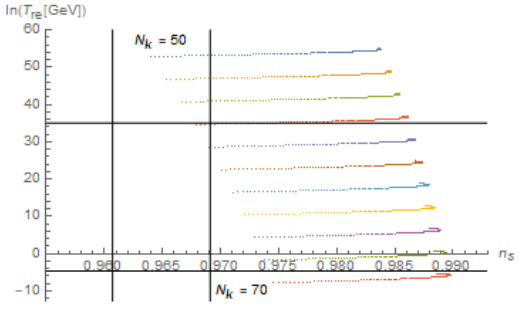

(b) The (log) reheating temperature of the RCHI$_8$ model against the spectral index n_s over $50 \leq N_k \leq 70$.

Figure A.10: Numerical solutions of (n_s, r) and the reheating temperature of the $RCHI_8$ model.

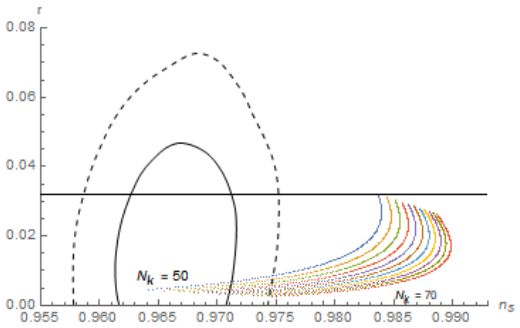

(a) Numerical solutions of the tensor-scalar ratio r and spectral index n_s for the RCHI$_9$ model over the $50 \leq N_k \leq 70$.

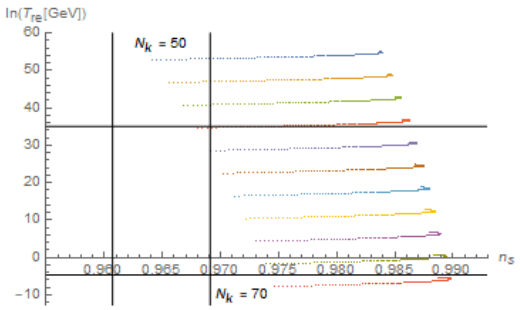

(b) The (log) reheating temperature of the RCHI$_9$ model against the spectral index n_s over $50 \leq N_k \leq 70$.

Figure A.11: Numerical solutions of (n_s, r) and the reheating temperature of the $RCHI_9$ model.

Appendix B

B.1 Bianchi Numerical Solution Hamiltonians

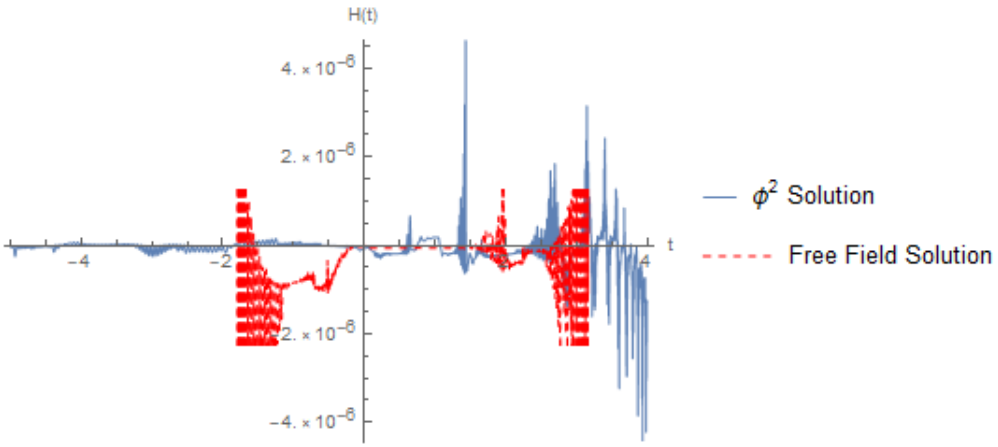

Figure B.1: Numerical solution Hamiltonian for the Bianchi I + free field (red, dashed) and harmonic potential (blue) models. The discretised equations of motion for the free field model become numerically faster than the harmonic potential model thus the numerical solution is valid over a smaller time domain.

In figure B.2a we plot the numerical solution Hamiltonians for Bianchi IX, the numerical solution Hamiltonians are larger in magnitude than the previous cases we have looked at in this paper, however the Hamiltonian itself is still much smaller than the individual terms that it is comprised of. For example consider the first term in the Hamiltonian 5.239

$$\mathcal{H}_1 = \frac{1}{2} p_\beta^2 \cos^2 \beta \tag{B.1}$$

The relative size of $\mathcal{H}/\mathcal{H}_1$ is typically small except where $\mathcal{H}_1 \to 0$, as demonstrated in figure B.2b

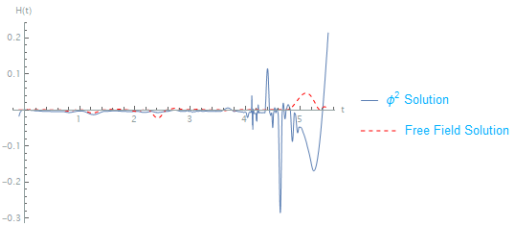

(a) Bianchi IX numerical solution Hamiltonian for the free field (red, dashed) and harmonic potential models.

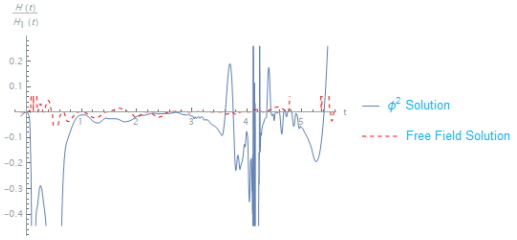

(b) Plot of the ratio $\mathcal{H}/\mathcal{H}_1$ for the Bianchi IX numerical solution Hamiltonians.

Figure B.2: Numerical solutions of the Bianchi IX + matter Hamiltonians and comparison of the Hamiltonian to its first term.

B.2 Gnomonic Projection Example

Consider the motion of a free-particle in two dimensions, in the standard symplectic mechanics context. The Lagrangian for such a system is simply

$$\mathcal{L} = \frac{1}{2}\left(\dot{x}^2 + \dot{y}^2\right) \tag{B.2}$$

and the solutions, which are straight lines on the $\mathbb{R}^2$ plane are of course obtained trivially. The solutions are characterised by two constant momenta (p_x, p_y) each associated with one of the coordinates on the plane

$$x(t) = x_0 + p_x t, \quad y(t) = y_0 + p_y t \tag{B.3}$$

In this appendix we show explicitly how, after making a gnomonic projection to shape space, the solutions of the equations of motion are great circles on S^2. Recall that the gnomonic projection is a compactification onto the surface of a sphere, in this case a 2-sphere. This projection takes a unit sphere tangent to the plane at the origin and draws a straight line from a point $P(x, y)$ on the plane to the

centre of the tangent sphere. $P(x, y)$ is then identified with the coordinates on the 2-sphere (α, β) where the line intersects the sphere. The shape space coordinates are the angle subtended from the pole β and the azimuthal angle α. Explicitly the projection map is written as

$$\begin{pmatrix} x \\ y \end{pmatrix} = |\tan\beta| \begin{pmatrix} \cos\alpha \\ \sin\alpha \end{pmatrix} \tag{B.4}$$

In these shape space coordinates the Lagrangian in

$$\mathcal{L} = \frac{1}{2}\left(\dot{\beta}^2 \sec^4\beta + \dot{\alpha}^2 \tan^2\beta\right) \tag{B.5}$$

From which one may find the canonical momenta

$$p_\alpha = \dot{\alpha}\tan^2\beta, \quad p_\beta = \dot{\beta}\sec^4\beta \tag{B.6}$$

and obtain the Hamiltonian through a Legendre transformation

$$\mathcal{H} = \frac{1}{2}p_\beta^2 \cos^4\beta + \frac{p_\alpha^2}{2\tan^2\beta} \tag{B.7}$$

One may now simply use the symplectic Hamiltons equations of motion [16]

$$\dot{q}_i = \frac{\partial\mathcal{H}}{\partial p^i}, \quad \dot{p}^i = -\frac{\partial\mathcal{H}}{\partial q_i} \tag{B.8}$$

to obtain

$$\dot{\alpha} = \frac{p_\alpha}{\tan^2\beta}, \quad \dot{p}_\alpha = 0 \tag{B.9}$$

$$\dot{\beta} = p_\beta \cos^4\beta, \quad \dot{p}_\beta = 2p_\beta^2 \cos^3\beta\sin\beta + p_\alpha^2 \frac{\cos\beta}{\sin^3\beta} \tag{B.10}$$

In symplectic mechanics, the Hamiltonian is a conserved, constant quantity and

therefore one may determine that

$$\frac{d\alpha}{d\beta} = \frac{\dot{\alpha}}{\dot{\beta}} = \frac{p_\alpha}{\sin^2\beta\sqrt{2\mathcal{H} - p_\alpha^2\cot^2\beta}} \tag{B.11}$$

Equation B.11 has the solution

$$\cos(\alpha - \alpha_0) = \frac{p_\alpha}{\sqrt{2\mathcal{H}}\tan\beta} \tag{B.12}$$

which is the equation of a great circle on the 2-sphere, whose orientation relative to the $\mathbb{R}^2$ is controlled by $p_\alpha/\sqrt{2\mathcal{H}}$.

References

[1] J. Hoffmann and D. Sloan, "Squared quartic hilltop inflation," *Phys. Rev. D*, vol. 104, no. 12, p. 123542, 2021.

[2] J. Hoffmann and D. Sloan, "Regularization of single field inflation models," *Phys. Rev. D*, vol. 107, no. 2, p. 023502, 2023.

[3] J. Hoffmann and D. Sloan, "Continuation of Bianchi Spacetimes Through The Big Bang," 5 2024.

[4] N. Aghanim, Y. Akrami, M. Ashdown, J. Aumont, C. Baccigalupi, M. Ballardini, A. J. Banday, R. B. Barreiro, N. Bartolo, S. Basak, R. Battye, K. Benabed, J.-P. Bernard, M. Bersanelli, P. Bielewicz, J. J. Bock, J. R. Bond, J. Borrill, F. R. Bouchet, F. Boulanger, M. Bucher, C. Burigana, R. C. Butler, E. Calabrese, J.-F. Cardoso, J. Carron, A. Challinor, H. C. Chiang, J. Chluba, L. P. L. Colombo, C. Combet, D. Contreras, B. P. Crill, F. Cuttaia, P. de Bernardis, G. de Zotti, J. Delabrouille, J.-M. Delouis, E. Di Valentino, J. M. Diego, O. Doré, M. Douspis, A. Ducout, X. Dupac, S. Dusini, G. Efstathiou, F. Elsner, T. A. Enßlin, H. K. Eriksen, Y. Fantaye, M. Farhang, J. Fergusson, R. Fernandez-Cobos, F. Finelli, F. Forastieri, M. Frailis, A. A. Fraisse, E. Franceschi, A. Frolov, S. Galeotta, S. Galli, K. Ganga, R. T. Génova-Santos, M. Gerbino, T. Ghosh, J. González-Nuevo, K. M. Górski, S. Gratton, A. Gruppuso, J. E. Gudmundsson, J. Hamann, W. Handley, F. K. Hansen, D. Herranz, S. R. Hildebrandt, E. Hivon, Z. Huang, A. H. Jaffe, W. C. Jones, A. Karakci, E. Keihänen, R. Keskitalo,

K. Kiiveri, J. Kim, T. S. Kisner, L. Knox, N. Krachmalnicoff, M. Kunz, H. Kurki-Suonio, G. Lagache, J.-M. Lamarre, A. Lasenby, M. Lattanzi, C. R. Lawrence, M. Le Jeune, P. Lemos, J. Lesgourgues, F. Levrier, A. Lewis, M. Liguori, P. B. Lilje, M. Lilley, V. Lindholm, M. López-Caniego, P. M. Lubin, Y.-Z. Ma, J. F. Macías-Pérez, G. Maggio, D. Maino, N. Mandolesi, A. Mangilli, A. Marcos-Caballero, M. Maris, P. G. Martin, M. Martinelli, E. Martínez-González, S. Matarrese, N. Mauri, J. D. McEwen, P. R. Meinhold, A. Melchiorri, A. Mennella, M. Migliaccio, M. Millea, S. Mitra, M.-A. Miville-Deschênes, D. Molinari, L. Montier, G. Morgante, A. Moss, P. Natoli, H. U. Nørgaard-Nielsen, L. Pagano, D. Paoletti, B. Partridge, G. Patanchon, H. V. Peiris, F. Perrotta, V. Pettorino, F. Piacentini, L. Polastri, G. Polenta, J.-L. Puget, J. P. Rachen, M. Reinecke, M. Remazeilles, A. Renzi, G. Rocha, C. Rosset, G. Roudier, J. A. Rubiño-Martín, B. Ruiz-Granados, L. Salvati, M. Sandri, M. Savelainen, D. Scott, E. P. S. Shellard, C. Sirignano, G. Sirri, L. D. Spencer, R. Sunyaev, A.-S. Suur-Uski, J. A. Tauber, D. Tavagnacco, M. Tenti, L. Toffolatti, M. Tomasi, T. Trombetti, L. Valenziano, J. Valiviita, B. Van Tent, L. Vibert, P. Vielva, F. Villa, N. Vittorio, B. D. Wandelt, I. K. Wehus, M. White, S. D. M. White, A. Zacchei, and A. Zonca, "Planck2018 results: Vi. cosmological parameters," *Astronomy amp; Astrophysics*, vol. 641, p. A6, Sept. 2020.

[5] K. Dimopoulos, "An analytic treatment of quartic hilltop inflation," *Phys. Lett. B*, vol. 809, p. 135688, 2020.

[6] S. Krantz and H. Parks, "The implicit function theorem : History, theory, and applications / s.g. krantz, h.r. parks.," 01 2003.

[7] P. Mann, *Lagrangian and Hamiltonian Dynamics*. Oxford University Press, 06 2018.

[8] E. Noether, "Invariante variationsprobleme," *Nachrichten von der Gesellschaft der Wissenschaften zu Göttingen, Mathematisch-Physikalische Klasse*, vol. 1918, pp. 235–257, 1918.

[9] J. José and E. Saletan, *Classical Dynamics: A Contemporary Approach*. Cambridge University Press, 1998.

[10] L. Hand and J. Finch, *Analytical Mechanics*. Cambridge University Press, 1998.

[11] J. Baez and J. P. Muniain, *Gauge fields, knots and gravity*. 1995.

[12] K. Vogtmann, A. Weinstein, and V. Arnol'd, *Mathematical Methods of Classical Mechanics*. Graduate Texts in Mathematics, Springer New York, 1997.

[13] A. Bravetti, H. Cruz, and D. Tapias, "Contact hamiltonian mechanics," *Annals of Physics*, vol. 376, p. 17–39, Jan. 2017.

[14] A. Weinstein, "Symplectic geometry," *Bulletin (New Series) of the American Mathematical Society*, vol. 5, no. 1, pp. 1 – 13, 1981.

[15] X. Gràcia, "Fibre derivatives: Some applications to singular lagrangians," *Reports on Mathematical Physics*, vol. 45, no. 1, pp. 67–84, 2000.

[16] M. de León and M. Lainz, "A review on contact hamiltonian and lagrangian systems," *arXiv preprint arXiv:2011.05579*, 2020.

[17] H. Geiges, "Contact geometry," *arXiv preprint math/0307242*, 2003.

[18] H. Geiges, *An Introduction to Contact Topology*. Cambridge Studies in Advanced Mathematics, Cambridge University Press, 2008.

[19] R. Mrugala, J. D. Nulton, J. Christian Schön, and P. Salamon, "Contact structure in thermodynamic theory," *Reports on Mathematical Physics*, vol. 29, no. 1, pp. 109–121, 1991.

[20] G. Hernández and E. A. Lacomba, "Contact riemannian geometry and thermodynamics," *Differential Geometry and its Applications*, vol. 8, no. 3, pp. 205–216, 1998.

[21] A. Ghosh and C. Bhamidipati, "Contact geometry and thermodynamics of black holes in ads spacetimes," *Physical Review D*, vol. 100, no. 12, p. 126020, 2019.

[22] A. A. Simoes, M. de León, M. L. Valcázar, and D. M. de Diego, "Contact geometry for simple thermodynamical systems with friction," *Proceedings of the Royal Society A: Mathematical, Physical and Engineering Sciences*, vol. 476, no. 2241, p. 20200244, 2020.

[23] S. G. Rajeev, "A Hamilton Jacobi formalism for thermodynamics," *Annals of Physics*, vol. 323, pp. 2265–2285, Sept. 2008.

[24] "Liouville's theorem and the canonical measure for nonconservative systems from contact geometry," *Journal of Physics A: Mathematical and Theoretical*, vol. 48, no. 24, p. 245001, 2015.

[25] M. De Leon and M. Lainz Valcázar, "Singular lagrangians and precontact hamiltonian systems," *International Journal of Geometric Methods in Modern Physics*, vol. 16, no. 10, p. 1950158, 2019.

[26] D. Sloan, "New action for cosmology," *Physical Review D*, vol. 103, no. 4, p. 043524, 2021.

[27] R. M. Wald, *General Relativity*. Chicago, USA: Chicago Univ. Pr., 1984.

[28] C. W. Misner, K. S. Thorne, and J. A. Wheeler, *Gravitation*. San Francisco: W. H. Freeman, 1973.

[29] S. W. Hawking and G. F. R. Ellis, *The Large Scale Structure of Space-Time*. Cambridge Monographs on Mathematical Physics, Cambridge University Press, 2 2023.

[30] S. M. Carroll, *Spacetime and Geometry: An Introduction to General Relativity*. Cambridge University Press, 7 2019.

[31] R. Bishop and R. Crittenden, "Geometry of manifolds," 1964.

[32] V. P. Frolov and A. Zelnikov, *Introduction to black hole physics*. OUP Oxford, 2011.

[33] B. C. Hall, "An Elementary Introduction to Groups and Representations," *arXiv e-prints*, pp. math–ph/0005032, May 2000.

[34] J. W. York, "Role of conformal three-geometry in the dynamics of gravitation," *Phys. Rev. Lett.*, vol. 28, pp. 1082–1085, Apr 1972.

[35] G. W. Gibbons and S. W. Hawking, "Action integrals and partition functions in quantum gravity," *Phys. Rev. D*, vol. 15, pp. 2752–2756, May 1977.

[36] M. Bojowald, *Canonical Gravity and Applications: Cosmology, Black Holes, and Quantum Gravity*. Cambridge University Press, 2010.

[37] L. Modesto and C. Rovelli, "Particle scattering in loop quantum gravity," *Phys. Rev. Lett.*, vol. 95, p. 191301, 2005.

[38] P. Frisoni, "Introduction to Loop Quantum Gravity: Rovelli's lectures on LQG," *arXiv e-prints*, p. arXiv:2305.12215, May 2023.

[39] P. K. Townsend, "Black Holes," *arXiv e-prints*, pp. gr–qc/9707012, July 1997.

[40] M. E. Peskin and D. V. Schroeder, *An Introduction to quantum field theory*. Reading, USA: Addison-Wesley, 1995.

[41] M. D. Schwartz, *Quantum Field Theory and the Standard Model*. Cambridge University Press, 3 2014.

[42] D. J. Fixsen, "The temperature of the cosmic microwave background," *The Astrophysical Journal*, vol. 707, p. 916–920, Nov. 2009.

[43] A. Challinor, "Cmb anisotropy science: a review," *Proceedings of the International Astronomical Union*, vol. 8, p. 42–52, Aug. 2012.

[44] B. E. Corey and D. T. Wilkinson, "A Measurement of the Cosmic Microwave Background Anisotropy at 19 GHz," in *Bulletin of the American Astronomical Society*, vol. 8, p. 351, Mar. 1976.

[45] G. F. Smoot, M. V. Gorenstein, and R. A. Muller, "Detection of Anisotropy in the Cosmic Blackbody Radiation," , vol. 39, pp. 898–901, Oct. 1977.

[46] N. J. Secrest, S. v. Hausegger, M. Rameez, R. Mohayaee, S. Sarkar, and J. Colin, "A test of the cosmological principle with quasars," *The Astrophysical Journal Letters*, vol. 908, p. L51, Feb. 2021.

[47] C. O'Raifeartaigh, M. O'Keeffe, W. Nahm, and S. Mitton, "Einstein's 1917 static model of the universe: a centennial review," *The European Physical Journal H*, vol. 42, p. 431–474, July 2017.

[48] E. Hubble, "A Relation between Distance and Radial Velocity among Extra-Galactic Nebulae," *Proceedings of the National Academy of Science*, vol. 15, pp. 168–173, Mar. 1929.

[49] A. G. Riess, W. Yuan, L. M. Macri, D. Scolnic, D. Brout, S. Casertano, D. O. Jones, Y. Murakami, G. S. Anand, L. Breuval, T. G. Brink, A. V. Filippenko, S. Hoffmann, S. W. Jha, W. D'arcy Kenworthy, J. Mackenty, B. E. Stahl, and W. Zheng, "A comprehensive measurement of the local value of the hubble constant with 1 km s1 mpc1 uncertainty from the hubble space telescope and the sh0es team," *The Astrophysical Journal Letters*, vol. 934, p. L7, July 2022.

[50] A. G. Riess, G. S. Anand, W. Yuan, S. Casertano, A. Dolphin, L. M. Macri, L. Breuval, D. Scolnic, M. Perrin, and R. I. Anderson, "Crowded no more: The accuracy of the hubble constant tested with high resolution observations of cepheids by jwst," 2023.

[51] M. Kamionkowski and A. G. Riess, "The hubble tension and early dark energy," 2022.

[52] W. L. Freedman, "Cosmology at at crossroads: Tension with the hubble constant," 2017.

[53] J.-P. Hu and F.-Y. Wang, "Hubble tension: The evidence of new physics," 2023.

[54] A. G. Riess, L. Macri, S. Casertano, H. Lampeitl, H. C. Ferguson, A. V. Filippenko, S. W. Jha, W. Li, and R. Chornock, "A 3

[55] A. G. Riess, L. M. Macri, S. L. Hoffmann, D. Scolnic, S. Casertano, A. V. Filippenko, B. E. Tucker, M. J. Reid, D. O. Jones, J. M. Silverman, R. Chornock, P. Challis, W. Yuan, P. J. Brown, and R. J. Foley, "A 2.4

[56] S. Blundell, S. Blundell, and K. Blundell, *Concepts in Thermal Physics*. Oxford University Press, 2006.

[57] C. L. Bennett, D. Larson, J. L. Weiland, N. Jarosik, G. Hinshaw, N. Odegard, K. M. Smith, R. S. Hill, B. Gold, M. Halpern, E. Komatsu, M. R. Nolta, L. Page, D. N. Spergel, E. Wollack, J. Dunkley, A. Kogut, M. Limon, S. S. Meyer, G. S. Tucker, and E. L. Wright, "Nine-year wilkinson microwave anisotropy probe (wmap) observations: Final maps and results," *The Astrophysical Journal Supplement Series*, vol. 208, p. 20, Sept. 2013.

[58] D. J. Fixsen, E. S. Cheng, D. A. Cottingham, J. Eplee, R. E., R. B. Isaacman, J. C. Mather, S. S. Meyer, P. D. Noerdlinger, R. A. Shafer, R. Weiss, E. L. Wright, C. L. Bennett, N. W. Boggess, T. Kelsall, S. H. Moseley, R. F. Silverberg, G. F. Smoot, and D. T. Wilkinson, "Cosmic Microwave Background Dipole Spectrum Measured by the COBE FIRAS Instrument," , vol. 420, p. 445, Jan. 1994.

[59] E. Corbelli and P. Salucci, "The extended rotation curve and the dark matter halo of m33," *Monthly Notices of the Royal Astronomical Society*, vol. 311, p. 441–447, Jan. 2000.

[60] N. Aghanim, Y. Akrami, F. Arroja, M. Ashdown, J. Aumont, C. Baccigalupi, M. Ballardini, A. J. Banday, R. B. Barreiro, N. Bartolo, S. Basak, R. Battye, K. Benabed, J.-P. Bernard, M. Bersanelli, P. Bielewicz, J. J. Bock, J. R. Bond, J. Borrill, F. R. Bouchet, F. Boulanger, M. Bucher, C. Burigana, R. C. Butler, E. Calabrese, J.-F. Cardoso, J. Carron, B. Casaponsa, A. Challinor, H. C. Chiang, L. P. L. Colombo, C. Combet, D. Contreras, B. P. Crill, F. Cuttaia, P. de Bernardis, G. de Zotti, J. Delabrouille, J.-M. Delouis, F.-X. Désert, E. Di Valentino, C. Dickinson, J. M. Diego, S. Donzelli, O. Doré, M. Douspis, A. Ducout, X. Dupac, G. Efstathiou, F. Elsner, T. A. Enßlin, H. K. Eriksen, E. Falgarone, Y. Fantaye, J. Fergusson, R. Fernandez-Cobos, F. Finelli, F. Forastieri, M. Frailis, E. Franceschi, A. Frolov, S. Galeotta, S. Galli, K. Ganga, R. T. Génova-Santos, M. Gerbino, T. Ghosh, J. González-Nuevo, K. M. Górski, S. Gratton, A. Gruppuso, J. E. Gudmundsson, J. Hamann, W. Handley, F. K. Hansen, G. Helou, D. Herranz, S. R. Hildebrandt, E. Hivon, Z. Huang, A. H. Jaffe, W. C. Jones, A. Karakci, E. Keihänen, R. Keskitalo, K. Kiiveri, J. Kim, T. S. Kisner, L. Knox, N. Krachmalnicoff, M. Kunz, H. Kurki-Suonio, G. Lagache, J.-M. Lamarre, M. Langer, A. Lasenby, M. Lattanzi, C. R. Lawrence, M. Le Jeune, J. P. Leahy, J. Lesgourgues, F. Levrier, A. Lewis, M. Liguori, P. B. Lilje, M. Lilley, V. Lindholm, M. López-Caniego, P. M. Lubin, Y.-Z. Ma, J. F. Macías-Pérez, G. Maggio, D. Maino, N. Mandolesi, A. Mangilli, A. Marcos-Caballero, M. Maris, P. G. Martin, M. Martinelli, E. Martínez-González, S. Matarrese, N. Mauri, J. D. McEwen, P. D. Meerburg, P. R. Meinhold, A. Melchiorri, A. Mennella, M. Migliaccio, M. Millea, S. Mitra, M.-A. Miville-Deschênes, D. Molinari, A. Moneti, L. Montier, G. Morgante, A. Moss, S. Mottet, M. Münchmeyer, P. Natoli, H. U. Nørgaard-Nielsen, C. A. Oxborrow, L. Pagano, D. Paoletti,

B. Partridge, G. Patanchon, T. J. Pearson, M. Peel, H. V. Peiris, F. Perrotta, V. Pettorino, F. Piacentini, L. Polastri, G. Polenta, J.-L. Puget, J. P. Rachen, M. Reinecke, M. Remazeilles, C. Renault, A. Renzi, G. Rocha, C. Rosset, G. Roudier, J. A. Rubiño-Martín, B. Ruiz-Granados, L. Salvati, M. Sandri, M. Savelainen, D. Scott, E. P. S. Shellard, M. Shiraishi, C. Sirignano, G. Sirri, L. D. Spencer, R. Sunyaev, A.-S. Suur-Uski, J. A. Tauber, D. Tavagnacco, M. Tenti, L. Terenzi, L. Toffolatti, M. Tomasi, T. Trombetti, J. Valiviita, B. Van Tent, L. Vibert, P. Vielva, F. Villa, N. Vittorio, B. D. Wandelt, I. K. Wehus, M. White, S. D. M. White, A. Zacchei, and A. Zonca, "Planck2018 results: I. overview and the cosmological legacy ofplanck," *Astronomy amp; Astrophysics*, vol. 641, p. A1, Sept. 2020.

[61] W. Hu and S. Dodelson, "Cosmic microwave background anisotropies," *Annual Review of Astronomy and Astrophysics*, vol. 40, p. 171–216, Sept. 2002.

[62] D. Baumann, "Tasi lectures on inflation," 2012.

[63] A. R. Liddle, P. Parsons, and J. D. Barrow, "Formalizing the slow roll approximation in inflation," *Phys. Rev. D*, vol. 50, pp. 7222–7232, 1994.

[64] H. Bazrafshan Moghaddam, *Reheating in Early Universe Cosmology*. PhD thesis, McGill U., 2017.

[65] R. Allahverdi, R. Brandenberger, F.-Y. Cyr-Racine, and A. Mazumdar, "Reheating in inflationary cosmology: Theory and applications," *Annual Review of Nuclear and Particle Science*, vol. 60, p. 27–51, Nov. 2010.

[66] J. L. Cook, E. Dimastrogiovanni, D. A. Easson, and L. M. Krauss, "Reheating predictions in single field inflation," *JCAP*, vol. 04, p. 047, 2015.

[67] M. A. Amin, M. P. Hertzberg, D. I. Kaiser, and J. Karouby, "Nonperturbative dynamics of reheating after inflation: A review," *International Journal of Modern Physics D*, vol. 24, p. 1530003, Dec. 2014.

[68] P. Creminelli, D. L. Nacir, M. Simonović, G. Trevisan, and M. Zaldarriaga, "¡mml:math xmlns:mml="http://www.w3.org/1998/math/mathml" display="inline"¿¡mml:msup¿¡mml:mi¿¡/mml:mi¿¡mml:mn¿2¡/mml:mn¿¡/mml:msup¿¡/mml:m at its endpoint," *Physical Review D*, vol. 90, Oct. 2014.

[69] L. Kofman, A. Linde, and A. A. Starobinsky, "Reheating after inflation," *Physical Review Letters*, vol. 73, p. 3195–3198, Dec. 1994.

[70] A. Linde, "Particle physics and inflationary cosmology," 2005.

[71] Y. Akrami, F. Arroja, M. Ashdown, J. Aumont, C. Baccigalupi, M. Ballardini, A. J. Banday, R. B. Barreiro, N. Bartolo, S. Basak, K. Benabed, J.-P. Bernard, M. Bersanelli, P. Bielewicz, J. J. Bock, J. R. Bond, J. Borrill, F. R. Bouchet, F. Boulanger, M. Bucher, C. Burigana, R. C. Butler, E. Calabrese, J.-F. Cardoso, J. Carron, A. Challinor, H. C. Chiang, L. P. L. Colombo, C. Combet, D. Contreras, B. P. Crill, F. Cuttaia, P. de Bernardis, G. de Zotti, J. Delabrouille, J.-M. Delouis, E. Di Valentino, J. M. Diego, S. Donzelli, O. Doré, M. Douspis, A. Ducout, X. Dupac, S. Dusini, G. Efstathiou, F. Elsner, T. A. Enßlin, H. K. Eriksen, Y. Fantaye, J. Fergusson, R. Fernandez-Cobos, F. Finelli, F. Forastieri, M. Frailis, E. Franceschi, A. Frolov, S. Galeotta, S. Galli, K. Ganga, C. Gauthier, R. T. Génova-Santos, M. Gerbino, T. Ghosh, J. González-Nuevo, K. M. Górski, S. Gratton, A. Gruppuso, J. E. Gudmundsson, J. Hamann, W. Handley, F. K. Hansen, D. Herranz, E. Hivon, D. C. Hooper, Z. Huang, A. H. Jaffe, W. C. Jones, E. Keihänen, R. Keskitalo, K. Kiiveri, J. Kim, T. S. Kisner, N. Krachmalnicoff, M. Kunz, H. Kurki-Suonio, G. Lagache, J.-M. Lamarre, A. Lasenby, M. Lattanzi, C. R. Lawrence, M. Le Jeune, J. Lesgourgues, F. Levrier, A. Lewis, M. Liguori, P. B. Lilje, V. Lindholm, M. López-Caniego, P. M. Lubin, Y.-Z. Ma, J. F. Macías-Pérez, G. Maggio, D. Maino, N. Mandolesi, A. Mangilli, A. Marcos-Caballero, M. Maris, P. G. Martin, E. Martínez-González, S. Matarrese, N. Mauri, J. D. McEwen,

P. D. Meerburg, P. R. Meinhold, A. Melchiorri, A. Mennella, M. Migliaccio, S. Mitra, M.-A. Miville-Deschênes, D. Molinari, A. Moneti, L. Montier, G. Morgante, A. Moss, M. Münchmeyer, P. Natoli, H. U. Nørgaard-Nielsen, L. Pagano, D. Paoletti, B. Partridge, G. Patanchon, H. V. Peiris, F. Perrotta, V. Pettorino, F. Piacentini, L. Polastri, G. Polenta, J.-L. Puget, J. P. Rachen, M. Reinecke, M. Remazeilles, A. Renzi, G. Rocha, C. Rosset, G. Roudier, J. A. Rubiño-Martín, B. Ruiz-Granados, L. Salvati, M. Sandri, M. Savelainen, D. Scott, E. P. S. Shellard, M. Shiraishi, C. Sirignano, G. Sirri, L. D. Spencer, R. Sunyaev, A.-S. Suur-Uski, J. A. Tauber, D. Tavagnacco, M. Tenti, L. Toffolatti, M. Tomasi, T. Trombetti, J. Valiviita, B. Van Tent, P. Vielva, F. Villa, N. Vittorio, B. D. Wandelt, I. K. Wehus, S. D. M. White, A. Zacchei, J. P. Zibin, and A. Zonca, "Planck2018 results: X. constraints on inflation," *Astronomy amp; Astrophysics*, vol. 641, p. A10, Sept. 2020.

[72] J.-O. Gong, "Multi-field inflation and cosmological perturbations," *International Journal of Modern Physics D*, vol. 26, p. 1740003, Jan. 2017.

[73] L. Iacconi and D. J. Mulryne, "Multi-field inflation with large scalar fluctuations: non-gaussianity and perturbativity," 2023.

[74] Y. Akrami *et al.*, "Planck 2018 results. X. Constraints on inflation," *Astron. Astrophys.*, vol. 641, p. A10, 2020.

[75] L. Boubekeur and D. H. Lyth, "Hilltop inflation," *JCAP*, vol. 07, p. 010, 2005.

[76] W. H. Kinney and K. T. Mahanthappa, "Inflation from symmetry breaking below the Planck scale," *Phys. Lett. B*, vol. 383, pp. 24–27, 1996.

[77] K. Freese, J. A. Frieman, and A. V. Olinto, "Natural inflation with pseudo nambu-goldstone bosons," *Phys. Rev. Lett.*, vol. 65, pp. 3233–3236, Dec 1990.

[78] F. C. Adams, J. R. Bond, K. Freese, J. A. Frieman, and A. V. Olinto, "Natural inflation: Particle physics models, power law spectra for large scale structure, and constraints from COBE," *Phys. Rev. D*, vol. 47, pp. 426–455, 1993.

[79] L. Knox and A. Olinto, "Initial conditions for natural inflation," *Phys. Rev. D*, vol. 48, pp. 946–949, Jul 1993.

[80] W. H. Kinney and K. T. Mahanthappa, "Natural inflation from Fermion loops," *Phys. Rev. D*, vol. 52, pp. 5529–5537, 1995.

[81] K. Kumekawa, T. Moroi, and T. Yanagida, "Flat potential for inflaton with a discrete R invariance in supergravity," *Prog. Theor. Phys.*, vol. 92, pp. 437–448, 1994.

[82] J. A. Adams, G. G. Ross, and S. Sarkar, "Natural supergravity inflation," *Phys. Lett. B*, vol. 391, pp. 271–280, 1997.

[83] K. I. Izawa and T. Yanagida, "Natural new inflation in broken supergravity," *Phys. Lett. B*, vol. 393, pp. 331–336, 1997.

[84] K. I. Izawa, M. Kawasaki, and T. Yanagida, "R invariant topological inflation," *Prog. Theor. Phys.*, vol. 101, pp. 1129–1133, 1999.

[85] W. Buchmuller, K. Hamaguchi, M. Ratz, and T. Yanagida, "Gravitino and Goldstino at Colliders," *arXiv e-prints*, pp. hep–ph/0403203, Mar. 2004.

[86] L. Covi, "Models of inflation, supersymmetry breaking and observational constraints," in *3rd International Heidelberg Conference on Dark Matter in Astro and Particle Physics*, Springer-Verlag, Berlin, Heidelberg, 7 2000.

[87] M. Kawasaki and M. Yamaguchi, "Supersymmetric topological inflation model," *Phys. Rev. D*, vol. 65, p. 103518, May 2002.

[88] P. Binétruy and M. K. Gaillard, "Candidates for the Inflaton Field in Superstring Models," *Phys. Rev. D*, vol. 34, pp. 3069–3083, 1986.

[89] D. H. Lyth, *Particle Physics Models of Inflation*, pp. 81–118. Berlin, Heidelberg: Springer Berlin Heidelberg, 2007.

[90] P. J. Steinhardt and M. S. Turner, "Prescription for successful new inflation," *Phys. Rev. D*, vol. 29, pp. 2162–2171, May 1984.

[91] A. Linde, "Chaotic inflation," *Physics Letters B*, vol. 129, no. 3, pp. 177–181, 1983.

[92] J. Martin, C. Ringeval, and V. Vennin, "Encyclopaedia inflationaris," 2023.

[93] D. H. Lyth and A. Riotto, "Particle physics models of inflation and the cosmological density perturbation," *Physics Reports*, vol. 314, p. 1–146, June 1999.

[94] R. Kallosh and A. Linde, "On hilltop and brane inflation after Planck," *JCAP*, vol. 09, p. 030, 2019.

[95] J. Martin, C. Ringeval, and V. Vennin, "Encyclopædia Inflationaris," *Phys. Dark Univ.*, vol. 5-6, pp. 75–235, 2014.

[96] D. Chowdhury, J. Martin, C. Ringeval, and V. Vennin, "Assessing the scientific status of inflation after Planck," *Phys. Rev. D*, vol. 100, no. 8, p. 083537, 2019.

[97] J. Martin and C. Ringeval, "First CMB Constraints on the Inflationary Reheating Temperature," *Phys. Rev. D*, vol. 82, p. 023511, 2010.

[98] G. Steigman, "Primordial Nucleosynthesis in the Precision Cosmology Era," *Ann. Rev. Nucl. Part. Sci.*, vol. 57, pp. 463–491, 2007.

[99] A. R. Liddle, "The Inflationary energy scale," *Phys. Rev. D*, vol. 49, pp. 739–747, 1994.

[100] M. Y. Khlopov and A. D. Linde, "Is It Easy to Save the Gravitino?," *Phys. Lett. B*, vol. 138, pp. 265–268, 1984.

[101] M. Kawasaki, K. Kohri, and T. Moroi, "Hadronic decay of late - decaying particles and Big-Bang Nucleosynthesis," *Phys. Lett. B*, vol. 625, pp. 7–12, 2005.

[102] E. J. Copeland and O. Seto, "Reheating and gravitino production in braneworld inflation," *Phys. Rev. D*, vol. 72, p. 023506, 2005.

[103] R. Kallosh, L. Kofman, A. D. Linde, and A. Van Proeyen, "Gravitino production after inflation," *Phys. Rev. D*, vol. 61, p. 103503, 2000.

[104] J. B. Munoz and M. Kamionkowski, "Equation-of-State Parameter for Reheating," *Phys. Rev. D*, vol. 91, no. 4, p. 043521, 2015.

[105] W. H. Kinney and K. T. Mahanthappa, "Inflation at low scales: General analysis and a detailed model," *Phys. Rev. D*, vol. 53, pp. 5455–5467, 1996.

[106] K. D. Lozanov, "Lectures on Reheating after Inflation," 7 2019.

[107] J. Rubio, "Higgs inflation," *Front. Astron. Space Sci.*, vol. 5, p. 50, 2019.

[108] D. I. Kaiser, "Primordial spectral indices from generalized einstein theories," *Phys. Rev. D*, vol. 52, pp. 4295–4306, Oct 1995.

[109] D. I. Kaiser, "Induced-gravity inflation and the density perturbation spectrum," *Physics Letters B*, vol. 340, no. 1, pp. 23–28, 1994.

[110] J. J. van der Bij, "Can gravity play a role at the electroweak scale?," *Int. J. Phys.*, vol. 1, p. 63, 1995.

[111] J. J. van der Bij, "Can gravity make the Higgs particle decouple?," *Acta Phys. Polon. B*, vol. 25, pp. 827–832, 1994.

[112] A. O. Barvinsky, A. Y. Kamenshchik, and A. A. Starobinsky, "Inflation scenario via the Standard Model Higgs boson and LHC," *JCAP*, vol. 11, p. 021, 2008.

[113] S. Ferrara, R. Kallosh, A. Linde, A. Marrani, and A. Van Proeyen, "Superconformal Symmetry, NMSSM, and Inflation," *Phys. Rev. D*, vol. 83, p. 025008, 2011.

[114] F. Bezrukov, A. Magnin, M. Shaposhnikov, and S. Sibiryakov, "Higgs inflation: consistency and generalisations," *JHEP*, vol. 01, p. 016, 2011.

[115] J. L. F. Barbon and J. R. Espinosa, "On the Naturalness of Higgs Inflation," *Phys. Rev. D*, vol. 79, p. 081302, 2009.

[116] S. C. Park and S. Yamaguchi, "Inflation by non-minimal coupling," *JCAP*, vol. 08, p. 009, 2008.

[117] C. Germani and A. Kehagias, "New Model of Inflation with Non-minimal Derivative Coupling of Standard Model Higgs Boson to Gravity," *Phys. Rev. Lett.*, vol. 105, p. 011302, 2010.

[118] Y. N. Obukhov, "Spin driven inflation," *Phys. Lett. A*, vol. 182, pp. 214–216, 1993.

[119] E. D. Stewart, "Inflation, supergravity and superstrings," *Phys. Rev. D*, vol. 51, pp. 6847–6853, 1995.

[120] G. R. Dvali and S. H. H. Tye, "Brane inflation," *Phys. Lett. B*, vol. 450, pp. 72–82, 1999.

[121] M. Cicoli, C. P. Burgess, and F. Quevedo, "Fibre Inflation: Observable Gravity Waves from IIB String Compactifications," *JCAP*, vol. 03, p. 013, 2009.

[122] G. F. Giudice and H. M. Lee, "Unitarizing Higgs Inflation," *Phys. Lett. B*, vol. 694, pp. 294–300, 2011.

[123] R. Kallosh, A. Linde, and Y. Yamada, "Planck 2018 and Brane Inflation Revisited," *JHEP*, vol. 01, p. 008, 2019.

[124] J. Martin, "Inflation and precision cosmology," *Braz. J. Phys.*, vol. 34, pp. 1307–1321, 2004.

[125] L.-F. Li, *Introduction to Renormalization in Field Theory*, pp. 465–491. 2013.

[126] R. D. Ball and R. S. Thorne, "Renormalizability of effective scalar field theory," *Annals Phys.*, vol. 236, pp. 117–204, 1994.

[127] J. Hoffmann and D. Sloan, "Continuation of bianchi spacetimes through the big bang," *Phys. Rev. D*, vol. 110, p. 063539, Sep 2024.

[128] S. W. Hawking and R. Penrose, "The Singularities of Gravitational Collapse and Cosmology," *Proceedings of the Royal Society of London Series A*, vol. 314, pp. 529–548, Jan. 1970.

[129] C. Clarke and A. Królak, "Conditions for the occurence of strong curvature singularities," *Journal of Geometry and Physics*, vol. 2, no. 2, pp. 127–143, 1985.

[130] A. Liddle, *An Introduction to Modern Cosmology.* Wiley, Hoboken, New Jersey, 2015.

[131] G. Horowitz, "Singularity resolution in string theory," in *APS April Meeting Abstracts*, APS Meeting Abstracts, p. B7.003, American Physical Society, Apr. 2008.

[132] M. Natsuume, "The Singularity problem in string theory," in *Meeting of Frontier of Cosmology and Gravitation*, 8 2001.

[133] G. W. Gibbons, G. T. Horowitz, and P. K. Townsend, "Higher-dimensional resolution of dilatonic black-hole singularities," *Classical and Quantum Gravity*, vol. 12, p. 297–317, Feb. 1995.

[134] B.-F. Li and P. Singh, "Loop quantum cosmology: Physics of singularity resolution and its implications," in *Handbook of Quantum Gravity*, pp. 1–55, Springer, 2023.

[135] R. Gambini, J. Olmedo, and J. Pullin, "Quantum black holes in Loop Quantum Gravity," *Class. Quant. Grav.*, vol. 31, p. 095009, 2014.

[136] R. Gambini, J. Olmedo, and J. Pullin, *Quantum Geometry and Black Holes.* 2023.

[137] A. Ashtekar, T. Pawlowski, and P. Singh, "Quantum nature of the big bang," *Phys. Rev. Lett.*, vol. 96, p. 141301, 2006.

[138] M. Bojowald, "Absence of singularity in loop quantum cosmology," *Phys. Rev. Lett.*, vol. 86, pp. 5227–5230, 2001.

[139] M. Bojowald, "Loop quantum cosmology," *Living Rev. Rel.*, vol. 8, p. 11, 2005.

[140] F. Mercati, "A shape dynamics tutorial," *arXiv preprint arXiv:1409.0105*, 2014.

[141] J. Barbour, *Shape Dynamics. An Introduction*, pp. 257–297. Basel: Springer Basel, 2012.

[142] J. B. Barbour and B. Bertotti, "Mach's Principle and the Structure of Dynamical Theories," *Proc. Roy. Soc. Lond. A*, vol. 382, pp. 295–306, 1982.

[143] D. Sloan, "Dynamical similarity," *Physical Review D*, vol. 97, June 2018.

[144] T. A. Koslowski, F. Mercati, and D. Sloan, "Through the big bang: Continuing Einstein's equations beyond a cosmological singularity," *Phys. Lett. B*, vol. 778, pp. 339–343, 2018.

[145] D. Sloan, "Scalar Fields and the FLRW Singularity," *Class. Quant. Grav.*, vol. 36, no. 23, p. 235004, 2019.

[146] A. Bravetti, C. Jackman, and D. Sloan, "Scaling symmetries, contact reduction and poincaré's dream," *Journal of Physics A: Mathematical and Theoretical*, vol. 56, no. 43, p. 435203, 2023.

[147] D. Sloan, "Herglotz action for homogeneous cosmologies," *Classical and Quantum Gravity*, vol. 40, no. 11, p. 115008, 2023.

[148] D. Sloan, "Scale symmetry and friction," *Symmetry*, vol. 13, no. 9, p. 1639, 2021.

[149] R. Jha, "Introduction to Hamiltonian formulation of general relativity and homogeneous cosmologies," *SciPost Phys. Lect. Notes*, vol. 73, p. 1, 2023.

[150] P. A. M. Dirac, "Generalized hamiltonian dynamics," *Canadian Journal of Mathematics*, vol. 2, p. 129–148, 1950.

[151] L. D. Landau and E. M. Lifschits, *The Classical Theory of Fields*, vol. Volume 2 of *Course of Theoretical Physics*. Oxford: Pergamon Press, 1975.

[152] G. MONTANI, M. V. BATTISTI, R. BENINI, and G. IMPONENTE, "Classical and quantum features of the mixmaster singularity," *International Journal of Modern Physics A*, vol. 23, p. 2353–2503, July 2008.

[153] R. Kantowski and R. K. Sachs, "Some Spatially Homogeneous Anisotropic Relativistic Cosmological Models," *Journal of Mathematical Physics*, vol. 7, pp. 443–446, 03 1966.

[154] G. Montani, M. V. Battisti, R. Benini, and G. Imponente, "Classical and quantum features of the mixmaster singularity," *International Journal of Modern Physics A*, vol. 23, no. 16n17, pp. 2353–2503, 2008.

[155] M. V. Battisti, A. Marciano, and C. Rovelli, "Triangulated loop quantum cosmology: Bianchi ix universe and inhomogeneous perturbations," *Physical Review D—Particles, Fields, Gravitation, and Cosmology*, vol. 81, no. 6, p. 064019, 2010.

[156] R. S. Palais, "The principle of symmetric criticality," *Communications in Mathematical Physics*, vol. 69, no. 1, pp. 19–30, 1979.

[157] M. E. Fels and C. G. Torre, "The principle of symmetric criticality in general relativity," *Classical and Quantum Gravity*, vol. 19, no. 4, p. 641, 2002.

[158] S. Hawking, "On the Rotation of the Universe," *Monthly Notices of the Royal Astronomical Society*, vol. 142, pp. 129–141, 01 1969.

[159] M. A. MacCallum and A. H. Taub, "Variational principles and spatially-homogeneous universes, including rotation.," *Commun. Math. Phys. 25: No. 3, 173-89(1972).*

[160] J. Ryan, Michael P., "Hamiltonian cosmology: Death and transfiguration," *Journal of Mathematical Physics*, vol. 15, pp. 812–815, 06 1974.

[161] A. Ashtekar, A. Henderson, and D. Sloan, "A Hamiltonian Formulation of the BKL Conjecture," *Phys. Rev. D*, vol. 83, p. 084024, 2011.

[162] C. W. Misner, "The Isotropy of the Universe," , vol. 151, p. 431, Feb. 1968.

[163] C. W. Misner, "Mixmaster universe," *Physical Review Letters*, vol. 22, no. 20, p. 1071, 1969.

[164] C. W. Misner, "Mixmaster universe," *Phys. Rev. Lett.*, vol. 22, pp. 1071–1074, May 1969.

[165] V. Ardourel and J. Jebeile, "Numerical instability and dynamical systems," *European Journal for Philosophy of Science*, vol. 11, pp. 1–21, May 2021.

[166] R. Steinbauer, "The singularity theorems of general relativity and their low regularity extensions," *Jahresbericht der Deutschen Mathematiker-Vereinigung*, vol. 125, no. 2, pp. 73–119, 2023.

[167] A. D. Rendall, "The Nature of spacetime singularities," *100 Years Of Relativity : space-time structure: Einstein and beyond*, pp. 76–92, 2005.

[168] T. Thiemann, *Modern Canonical Quantum General Relativity.* Cambridge Monographs on Mathematical Physics, Cambridge University Press, 2007.

[169] A. Ashtekar, T. Pawlowski, and P. Singh, "Quantum Nature of the Big Bang: An Analytical and Numerical Investigation. I.," *Phys. Rev. D*, vol. 73, p. 124038, 2006.

[170] A. Ashtekar, T. Pawlowski, P. Singh, and K. Vandersloot, "Loop quantum cosmology of $k = 1$ frw models," *Phys. Rev. D*, vol. 75, p. 024035, Jan 2007.

[171] Łukasz Szulc, W. Kamiński, and J. Lewandowski, "Closed friedmann–robertson–walker model in loop quantum cosmology," *Classical and Quantum Gravity*, vol. 24, p. 2621, apr 2007.

[172] A. Ashtekar and A. Barrau, "Loop quantum cosmology: from pre-inflationary dynamics to observations," *Classical and Quantum Gravity*, vol. 32, p. 234001, nov 2015.

[173] H. Gomes and T. Koslowski, "Frequently asked questions about shape dynamics," *Foundations of Physics*, vol. 43, p. 1428–1458, Nov. 2013.

[174] F. Mercati and D. Sloan, "Traversing through a black hole singularity," *Phys. Rev. D*, vol. 106, no. 4, p. 044015, 2022.

[175] M. de Cesare and E. Wilson-Ewing, "A generalized kasner transition for bouncing bianchi i models in modified gravity theories," *Journal of Cosmology and Astroparticle Physics*, vol. 2019, p. 039–039, Dec. 2019.

[176] "Problem of time in quantum gravity," *Annalen der Physik*, vol. 524, no. 12, pp. 757–786, 2012.

[177] J. Barbour, T. Koslowski, and F. Mercati, "The solution to the problem of time in shape dynamics," *Classical and Quantum Gravity*, vol. 31, p. 155001, July 2014.

[178] J. Barbour, T. Koslowski, and F. Mercati, "Identification of a gravitational arrow of time," *Physical review letters*, vol. 113, no. 18, p. 181101, 2014.

[179] G. Herczeg and A. Waldron, "Contact geometry and quantum mechanics," *Physics Letters B*, vol. 781, p. 312–315, June 2018.

[180] R. Casals, G. Herczeg, and A. Waldron, "Dynamical quantization of contact structures," *arXiv preprint arXiv:2103.16645*, 2021.

[181] S. Rajeev, "Quantization of contact manifolds and thermodynamics," *Annals of Physics*, vol. 323, p. 768–782, Mar. 2008.

[182] S. Fitzpatrick, "On the geometric quantization of contact manifolds," *Journal of Geometry and Physics*, vol. 61, p. 2384–2399, Dec. 2011.

[183] K. Wernli, "Six lectures on geometric quantization," *Proceedings of Science*, vol. 435, p. 005, 2023.

[184] Y. Akrami *et al.*, "Planck 2018 results. X. Constraints on inflation," *Astron. Astrophys.*, vol. 641, p. A10, 2020.

[185] J. B. Barbour and B. Bertotti, "Mach's Principle and the Structure of Dynamical Theories," *Proceedings of the Royal Society of London Series A*, vol. 382, pp. 295–306, Aug. 1982.

[186] D. Sloan, "Dynamical Similarity in Field Theories," 7 2024.